Flow Science Incorporated
420 Neff Avenue, Suite 230, Harrisonburg, VA 22801
(540) 442-8433 • FAX (540) 442-8863

Reservoir Augmentation Demonstration Project: Limnology and Reservoir Detention Study of San Vicente Reservoir - Calibration of the Water Quality Model

Prepared for
City of San Diego
600 B Street, Suite 600,
San Diego, CA 92101

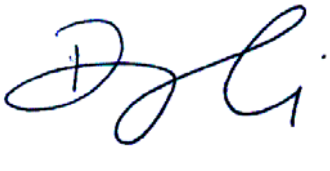

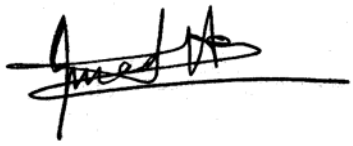

Prepared By
Li Ding, Ph.D., P.E. (VA)
Senior Engineer

Reviewed By
Imad A. Hannoun, Ph.D., P.E. (VA)
President

Reviewed By
E. John List, Ph.D., P.E.
Principal Consultant

FSI V094005
May 01, 2012

Table of Contents

List of Tables

Chapter 3

Chapter 4

Chapter 5

List of Figures

SUMMARY

San Vicente Reservoir (SVR) is located near Lakeside, California, and is used as a source of drinking water supply by the City of San Diego (City), its owner and operator. The reservoir currently has a capacity of about 90,000 acre-feet. San Vicente Reservoir is undergoing an enlargement that will raise the dam 117 feet and increase the reservoir's storage to 247,000 acre-feet at the spillway level (or 242,000 acre-feet at the maximum operation level).

A water reuse project, entitled Reservoir Augmentation, is being studied by the City. If implemented at full-scale, Reservoir Augmentation would bring advanced treated recycled water from the North City Water Reclamation Plant to SVR via a pipeline. The advanced treated recycled water would be blended with other water in the reservoir. The current project – the Reservoir Augmentation Demonstration Project – will not actually put any advanced treated recycled water into the reservoir; rather it will study and demonstrate the Reservoir Augmentation process. A component of the Reservoir Augmentation Demonstration Project (Demonstration Project) is the Limnology and Reservoir Detention Study of San Vicente Reservoir.

As part of the Limnology Study, the City has requested that Flow Science Incorporated (FSI) develop a three-dimensional water quality model that can accurately predict hydrodynamics and water quality of the existing and expanded SVR. It is anticipated that this model will be utilized to (1) establish residence time requirement for advanced treated recycled water in the reservoir and assess the short-circuiting of the advanced treated recycled water to the outlet structure; and (2) evaluate the effects of the advanced treated recycled water on water quality and eutrophication in the reservoir. This Technical Memorandum focuses on the development, calibration and validation of the three-dimensional water quality model for SVR.

Flow Science used two comprehensive and coupled three-dimensional computer models to simulate the hydrodynamics and water bio-chemistry of SVR. The models include a three-dimensional hydrodynamic module (Estuary Lake and Coastal Ocean Model, or ELCOM) and a water quality module (Computational Aquatic Ecosystem DYnamics Model, or CAEDYM). ELCOM simulates water velocities, temperatures, concentrations of salinity (*i.e.*, conductivity) and tracers; CAEDYM computes changes in dissolved oxygen (DO), nutrients, organic matter, pH and chlorophyll *a*. The coupled models are used to study the spatial and temporal relationships between physical, biological, and chemical variables in SVR.

The modeling domain includes the existing portion of the reservoir as well as the proposed expanded portion of the reservoir. A fine grid with a horizontal resolution of 50 × 50 m was used in the ELCOM calibration while a coarse grid with a horizontal resolution of 100 × 100 m was used in the CAEDYM calibration. This was necessitated by the large computer requirements and the desire to limit computation time to several

days per model run for a two-year simulation. A variable grid size was used in the vertical dimension with a grid size of 1.64 ft (0.5 m) near the surface, and expanding in size with depth. The calibration was conducted for the two-year period of 2006-2007. The input data required by the calibration were either based on measured data or derived from these data. ELCOM requires limited calibration effort in that the physical aspects of water movements in reservoirs are fairly well understood. The CAEDYM model was calibrated by adjusting some model bio-chemical parameters so that the simulation results best match measured field data.

The calibrated/validated ELCOM model shows good agreement with the measured data for both water temperature and conductivity. The calibration involved reconstruction of some meteorological data during periods where data were unavailable. It also involved an adjustment for the outlet port openings during the second half of 2007. As will be discussed in detail in the report, the City-specified field reports of the ports open during a portion of 2007 are at variance with the basic thermodynamics of the system. It is demonstrated later in this report that the open ports must have been at or above the thermocline level and not in the hypolimnion, as specified. In the future, it is recommended that outflow temperatures from SVR be recorded so that they can provide verification of the field record of port openings.

The onset and duration of thermal stratification as well as the deepening rate of the thermocline were predicted accurately by the model. Furthermore, the water conductivity, a measure of salinity, was well predicted by the model. It is noted that future modeling of the hydrodynamics at SVR would benefit from a full set of meteorological data gathered at SVR (the City stopped gathering on-site meteorological data in March 2007). An analysis presented herein shows that the meteorological data measured at the nearby California Irrigation Management Information System (CIMIS) station in Escondido differ in significant aspects from data gathered at SVR.

After the model was calibrated, a validation was performed to compare the model against the results of previous field studies. The field studies involved two separate episodes of tracer injection in the reservoir (winter 1995 and summer 1995). The field studies clearly showed the impacts of stratification (or lack thereof) on the mixing and dispersion of the tracer. The ELCOM model was capable of replicating the main features of the tracer study. Due to the nature of the tracer used in those studies (Lanthanum Chloride), a significant amount of tracer was lost due to coagulation/flocculation and subsequent settling. A simple coagulation/settling model was added to ELCOM. After the implementation of the coagulation/settling model, very good agreement between the model and the data was obtained. This validation provides strong verification and assurance that the model performance is accurate.

The calibration of the water quality model CAEDYM was carried out after the ELCOM calibration and verification process. The comparison between simulation results and measured in-reservoir field data involved water quality parameters including

dissolved oxygen (DO), pH, nutrients (nitrogen and phosphorus), chlorophyll *a* and Secchi depth. It is noted that some assumptions had to be made in order to calibrate the model. For example, assumptions on nutrient levels for the Aqueduct inflows during the "Bypassing Period" were needed to characterize nutrient loadings because there are only limited nutrient data available for the Aqueduct inflow.

The calibrated CAEDYM model shows overall good agreements with measured data. The simulated DO concentrations capture the major trends in the measured DO concentrations, including the onset, duration, and magnitude of periods of anoxia in the hypolimnion, the depth to the top of the anoxic (*i.e.,* "without oxygen") region, the DO decay rate in the spring in the hypolimnion, and the high surface DO concentrations in the spring (and sometimes fall) that are due to algae blooms. The simulated pH values closely match the measured data and are on average within 0.3 of the measured values. The calibrated model also replicates the major trends in the measured nutrient (phosphorus and nitrogen) concentrations. It is noted, however, that some of the field data are below the detection limit. The available in-reservoir chlorophyll *a* data were qualitatively measured using a fluorometer that has not been calibrated. The calibration of chlorophyll *a* had to be conducted indirectly through the calibration of Secchi depth. The final calibration run shows a fairly good agreement with the measured Secchi depths, indicating a fairly good calibration for chlorophyll *a*.

At this point, it is believed that the model calibration/validation is nearly complete. The calibrated/validated model will undergo peer review. After that, the model will be applied to the study of the expanded reservoir as well as the evaluation of the mixing of the advanced treated recycled water within the reservoir. The planned modification of Aqueduct release locations/facilities into the expanded SVR and outlet structure/port depths will be incorporated into the model.

Finally, it is noted that future evaluations of water quality at SVR would benefit from more frequent sampling of nutrients and chlorophyll *a* within the reservoir, lower nutrient detection limits, and an increased use of duplicate samples or periodic sampling audits. It is recommended that nutrient samples be collected more frequently for the inflows and within the water column. It is further recommended that the collection of chlorophyll *a* samples be resumed. Composite samples should be collected from the reservoir surface in order to analyze chlorophyll *a* concentrations in the laboratory. This would allow for calibration of the optical fluorometer data and improve the usefulness and interpretation of those data.

1. INTRODUCTION

1.1 BACKGROUND AND OBJECTIVES

San Vicente Reservoir (SVR) is located near Lakeside, California, and is used as a drinking water supply by the City of San Diego (City), its owner and operator (**Figure 1**). The reservoir currently has a capacity of about 90,000 acre-feet. San Vicente Reservoir is undergoing an enlargement that will raise the dam by 117 feet and increase the reservoir's storage to 247,000 acre-feet at the spillway level (or 242,000 acre-feet at the maximum operation level).

A water reuse project, entitled Reservoir Augmentation, is being studied by the City. If implemented at full-scale, Reservoir Augmentation would bring advanced treated recycled water from the North City Water Reclamation Plant to SVR via a pipeline. The City's Reservoir Augmentation program consists of three phases (Welch, 1997; City of San Diego, 2008).

- In Phase One, a comprehensive evaluation of all viable options to maximize the amount of water reuse in San Diego was undertaken. It included analysis and research on the health effects of reuse options, and included a public participation process. The Reuse Study's stakeholders identified Reservoir Augmentation at the City's San Vicente Reservoir to be the preferred reuse strategy.

- Phase Two is the Reservoir Augmentation Demonstration Project (Demonstration Project). The Demonstration Project will: (1) design, construct, operate, and test a demonstration-scale advanced water treatment (AWT) plant at the North City Water Reclamation Plant which will produce advanced treated recycled water; (2) conduct a limnology study of SVR to evaluate the water quality effects of bringing advanced treated recycled water into the reservoir, establish residence time and assess short-circuiting for advanced treated recycled water in the reservoir; (3) convene an Independent Advisory Panel (IAP) to provide independent expert oversight of the Demonstration Project; (4) define the State's regulatory requirements for the Reservoir Augmentation program; (5) perform an independent energy and economic analysis for the Reservoir Augmentation program; (6) and conduct a public outreach and education program regarding Reservoir Augmentation.

- If the Demonstration Project meets regulatory requirements and provides evidence of the viability of the Reservoir Augmentation process, the City could choose to proceed with Phase Three, the full-scale Reservoir Augmentation Project. Phase Three would create a new potable water supply for the City of San Diego and the region from advanced treated recycled water.

A component of the Demonstration Project is the Limnology and Reservoir Detention Study of San Vicente Reservoir (Limnology Study). As part of the Limnology Study, the City has requested that Flow Science Incorporated (FSI) develop a three-dimensional water quality model that can accurately predict hydrodynamics and water quality of the existing and expanded SVR. It is anticipated that this model will be utilized to (1) establish residence time requirement for advanced treated recycled water in the reservoir and assess the short-circuiting of the advanced treated recycled water to the outlet structure; and (2) evaluate the effects of the advanced treated recycled water on water quality and eutrophication in the reservoir.

This Technical Memorandum (TM) focuses on the development, calibration and validation of the three-dimensional water quality modeling for SVR. This work has been performed by Flow Science Incorporated (FSI) of Pasadena, California, under contract to the City of San Diego, California.

1.2 PREVIOUS STUDIES

FSI has previously performed various hydraulic and water quality modeling evaluations of SVR. The current work builds on these previous evaluations.

In the early 1990s, FSI conducted an analysis to evaluate the feasibility of introducing some highly-treated tertiary effluent into SVR (FSI, 1994). The study comprised one-dimensional reservoir modeling, a field study and data analysis. In 1995, the City conducted two field tracer studies in SVR that were completed in the winter and summer of 1995 (FSI, 1995). The work was used to enhance understanding of the water circulation patterns in the reservoir and help identify the fate and transport of the Aqueduct inflow. The results of that work have been used here to validate the three-dimensional water quality model developed in this study.

In 1997, FSI evaluated the hypolimnetic oxygen demand in SVR (FSI, 1997). As part of that project, FSI developed calibrated models of temperature and DO in SVR for 1992-1994 using the one-dimensional Dynamic Reservoir Simulation Model – Water Quality (DYRESM-WQ). In 2001, FSI revised the estimated hypolimnetic oxygen demand for SVR based on more extensive reservoir profiling data from 1992-2000. These data were used to develop recommendations for sizing a diffused oxygen input system and to develop performance specifications and design criteria for such a system (FSI, 2001).

In 2005, FSI developed a calibrated one-dimensional DYRESM-WQ model of temperature, conductivity (*i.e.,* salinity), and dissolved oxygen (DO) for SVR for the period 1999-2000 (FSI, 2005a). The model was then used to perform an assessment of water quality in the reservoir after the proposed dam raise and expansion. The purpose of the modeling work was to identify the effects of the reservoir expansion and new inlet and outlet facilities on water quality and possible design and management options for

maintaining or enhancing water quality. In particular, the focus of the work was on identifying the optimum elevations for the seven ports in the outlet tower that is being constructed as part of the dam-raise project. The work defined the port elevations so that the City and the Water Authority can selectively withdraw the best-available water in the reservoir at different lake elevations and for different operating conditions.

Most recently, in 2009, FSI re-calibrated the SVR one-dimensional DYRESM-WQ model developed in 2005 for the period 2006-2007 (FSI, 2009) using newly-obtained in-reservoir nutrient and chlorophyll *a* data that were either insufficient, or non-existent, for the previous calibration period (1999-2000). The calibrated DYRESM-WQ model was then used to evaluate water quality effects within the reservoir during dam construction drawdown conditions, when the water surface elevation levels (WSELs) in the reservoir would be reduced from around 620 ft to around 590 ft during the dam-raise construction.

The current project builds upon knowledge gained from the development of these models and analysis and the associated database of information on SVR.

1.3 TECHNICAL MEMORANDUM ORGANIZATION

This TM provides a detailed description of the three-dimensional water quality modeling performed for SVR. **Chapter 2** of the report provides details of the modeling approach and setup, including a description of the computer code used in the model and its required inputs. **Chapter 3** describes the calibration of the hydrodynamic part of the model, including details on the calibration setup and field data used for the calibration. Then, the calibration validation of the hydrodynamic part of the model (ELCOM) is presented in **Chapter 4**. **Chapter 5** provides details of the calibration of the water quality part of the model (CAEDYM). Conclusions and discussion are provided in **Chapter 6**.

2. MODELING APPROACH AND SETUP

2.1 ELCOM AND CAEDYM DESCRIPTION

FSI used comprehensive computer modeling to simulate the hydrodynamics and water quality for this study. The models used include a three-dimensional hydrodynamic module (Estuary Lake and Costal Ocean Model, or ELCOM) and a water quality module (Computational Aquatic Ecosystem DYnamics Model, or CAEDYM). ELCOM simulates water velocities, temperatures, concentrations of salinity (*i.e.*, conductivity) and tracers; CAEDYM computes changes in dissolved oxygen (DO), nutrients, organic matter, pH and chlorophyll *a*. By coupling these two modules, the models can be used to study the spatial and temporal relationships between physical, biological, and chemical variables in San Vicente Reservoir (see **Figure 2**[1]).

Both the ELCOM and CAEDYM models were developed at the Centre for Water Research at the University of Western Australia. They have been used in predicting water quality in many lakes and reservoirs throughout the world and a more detailed description of them is included in **Appendix A**.

Compared to the one-dimensional DYRESM-WQ model used in the previous studies of SVR, both ELCOM and CAEDYM are more advanced computer models that are capable of simulating sophisticated hydrodynamic and biogeochemical processes in three dimensions. More importantly, as three-dimensional models, they can track the horizontal and vertical movement of the advanced treated recycled water in the reservoir. Therefore, water quality effects induced by the advanced treated recycled water can be evaluated both temporally and spatially. By comparison, DYRESM-WQ is a one-dimensional model that focuses on identifying the vertical gradients in the reservoir.

ELCOM can run independently of CAEDYM to predict only reservoir hydrodynamics and parameters such as water velocities, temperatures and tracer concentrations. However, CAEDYM needs to be run coupled with ELCOM because it relies on ELCOM to provide the hydrodynamic "driver" to transport and mix the biological and chemical water quality parameters that are the essence of CAEDYM.

[1] Note that Figure 2 illustrates some processes that do not occur or are not modeled in SVR and are therefore not included in the modeling.

2.2 APPROACH

The approach to studying water quality effects of the advanced treated recycled water using a computer model consists of the following steps:

- Select an appropriate hydrodynamic and water quality computer models for the SVR model, which in this case are ELCOM and CAEDYM;
- Obtain and assemble existing data for calibration and validation of the SVR model;
- Set up the SVR model and associated input data files;
- Perform ELCOM simulations necessary to calibrate and validate the hydrodynamic part of the SVR model;
- Perform ELOCM-CAEDYM simulations necessary to calibrate the water quality part of the SVR model;
- Extend the model to the enlarged reservoir;
- Determine the future scenarios and associated input data;
- Apply the calibrated SVR model to different future scenarios and evaluate water quality changes induced by the Demonstration Project.

This report focuses on the first five steps, which involve the calibration and validation of the SVR water quality model.

2.3 MODEL SETUP

2.3.1 Model Domain and Grid

The model domains include the existing portion of the reservoir (WSEL = 650 ft) and the expanded portion of the reservoir (WSEL = 780 ft) (see **Figure 1**). However, the calibration/validation work discussed herein only considers the existing reservoir.

Bathymetry contour data for the reservoir were provided by the City with contour intervals varying from 2 ft to 10 ft, from which the model computational grid was created. The horizontal resolution of the grid for the ELCOM runs is 50 × 50 m (see **Figure 3**). The model grid was rotated 42 degrees counter-clockwise from North in order to align the major channels of the reservoir with the model grid axes to reduce numerical

errors. A two-year ELCOM simulation using this grid takes approximately 7 days on a fast personal computer. In order to control the run time for ELCOM-CAEDYM, a 100 × 100 m grid was used, as will be discussed in **Chapter 5**.

A variable grid size was used in the vertical dimension. A vertical grid size of 1.64 ft (0.5 m) was used near the top of the reservoir in order to provide a high resolution for resolving vertical stratification in the reservoir. Below this a stretched grid was used in order to decrease the number of cells needed and to improve computational efficiency. Each stretched cell is 6 percent larger in the vertical direction than the cell directly above it (i.e., stretch ratio or the ratio of grid sizes for adjacent cells = 1.06). This is possible because vertical gradients of water parameters such as temperature and conductivity within the hypolimnion tend to be small. The same vertical resolution was used for both ELCOM and ELCOM-CAEDYM.

2.3.2 Modeling Period

The period of 2006-2007 was chosen as the model calibration period for the following reasons:

- Measurements of daily Aqueduct inflow volumes began in late 2006;
- It had as dense a data set as other years since nutrient sampling began in 2003;
- Most data sets in this period have been evaluated, cleaned (by removing seemingly erroneous data), and verified in the most recent SVR study conducted by FSI (FSI, 2009) and are ready to use;
- Field data in 2007 showed faster rates of DO decay and smaller Secchi depths than in previous years, which provided a more conservative basis for the calibration.

2.3.3 Model Inputs

The input data required by the modeling include flow rates for inflows and outflows, inflow water quality, and meteorological forcing functions (rainfall, air temperature, wind speed and direction, relative humidity, solar influx) over the modeling period. The input data used in this study were either based on measured data or derived from these data. The sources and derivation of these data are discussed in more detail in the next three chapters.

3. ELCOM CALIBRATION

3.1 OVERVIEW

Model calibration is the process of adjusting some model parameters and sometimes correcting seemingly erroneous input data in an attempt to match the simulation results with measured field data. In this study, the calibration of the hydrodynamic model ELCOM was carried out first. The comparison between simulation results and measured in-reservoir field data involved the following parameters: water surface elevation (WSEL), water temperature and conductivity.

The in-reservoir field data were measured and provided by the City. **Appendix B** includes plots of the historical in-reservoir water temperature data since 1992 and conductivity data since 1999, as well WSEL data since 1990. During the calibration period (year 2006-2007), WSELs were measured daily while temperature and conductivity profiles were measured weekly. Most of these inputs were obtained by FSI for the recent study in 2009 (FSI, 2009).

3.2 ELCOM CALIBRATION SETUP

3.2.1 Computational Grid Setup and Initial Conditions

As described in **Chapter 2**, the model grid with a constant horizontal grid size of 50 × 50 m and a variable vertical grid size was used for ELCOM calibration (see **Figure 3**).

The initial reservoir temperature profile at the beginning of 2006 was based on in-reservoir measured data from Station A (near the outlet tower, see **Figure 1**) on January 3, 2006, as shown in **Appendix B**.

Since ELCOM requires salinity as an input, but only conductivity is generally measured in the reservoir and in the inflows, salinity values were estimated from the conductivity data. The in-reservoir salinity is estimated to be approximately equal to the total dissolved solids (TDS) concentration, and the TDS concentration and salinity can be estimated according to the following formula developed from comparisons of available measured TDS and conductivity data using a least squares best fit to a linear relation (FSI, 2009):

$$\text{TDS (mg/L)} = \text{Salinity (mg/L)} = 0.65 * \text{Conductivity (}\mu\text{S/cm)} \qquad \text{[Eqn. 1]}$$

As suggested in the previous SVR modeling study (FSI, 2009), conductivity data from January 9, 2006, were used for the initial conditions for the computation. The calibration was performed as one continuous two-year simulation,

3.2.2 Flow Rate Inputs

Three surface inflows were included in the model calibration. These include the First San Diego Aqueduct (Aqueduct), stream inflows (Runoff), and water transfers from Sutherland Reservoir. The Aqueduct consists of two pipelines that extend from the Metropolitan Water District of Southern California's (MWD's) Colorado River Aqueduct near San Jacinto, California, and terminate at the north-west corner of SVR (**Figure 1**). The Aqueduct inflow cascades down a steep, natural channel and enters the reservoir at the surface. Runoff enters the reservoir as a surface inflow through several tributaries, with San Vicente Creek being the dominant Runoff inflow. When water is transferred from Sutherland Reservoir, it enters San Vicente Reservoir at the north end of the reservoir via San Vicente Creek.

The only modeled outflow in the calibration is the withdrawal from the existing outlet tower located near the center of the upstream face of the dam (see **Figure 1**). It consists of a vertical outlet tower with six tiers, three of which can also be equipped with an optional 20 ft riser. The multiple tier elevations allow for selective withdrawal of the water at desired depths. A detailed discussion of modeled withdrawal elevations is included in **Section 3.2.5**.

Total monthly flow volumes for each of the three inflows and the outflow were provided by the City. In addition, daily Aqueduct inflow volumes were provided starting in November 2006, and daily outflow (draft) volumes were provided for the entire calibration period. During those times when daily Aqueduct inflow volumes were not available, the monthly inflow data were used for the average daily inflow volumes. The monthly inflow data were also used for the average daily inflow volumes for the Runoff and Sutherland Reservoir inflows. Note that the Runoff volumes are not measured directly; instead, they are determined from other known values based on a mass balance computation.

However, the calculated reservoir storage using the inflow/outflow rates provided by the City does not match the measured storage volumes and it varied by as much as 40 Million Gallon (MG) (about 0.2% of the total reservoir volume) from the measured volumes in June 2006 and April, May, and December 2007. Thus, as part of WSEL calibration, a correction was made to the Aqueduct inflow or outlet flows (depending upon whether additional inflows or outflows were needed to correct the storage) to improve the WSEL results. Details on the correction method can be found in the previous SVR model calibration study (FSI, 2009). A plot of the resulting inflow and outflow volumes used in the model calibration, as compared to the measured volumes, is included in **Figures 4** and **5**.

As shown, the Aqueduct comprises the major inflow source to SVR with maximum flow rates generally occurring in the winter and spring. Runoff inflows were much less

than the Aqueduct inflows during this period, with maximum Runoff occurring in the winter and spring. The controlled inflows from Sutherland Reservoir occurred in March, November, and December 2007.

3.2.3 Inflow Temperatures and Conductivity Inputs

Temperature and salinity of all inflows are the parameters required as inputs in the ELCOM calibration; but these data were not available at all times for all inflows. Therefore several assumptions and estimates were made when preparing these input files for the calibration. A brief description of these assumptions is provided below for each inflow and details can be found in the previous SVR model calibration study (FSI, 2009). **Appendix C** (see **Figures C-1** through **C-6**) includes plots of the measured data and input data used in the model calibration for each inflow.

Aqueduct Inflows

Discharges from Lake Skinner generally supply the Aqueduct. Therefore, since Aqueduct temperature and conductivity data are not measured at the inlet to SVR, data measured at the Lake Skinner outlet (located 80 miles upstream) were used to characterize the Aqueduct inflow for most of the 2006-2007 calibration period under the assumption that these parameters in the Aqueduct do not change significantly from the Lake Skinner discharge to SVR. These data at Lake Skinner were obtained directly from MWD and included approximately bi-weekly temperature and conductivity (and some TDS data).

During the period from approximately October 2006 through January 2007, about 80% of the water in the Aqueduct was being supplied directly from the San Diego Canal while the remaining water was supplied by Lake Skinner (verbal communication with Dr. Rich Losee of MWD on June 4, 2008). Based on limited data obtained from MWD for the San Diego Canal, temperature and conductivity (*i.e.*, salinity) values during the "Bypassing Period" are comparable to data measured at the Lake Skinner outflow, so the more dense Lake Skinner outflow data were used. The final temperature and conductivity input values for the Aqueduct inflow as well as all the measured data were presented in **Figures C-1** and **C-2**.

Runoff Inflows

Temperature and conductivity data for the local tributaries to SVR were obtained from the City and sampled as often as monthly since 2003. Data were measured in San Vicente Creek (SV Creek) - both upstream and downstream of the confluence with the Sutherland Reservoir inflow - and in Barona Creek, Aqueduct Creek, Kimball Creek, and Tool Road Creek. Due to the lack of data for other tributaries, data measured in SV Creek were used to estimate the model inputs for other tributaries.

The Runoff conductivity can vary significantly depending upon whether it is composed of a small or large rain event, and stream data are not collected frequently enough to characterize the complex relationship between conductivity and flow rate. However, stream conductivity generally decreases with increasing flow rates. As suggested in the previous SVR model calibration study (FSI, 2009), salinity values were reduced in February 2006, March 2006, December 2007 for possible sustained runoff events that were not captured by monthly sampling data (per statements made by City and Water Authority personnel during 9/23/08 conference call). Otherwise there is no conductivity drop as demonstrated in the measured conductivity profile data. The final temperature and conductivity input values for the runoff as well as all the measured data are presented in **Figures C-3** and **C-4**.

Sutherland Reservoir Inflows

Water from Sutherland Reservoir is intermittently released from the hypolimnion and travels through an approximately 12-mile pipeline before discharging into SV Creek about 4.5 miles upstream of SVR. During the calibration period, inflows from Sutherland Reservoir occurred in March 2006 and November-December 2007. In-reservoir temperature and conductivity data were obtained from the City for Sutherland Reservoir. The temperature and conductivity values of inflows from Sutherland Reservoir were in general assumed to be equal to the values from the in-reservoir profile data measured from within the hypolimnion near the elevation of the sole Sutherland outlet located at EL 1940 ft.

As suggested in the previous SVR model calibration study (FSI, 2009), inflow temperatures in March 2007 were adjusted in order to decrease the density of the inflow relative to San Vicente Reservoir so that the Sutherland Reservoir inflow would insert at the surface as indicated by conductivity profile data taken from San Vicente Reservoir. This correction may be related to the heating of the water while it travels between the two reservoirs. The final temperature and conductivity input values for the Sutherland reservoir inflow as well as all the measured data are presented in **Figures C-5** and **C-6**.

3.2.4 Meteorological Inputs

The meteorological inputs required for the model, which features a complete thermodynamic calculation, include measurements of solar radiation, air temperature, wind speed, wind direction, relative humidity, and rainfall. The meteorological data at SVR are only available from January 1, 2006, through December 11, 2006, and January 1, 2007, through March 15, 2007, which were measured every 10 minutes by the City at a monitoring station on Lowell Island within San Vicente Reservoir (see **Figure 1**).

Initially, the remaining meteorological data for 2006 and 2007 were filled by data obtained from the California Irrigation Management Information System (CIMIS). Hourly CIMIS data were measured at Station 153 in Escondido, California, which is the closest operational CIMIS station during the calibration period and is more than 10 miles from SVR (see **Figure 6**). The ELCOM calibration run using this composite data set shows that the simulated temperature profiles track closely to the measured value in 2006 when the meteorological data from the City were used, while the model overestimates thermocline depths in the summer of 2007 when the CIMIS data were mostly used (see **Figure 7**). Several attempts were made to adjust the CIMIS data based on an evaluation of the overlapping City and CIMIS data, but they all failed to accurately reproduce the measured thermocline depths in the summer of 2007. It was concluded that the CIMIS meteorological data do not represent meteorological conditions at SVR, even with the adjustments, probably because of distance between these two places and the complex terrain surrounding SVR. In particular, it is noted that the wind velocity can have a significant impact on lake mixing and the depth of the thermocline, and as a result, using wind speed from a remote location with different wind patterns can lead to erroneous modeling results.

Due to the inadequacy of using the meteorological data from Escondido, the approach used herein involved constructing a composite meteorological data set by filling in the missing 2007 meteorological data from SVR with the corresponding 2006 data gathered by the City. For an approximately three-week period in December 2006 and 2007, there were no meteorological data available from the City. This period was filled by using the CIMIS data from Escondido (see **Table 1)**. Using this composite data set, the simulation results show very good agreement between the simulated and measured water temperatures between April and June 2007, but the model results start to deviate from the measured data after July 2007 (see **Figure 8**). As described later, the deviation in the second half of 2007 can be attributed to issues other than meteorological data. As a result, this composite meteorological data set was used in all the calibration runs. Graphical plots of the final meteorological data inputs are included in **Appendix C** (see **Figures C-7** through **C-12**).

Table 1. Details on the Composite Meteorological Data Used in the Model

Period	Data Source	Measured Location
1/1/2006 – 12/11/2006	City	Lowell Island
12/12/2006-12/31/2006	CIMIS	Escondido
1/1/2007 – 3/15/2007	City	Lowell Island
3/16/2007 – 12/11/2007	Using data between 3/16/2006 – 12/11/2006 from the City	Lowell Island
12/12/2007 – 12/31/2007	Using data between 12/12/2006 – 12/31/2006 from CIMIS	Escondido

3.2.5 Outflow Port Openings

The existing reservoir outlet tower consists of six tiers, three of which are also equipped with an optional 20 ft riser. A summary of the available withdrawal elevations from the ports on the current tower is included in **Table 2**.

Table 2. Available Withdrawal Elevations on Existing Outlet Tower

Port	Withdrawal Elevation
1	493 ft
2	510 ft
2 w/ 20 ft riser	530 ft
3	540 ft
3 w/20 ft riser	560 ft
4	570 ft
4 w/20 ft riser	590 ft
5	600 ft
6	630 ft

Based on records obtained from the City, outflows were withdrawn from Port No. 3 with a 20-ft riser (560 ft EL) and Port No. 4 (570 ft EL) from January through mid-June 2006. From mid-June 2006 through mid-September 2007, outflows were withdrawn from Port No. 2 with a 20-ft riser (530 ft EL) and Port No. 3 (540 ft EL). Starting in mid-September 2007, outflow withdrawal switched back to Port No. 3 with a 20-ft riser (560 ft EL) and Port No. 4 (570 ft EL).

The ELCOM calibration run using the outflow port openings described above shows that simulated thermocline depths match well with measured data in 2006 and the first half of 2007, but it predicted much deeper thermocline levels than shown by the in-reservoir data from July 2007 onward (see **Figures 7** and **8**). Historical temperature data between 2000 and 2007 (**Figure 9**) reveal that the thermocline depth in the summer of 2007 resided around 20 ft below the surface and is much shallower than those in previous years. However, there is no evidence indicating that meteorological conditions in 2007 at SVR, which was believed to be not much different from previous years (verbal communication with Jeff Pasek of the City), could lead to such a shallow thermocline depth.

This initial finding led to a more careful examination of the effect of inflows and outflows on thermocline depths at SVR. In the summers of 2006 and 2007, the Aqueduct flow was the major inflow source at SVR and entered the reservoir at the surface. Temperatures for the Aqueduct inflow were between 20 and 28 ^{o}C between early June and later September in both 2006 and 2007 (see **Figure 10**). If the 18 ^{o}C isotherm (see **Figure 11**) is used to represent the thermocline, the Aqueduct inflow should reside above the defined thermocline, given that it enters the reservoir at the surface with a relatively high temperature. The City reported withdrawal levels during this period were below the observed thermocline. As a result, the increase in thickness of epilimnion (the layer above the thermocline) at SVR would be expected to be greater than the thickness of the layer formed by the Aqueduct inflow during the same period (making due allowance for evaporation losses). For 2006, the thermocline (defined as the 18 ^{o}C isotherm) is observed to deepen by about 9.5 ft between early June and early September. During the same period, the thickness of the layer formed by the Aqueduct inflow would be 2.6 ft and the evaporation loss is calculated to be about 2 ft. The net thermocline deepening in this time period due to external forcing (wind, heating and cooling, etc.) can be calculated using the following equation:

Deepening due to external forcing (m) = Net observed thermocline deepening (m)
- Deepening due to inflow insertion (m)
+ Loss due to withdrawal above thermocline (m)
+ Loss due to evaporation (m) [Eqn. 2]

From Eqn. 2, the deepening of the thermocline due to external forcing is estimated to be 8.9 ft, calculated as 9.5 less 2.6 plus 2 ft. However, for 2007, the thermocline (defined as the 18 ^{o}C isotherm) is observed to deepen by about 6.6 ft between early June and early September, while the thickness of the layer formed by the Aqueduct inflow is 11 ft. Applying Eqn. 2, the deepening of the thermocline due to external forcing in 2007 is therefore estimated to be -2.4 ft, which is a clearly unrealistic answer. If the mixing in

2007 is considered to actually have deepened the thermocline by the same amount as 2006 (*i.e.*, 8.9 ft which is a reasonable assumption[2]), then the thermocline depth would be 11.3 ft deeper than observed (calculated using Eqn. 2).

It is therefore apparent that the measured depth of the thermocline in the summer of 2007 is not reasonable unless some outflows were withdrawn from the epilimnion during this period[3] (about 11.3 ft worth of outflow). During this time period, the recorded outflows were from Port No. 2 with a 20-ft riser (530 ft EL) and Port No. 3 (540 ft EL), at a depth of 60 and 50 ft below the observed thermocline, respectively. The total water withdrawn from the reservoir during this time was 3,300 MG, corresponding to a reservoir layer of 11 ft (at the level of the thermocline). The only explanation of the above discrepancy is that the recorded open ports during this period were not correct, and that an approximately 11.3 ft thick layer of water was withdrawn at or above the thermocline level. It is noted that the recorded open ports show a switch to higher ports (Port No. 3 with a 20-ft riser at 560 ft EL and Port No. 4 at 570 ft EL) in mid-September 2007. However, these recorded open ports were too deep (both were below the thermocline) and the switch was too late to explain the above-mentioned discrepancy. To correct for the discrepancy it was considered in the model that the switch to the upper ports occurred earlier (in mid-June 2007) and the switch was to the shallower ports (Port No. 4 with a 20-ft riser at 590 ft EL and Port No. 5 at 600 ft EL) (see **Figure 12**), both of which were above the observed thermocline in the summer of 2007. The corresponding model results incorporating this change show good agreement in matching the measured data regarding thermocline depth (see **Figure 13**).

3.3 CALIBRATION RESULTS

3.3.1 Water Surface Elevation

Figure 14 shows the measured versus simulated water surface elevations for the calibration based on the flow data provided by the City. As shown, the simulated water surface elevations are generally within 1 ft of the measured WSELs.

---

[2] We have conducted a few sensitivity test runs and the results indicated that reducing the wind speed by 30%, or decreasing sunlight penetration depth (due to higher algae concentrations) only reduced the thermocline deepening due to external forcing by 1-2 ft.

[3] It is noted here that the thermocline depth measurements were performed using three different instruments at different times, and all the instruments produced similar results, thus ruling out instrument error as a source of the discrepancy.

3.3.2 Temperature

Figure 15 shows a time series plot of the simulated versus measured temperatures for both 2006 and 2007 at the surface and bottom of the reservoir. **Figure 16** shows color contours of the simulated water temperatures in comparison to the measured data. In addition, comparisons of simulated and measured temperature profiles at selected dates are included in **Appendix C** (see **Figures C-13** through **C-15**). As presented, the simulated temperatures closely match the measured data and accurately predict the onset and duration of thermal stratification, as well as the depth of the thermocline.

A scatter plot of the measured and simulated temperature for years 2006 and 2007 is provided in **Figure 17**. The plot includes only surface and bottom temperature. In the plot, the 45-degree theoretical line with zero intercept represents what would be a "perfect" correlation between the simulated and measured data. Therefore, the nearer the plotted points are to the 45-degree line, the better is the simulation. The graph indicates a good calibration in temperature.

A statistical analysis of the calibration results versus the measured temperature produced the metrics presented in **Table 3**. These metrics quantitatively summarize the accuracy of the calibration results. For example, the computed Root Mean Square Errors (RMSE) indicate that the calibrated temperatures in 2006 are on average within 0.60 ^{o}C of the measured data, corresponding to 3.6% of the range in measured temperatures (relative RMSE = RMSE / $|T_{max} - T_{min}|$); and the calibrated temperatures in 2007 are on average within 1.03 ^{o}C of the measured data, corresponding to 6.2% of the range in measured temperatures. Mean error calculates the average of difference between the measured and simulated values. Thus, the model on average overestimates temperatures by 0.17 ^{o}C in 2006 and on average underestimates temperatures by 0.1 ^{o}C in 2007. These metrics indicate a good calibration.

Table 3. Temperature Calibration Metrics

PARAMETER	2006 RESULTS			2007 RESULTS		
	ROOT MEAN SQUARE ERROR (RMSE)	RELATIVE RMSE	MEAN ERROR	ROOT MEAN SQUARE ERROR (RMSE)	RELATIVE RMSE	MEAN ERROR
Surface and Bottom Temperature	0.60 °C	3.6 %	-0.17 °C	1.03 °C	6.2 %	0.1 °C

3.3.3 Conductivity

Figures 18 and **19** are comparison plots (time series and color contours, respectively) for the simulated and measured conductivities (*i.e.*, salinities). The simulated

conductivity data plotted in the figures are computed based on the in-reservoir relationships between conductivity, salinity, and TDS as given in Eqn. 1.

The resulting simulated conductivities capture the seasonal trends in both the surface and bottom conductivity values; the magnitudes of the simulated and measured conductivity data also track closely, particularly in 2006.

A scatter plot of the measured and simulated conductivity values for years 2006 and 2007 is provided in **Figure 20**. Statistical metrics are included in **Table 4**. The RMSE indicate that the calibrated conductivity values are on average within 15-30 µS/cm of the measured, corresponding to 10 – 20% of the range in measured conductivity. These indicate a good conductivity calibration for both years, especially given that an error of 30 µS/cm is common in field-measured conductivity (FSI, 2005b).

Table 4. Conductivity Calibration Metrics

PARAMETER	2006 RESULTS			2007 RESULTS		
	ROOT MEAN SQUARE ERROR (RMSE)	RELATIVE RMSE	MEAN ERROR	ROOT MEAN SQUARE ERROR (RMSE)	RELATIVE RMSE	MEAN ERROR
Surface and Bottom Conductivity	14.9 µS/cm	10.7 %	8.6 µS/cm	29.7 µS/cm	19.7 %	2.8 µS/cm

3.3.4 Animation of Aqueduct Tracer

An animation that shows transport and mixing of a conservative tracer injected into the Aqueduct inflow on July 1, 2006 is included in **Appendix D**. The tracer was added at a constant concentration of 100 to the Aqueduct inflow. The plan view plots the maximum value of the tracer concentrations for each vertical water column within the model domain. Two cross sections plot the tracer concentrations on the section connecting between Aqueduct inflow and the Dam and the section connecting between Kimball Arm and the Dam.

4. ELCOM VALIDATION

4.1 FIELD TRACER STUDIES

Model validation presented here involves simulating the periods of the tracer studies completed in 1995 using the previously-calibrated SVR model (**Chapter 3**). The ability of the calibrated model to reproduce observed field data in these tracer studies provides assurance of the predictive capability of the model.

Two tracer field studies were conducted by the City of San Diego in 1995: the winter study that was completed in January and February and the summer study that was completed between July and early September. In each study, a lanthanum (lanthanide) chloride solution was injected as a tracer into the Aqueduct inflow just before it enters the reservoir. Over the period of each study, tracer concentrations and other water quality parameters such as temperature, salinity and pH were measured at various reservoir stations (see **Figure 21**). **Table 5** presents a summary of information on field studies. A detailed description and analysis of the tracer studies can be found in the FSI report titled "San Vicente Water Reclamation Project: Results of Tracer Studies" (FSI, 1995).

Table 5. Summary of Information on Tracer Studies

Name	Injection Date	Injected Lanthanum Mass	Lake Condition	Sampling Period
Winter study	9:00 AM, 1/4/95-9:00 AM, 1/5/95	77.9 kg	Weak Stratification	1/6/95 – 2/7/95
Summer Study	10:00 AM, 7/24/95-10:00 AM, 7/25/95	154.5 kg	Strong Stratification	7/31/95 – 9/5/95

4.2 MODEL VALIDATION SETUP

4.2.1 Computational Grid and Model Inputs

The approach to setting up grid and input files for the model validation run is similar to that used in setting up the calibration run, except that 1995 data (inflows, outflow, meteorology) were used.

Since no meteorological data were collected at SVR in 1995, data at CIMIS Ramona Station (#98) were used as input in the validation run. Ramona Station is about 6 miles away from SVR. Note that the Ramona station was only in operation before 1999, and thus could not be used in the 2006/07 calibration to reconstruct missing meteorological data.

The winter validation run simulated a 45-day period starting on January 3, 1995 (1 day prior to the tracer injection) and ending on February 18, 1995. The initial conditions for the winter run were based on data measured at Station A on January 3, 1995.

The summer validation run simulated a 50-day period starting on July 21, 1995 (3 days prior to tracer injection) and ending on September 9, 1995. The initial conditions for the summer run were based on data measured at Station A on July 21, 1995.

4.2.2 Particle Settling

Both winter and summer tracer studies used lanthanum chloride as the tracer. Lanthanum, a coagulant used in the wastewater treatment, can bind with phosphate in water and form insoluble particles (Niquette, *et al.,* 2004, Recht, *et al*., 1970). After the particles are formed, they grow in size by attaching themselves to other large particles in the water (*i.e.,* "flocculation") and then settle within the water column and may deposit on the sediment. This lanthanum removal process by settling is evidenced in the exponential loss of total measured lanthanum mass in the reservoir over the time during the tracer studies (see **Figure 22**). For example, after 35 days from the initial injection of the lanthanum, there was about 15% of the lanthanum mass left in the water column for the winter tracer study (illustrated as red diamonds in **Figure 22**) and about 50% of the lanthanum remained in the water column in the summer tracer study (illustrated as green squares in **Figure 22**). These figures were obtained based on integrating the in-reservoir measured lanthanum concentration data at all stations. In contrast, after 35 days there would have been about 95% and 99% of the lanthanum left for the winter and summer studies, respectively, if the lanthanum were a conservative tracer (the contour plots for these runs are include in **Figures C-16** through **C-22** of **Appendix C**). This indicates that less than 5% of the lanthanum was withdrawn through outlets during the 35-day period and significant portion of the total injected lanthanum was lost through settling. It is also noted that the volume of water withdrawn from the reservoir during the winter and summer studies was approximately 4 and 10 % of the reservoir volume, respectively. Therefore, it is more appropriate to model lanthanum as particles that grow in size and settle rather than a conservative tracer.

Lanthanum chloride usually bonds with phosphate to form insoluble particles. In the winter study, most of injected lanthanum chloride was observed to reside close to the bottom of the reservoir, where phosphate is ample due to sediment release and lack of algae consumption at depth. In the summer study, most of lanthanum chloride resides in the epilimnion or at the level of the thermocline where phosphate level is low due to algae consumption. Therefore, more insoluble lanthanum phosphate particles are expected to form in the winter than in the summer. In addition, more large suspended particles in the reservoir were expected in the winter due to winter storms and runoff. These particles provide the medium to which lanthanum phosphate can attach.

Therefore, it is reasonable to apply different particle distributions and flocculation rates in the summer and winter simulations as described above.

In the validation run, the lanthanum coagulation/flocculation was modeled using a simplified representation as follows:

- Nine (9) different-sized particle groups (leading to different settling velocities) were used to represent the lanthanum in the reservoir. The settling velocity of each particle size group was calculated according to Stokes's Law, which suggests that the settling velocity increases in proportion to the square of the particle diameter. A summary of settling velocity for each particle size group is listed in **Table 6**.

- In the winter study, starting with the initial distribution among the particle size groups, it is assumed that 8% mass of each group particle moves to the next group with larger size daily (*i.e.*, a flocculation rate equal to 8% of mass / day). The simulated mass distributions of the particle groups on the sampling dates in the winter study are presented in **Figure 23**.

- In the summer study, two flocculation rates were used for each particle size group: 60% mass of each group has the flocculation rate of 0.9% of mass / day (*i.e.*, 0.9% mass of each group moves to the next group with larger size daily); and 40% mass of each group has the flocculation rate of 28% of mass / day (*i.e.*, 28% mass of each group moves to the next group with larger size daily). The simulated mass distributions of particle groups on the sampling dates in the summer study are presented in **Figure 23**. The use of different flocculation rates in summer and winter is discussed further below.

- These flocculation rates were selected mainly because they produce the best match to the rate of decrease in measured total lanthanum mass over the whole reservoir (see **Figure 24**).

Table 6. Settling Velocity for Simulated Particle Groups

Particle Size Group	Settling Velocity (m/day)
1	0.0
2	0.1
3	0.2
4	0.3
5	0.5
6	1.0
7	1.5
8	2.5
9	5.0

4.3 VALIDATION RESULTS

Figure 25 presents color contours of the simulated water temperature in comparison to the measured temperature data during the period of the winter tracer study. Note that the simulated temperature shows more diurnal fluctuations because the simulation results were plotted based on three-hour sampling, while the field data were measured once every few days. During the winter study, the reservoir was well-mixed initially and started to develop a weak stratification later. As presented, the simulated temperatures match well with the measured data and the model accurately predicts the onset and development of thermal stratification.

Figures 26 through **28** show color contours of measured and simulated lanthanum profiles in the winter tracer study along a continuous path joining Stations I, B, K, L, A, L, M, C, D, G, Q, and R as shown in **Figure 21**. The majority of the lanthanum stays close to the bottom of the reservoir and was rarely mixed to the surface (probably due to the settling of lanthanum and a weak stratification). This indicates that the Aqueduct inflows dove to the bottom of the reservoir in the winter after entering from the surface. (The inflow was slightly colder and therefore denser than the reservoir water during winter.) As presented, both the fate of the Aqueduct inflow and decrease of lanthanum concentrations over the time are well captured by the model.

Figures 29 through **33** are comparison plots of the simulated and measured temperatures and lanthanum concentrations for the summer tracer study. Due to the strong temperature stratification in the summer, the Aqueduct inflow, with its relatively higher temperature, stayed above the colder and denser water in the hypolimnion after entering at the surface as shown in the measured field data. Then, lanthanum started to settle as evidenced by the layer of lanthanum expanding vertically toward the bottom. Without the formation of lanthanum particles and subsequently settling, the lanthanum

would have mostly remained trapped at the thermocline and eventually mixed to the surface by wind (see **Figures C-16** through **C-22** of **Appendix C)**. Both the insertion level and settling were well captured by the model. The model was also able to accurately predict the horizontal extent of lanthanum plume in the reservoir.

The validation presented here introduced additional assumptions, such as particle distributions and flocculation rates other than those made in the calibration. However, both the particle distributions and flocculation rates were determined solely based on the measured decreasing mass of total lanthanum over the whole reservoir. The model was able to reproduce the three-dimensional details in measured lanthanum concentrations such as the insertion, horizontal extent and dilution of the plume, as well as the settling. This provides verification and confidence in the model performance.

5. CAEDYM CALIBRATION

5.1 OVERVIEW

The calibration of the water quality model CAEDYM was carried out after the ELCOM calibration was completed. The comparison between simulation results and measured in-reservoir field data involved the following water quality parameters: DO, pH, nutrients, chlorophyll *a* and Secchi depth.

The in-reservoir water quality data were obtained by the City and plots of these data are included in **Appendix B**. Secchi depths and DO profiles are measured weekly. Nutrients are measured monthly at the surface (*i.e.*, epilimnion) and 1 meter above the reservoir bottom (*i.e.*, within the hypolimnion). Surface grab samples of chlorophyll *a* were measured monthly through 2003 (**Figure B-21**); since 2004, chlorophyll *a* concentration profiles have been estimated using an optical fluorometer (**Figure B-11** through **B-15**). These in-reservoir data were used to specify the initial profile concentrations at the start of the calibration period as well as for comparison against the simulated results for CAEDYM calibration.

5.2 CAEDYM CALIBRATION SETUP

5.2.1 Computational Grid Setup and Initial Conditions

A grid with a horizontal resolution of 100 × 100 m as shown in **Figure** 34 (compared to the finer grid with a horizontal resolution of 50 × 50 m used in the ELCOM calibration) was used for the CAEDYM calibration in order to complete the two-year run in reasonable computation time (4 days on a fast PC). The vertical grid is the same as that in the ELCOM calibration. The ELCOM calibration run was conducted on both grids to evaluate any difference in the predicted hydrodynamic conditions. **Figure 35** shows a comparison of the predicted temperature profiles at Station A using the fine and coarse grids. **Figure 36** shows a time series of predicted surface and bottom conductivity using these two grids. The results indicate that using either the fine or coarse grids will result in almost the same predicted conductivity and very similar predicted temperature profiles. Therefore, it is appropriate to use the coarse grid in the CAEDYM calibration to provide both reasonable model run times as well as adequate model resolution.

The initial reservoir DO and pH concentrations at the beginning of 2006 were based on in-reservoir measured data from Station A (see **Figure 1**) on January 3, 2006, as shown in **Appendix B**. The initial conditions for nutrients were based on the first available measured data (*i.e.*, on January 26, 2006).

5.2.2 Inflow Water Quality Inputs

Water quality parameters such as pH, DO, nutrients and chlorophyll *a* of all inflows are required as inputs in the CAEDYM calibration; but these data were not measured at all times for all inflows. In the previous SVR modeling study (FSI, 2009), a lot of effort has been put into preparing and testing the input files for the water quality calibration based on several assumptions and estimates. These assumptions and estimates have been through peer review in the previous study and were adopted directly in this calibration. A brief description of these assumptions is provided below for each inflow and details can be found in the previous SVR model calibration study (FSI, 2009). **Appendix C** (see **Figures C-23** through **C-40**) includes plots of the measured data and input data used in the model calibration for each inflow.

Aqueduct Inflows

Similar to the ELCOM calibration, water quality data measured at the Lake Skinner outlet were used to characterize the Aqueduct inflow for most of the 2006-2007 calibration period. These data were obtained directly from MWD and included approximately bi-weekly total phosphate (TP), and nitrate for at least 2006-2007. Ortho-phosphate (OPO4, used interchangeably with soluble reactive phosphate, or SRP here) data were only available for 2001-2004, ammonia data were only available for 2000-2004, and total nitrogen (TN) data were not available at all. Assumptions made in developing the Aqueduct water quality input files (**Figures C-23** through **C-29**) are noted below:

- DO concentrations were assumed to be 100% saturated based on water temperature.
- Chlorophyll *a* concentrations were assumed to be 0 µg/L since releases from Lake Skinner are generally at depth.
- Concentrations of SRP were estimated as 40 percent of the TP concentrations based on comparisons of the limited OP data from 2001-2004 with the TP data.
- Ammonia concentrations were estimated as 20 percent of the nitrate concentrations based on comparisons of the limited ammonia data from 2000-2004 with the nitrate data.
- TN concentrations were estimated as 120 percent of the sum of the nitrate and ammonia concentrations

During the "Bypassing Period" (October 2006 through January 2007), about 80% of the water in the Aqueduct was being supplied directly from the San Diego Canal while

the remaining water was supplied by Lake Skinner. During this period, limited TP and nitrate, but not SRP, ammonia, and TN, data were obtained from MWD for the San Diego Canal. Assumptions made in developing the Aqueduct input data files during the Bypassing Period are noted below:

- DO concentrations were assumed to be 100 percent saturated based on water temperature.
- Chlorophyll *a* concentrations were assumed to be 0 µg/L.
- TP and nitrate concentrations measured at the San Diego Canal were used to represent those in the Aqueduct inflow. Concentrations of SRP were estimated as 40 percent of the TP concentrations. Ammonia concentrations were estimated as 20 percent of the nitrate concentrations. TN concentrations were estimated as 1.2 mg/L to reflect the fact that a majority of the water in the San Diego Canal at that time was from the State Water Project (SWP), and SWP water generally has high nutrient concentrations (verbal communication with Bill Taylor of MWD and Jeffery Pasek of the City).

Runoff Inflows

Water quality data for the local tributaries to SVR were obtained from the City and included DO, TP, OPO4, TN, nitrate, and ammonia data, measured as often as monthly since 2003. Similar to the ELCOM calibration, data measured in SV Creek were used to estimate the model inputs for other tributaries (**Figures C-30** through **C-36**).

Sutherland Reservoir Inflows

Due to the limited nutrient data available during the months in which the Sutherland Reservoir inflows occurred (**Figure C-37**), TP, SRP, and TN concentrations were estimated by computing the average concentrations from measurements taken within Sutherland Reservoir when destratified in the winter, a period when nutrients are generally not being quickly consumed. Nitrate data were all below the detection limit, so nitrate concentrations were estimated to be equal to the detection limit. Since ammonia concentration data were not collected, ammonia concentrations were estimated as 20% of the TN.

The pH, DO and chlorophyll *a* values of inflows from Sutherland Reservoir were assumed to be equal to the profile data measured within the hypolimnion near the elevation of the outlet (**Figures C-38** through **C-40**).

5.3 CALIBRATION RESULTS

5.3.1 Dissolved Oxygen

Comparison plots for the simulated and measured DO concentrations are provided in **Figures 37** and **38**. The measured data show that DO concentrations at the surface remained high throughout the years because of the supply of oxygen directly from the atmosphere by diffusion and because of oxygen produced by photosynthetic activity of algae at surface. At high rates of photosynthesis, oxygen production by algae exceeded the diffusion of oxygen out of the system and resulted in occasional oxygen supersaturation in the spring of 2006 and 2007. The DO at bottom was replenished through vertical mixing with the surface water with high DO concentrations during the reservoir destratified periods in the winter of 2006 and 2007. However, during the summer, strong stratification at SVR prevented such vertical mixing and DO at the bottom was quickly depleted by the decay of algae and other organic matter in the sediment (*i.e.*, Sediment Oxygen Demand or SOD). The water conditions in the hypolimnion became anoxic (*i.e.*, dissolved oxygen concentrations are 0 mg/L) in the spring and anoxia lasted through the fall for both years, until the reservoir became destratified in the winter.

The simulated DO concentrations capture the major trends in the measured DO concentrations, including the onset, duration, and magnitude of periods of anoxia in the hypolimnion, the depth to the top of the anoxic (*i.e.*, "without oxygen") region, and the high surface DO concentrations in the spring (and sometimes fall) that are due to algae blooms. A value of 1.5 g/m^2/day was used for SOD in the calibration as it achieved the best match to the rate of decrease in DO measured at bottom during the stratified periods. This value is at the high end of the range of 0.1 – 1.75 g/m^2/day for sediment oxygen demand measured at SVR in 2001 (Beutel, 2001), but is consistent with historic DO profile data (**Appendix B**) that show faster rates of DO decay at the bottom in 2006-2007 than in 2001 due to more algal productions in the reservoir evidenced by relatively smaller Secchi depths in 2006-2007.

A scatter plot of the measured and simulated DO concentrations for years 2006 and 2007 is provided in **Figure 39**. A statistical analysis of the calibration results versus the measured data produced the metrics presented in **Table 7**. The computed Root Mean Square Errors (RMSE) indicate that the calibrated DO concentrations are on average within 1.3 mg/L of the measured data, corresponding 7-9% of the range in measured DO concentrations. These indicate a good calibration for DO for both years.

Table 7. Dissolved Oxygen Calibration Metrics

PARAMETER	2006 RESULTS			2007 RESULTS		
	ROOT MEAN SQUARE ERROR (RMSE)	RELATIVE RMSE	MEAN ERROR	ROOT MEAN SQUARE ERROR (RMSE)	RELATIVE RMSE	MEAN ERROR
Surface and Bottom Dissolved Oxygen	1.26 mg/L	9.0 %	0.76 mg/L	1.03 mg/L	7.4 %	0.45 mg/L

5.3.2 pH

Figures 40 and **41** show comparison plots for the simulated and measured pH. The measured data show that pH increased in the spring and summer of each year when inorganic carbon was consumed by the photosynthetic activity of algae; pH values were reduced in the winter because of the release of CO_2 as a byproduct of algae respiration. The model accurately captures major trends in the measured pH and the simulated pH closely tracks measured data. It is noted in these figures that the measured surface pH on 11/5/07 and the measured bottom pH on 6/16/06, 4/23/07, 4/30/07, 7/16/07, 7/30/07, 11/5/07 and 11/19/07 are unusually low compared to other data. Thus, these data are considered as outliers and were excluded from the analysis described next. A scatter plot of the measured and simulated pH for years 2006 and 2007 is provided in **Figure 42**. A statistical analysis of the calibration results versus the measured data produced the metrics presented in **Table 8**. The computed Root Mean Square Errors (RMSE) indicates that the calibrated pH are on average within 0.3 of the measured data, corresponding to 10-15% of the range in measured pH values. These indicate a good pH calibration for both years, especially considering the small variation of pH during the two-year calibration period.

Table 8. pH Calibration Metrics

PARAMETER	2006 RESULTS			2007 RESULTS		
	ROOT MEAN SQUARE ERROR (RMSE)	RELATIVE RMSE	MEAN ERROR	ROOT MEAN SQUARE ERROR (RMSE)	RELATIVE RMSE	MEAN ERROR
Surface and Bottom pH	0.19	9.7 %	0.03	0.28	14.3 %	0.05

5.3.3 Nutrients

Figures 43 and 44 are plots of the simulated and measured SRP and TP concentrations, respectively. The measured surface SRP and TP data are usually below

the detection limits (*i.e.*, 0.008 and 0.08 mg/L P, respectively), and the bottom SRP and TP data are also below the detection limits in the winter and spring. Despite that, general trends in the measured phosphorus data can still be observed. At the surface, phosphorus levels were usually low due to consumption by algae. At the bottom, phosphorus concentrations were low at the beginning of 2006 when the reservoir was fully mixed. As the reservoir became stratified in the early spring of 2006, phosphorus concentrations started to increase due to the release of phosphorus from the sediment caused by anoxic conditions in the hypolimnion. However, after June 2006, phosphorus concentrations stayed relatively constant until the reservoir was fully mixed again in January 2007. This is due to the fact that the sediment release of phosphorus in spring probably exhausts the phosphorus storage in the sediments. In 2007, phosphorus concentrations increased slowly at the bottom through the year. As shown, the model captures these trends fairly well although the simulated bottom concentrations are slightly higher than the measured data.

Comparison plots of the simulated and measured ammonia, nitrate, and TN concentrations are provided in **Figures 45** through **47**, respectively. In these figures, ammonia concentrations are below the detection limit (*i.e.*, 0.04 mg/L N) at the surface throughout the year and at the bottom during the destratified period. The nitrate concentrations are below the detection limit (*i.e.*, 0.02 mg/L N) from about July through January of each year. The observed trends in measured ammonia data are similar to those in measured phosphorus data. However, the trends of nitrate concentrations at the bottom are the reverse of those in ammonia concentrations: nitrate concentrations are high when the reservoir is destratified and DO at bottom is high; nitrate concentrations decrease when the reservoir is stratified and DO at bottom is low. This is because ammonia in the sediment can convert to nitrate through a nitrification process if oxygen is present and, consequently, the sediment releases nitrate instead of ammonia. Once the bottom of the reservoir becomes anoxic, nitrate is depleted slowly by denitrification. As shown, the simulated ammonia and nitrate match the trends and magnitude of the measured data fairly well.

The simulated TN concentrations match the measured concentrations during the destratified periods and follow the general trends of the data, although the simulated TN concentrations are significantly lower than a few measured data points during the summer of 2006. These measured TN concentrations in the summer of 2006 are very high compared to those in summer of 2007. There are no evident sources of nitrogen that can explain such spikes.

5.3.4 Chlorophyll *a* and Secchi Depth

There are no measured chlorophyll *a* concentrations available in years 2006-2007 at SVR. Instead, chlorophyll *a* concentration profiles were estimated using an optical fluorometer and were provided by the City (**Figure B-11** through **B-15**). The optical

fluorometer measures fluorescence and, if calibrated, can make an estimate of relative chlorophyll *a* concentrations because algae fluoresce at characteristic wavelengths. Optical fluorometers can be used to collect profile measurements similar to a temperature or conductivity probe. Thus, they could provide more data (albeit of lower quality) more economically than could be obtained with grab samples and laboratory analysis. However, fluorometer readings can be corrupted by other particles present in the water column and indicate "false" algae blooms. For example, in SVR, the algae bloom that starts from August 2007 is probably a "false" algae bloom because the data show extremely high chlorophyll *a* concentrations (> 100 µg/L) at the depth below the thermocline but measured DO profiles show no evidence of high oxygen spikes/production at that depth to support the existence of such algae bloom (**Figure 48**). These high readings of fluorescence below the thermocline could, for example, be caused by the accumulation of surface algae and other particles at the thermocline due to settling flocculants such as manganese and iron hydroxides formed in the epilimnion. Manganese and iron hydroxides are insoluble under high DO conditions (*e.g.* in the epilimnion) and soluble under low DO conditions (*e.g.* in the hypolimnion). Therefore, if water is rich in manganese and iron hydroxides which are flocculants, they form flocs in the epilimninon under high DO conditions. These flocs catch algae and other particles as they settle at the thermocline, leading to concentrated algae and particles (thus high readings of fluorescence) at the thermocline. Similar processes involved in arsenic accumulation at the thermocline have been reported at Halls Brook Pond, Massachusetts (Ford, *et al.,* 2005 and 2006)

Since a fluorometer calibration had not been conducted at SVR, the simulated chlorophyll *a* concentrations by the SVR model were not compared directly against chlorophyll *a* data estimated using fluorometer data. Instead, the calibration of chlorophyll *a* was conducted through a "simulated" Secchi depth derived from a correlation between the simulated chlorophyll *a* concentrations and Secchi depth.

Secchi depth is a measure of the degree of transparency at the reservoir surface and, in a water body like SVR, is generally strongly correlated (for water with low inorganic turbidity) with chlorophyll *a* concentration since algae growth affects water clarity. Based on a study by Rast and Lee (1978) on various reservoirs, the following relationship was suggested:

$$\text{Log (Secchi Depth in m)} = -0.473 \text{ Log (Chlorophyll } a \text{ in µg/L)} + 0.803 \qquad \text{[Eqn. 4]}$$

Although CAEDYM does not simulate Secchi depth directly, the "simulated" Secchi depths can be derived from the simulated surface chlorophyll *a* concentrations using this formula. Therefore, a good calibration for Secchi depth can be translated into a good calibration for chlorophyll *a* concentrations.

The "simulated" Secchi depths are plotted against the measured Secchi depths in **Figure 49**. The measured Secchi depths are generally in the range of 3 to 5 m from

January through September 2006. However, between October and December 2006, the Secchi depths decreased significantly and remained low through June 2007. This period of small Secchi depth corresponds to the Bypassing Period when 80% of flow into the Aqueduct was coming directly from the San Diego Canal that has higher nutrient levels as discussed in **Section 5.2.2**. It is believed that the decrease in Secchi depth starting in October 2006 is predominantly due to chlorophyll *a* growth (verbal communication with Jeffery Pasek of the City) caused by a large influx of nutrient from the water in the San Diego Canal during the Bypassing Period.

The Secchi depth data in **Figure 49** suggest that the calibrated chlorophyll *a* concentrations during the Bypassing Period and through June 2007 are still a little lower than the data. But without more detailed information on the Aqueduct source water quality and direct chlorophyll *a* measurements, it was difficult to obtain a better correlation. A scatter plot of the measured and simulated Secchi depth for years 2006 and 2007 is provided in **Figure 50**. A statistical analysis of the calibration results versus the measured data produced the metrics presented in **Table 9**. The computed Root Mean Square Errors (RMSE) indicate that the calibrated Secchi depths are on average within 1.2 m of the measured data, corresponding to about 20% of the range in measured Secchi depth. These indicate a fairly good calibration for both Secchi depth and chlorophyll *a*, especially considering the unknown nutrient loadings during the Bypassing Period.

Table 9. Secchi Depth Calibration Metrics

PARAMETER	2006 RESULTS			2007 RESULTS		
	ROOT MEAN SQUARE ERROR (RMSE)	RELATIVE RMSE	MEAN ERROR	ROOT MEAN SQUARE ERROR (RMSE)	RELATIVE RMSE	MEAN ERROR
Secchi Depth	1.06 m	20.8 %	0.18 m	1.14 m	22.3 %	-0.87 m

6. CONCLUSIONS AND DISCUSSION

A three-dimensional water quality model has been applied, calibrated and verified for SVR. It is anticipated that this model will be used to study the dynamics, mixing, and residence time of advanced treated recycled water and its effects on eutrophication in the expanded SVR.

The modeling domain includes the existing portion of the reservoir as well as the proposed expanded portion of the reservoir. A fine grid with a horizontal resolution of 50 × 50 m was used in the ELCOM calibration while a coarse grid with a horizontal resolution of 100 × 100 m was used in the CAEDYM calibration. This was necessitated by the large computer requirements and the desire to limit computation time to several days per model run for a two-year simulation. A variable grid size was used in the vertical dimension with a grid size of 1.64 ft (0.5 m) near the surface, and expanding in size with depth. The calibration was conducted for the two-year period of 2006-2007. The input data required by the calibration were either based on measured data or derived from these data. ELCOM requires limited calibration effort in that the physical aspects of water movements in reservoirs are fairly well understood. The CAEDYM model was calibrated by adjusting some model bio-chemical parameters so that the simulation results best match measured field data.

The calibrated/validated ELCOM model shows good agreement with the measured data for both water temperature and conductivity. The calibration involved reconstruction of some meteorological data during periods where data were unavailable. It also involved an adjustment for the outlet port openings in the second half of 2007. As discussed in detail in the report, the City-specified field reports of the ports open during a portion of 2007 are at variance with the basic thermodynamics of the system. It is demonstrated later in this report that the open ports must have been at or above the thermocline level and not in the hypolimnion, as specified. In the future, it is recommended that outflow temperatures from SVR be recorded so that they can provide verification of the field record of port openings.

The onset and duration of thermal stratification as well as the deepening rate of the thermocline were predicted accurately by the model. Furthermore, the water conductivity, a measure of salinity, was well predicted by the model. It is noted that future modeling of the hydrodynamics at SVR would benefit from a full set of meteorological data gathered at SVR (the City stopped gathering on-site meteorological data in March 2007). An analysis presented herein shows that the meteorological data measured at the nearby California Irrigation Management Information System (CIMIS) station in Escondido differ in significant aspects from data gathered at SVR.

After the model was calibrated, a validation was performed to compare the model against the results of previous field studies. The field studies involved two separate episodes of tracer injection in the reservoir (winter 1995 and summer 1995). The field

studies clearly showed the impacts of stratification (or lack thereof) on the mixing and dispersion of the tracer. The ELCOM model was capable of replicating the main features of the tracer study. Due to the nature of the tracer used in those studies (Lanthanum Chloride), a significant amount of tracer was lost due to coagulation/flocculation and subsequent settling. A simple coagulation/settling model was added to ELCOM. After the implementation of the coagulation/settling model, very good agreement between the model and the data was obtained. This validation provides strong verification and assurance that the model performance is accurate.

The calibration of the water quality model CAEDYM was carried out after the ELCOM calibration and verification process. The comparison between simulation results and measured in-reservoir field data involved water quality parameters including dissolved oxygen (DO), pH, nutrients (nitrogen and phosphorus), chlorophyll *a* and Secchi depth. It is noted that some assumptions had to be made in order to calibrate the model. For example, assumptions on nutrient levels for the Aqueduct inflows during the "Bypassing Period" were needed to characterize nutrient loadings because there are only limited nutrient data available for the Aqueduct inflow.

The calibrated CAEDYM model shows overall good agreements with measured data. The simulated DO concentrations capture the major trends in the measured DO concentrations, including the onset, duration, and magnitude of periods of anoxia in the hypolimnion, the depth to the top of the anoxic (*i.e.*, "without oxygen") region, the DO decay rate in the spring in the hypolimnion, and the high surface DO concentrations in the spring (and sometimes fall) that are due to algae blooms. The simulated pH values closely match the measured data and are on average within 0.3 of the measured values. The calibrated model also replicates the major trends in the measured nutrient (phosphorus and nitrogen) concentrations. It is noted, however, that some of the field data are below the detection limit and real values of the nutrient concentrations on these days are unknown. The available in-reservoir chlorophyll *a* data were qualitatively measured using a fluorometer that has not been calibrated. The calibration of chlorophyll *a* had to be conducted indirectly through the calibration of Secchi depth. The final calibration run shows a fairly good agreement with the measured Secchi depths, indicating a fairly good calibration for chlorophyll *a*.

At this point, it is believed that the model calibration/validation is nearly complete. The calibrated/validated model will undergo peer review. After that, the model will be applied to the study of the expanded reservoir as well as the evaluation of the mixing of the advanced treated recycled water within the reservoir. The planned modification of Aqueduct release locations/facilities into the expanded SVR and outlet structure/port depths will be incorporated into the model.

Future evaluations and modeling of water quality at SVR would benefit from more frequent sampling of nutrients and chlorophyll *a* within the reservoir, also from lower nutrient detection limits, and an increased use of duplicate samples or periodic sampling

audits. It is recommended that nutrient samples be collected more frequently and at additional depths throughout the water column. This would increase the data resolution and reliability, improve understanding of the reservoir behavior, and allow for a more precise water quality calibration. It is further recommended that the collection of chlorophyll *a* samples be resumed. Composite samples should be collected from the reservoir surface in order to analyze chlorophyll *a* concentrations in the laboratory. This would allow for calibration of the optical fluorometer data and improve the usefulness and interpretation of that data. Finally, it is recommended that more frequent sampling of nutrients and other parameters be conducted for the inflows (especially the Runoff, and the Aqueduct inflow during bypassing conditions).

7. REFERENCES

Beutel, M. (2001). "San Vicente Reservoir: Sediment-Water Interface Study," dated July 2001 and submitted to the San Diego Water Department.

City of San Diego (2008). "IPR Description for BOR Grant 122208 MS," obtained from Jeffery Pasek of the City of San Diego through email on December 23, 2008

Flow Science Incorporated (1994). "Water Recycling Conceptual Feasibility Study, San Vicente Reservoir, prepare for Montgomery Watson on behalf of Water Authority," FSI Project No. C938088, Pasadena, CA

Flow Science Incorporated (1995). "San Vicente Water Reclamation Project: Results of Tracer Studies, prepared for Montgomery Watson," FSI Project No. P941003, Pasadena, CA.

Flow Science Incorporated (1997). "San Vicente Reservoir Hypolimnetic Oxygenation System Design Support, prepared for Boyle Engineering Corp. on behalf of City of San Diego Water Department," FSI Project No. P974005, Pasadena, CA.

Flow Science Incorporated (2001). "Analysis and Modeling For San Diego Reservoir Oxygenation System, prepared for Boyle Engineering Corp. on behalf of City of San Diego Water Department," FSI Project No. V044091, Pasadena, CA.

Flow Science Incorporated (2005a). "Water Quality Assessment For San Vicente Reservoir Enlargement, prepared for GEI Consultants, Inc. on behalf of Water Authority," FSI Project No. V044091, Pasadena, CA.

Flow Science Incorporated (2005b). "Lake Mead ELCOM/CAEDYM Modeling, prepared for Black & Veatch on behalf of Clean Water Coalition," FSI Project No. S014004, Pasadena, CA.

Flow Science Incorporated (2009). "Water Quality Assessment of San Vicente Reservoir During Construction Drawdown Conditions, prepared for GEI Consultants, Inc. on behalf of Water Authority," FSI Project No. V074117, Pasadena, CA.

Ford, R.G., R.T. Wilkin, C.J. Paul, F. Beck and T. Lee (2005). "Field Study of the Fate of Arsenic, Lead, and Zinc at the Ground-Water/Surface-Water Interface," EPA/600/R-05/161, U.S. Environmental Protection Agency, Ada, Oklahoma.

Ford, R.G., R.T. Wilkin and G. Hernandez (2006). "Arsenic Cycling within the Water Column of a Small Lake Receiving Contaminated Ground-water Discharge," Chemical Geology, Vol. 228. No.1-3, p137-155.

Niquette, P., F. Monette, A. Azzouz and H. Hausler (2004). "Impacts of Substituting Aluminum-Based Coagulants in Drinking Water Treatment," Water Quality Research Journal of Canada, Vol. 39, No.3 p303-310.

Rast, W. and G.F. Lee (1978). "Summary Analysis of the North American (U.S. portion) OECD Eutrophycation Project: Nutrient loading – lake response relationships and trophic state indices," Ecological Research Serries, No. EPA-600/3-78-008, U.S. Environmental Protection Agency, Corvallis, Oregon, 454p.

Recht, H.L., M. Ghassemi and E.V. Kleber (1970). "Percipitation of Phosphate from Water and Wastewater using Lanthanum Salts," Presented at the 5th International Water Polluation Research Conference, San Francisco, California. P.I-17/1-I-17/12, July-August.

Welch, M.R. (1997). "Draft Report: San Vicente Reservoir Management Program – Water Repurification Project, prepare for Montgomery Watson on behalf of City of San Diego", dated on November 1997 and submitted to the City of San Diego.

FIGURES

San Vicente Reservoir

Plan View of Existing and Expanded Reservoir and Inflow/Outflow Locations

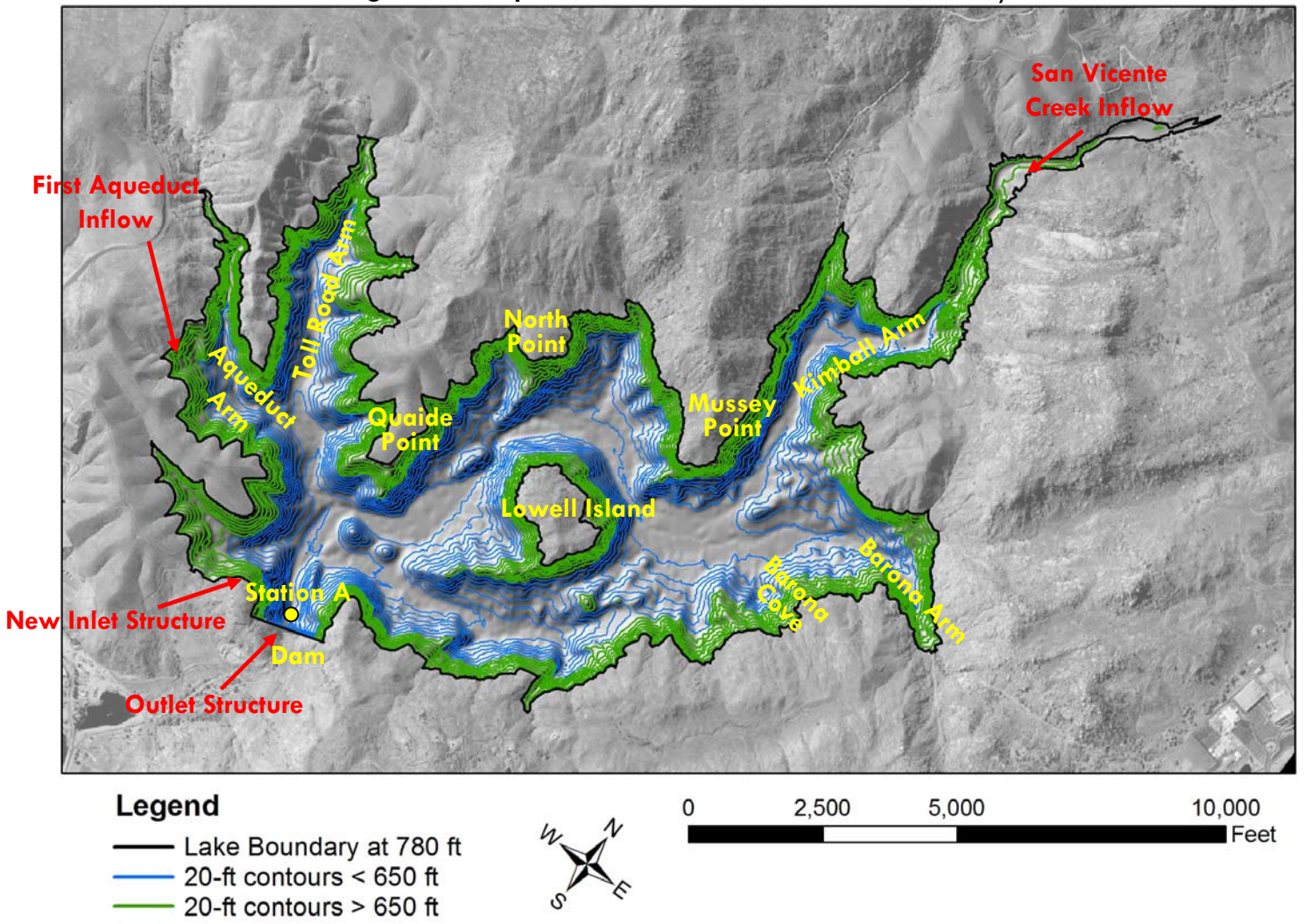

FSI V094005
May 01, 2012

Figure 1

FLOW SCIENCE®

ELCOM-CAEDYM

Schematic of Processes Modeled in ELCOM-CAEDYM

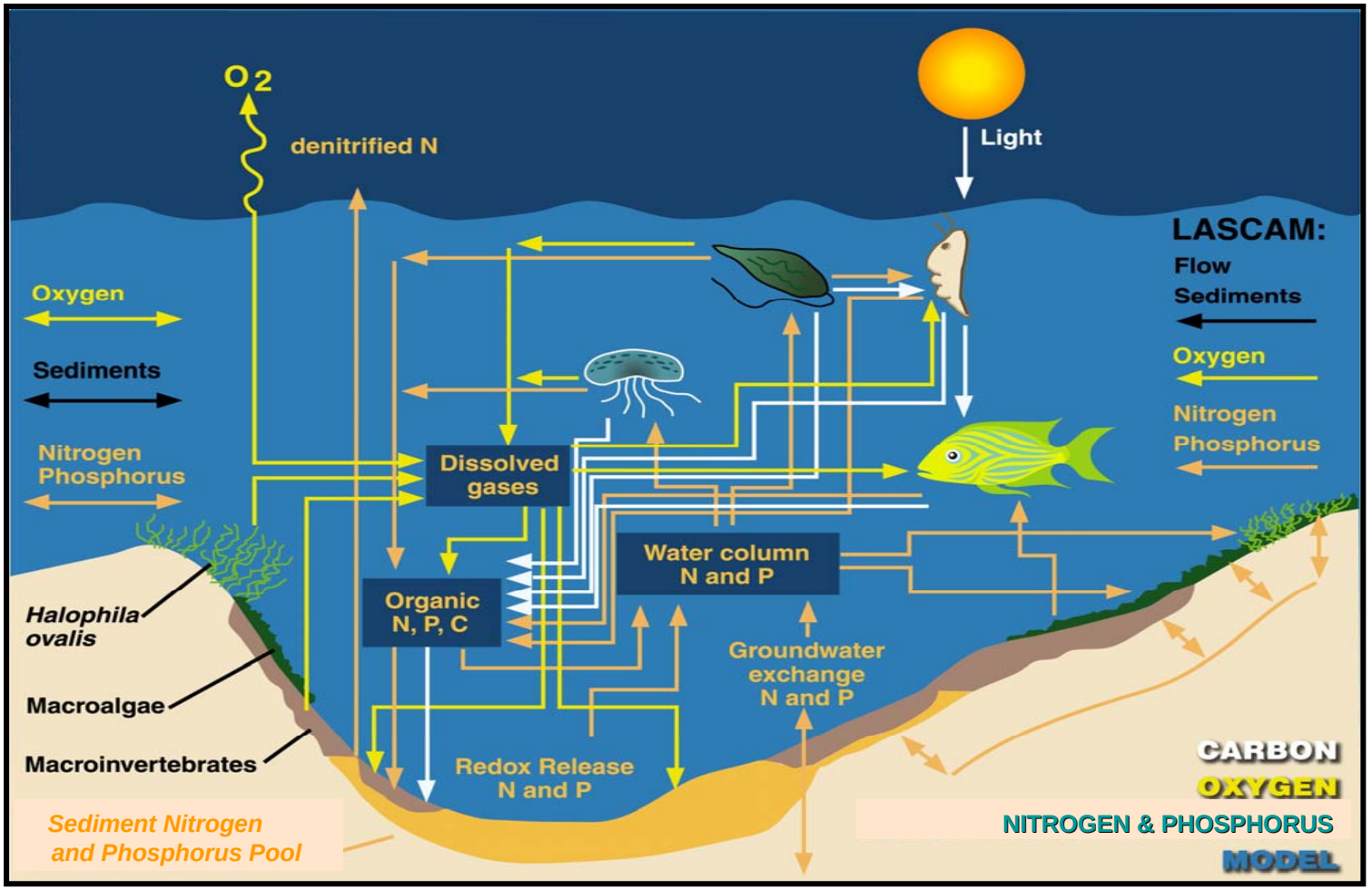

Figure 2

FLOW SCIENCE®

San Vicente Reservoir 50-m ELCOM Computational Grid

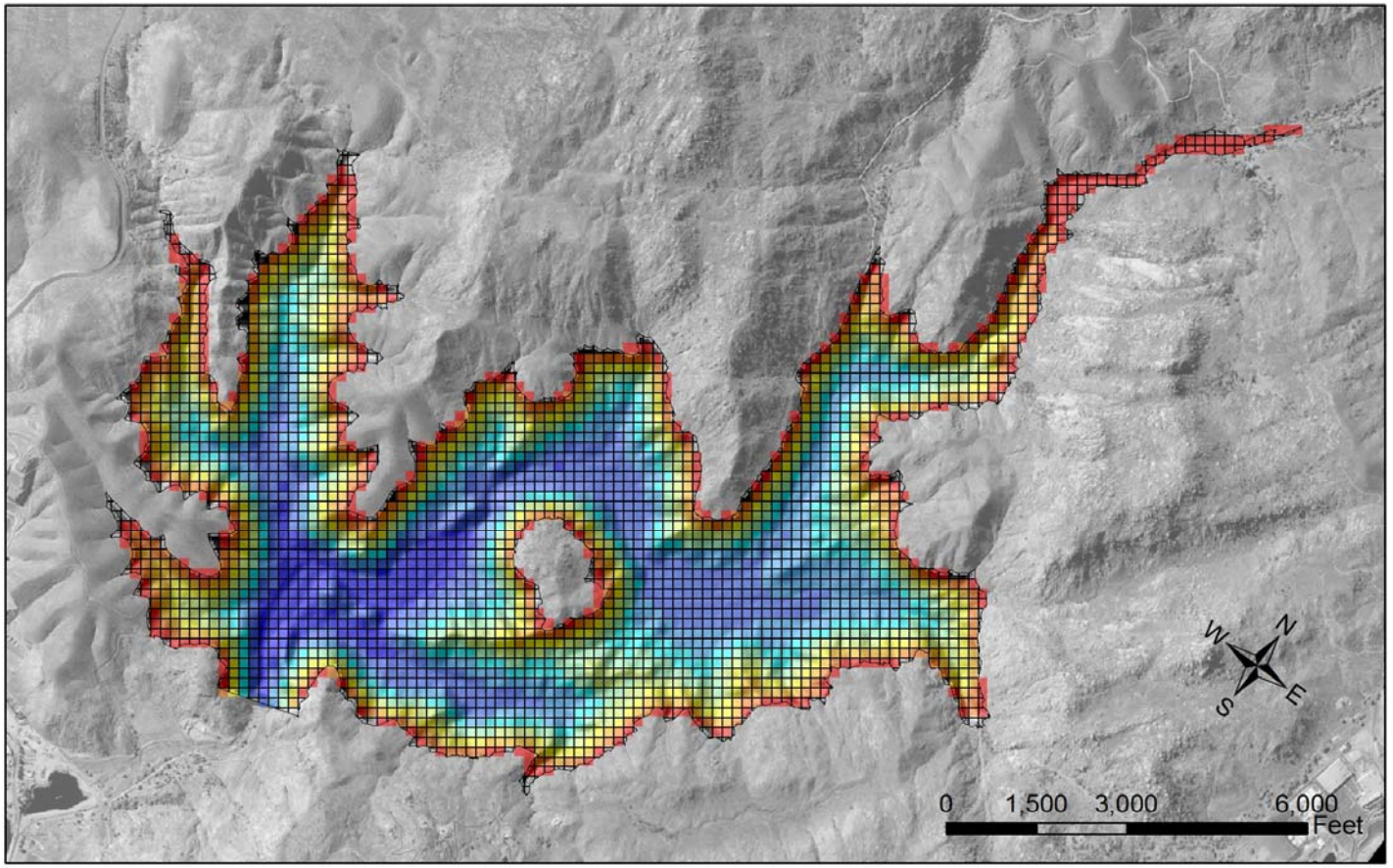

San Vicente
50-m ELCOM Grid

Legend

Lake Boundary at 780 ft

Elevation (ft)			
480 - 510	541 - 569	630 - 659	719 - 748
511 - 540	570 - 599	660 - 689	749 - 778
	600 - 629	690 - 718	

Figure 3

FSI V094005
May 01, 2012

FLOW SCIENCE®

San Vicente Reservoir

Measured/Modeled Inflow Volumes

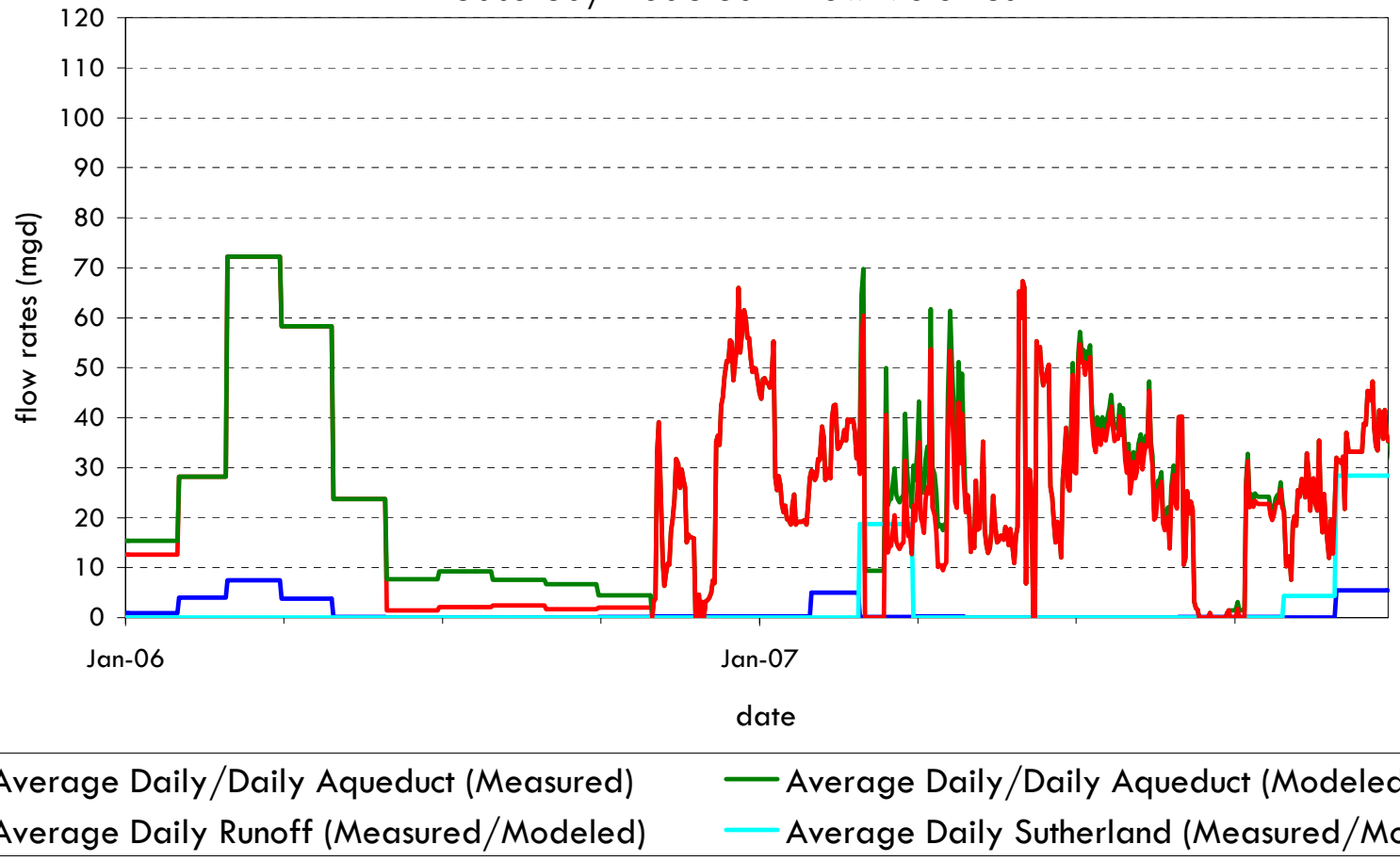

FSI V094005
May 01, 2012

Figure 4

FLOW SCIENCE®

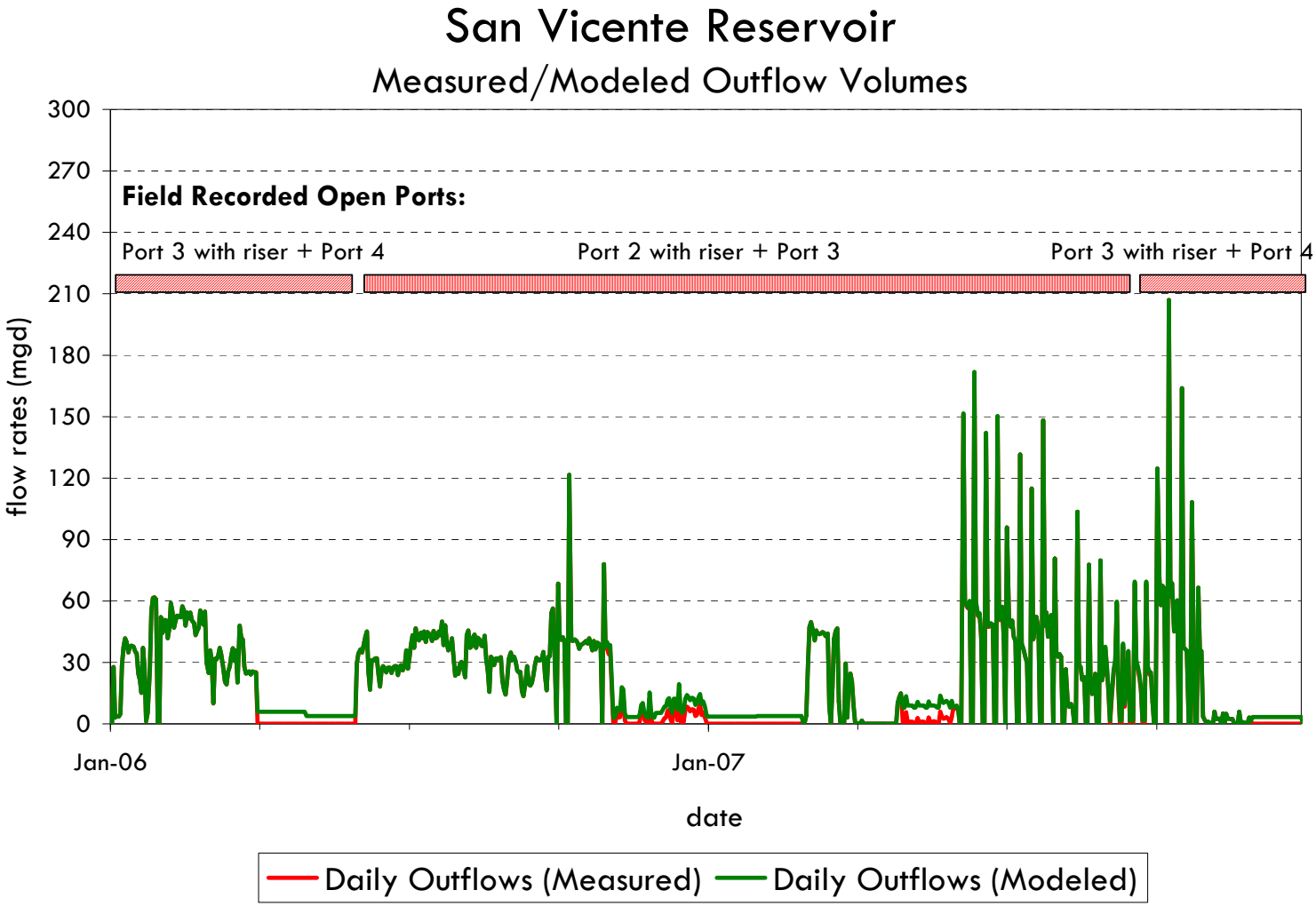

FSI V094005
May 01, 2012

Figure 5

FLOW SCIENCE®

Map of Meteorological Stations

FSI V094005
May 01, 2012

Figure 6

FLOW SCIENCE®

San Vicente Reservoir

Station A – Simulated Temperature Using CIMIS Meteorological Data After March 2007

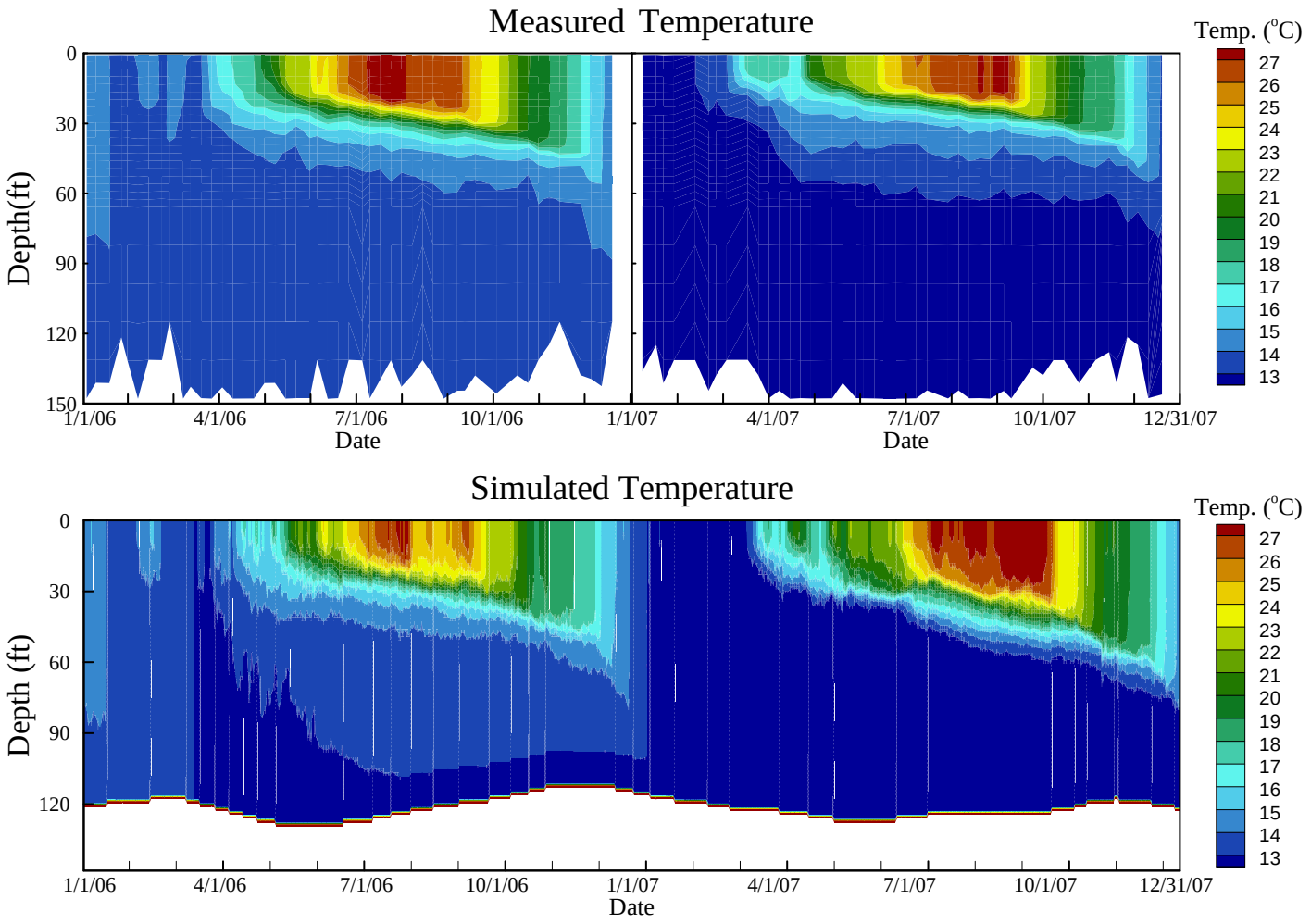

Figure 7

FSI V094005
May 01, 2012

FLOW SCIENCE®

San Vicente Reservoir - Station A Temperature Calibration

Impact of Using Different Meteorological Inputs

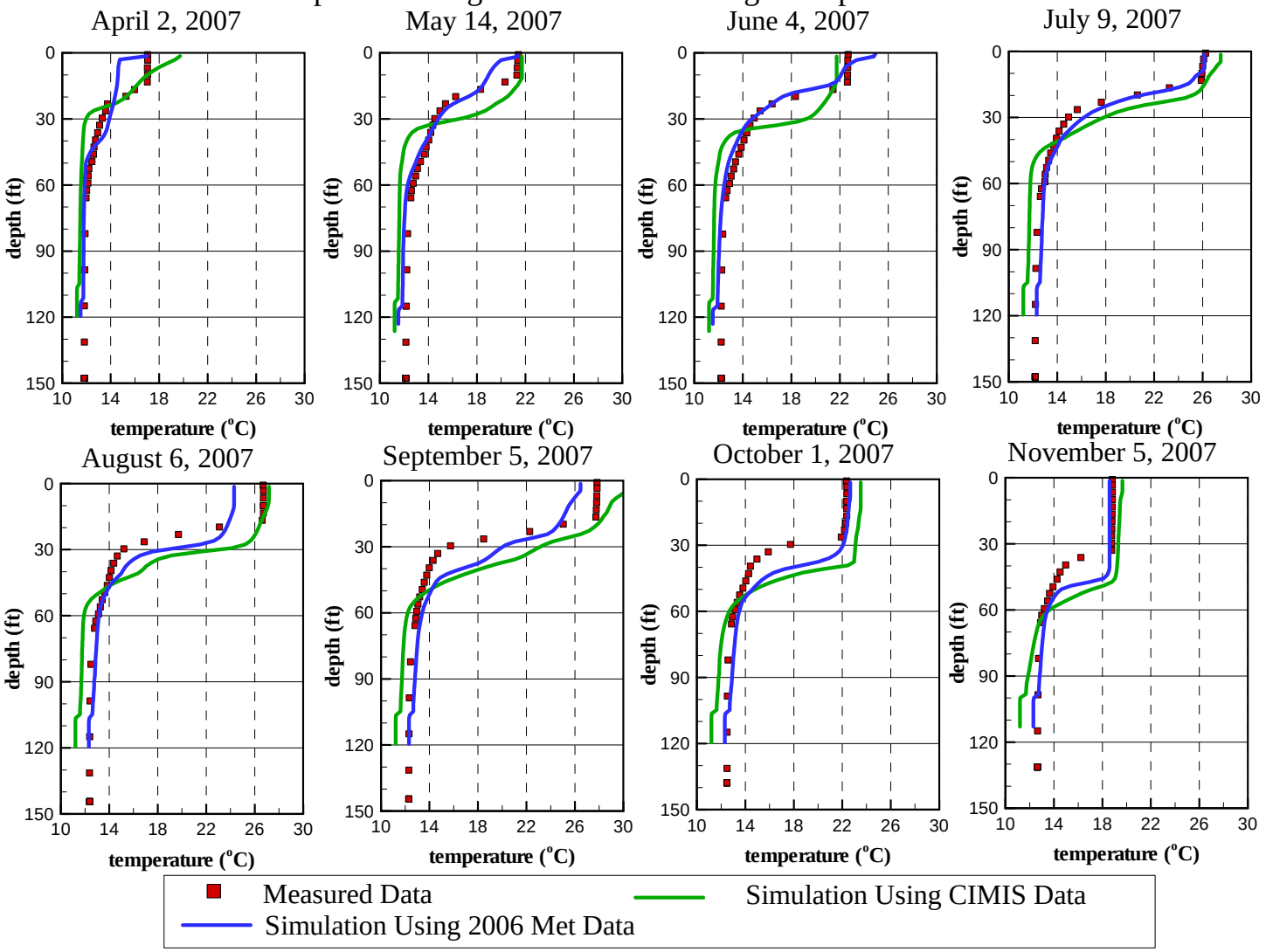

FSI V094005
May 01, 2012

Figure 8

FLOW SCIENCE®

San Vicente Reservoir

Station A - Measured Temperature Contours (2000-2007)

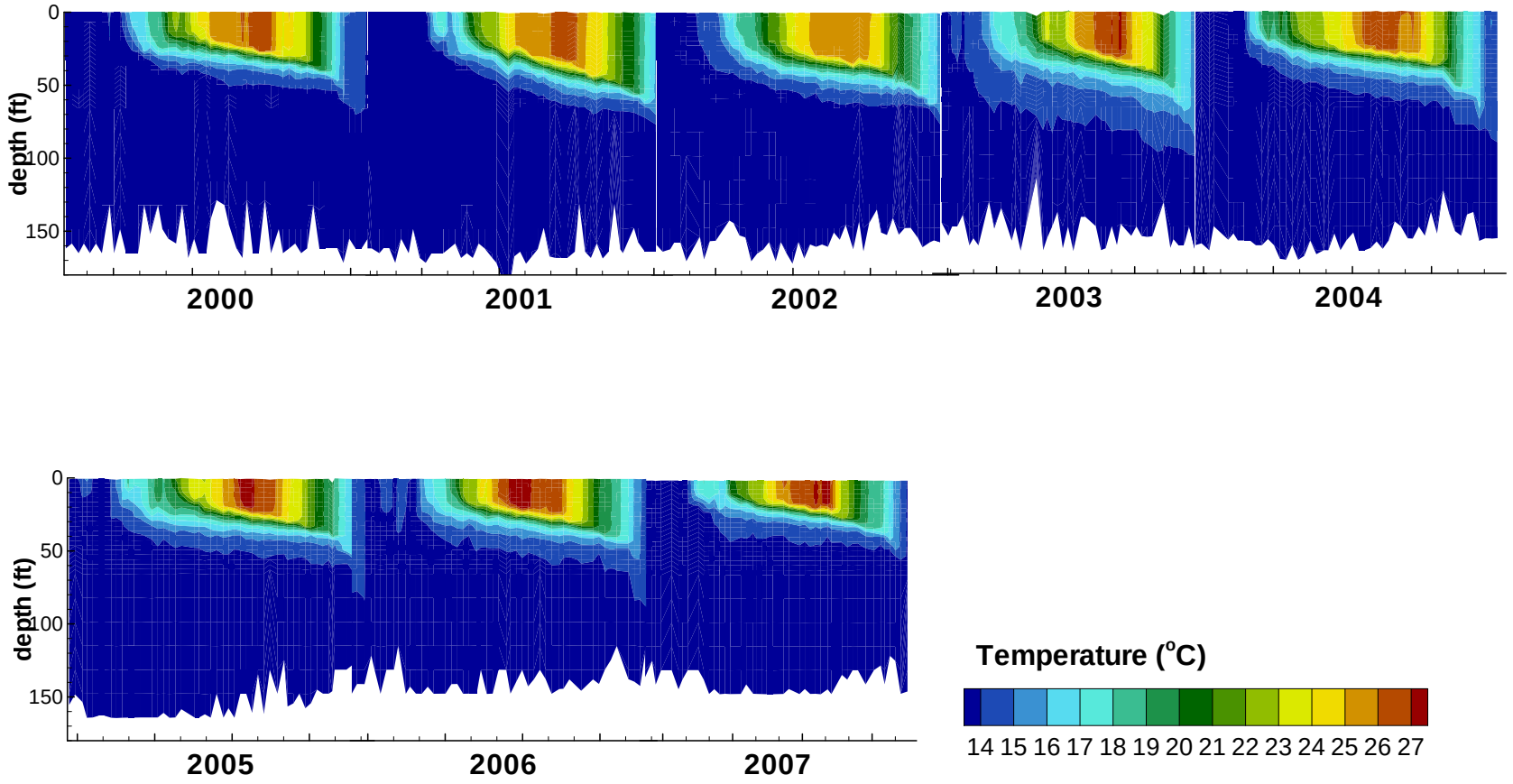

FSI V094005
May 01, 2012

Figure 9

FLOW SCIENCE®

San Vicente Reservoir

Comparison of 2006 and 2007 Measured Aqueduct Inflow Rates and Temperatures

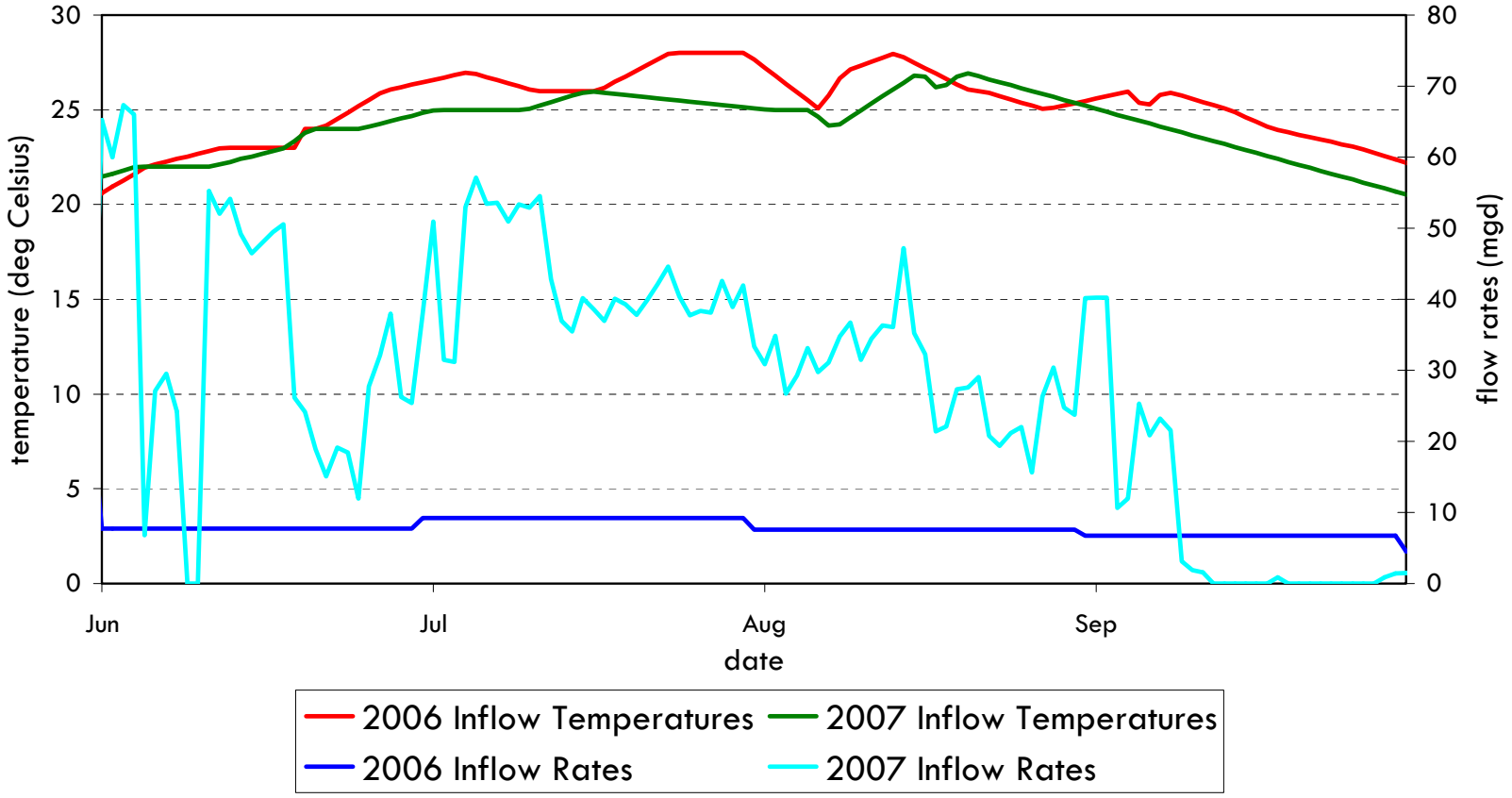

FSI V094005
May 01, 2012

Figure 10

FLOW SCIENCE®

San Vicente Reservoir

Station A - 2006-2007 Measured Temperature Profiles

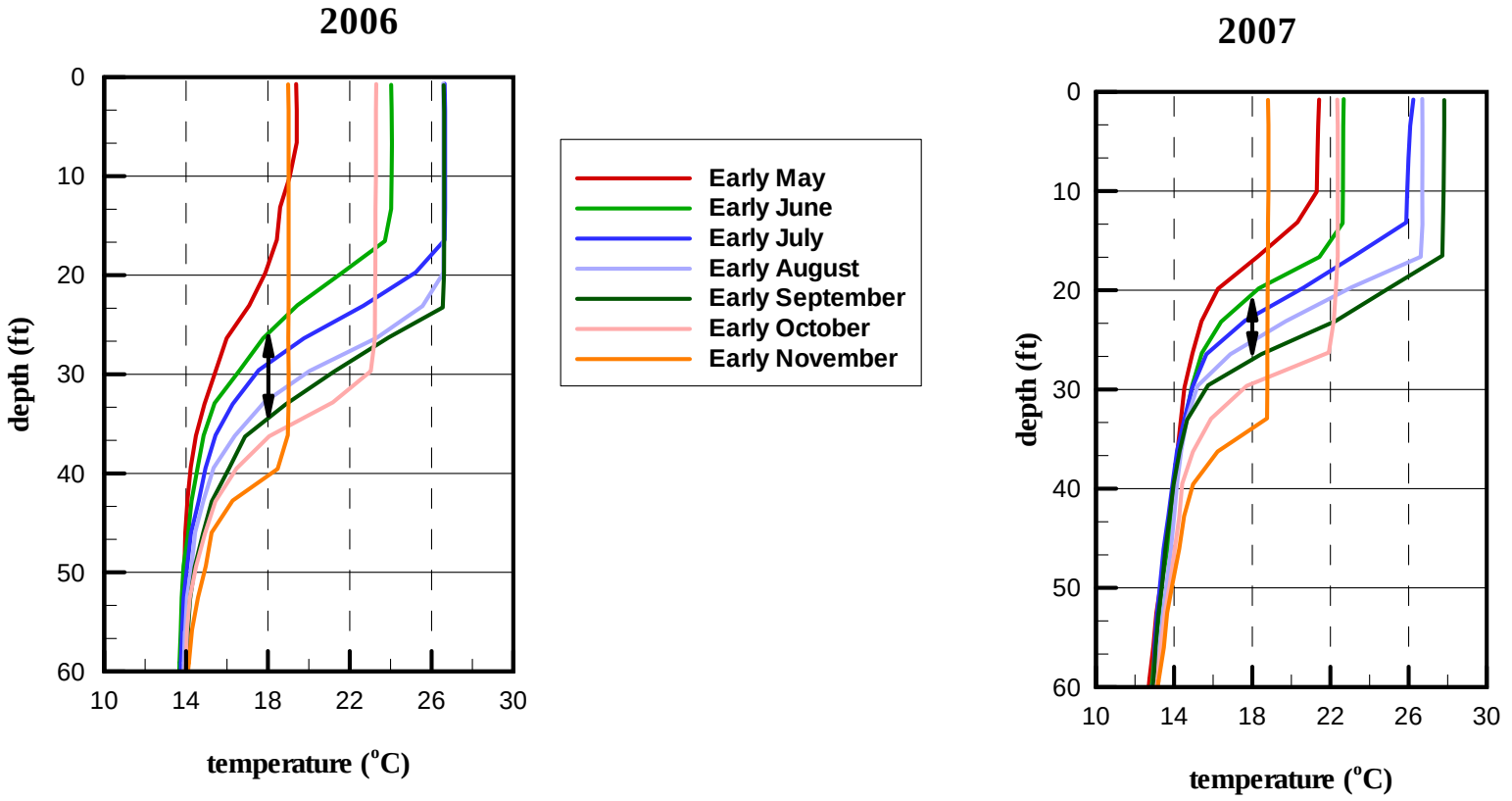

↔ Thermocline Deepening Between Early June and Early September

FSI V094005
May 01, 2012

Figure 11

FLOW SCIENCE®

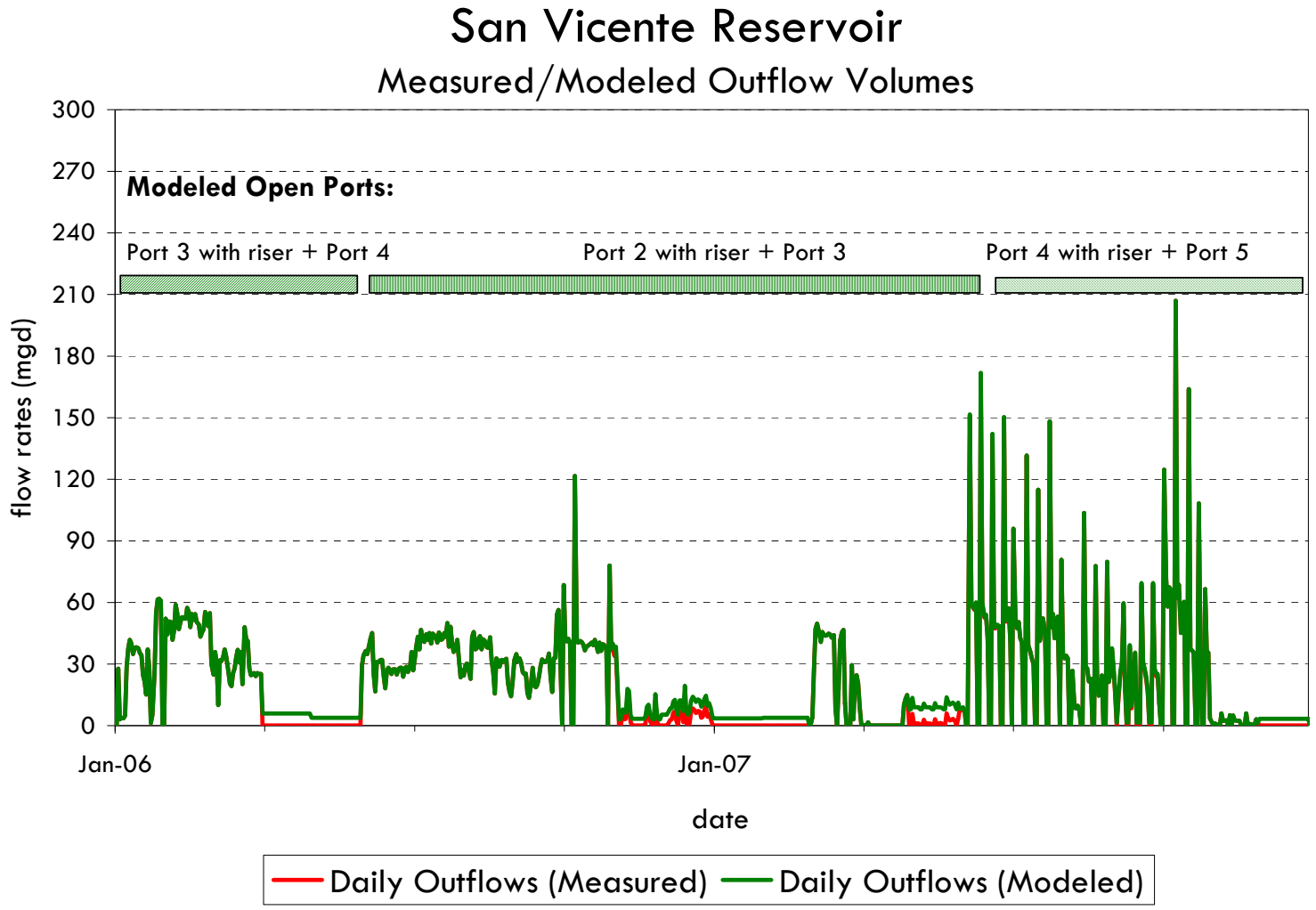

FSI V094005
May 01, 2012

Figure 12

FLOW SCIENCE®

San Vicente Reservoir - Station A Temperature Calibration

Impact of Opening Different Outlet Ports

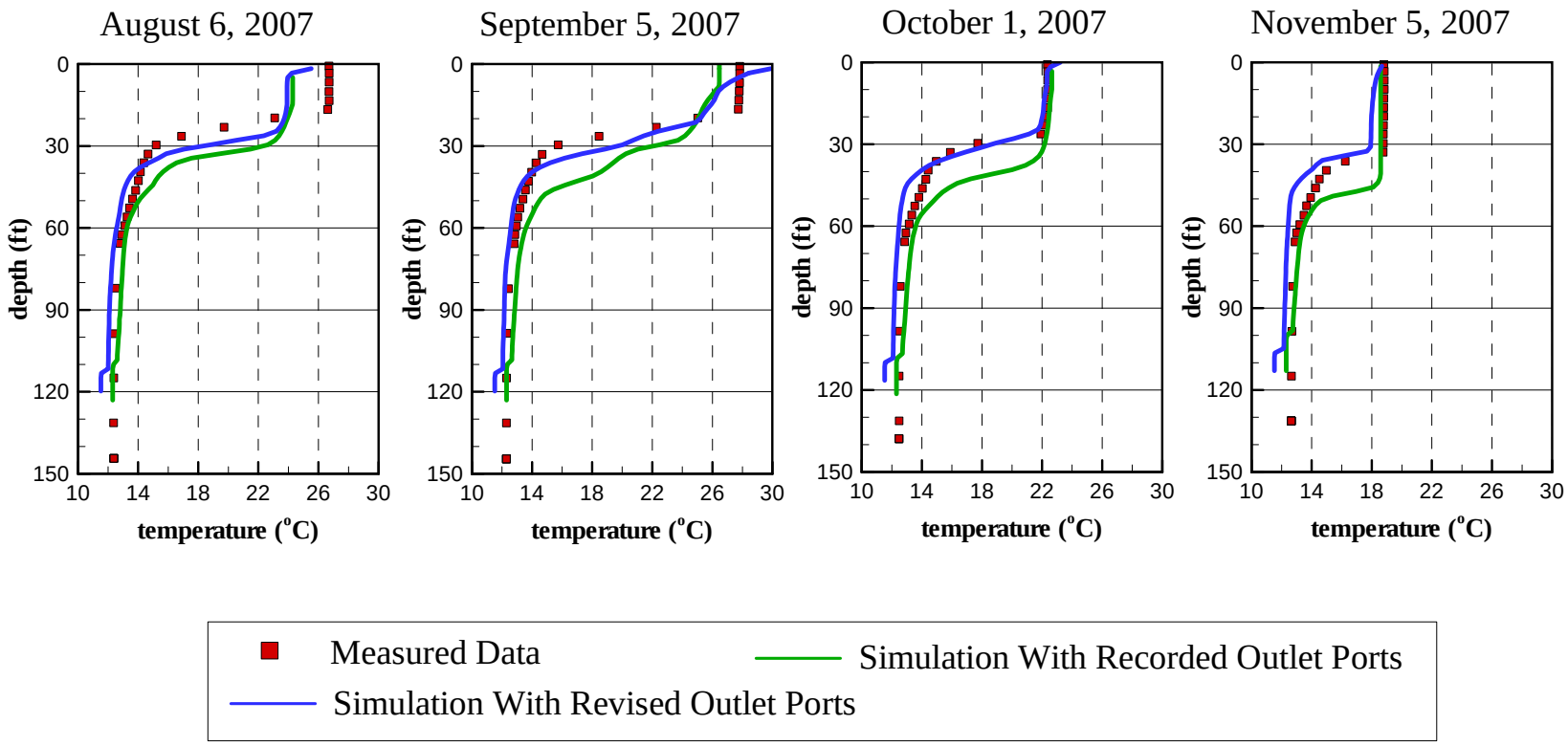

FSI V094005
May 01, 2012

Figure 13

FLOW SCIENCE®

San Vicente Reservoir

Measured vs Simulated Water Surface Elevations

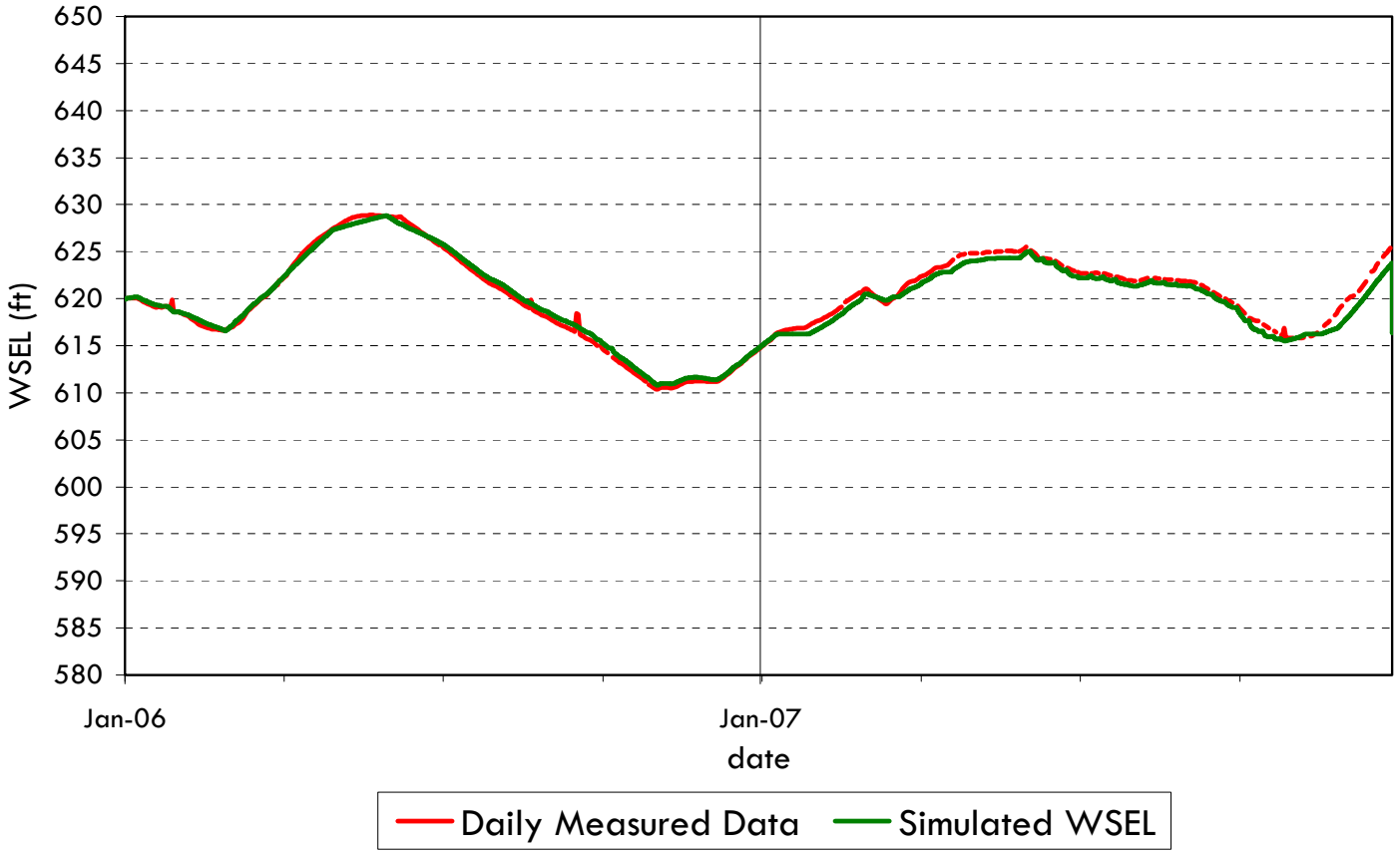

FSI V094005
May 01, 2012

Figure 14

FLOW SCIENCE®

San Vicente Reservoir Station A - Water Temperature Calibration

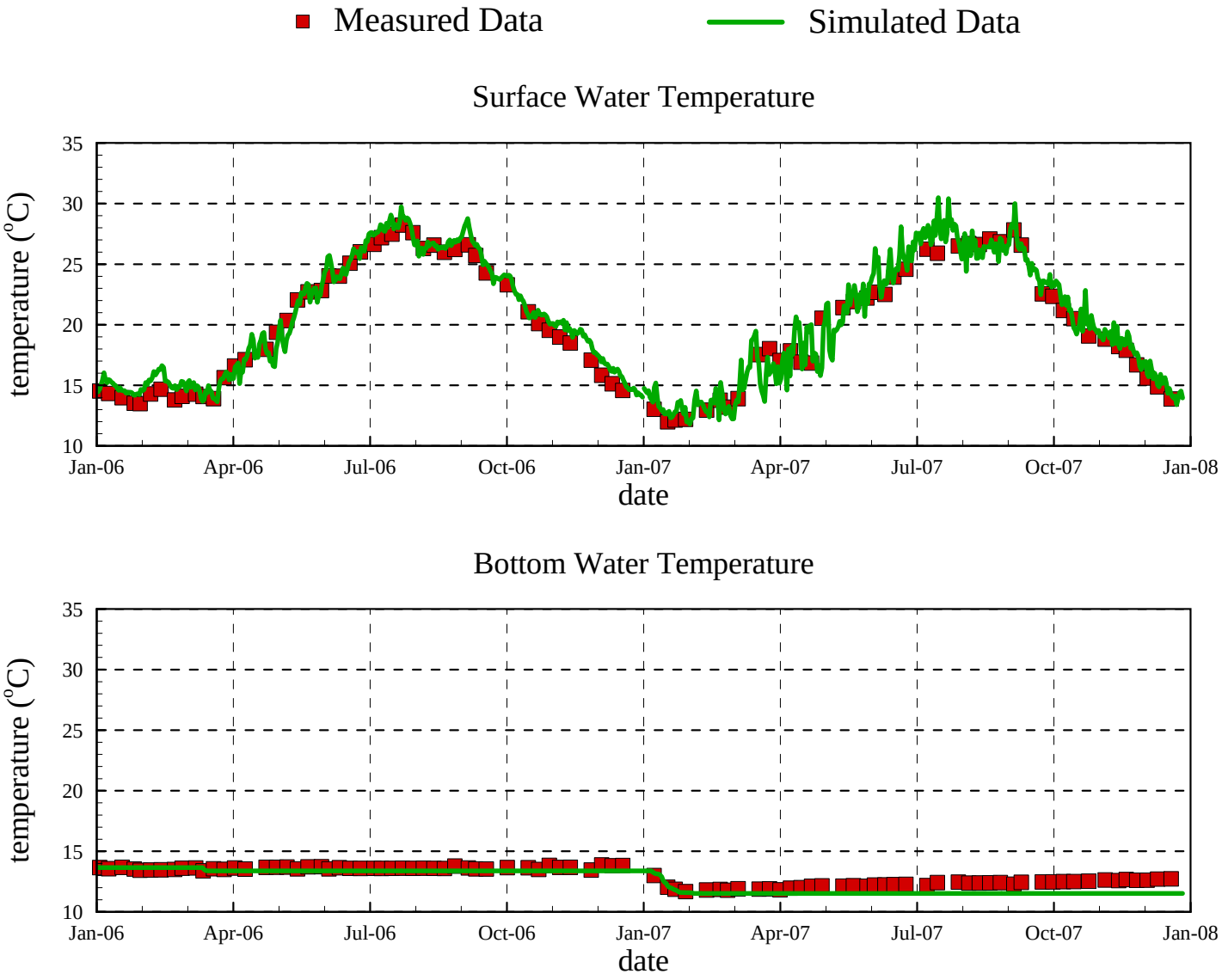

FSI V094005
May 01, 2012

Figure 15

FLOW SCIENCE®

San Vicente Reservoir

Station A - Water Temperature Calibration

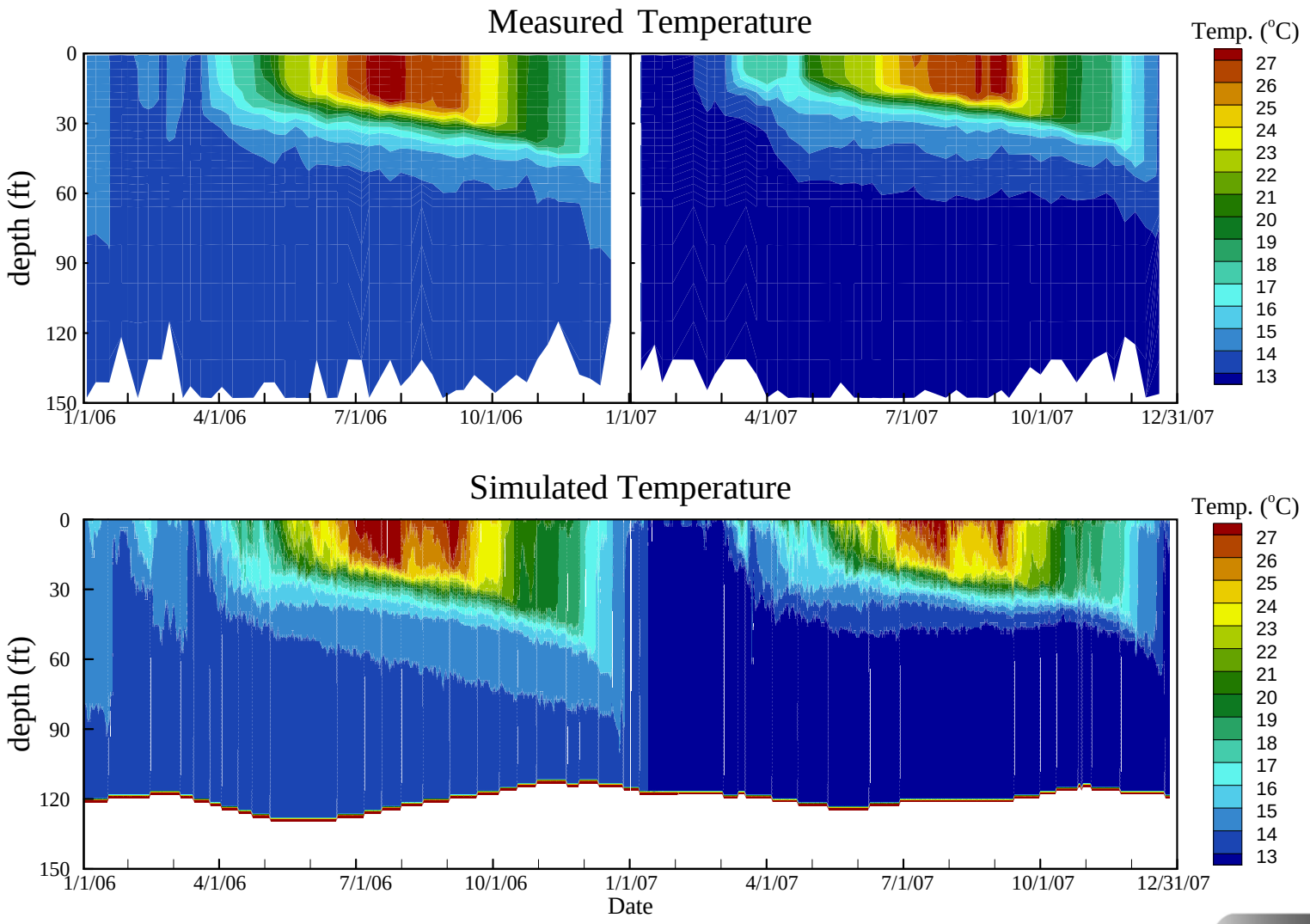

Figure 16

FSI V094005
May 01, 2012

FLOW SCIENCE®

San Vicente Reservoir

Scatter Plot of Measured vs. Simulated Temperature

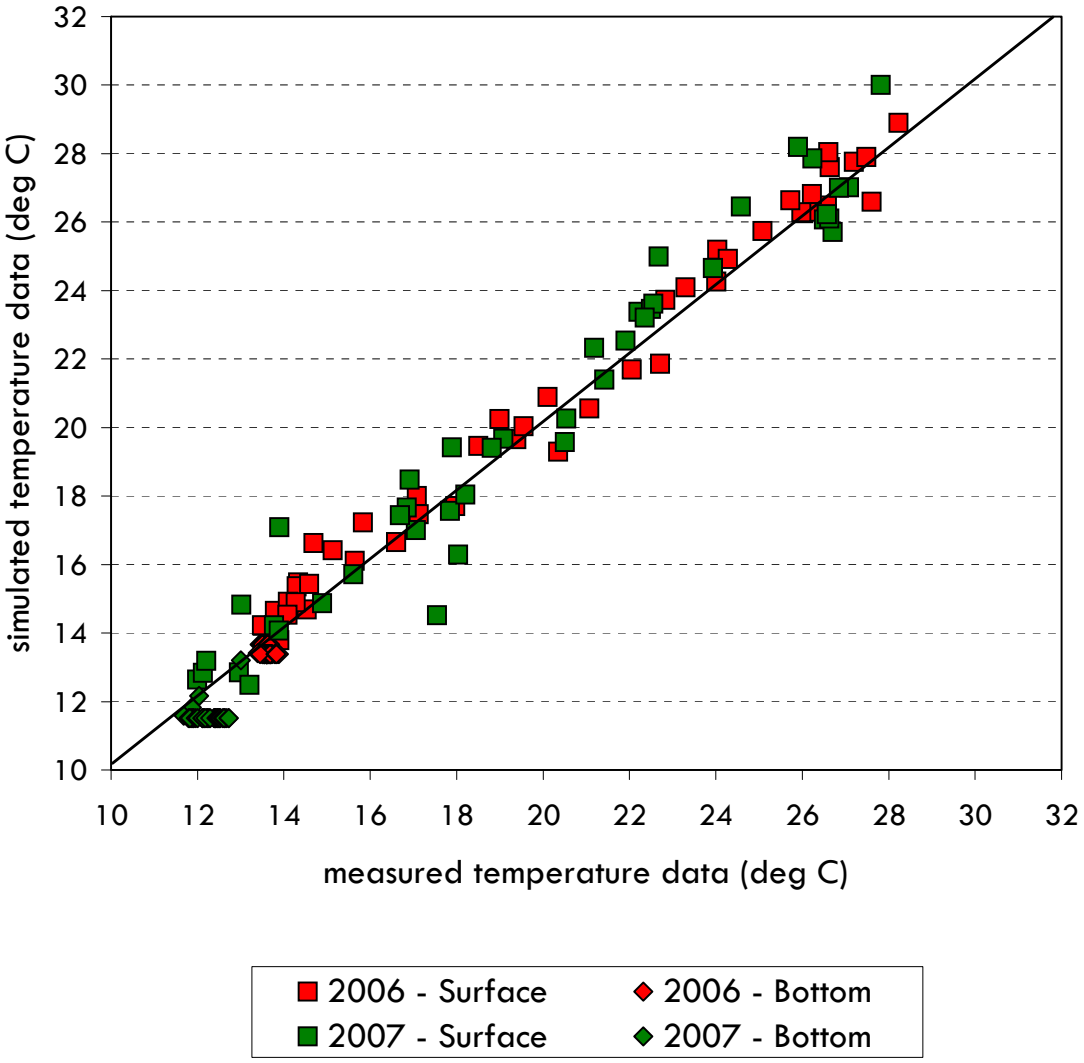

Figure 17

FSI V094005
May 01, 2012

FLOW SCIENCE®

San Vicente Reservoir Station A - Conductivity Calibration

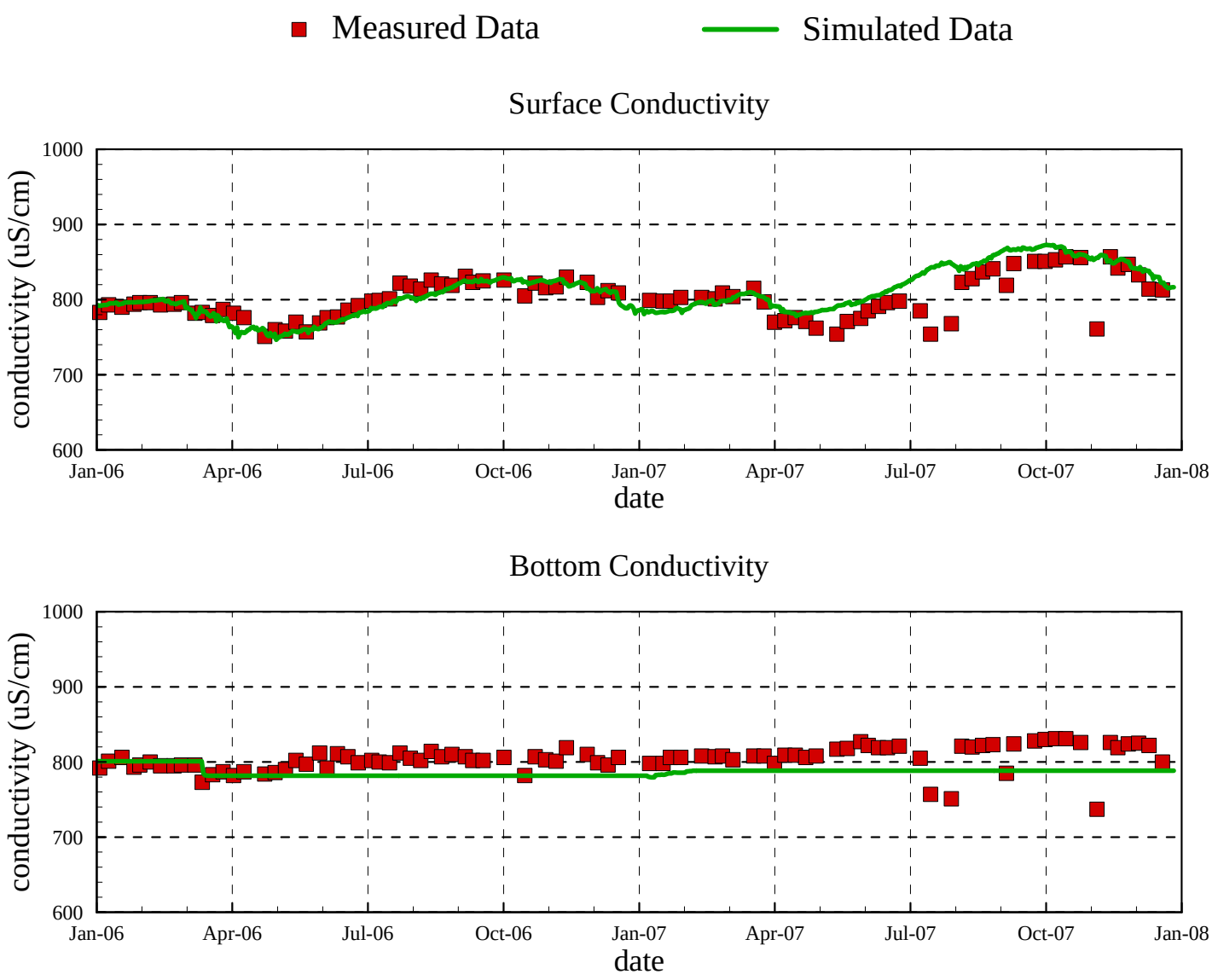

FSI V094005
May 01, 2012

Figure 18

FLOW SCIENCE®

San Vicente Reservoir
Station A - Conductivity Calibration

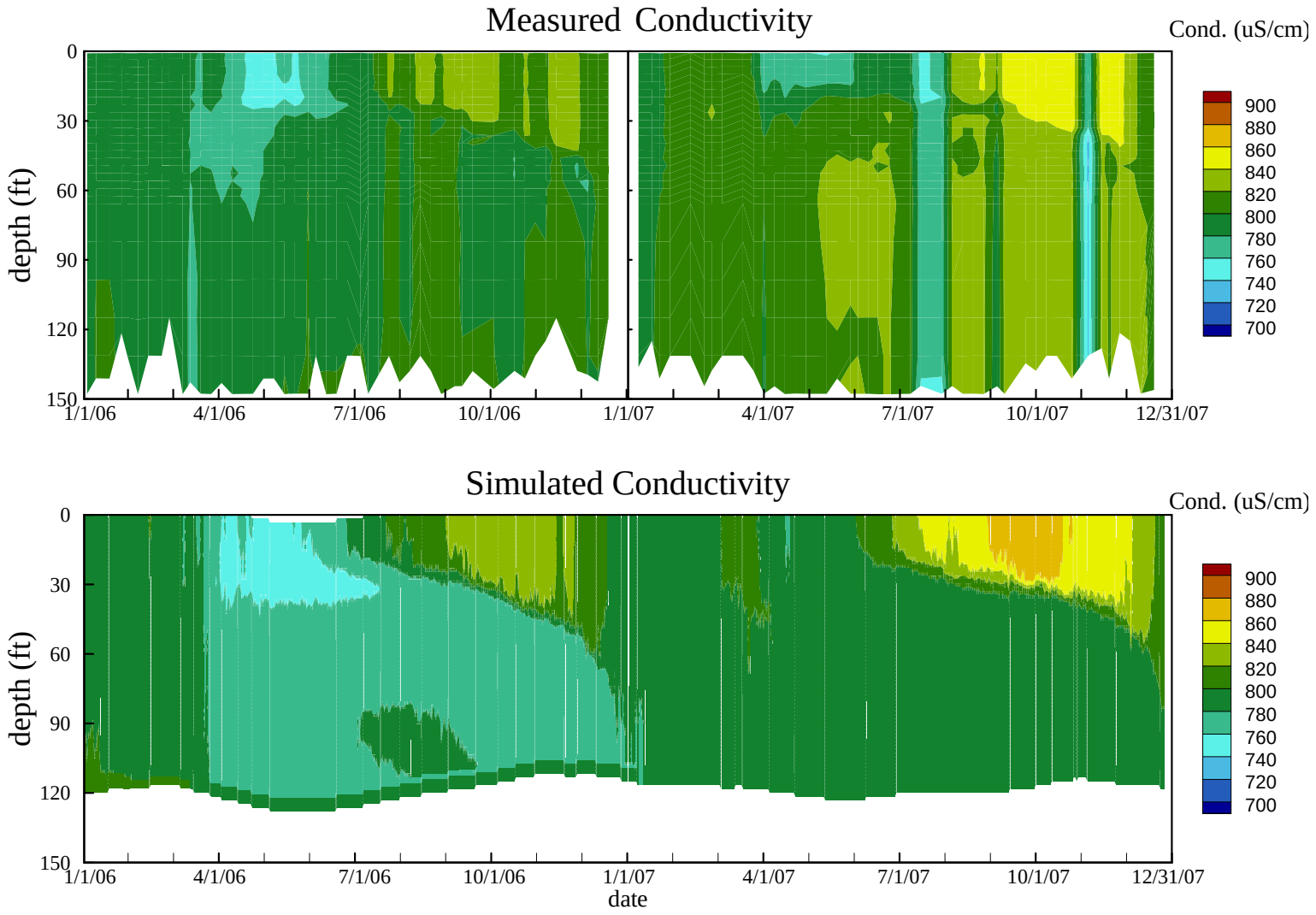

FSI V094005
May 01, 2012

Figure 19

FLOW SCIENCE®

San Vicente Reservoir

Scatter Plot of Measured vs. Simulated Conductivity

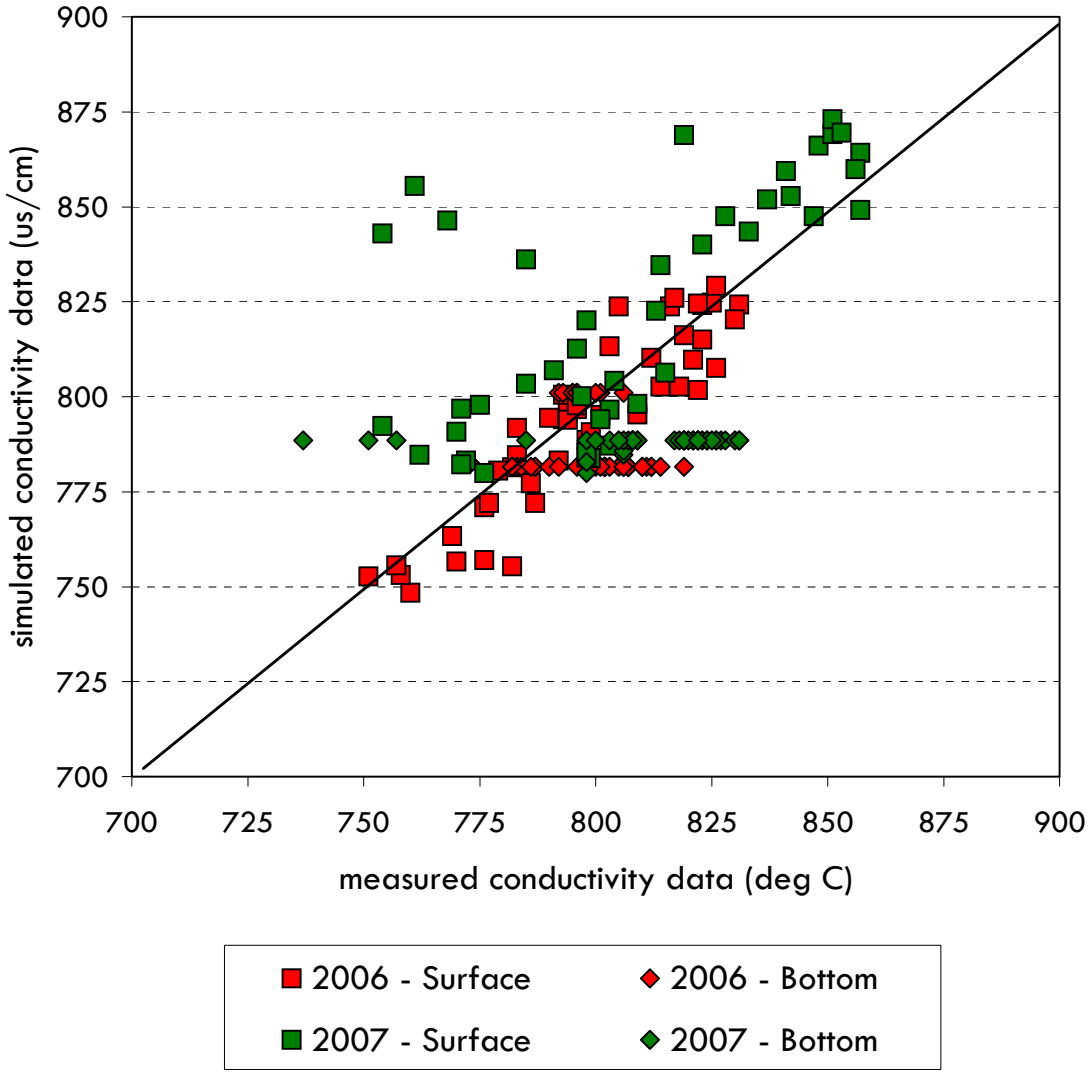

Figure 20

FSI V094005
May 01, 2012

FLOW SCIENCE®

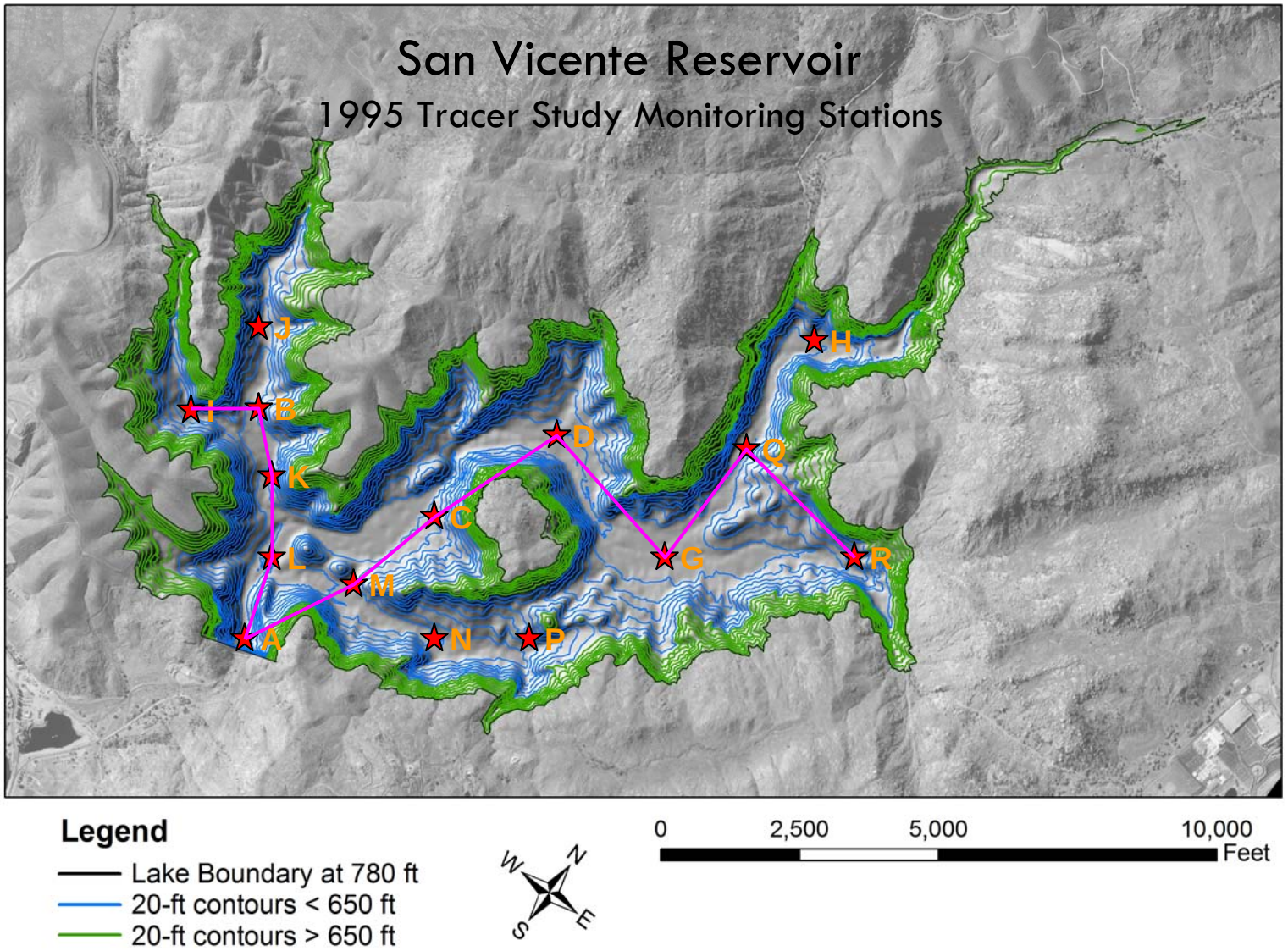

FSI V094005
May 01, 2012

Figure 21

FLOW SCIENCE®

San Vicente Reservoir

1995 Tracer Studies - Percent of Total Initial Mass of Lanthanum in the Reservoir versus Time

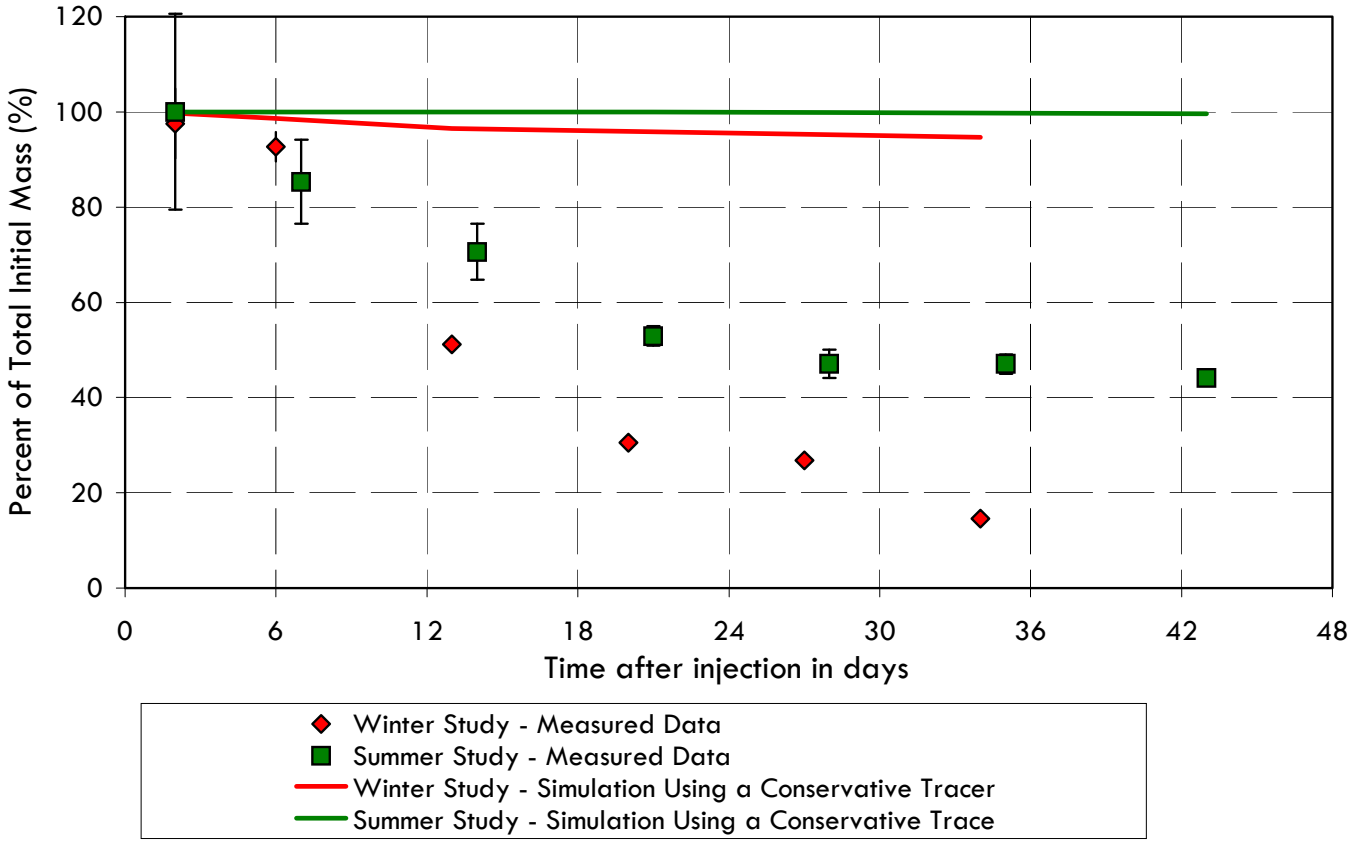

FSI V094005
May 01, 2012

Figure 22

FLOW SCIENCE®

San Vicente Reservoir

1995 Tracer Studies – Simulated Mass Distribution of Particles

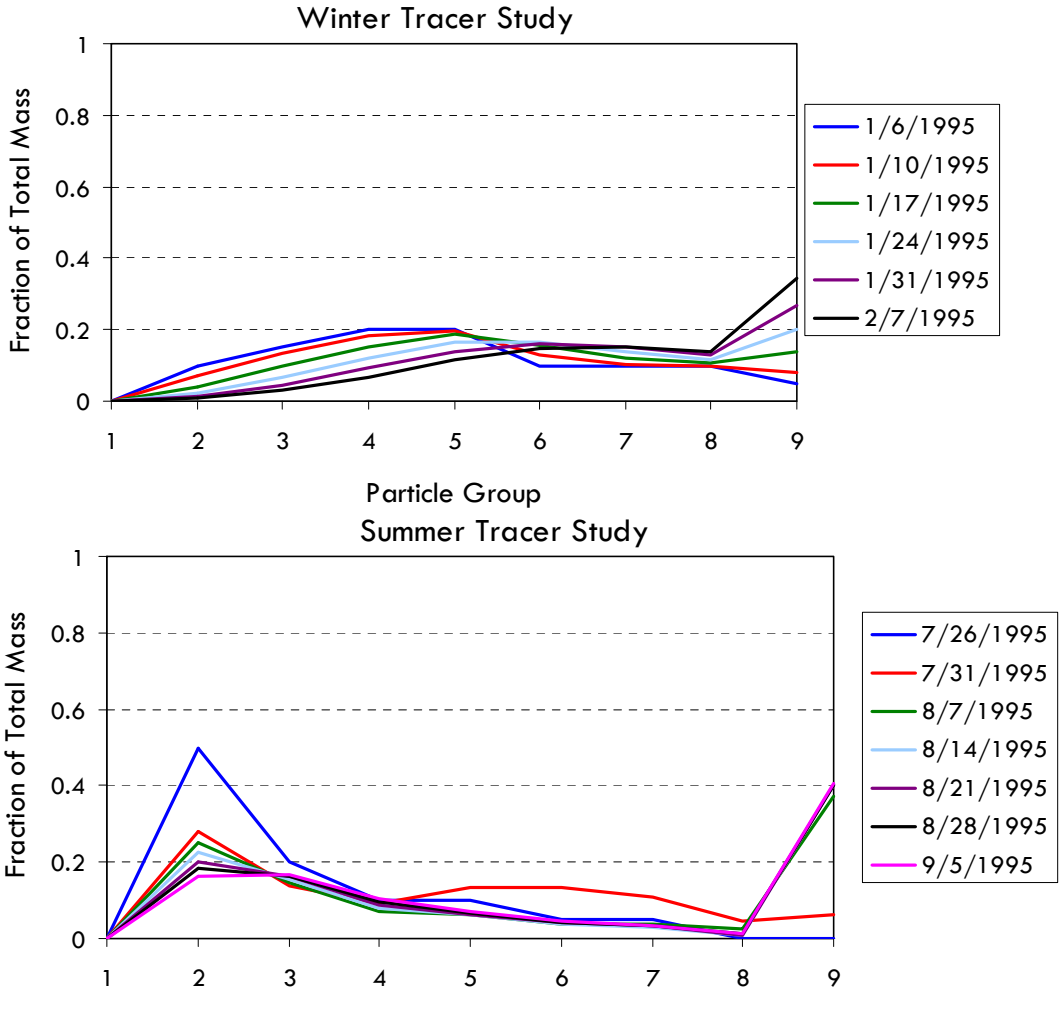

Figure 23

FSI V094005
May 01, 2012

FLOW SCIENCE®

San Vicente Reservoir

1995 Tracer Studies - Percent of Total Initial Mass of Lanthanum in the Reservoir versus Time

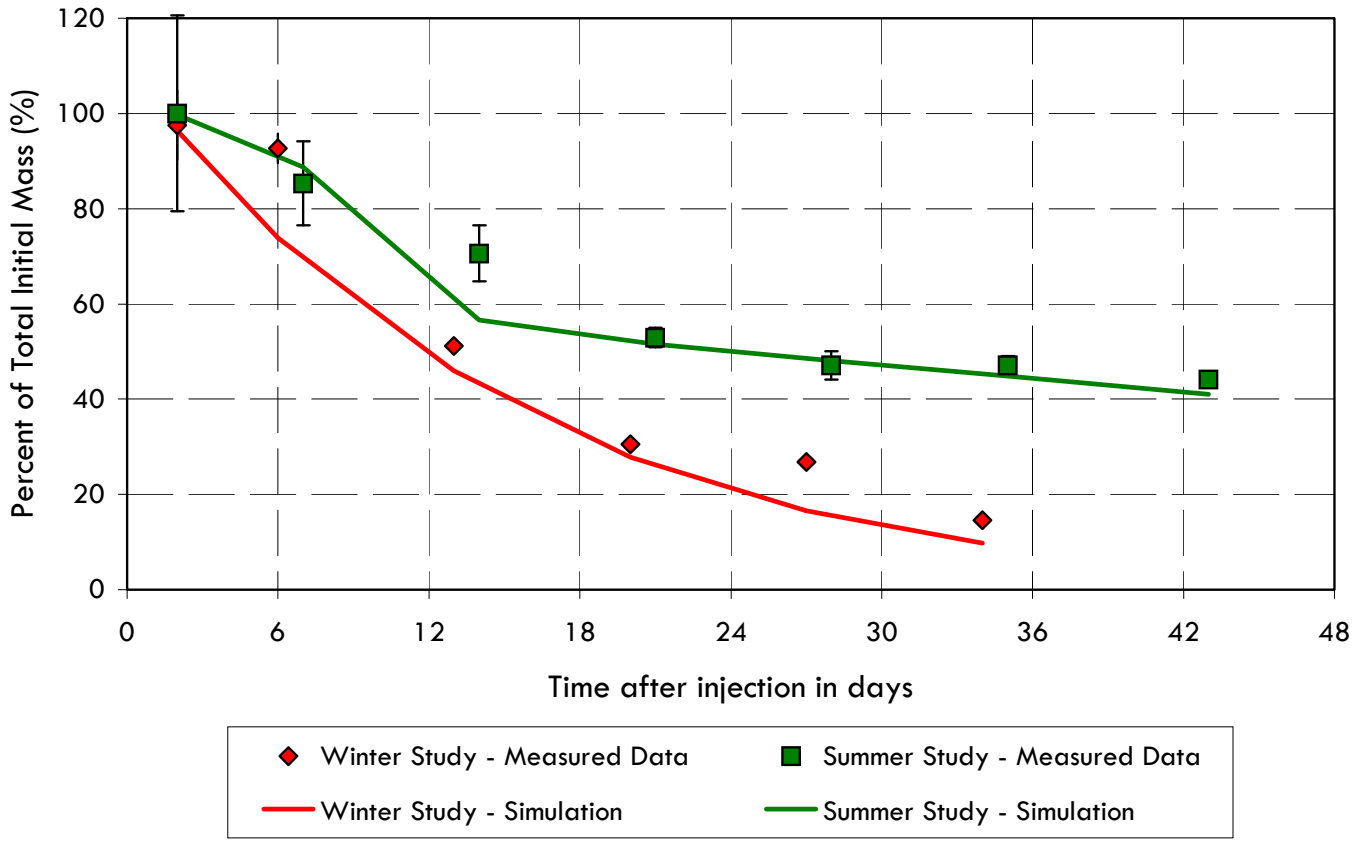

FSI V094005
May 01, 2012

Figure 24

FLOW SCIENCE®

San Vicente Reservoir
Station A - Water Temperature in 1995 Winter Tracer Study

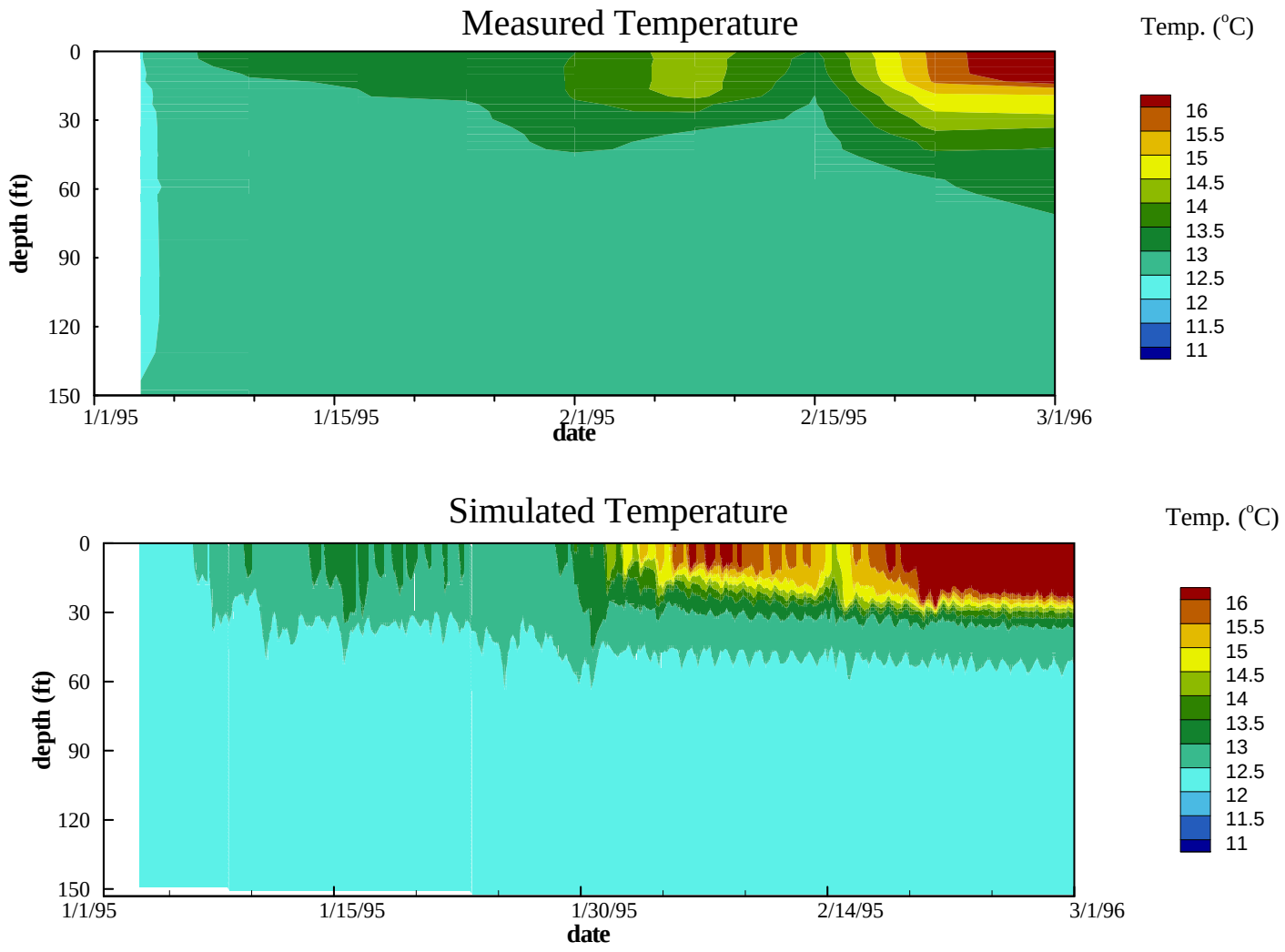

FSI V094005
May 01, 2012

Figure 25

FLOW SCIENCE®

San Vicente Reservoir

1995 Tracer Winter Study – Measured versus Simulated Lanthanum Concentrations

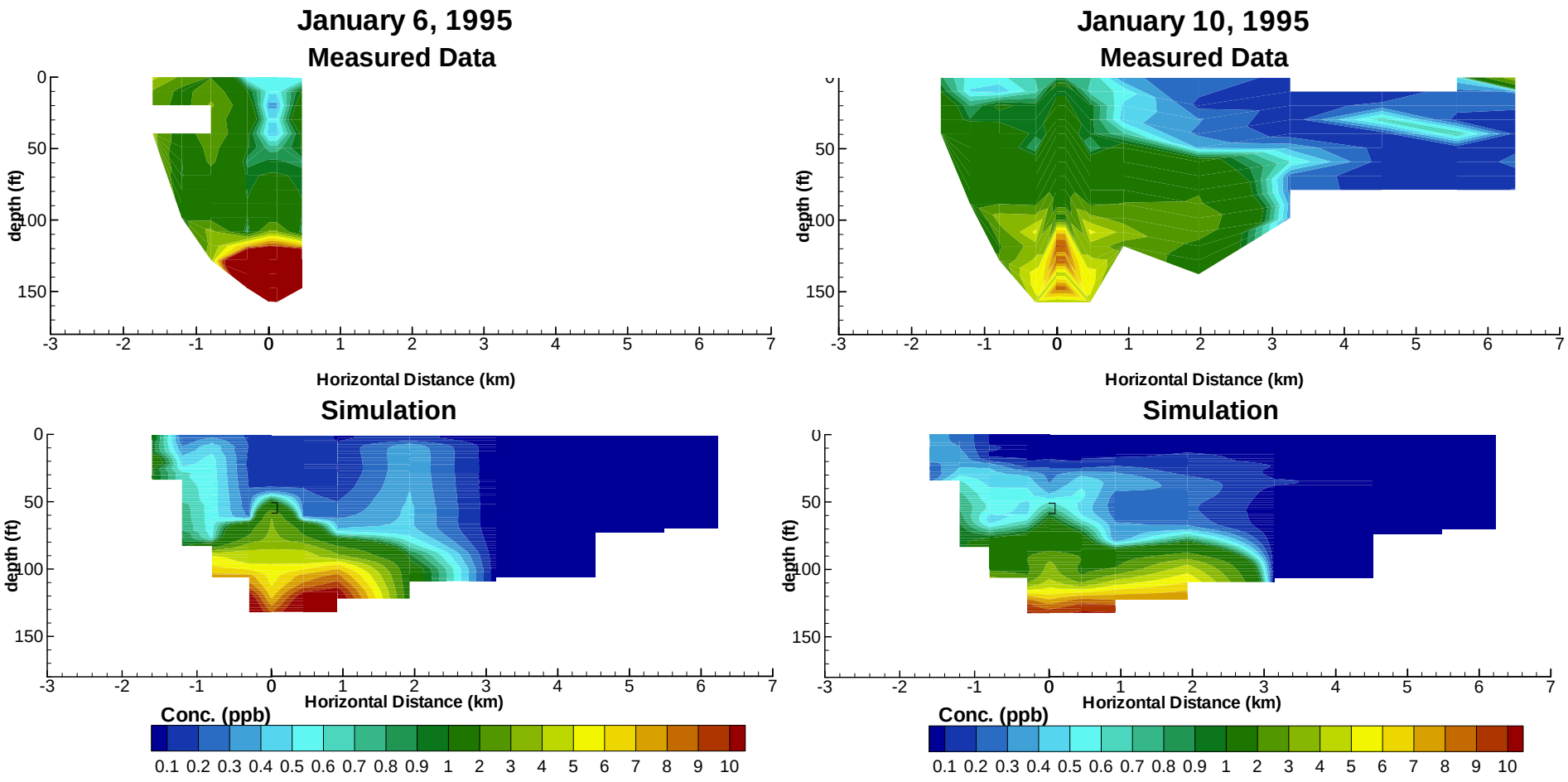

FSI V094005
May 01, 2012

Figure 26

FLOW SCIENCE®

San Vicente Reservoir

1995 Winter Tracer Study – Measured versus Simulated Lanthanum Concentrations

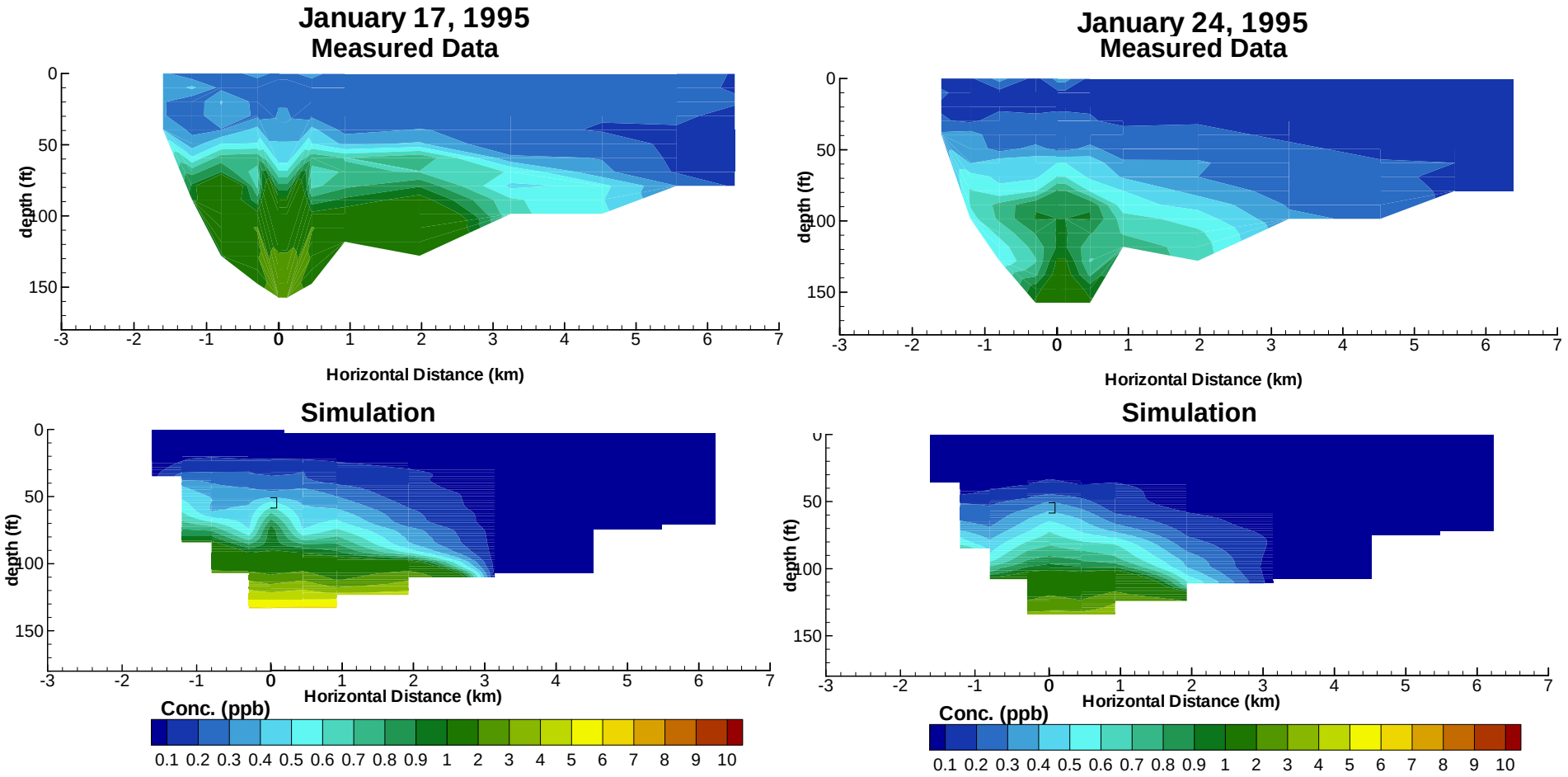

FSI V094005
May 01, 2012

Figure 27

FLOW SCIENCE®

San Vicente Reservoir

1995 Winter Tracer Study – Measured versus Simulated Lanthanum Concentrations

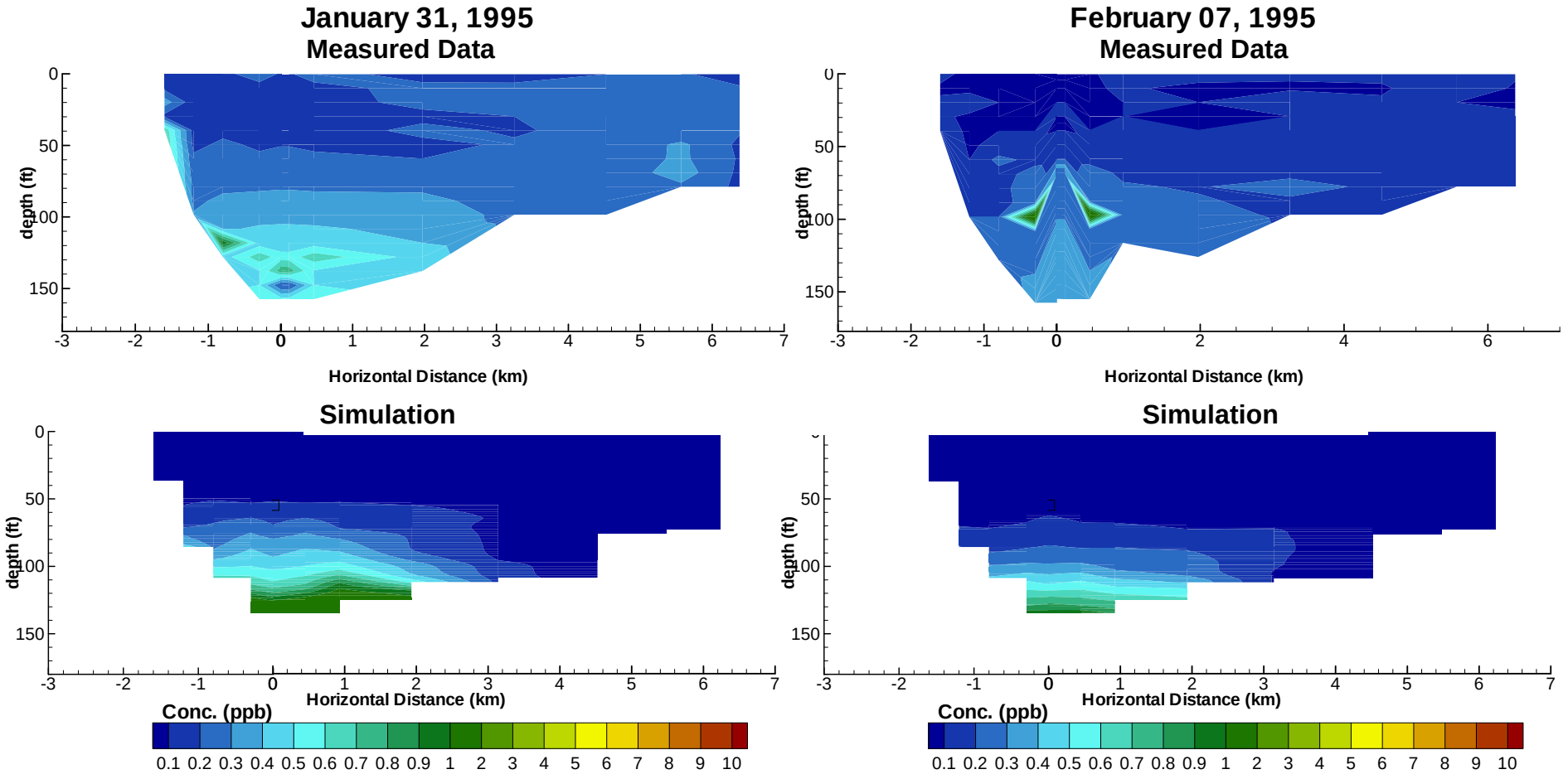

FSI V094005
May 01, 2012

Figure 28

FLOW SCIENCE®

San Vicente Reservoir
Station A - Water Temperature Calibration

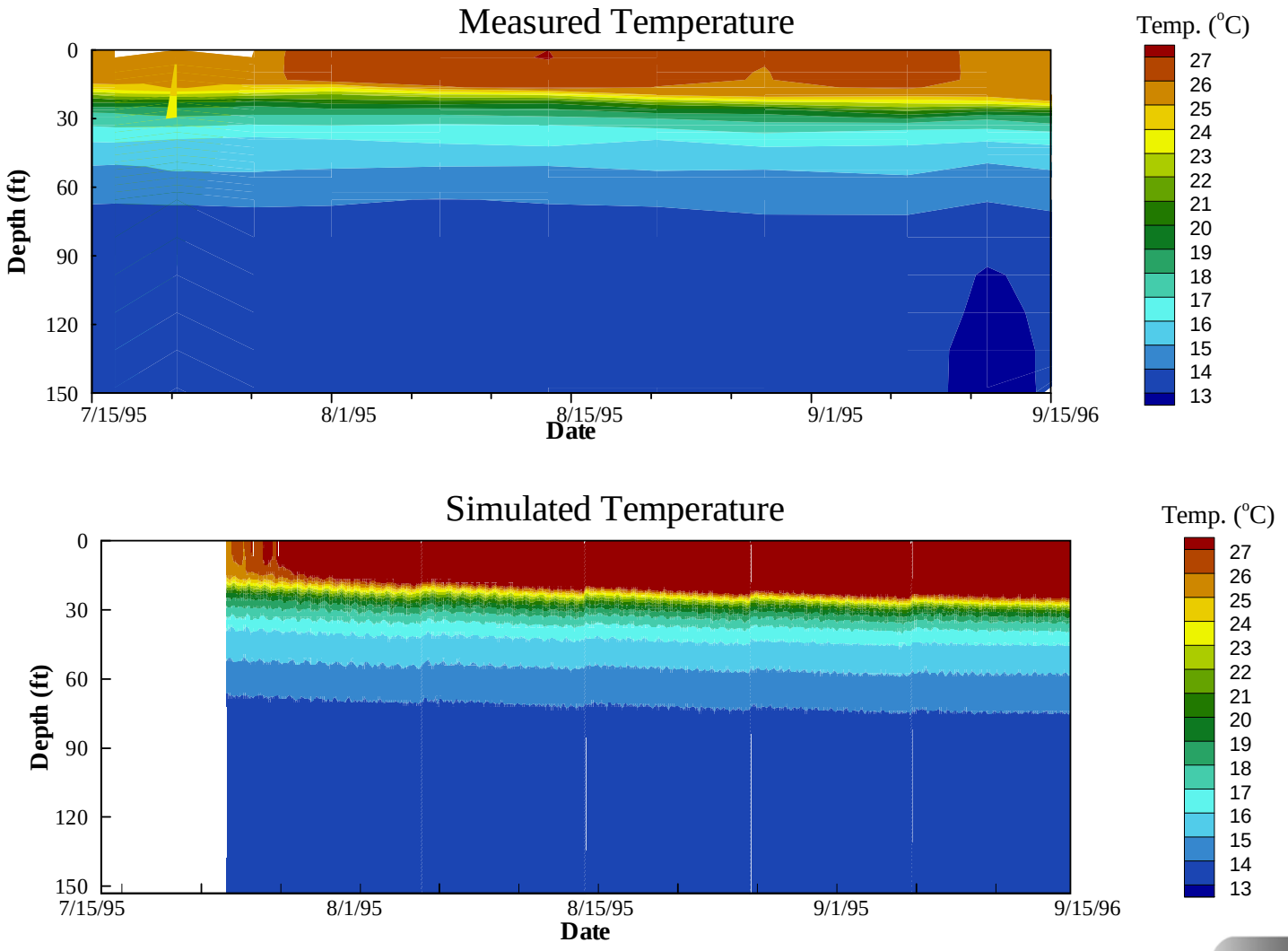

Figure 29

FSI V094005
May 01, 2012

FLOW SCIENCE®

San Vicente Reservoir

1995 Summer Tracer Study – Measured versus Simulated Lanthanum Concentrations

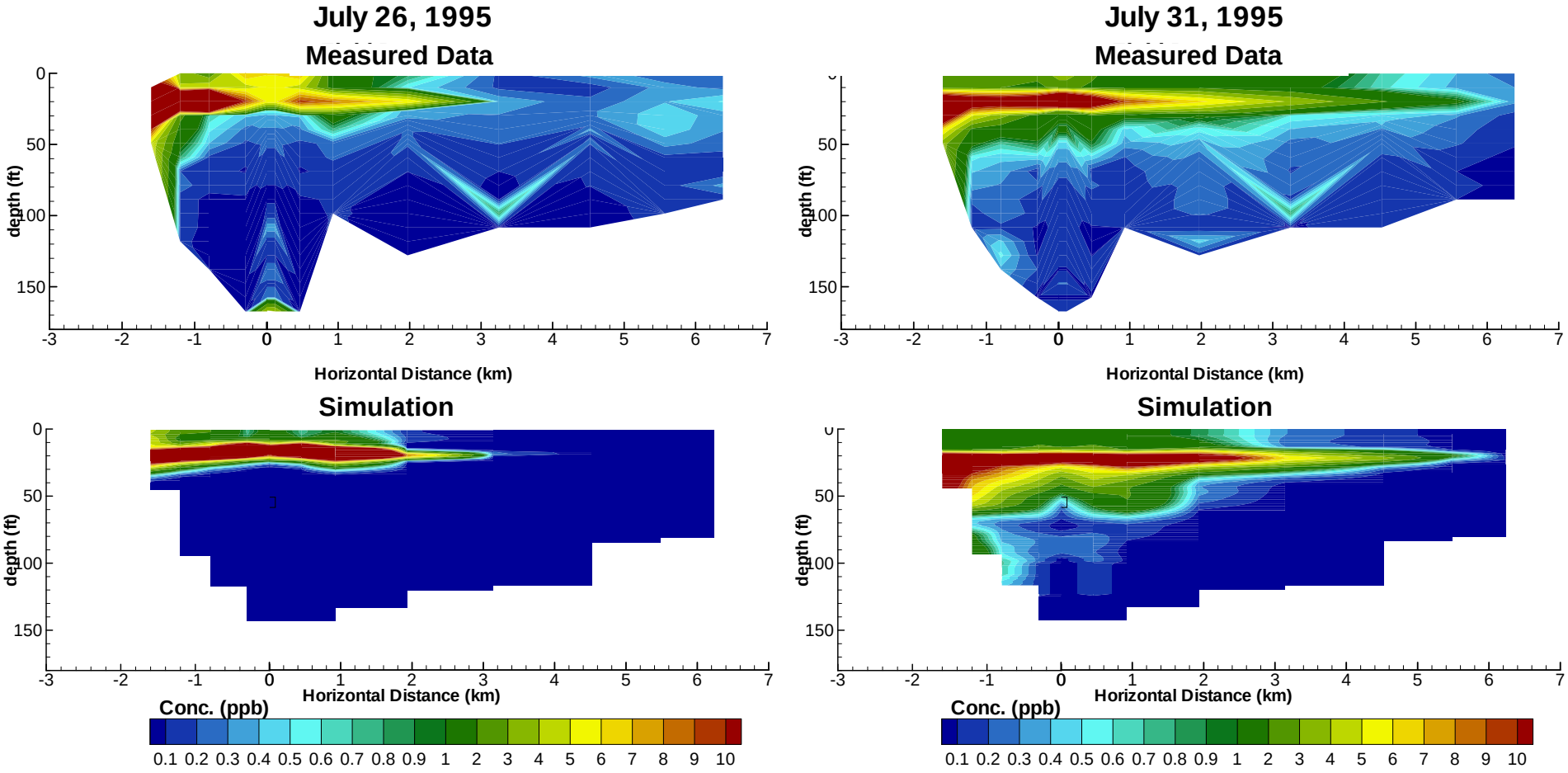

FSI V094005
May 01, 2012

Figure 30

FLOW SCIENCE®

San Vicente Reservoir

1995 Summer Tracer Study – Measured versus Simulated Lanthanum Concentrations

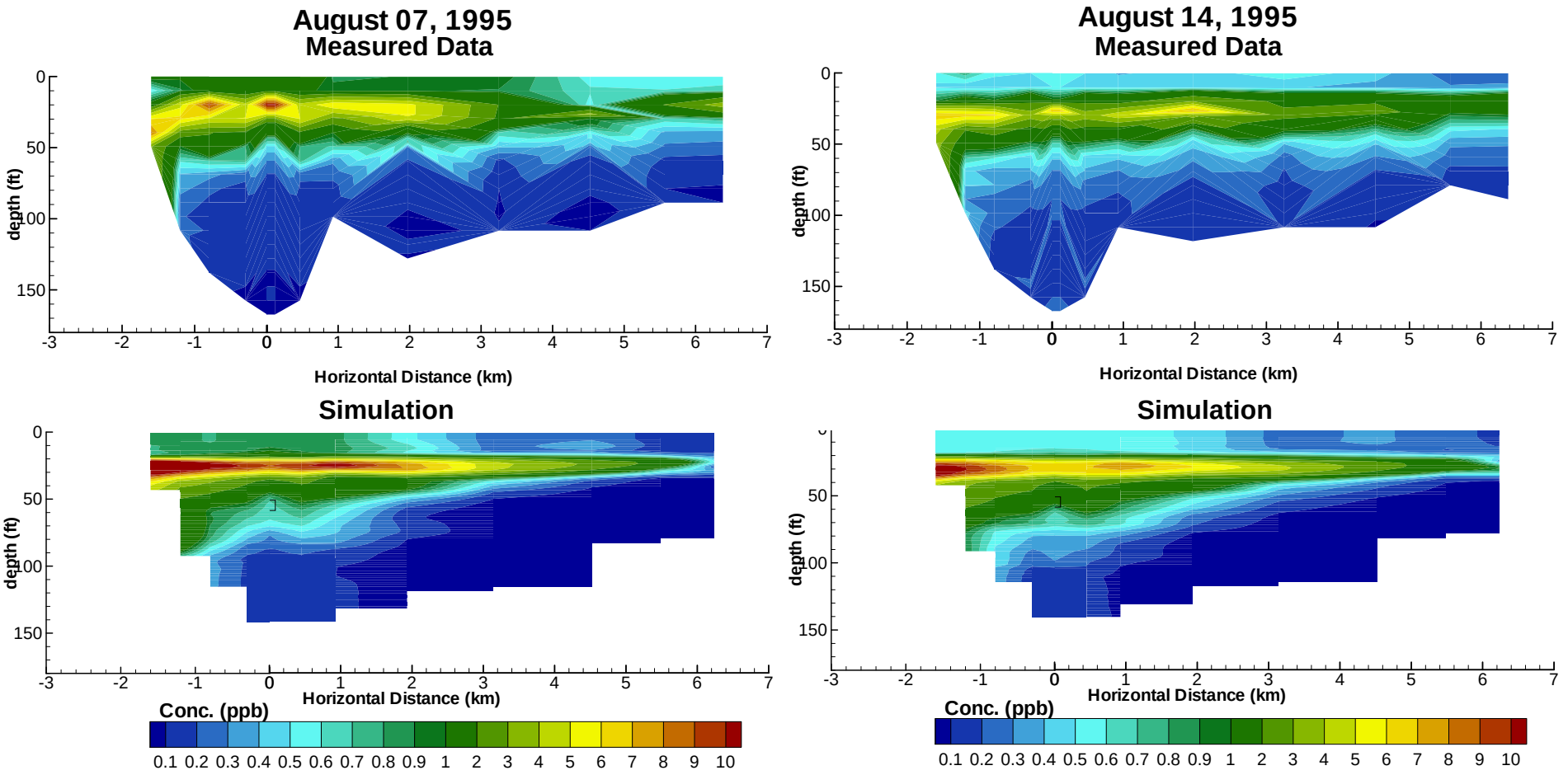

FSI V094005
May 01, 2012

Figure 31

FLOW SCIENCE®

San Vicente Reservoir

1995 Summer Tracer Study – Measured versus Simulated Lanthanum Concentrations

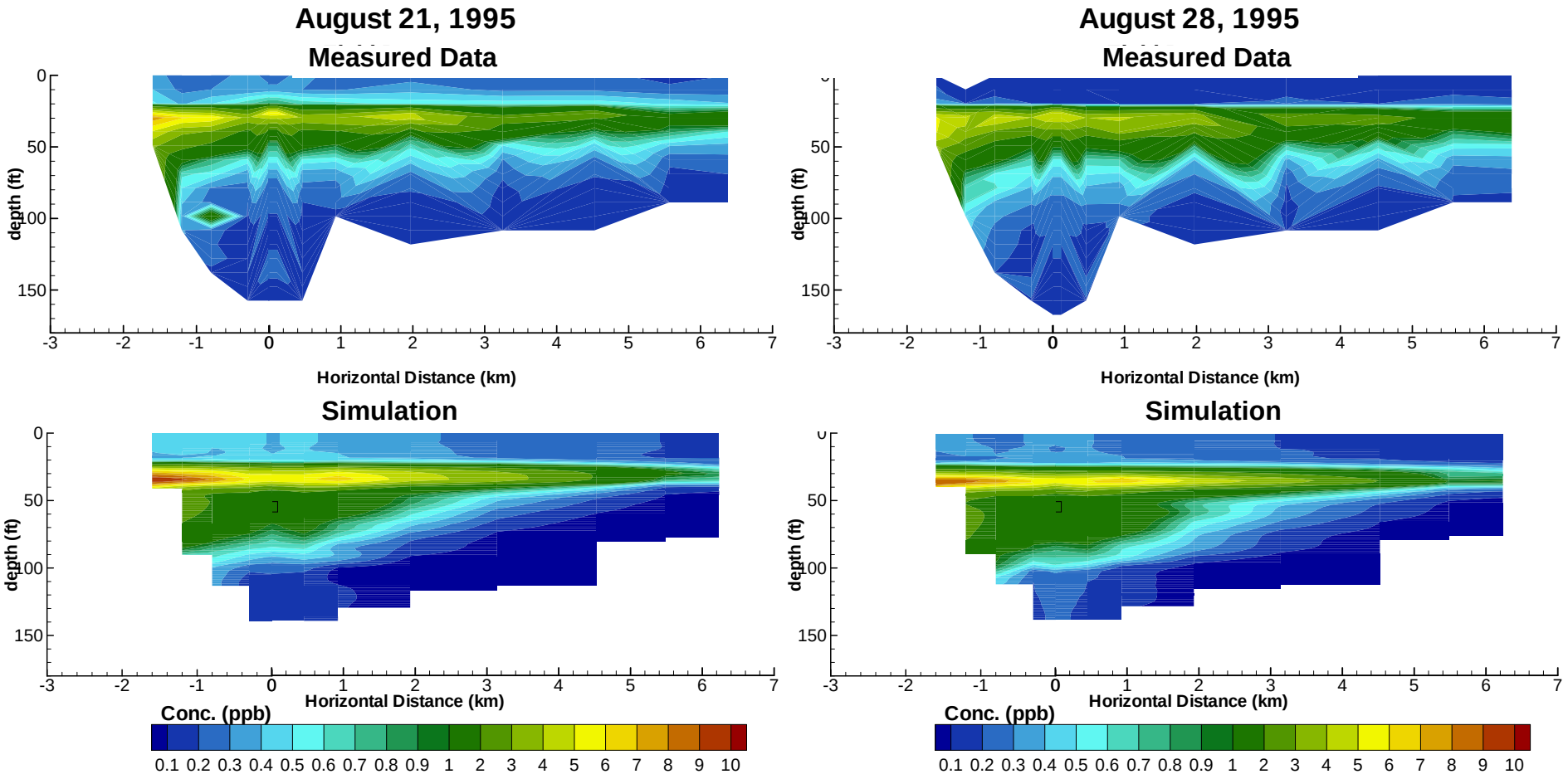

FSI V094005
May 01, 2012

Figure 32

FLOW SCIENCE®

San Vicente Reservoir

1995 Summer Tracer Study – Measured versus Simulated Lanthanum Concentrations

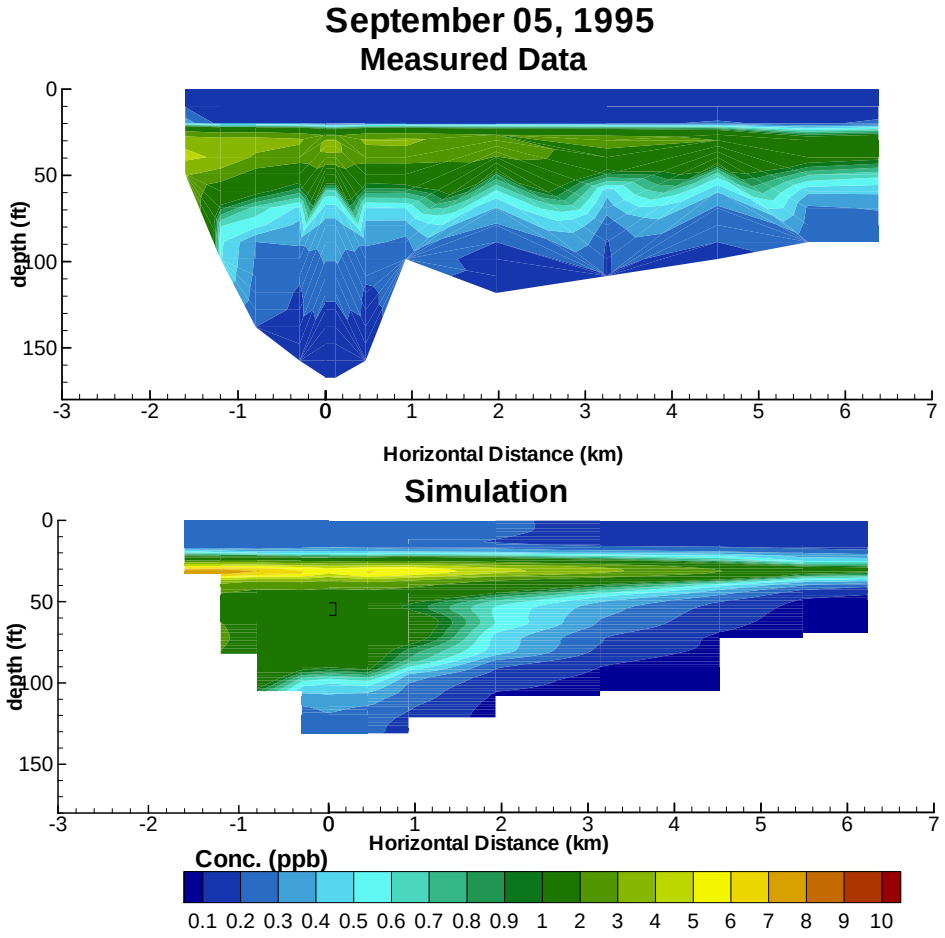

FSI V094005
May 01, 2012

Figure 33

FLOW SCIENCE®

San Vicente Reservoir 100-m ELCOM-CAEDYM Computational Grid

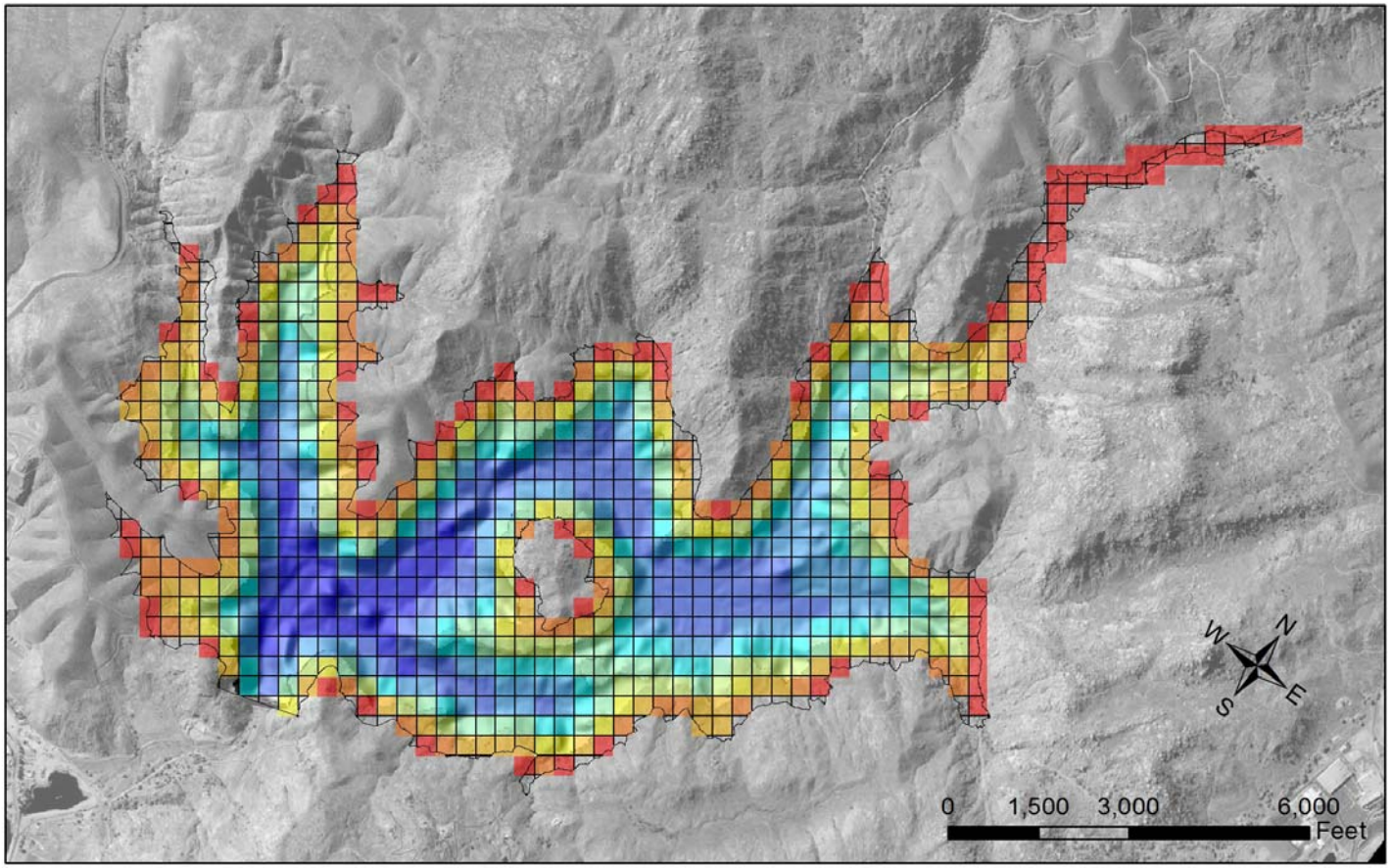

San Vicente
100-m ELCOM Grid

Legend

Lake Boundary at 780 ft

Elevation (ft)

480 - 510	541 - 569	630 - 659	719 - 748
511 - 540	570 - 599	660 - 689	749 - 778
	600 - 629	690 - 718	

FSI V094005
May 01, 2012

Figure 34

FLOW SCIENCE®

San Vicente Reservoir Station A - Water Temperature Simulation

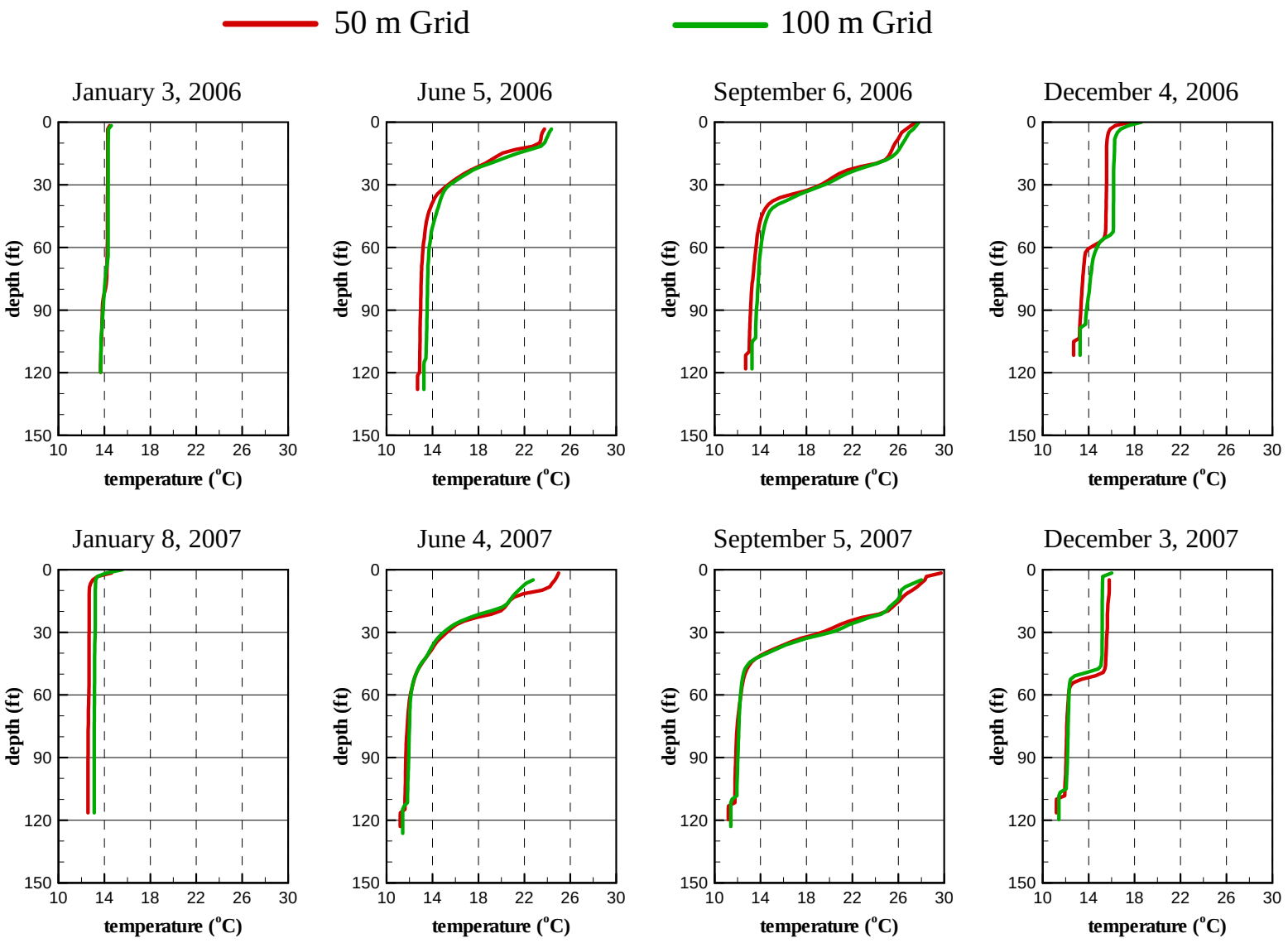

FSI V094005
May 01, 2012

Figure 35

FLOW SCIENCE®

San Vicente Reservoir Station A - Conductivity Simulation

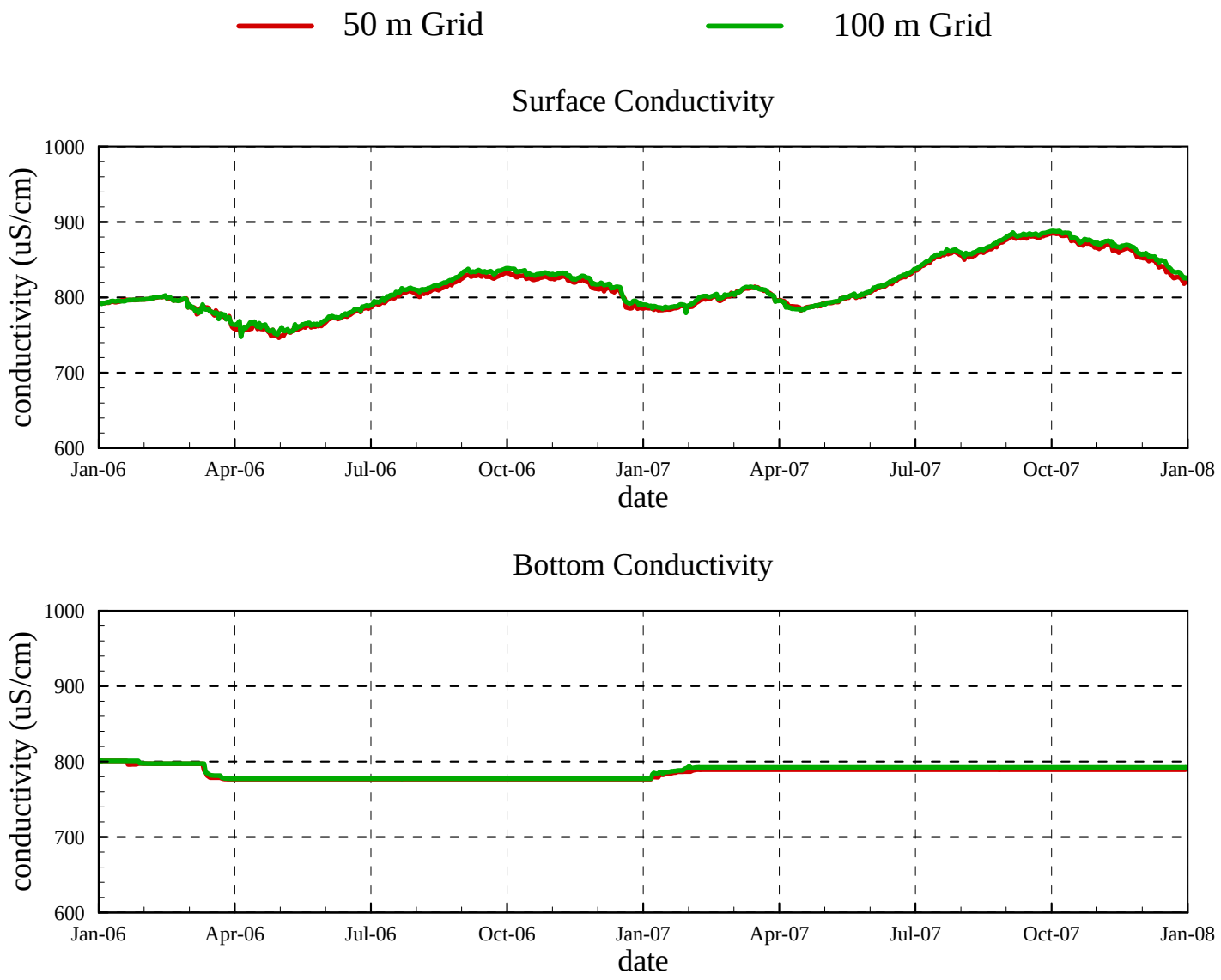

FSI V094005
May 01, 2012

Figure 36

FLOW SCIENCE®

San Vicente Reservoir Station A - Dissolved Oxygen Calibration

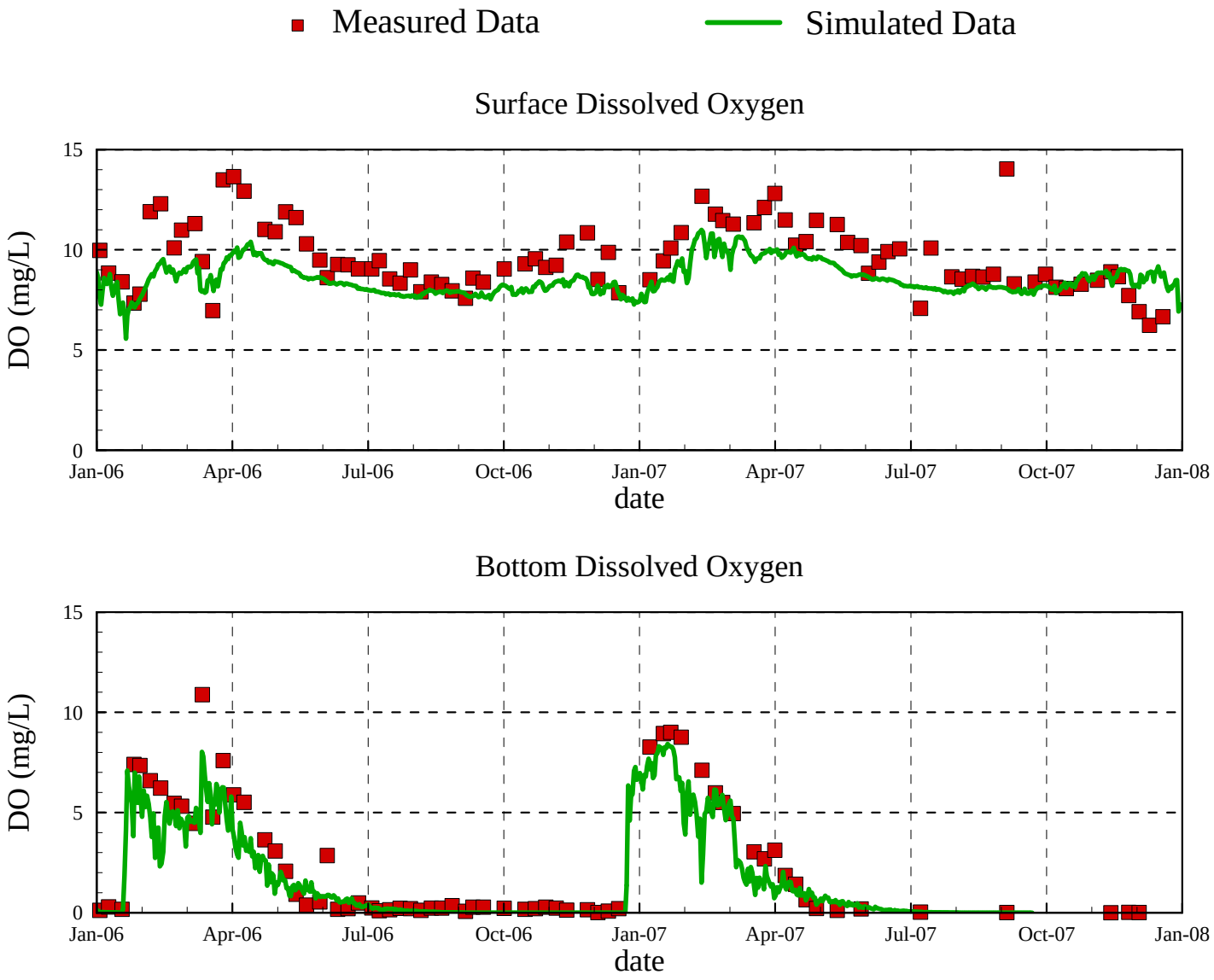

Figure 37

FSI V094005
May 01, 2012

FLOW SCIENCE®

San Vicente Reservoir

Station A - Dissolved Oxygen Calibration

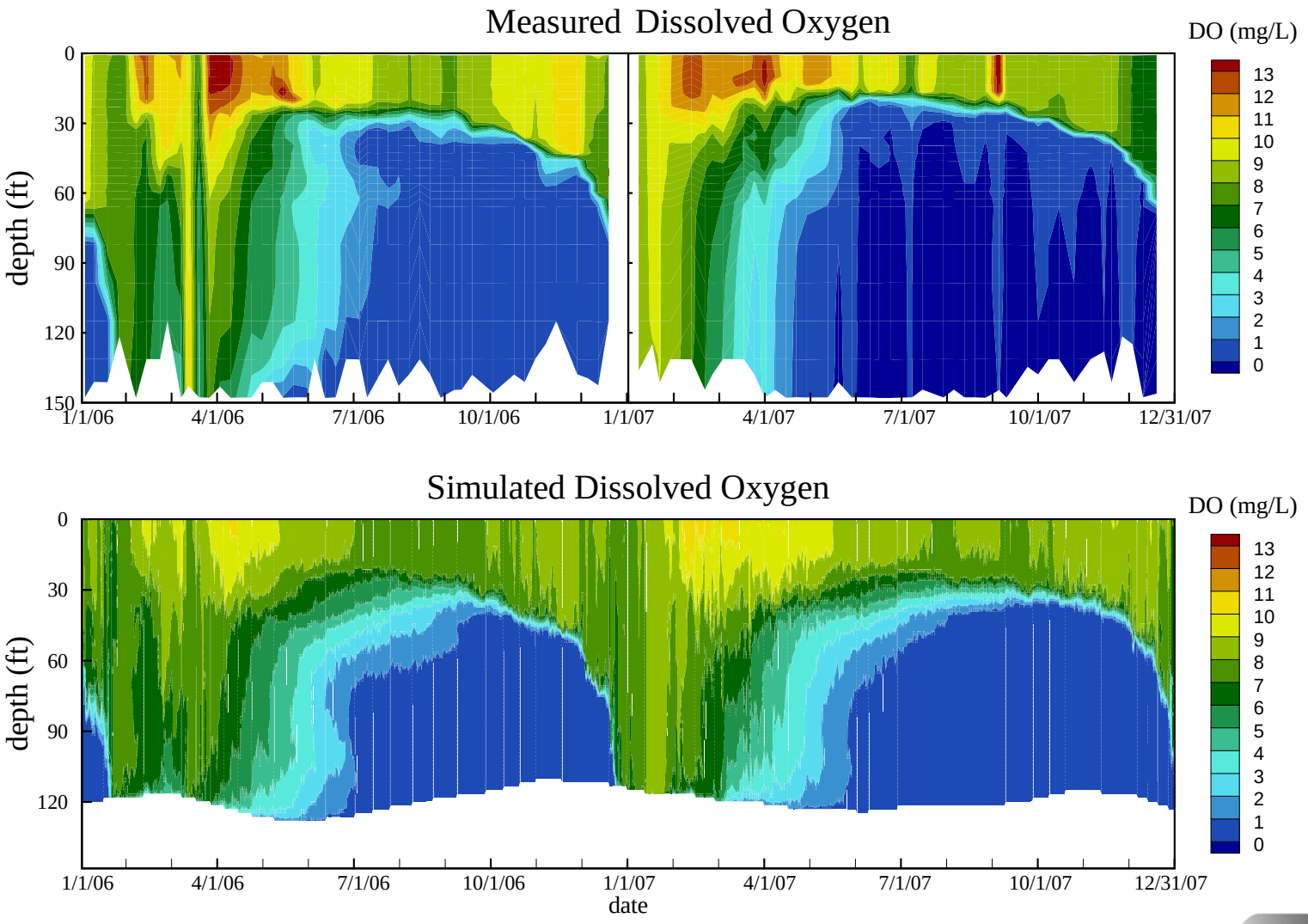

Figure 38

FSI V094005
May 01, 2012

FLOW SCIENCE®

San Vicente Reservoir

Scatter Plot of Measured vs. Simulated Dissolved Oxygen

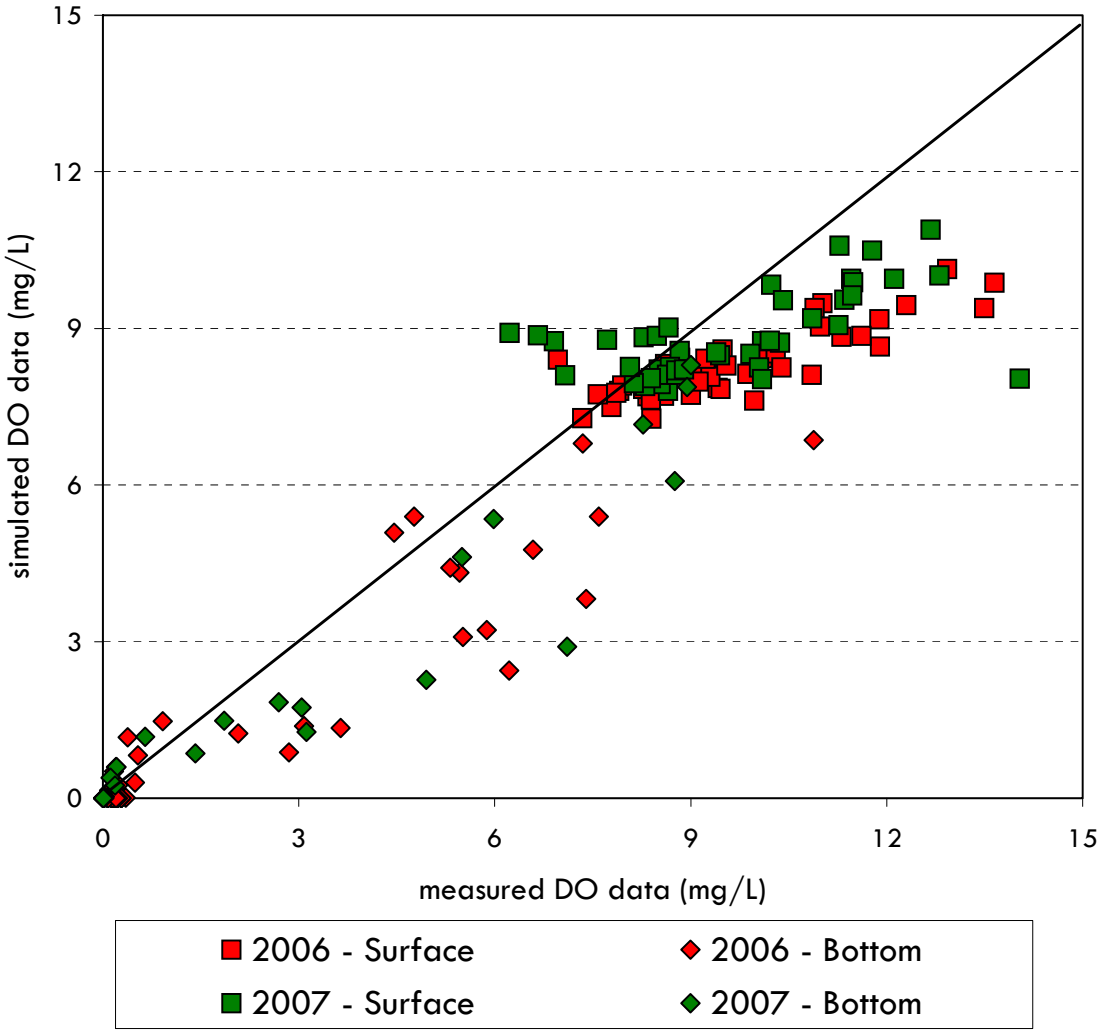

Figure 39

FSI V094005
May 01, 2012

FLOW SCIENCE®

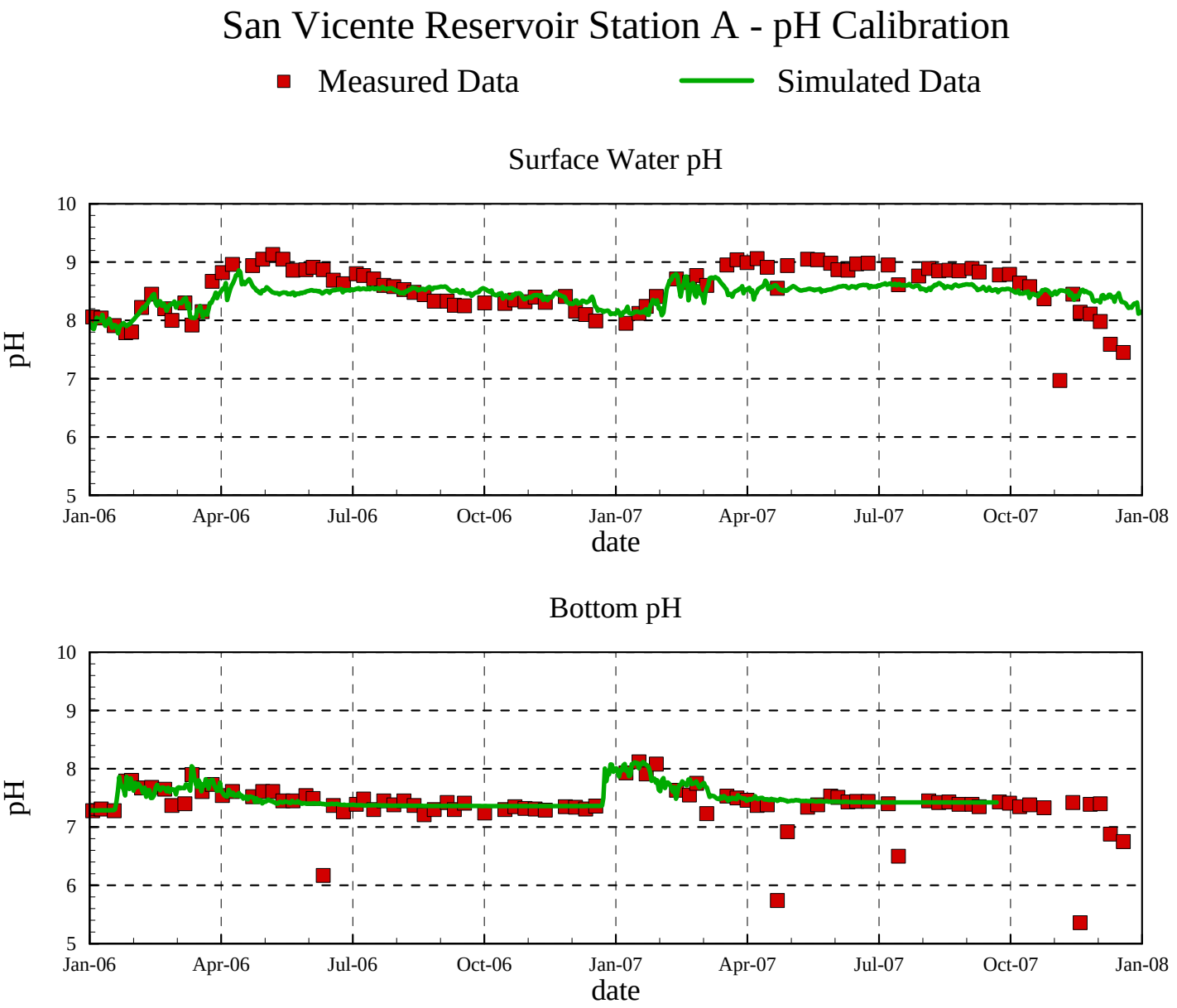

Figure 40

FSI V094005
May 01, 2012

FLOW SCIENCE®

San Vicente Reservoir

Station A - pH Calibration

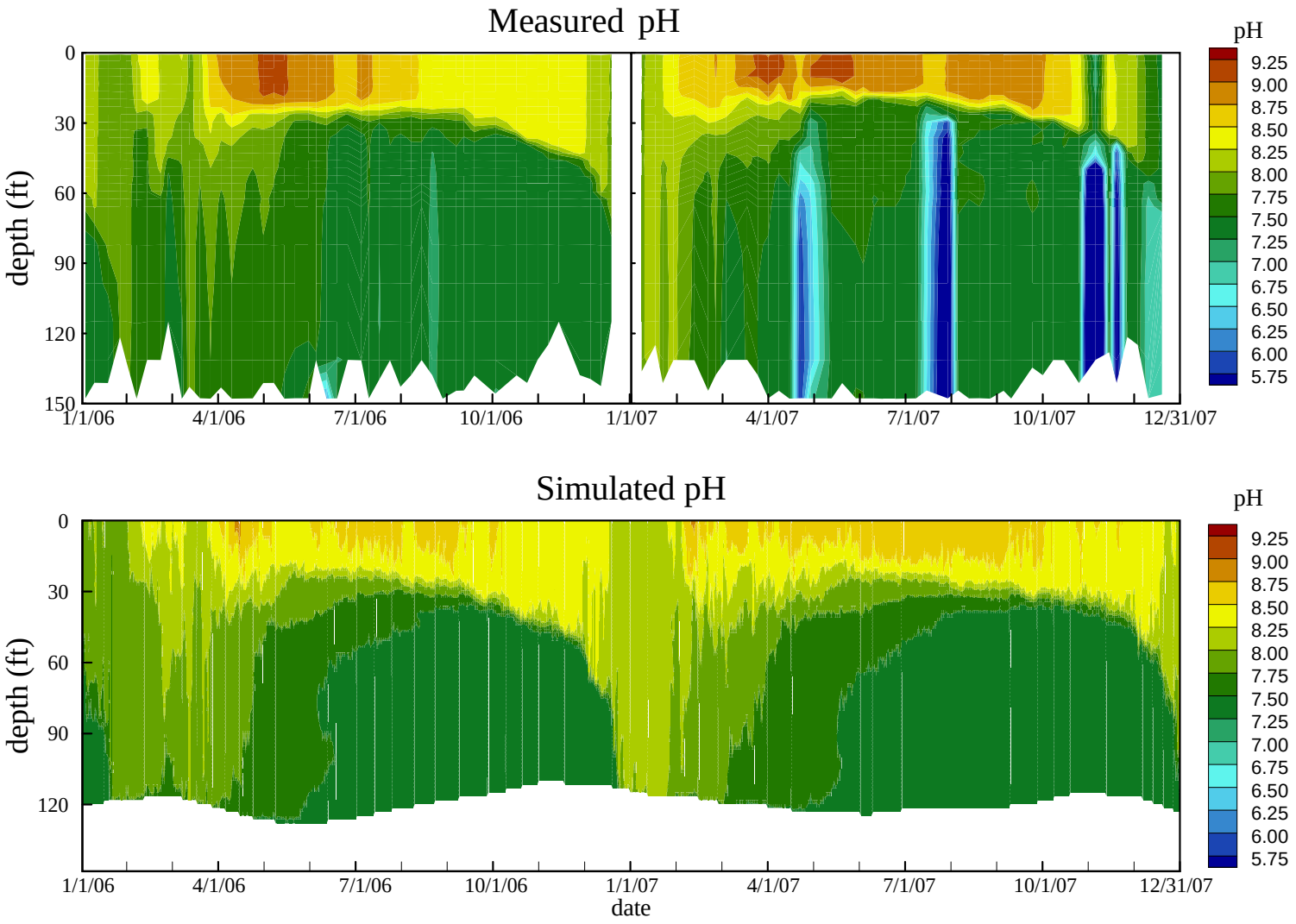

FSI V094005
May 01, 2012

Figure 41

FLOW SCIENCE®

San Vicente Reservoir

Scatter Plot of Measured vs. Simulated pH

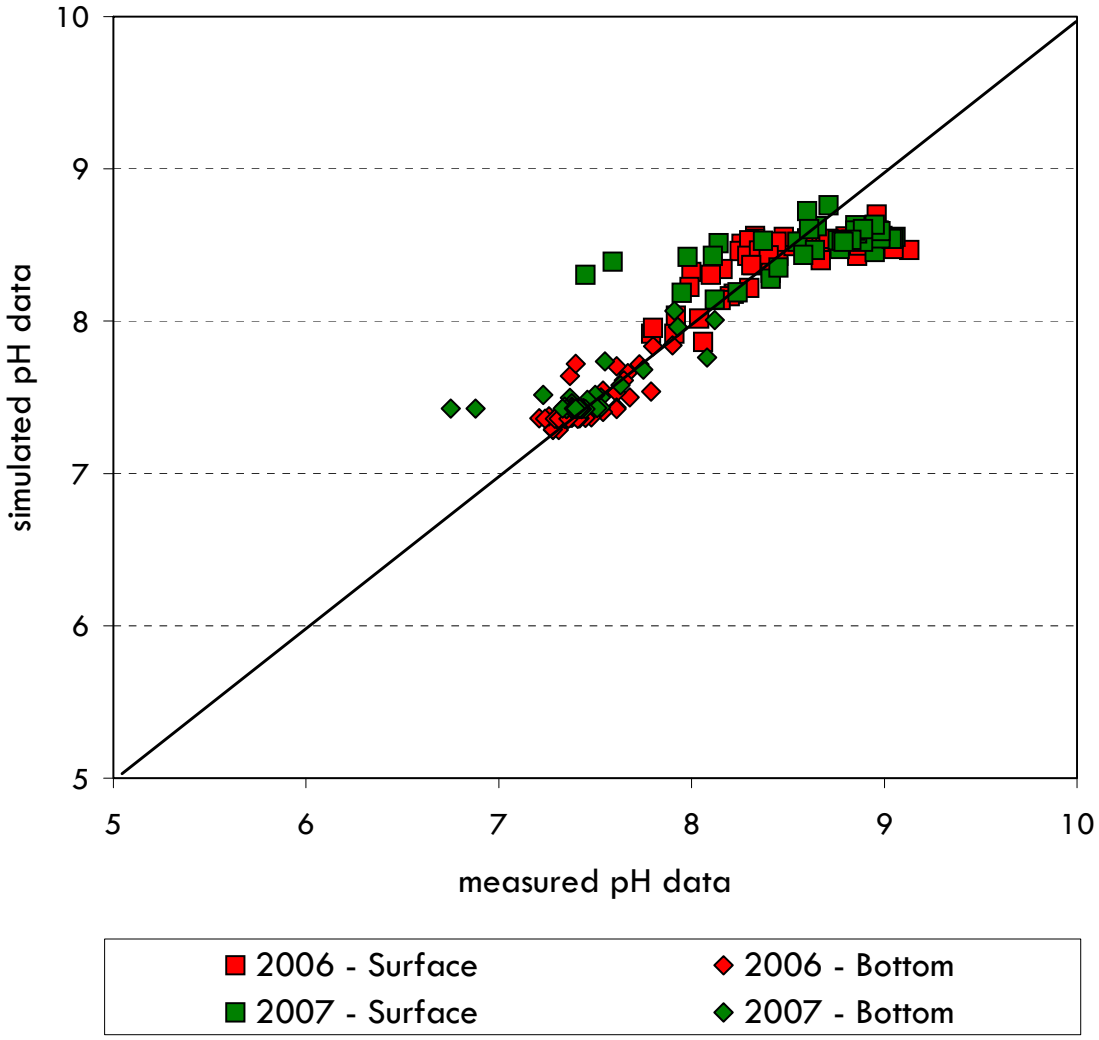

Figure 42

FSI V094005
May 01, 2012

FLOW SCIENCE®

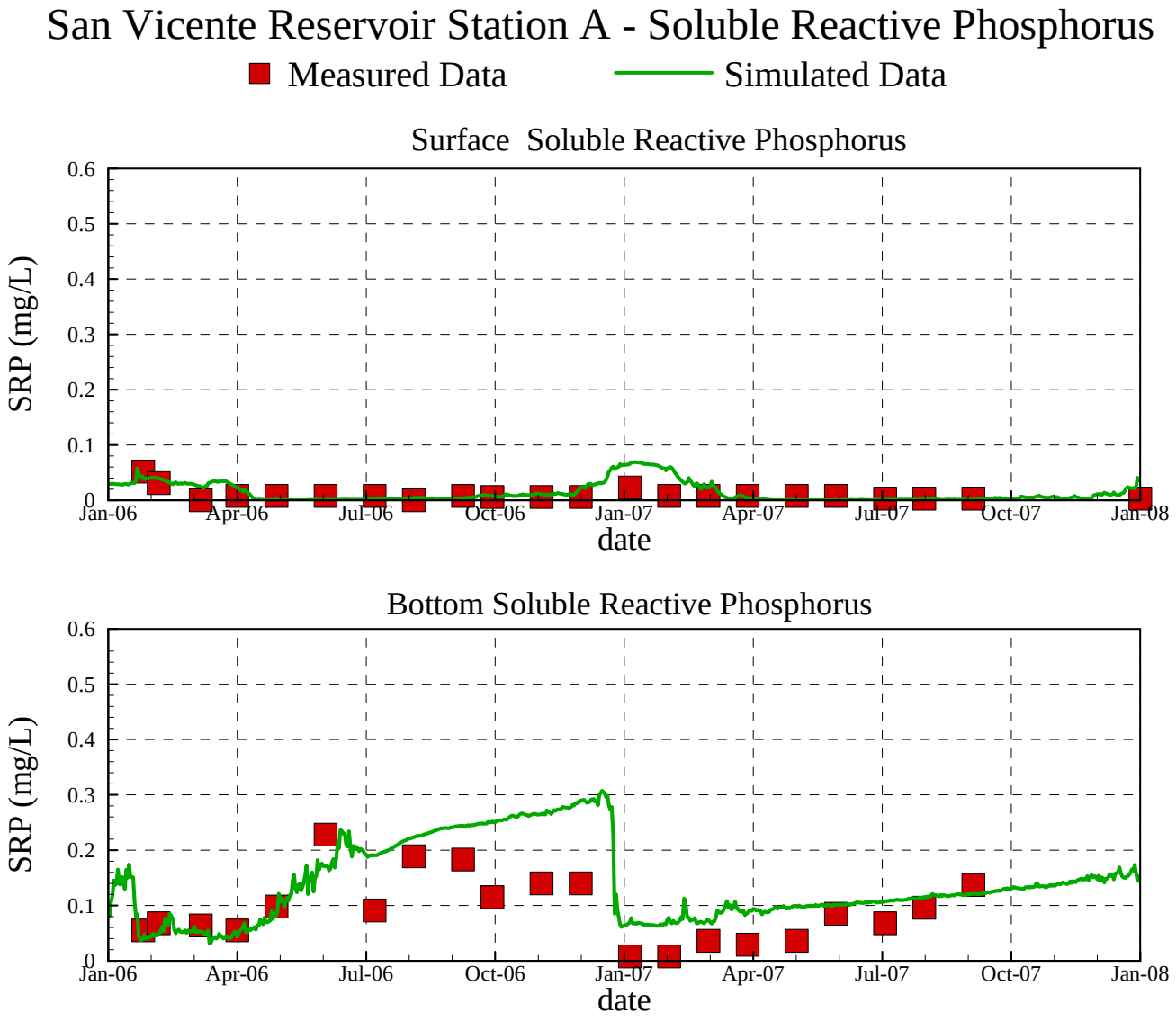

FSI V094005
May 01, 2012

Figure 43

FLOW SCIENCE®

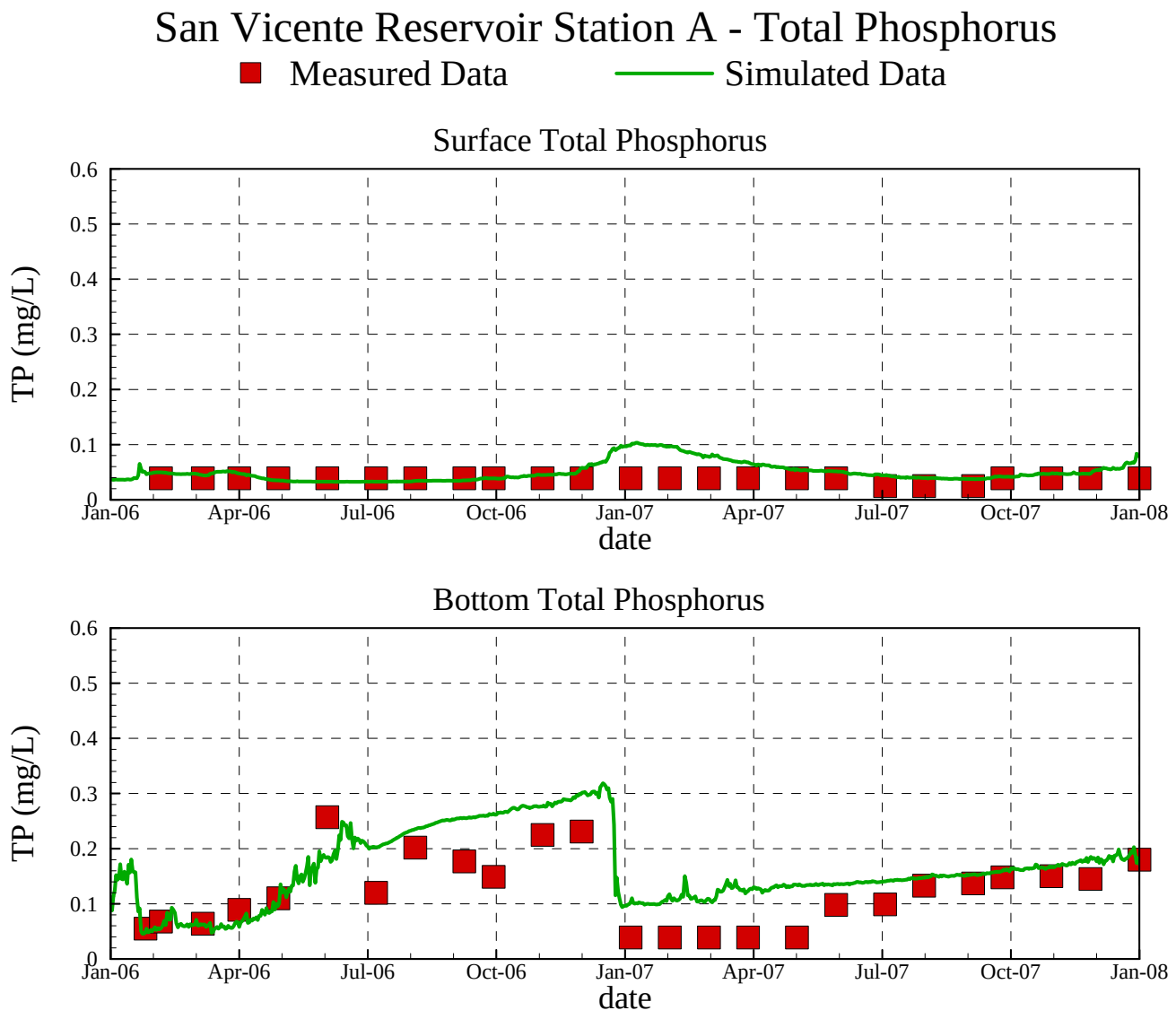

FSI V094005
May 01, 2012

Figure 44

FLOW SCIENCE®

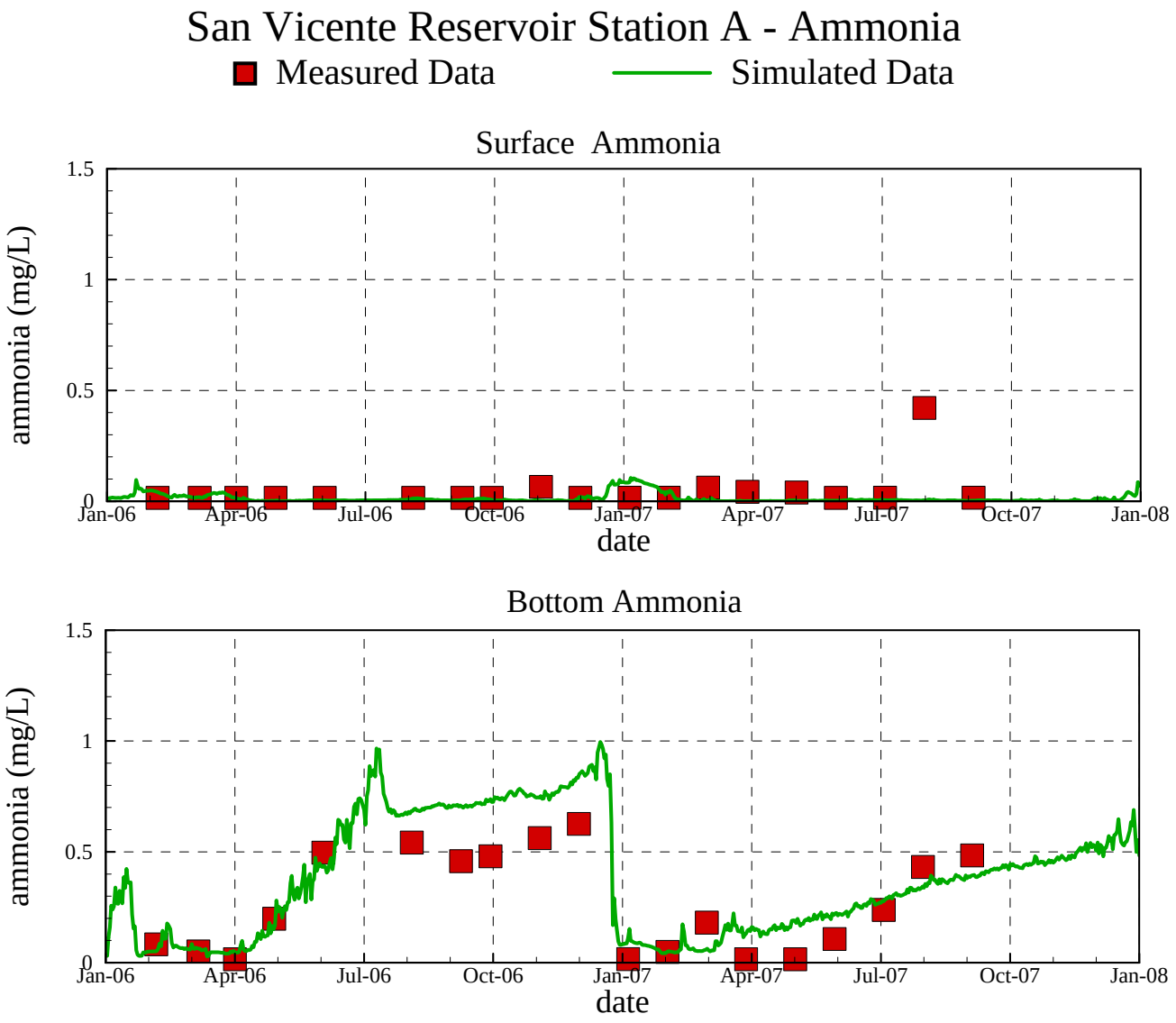

FSI V094005
May 01, 2012

Figure 45

FLOW SCIENCE®

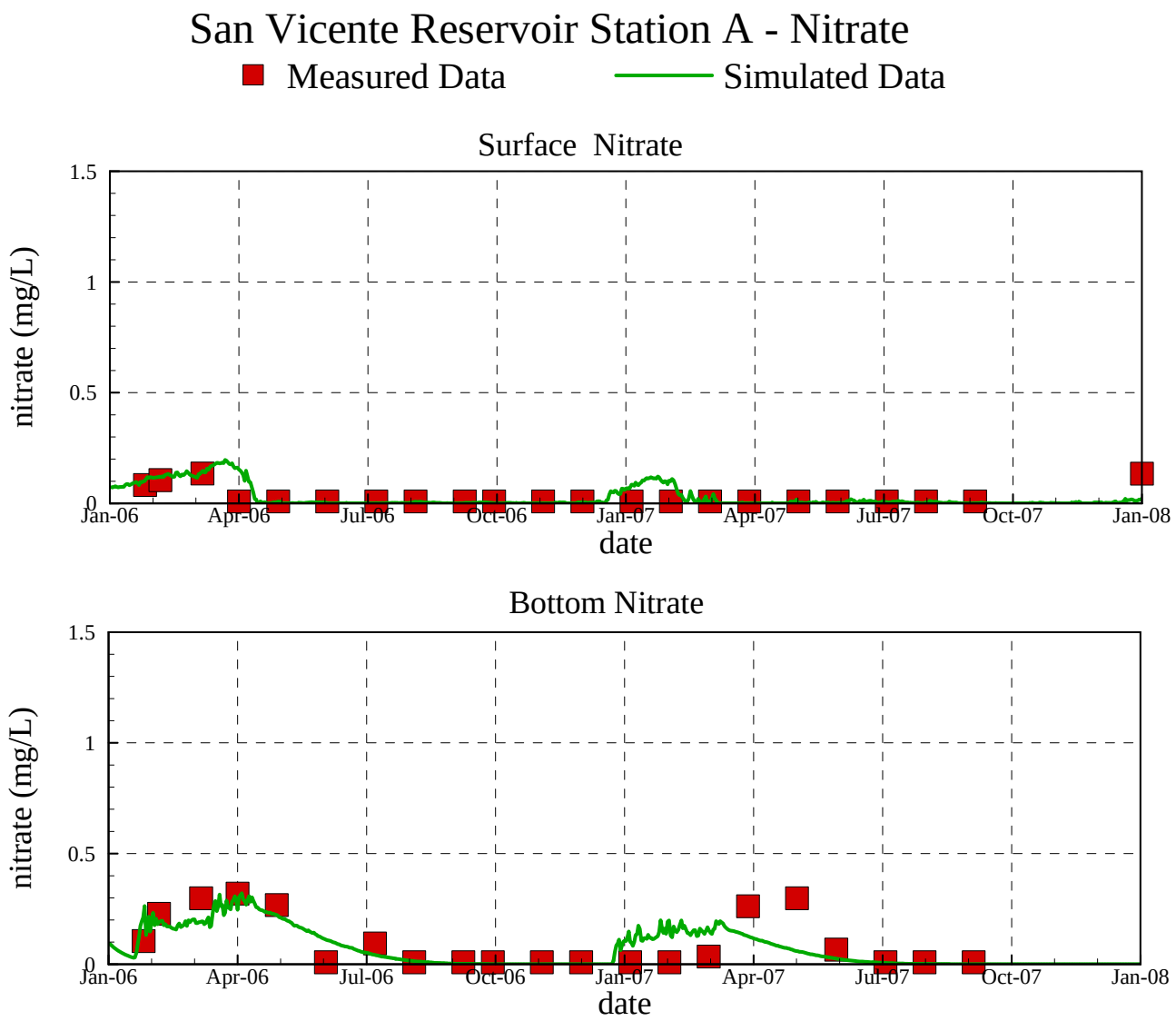

Figure 46

FSI V094005
May 01, 2012

FLOW SCIENCE®

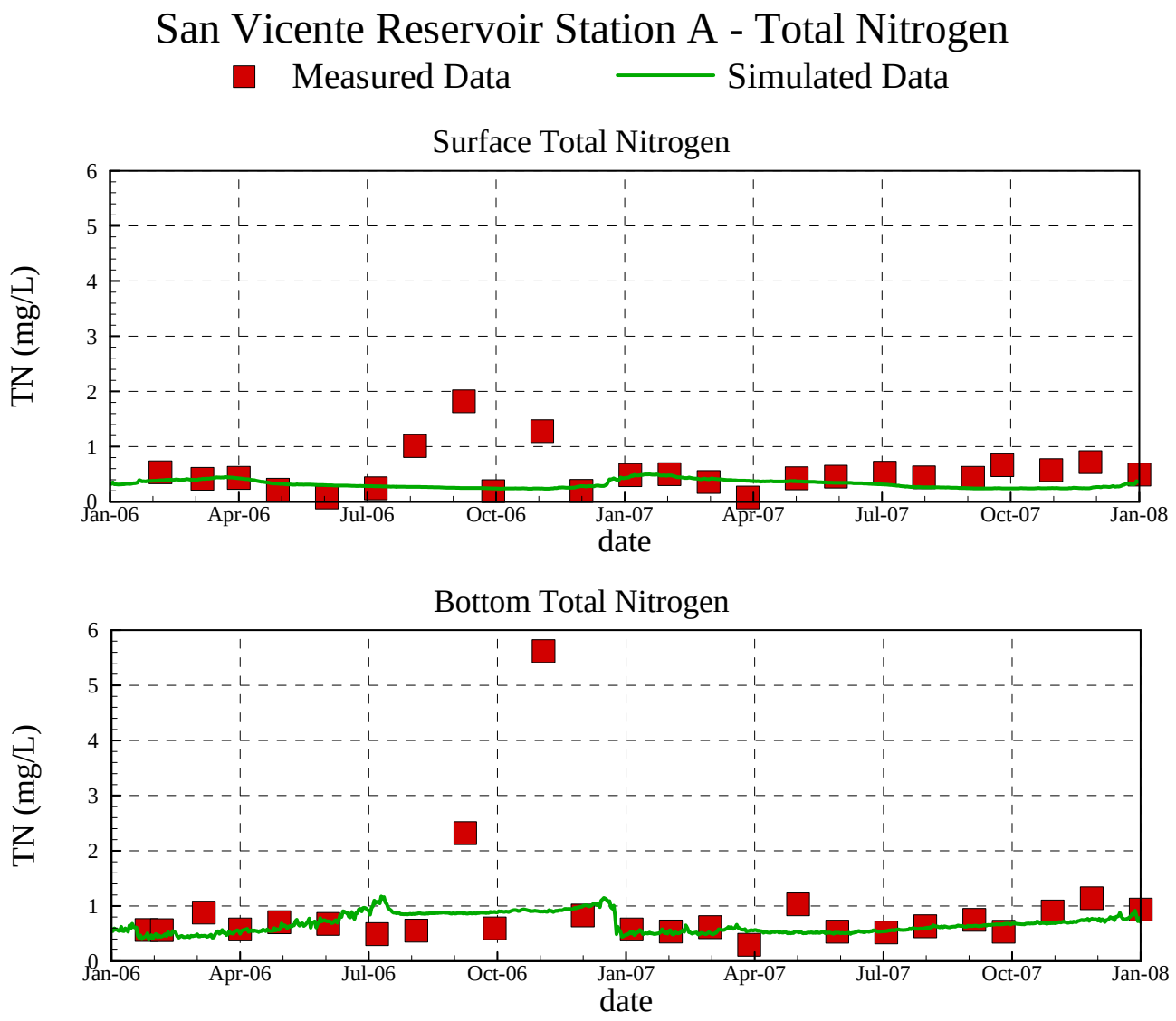

FSI V094005
May 01, 2012

Figure 47

FLOW SCIENCE®

San Vicente Reservoir

Station A – Chlorophyll a Concentrations

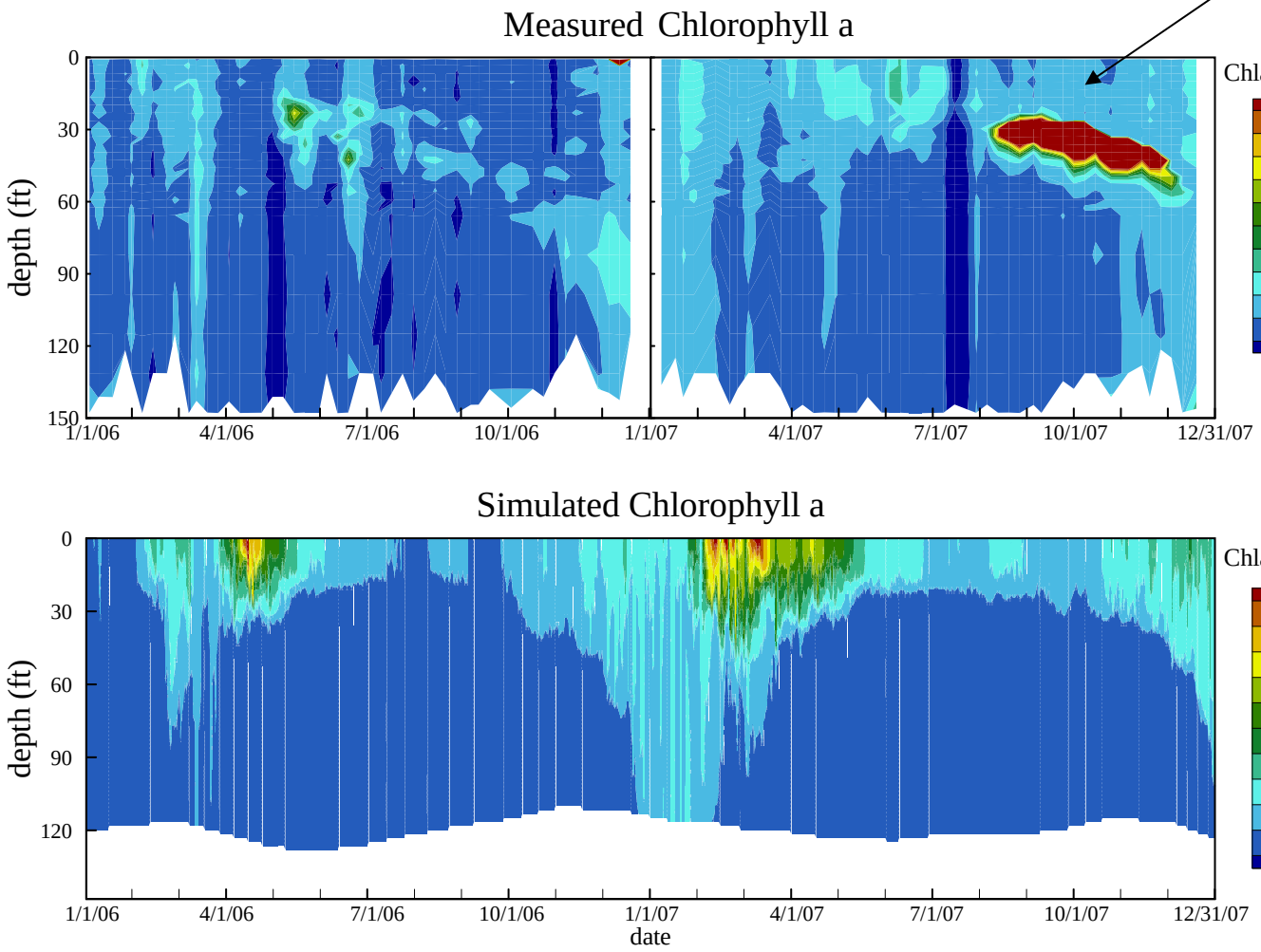

Measured DO, chlorophyll a and temperature profiles on 9/24/2007

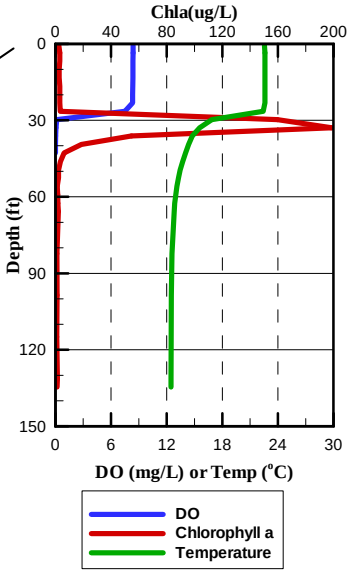

FSI V094005
May 01, 2012

Figure 48

FLOW SCIENCE®

San Vicente Reservoir Station A - Secchi Depth Calibration

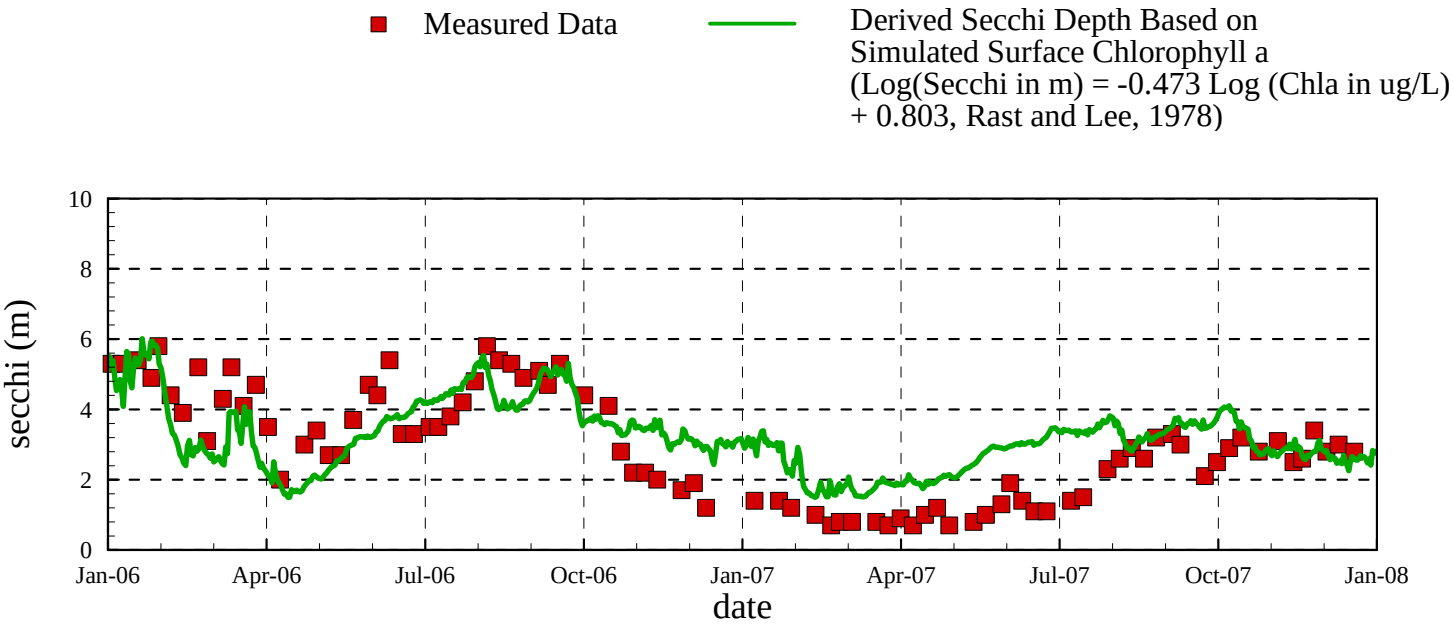

FSI V094005
May 01, 2012

Figure 49

FLOW SCIENCE®

San Vicente Reservoir

Scatter Plot of Measured vs. Simulated Secchi Depth

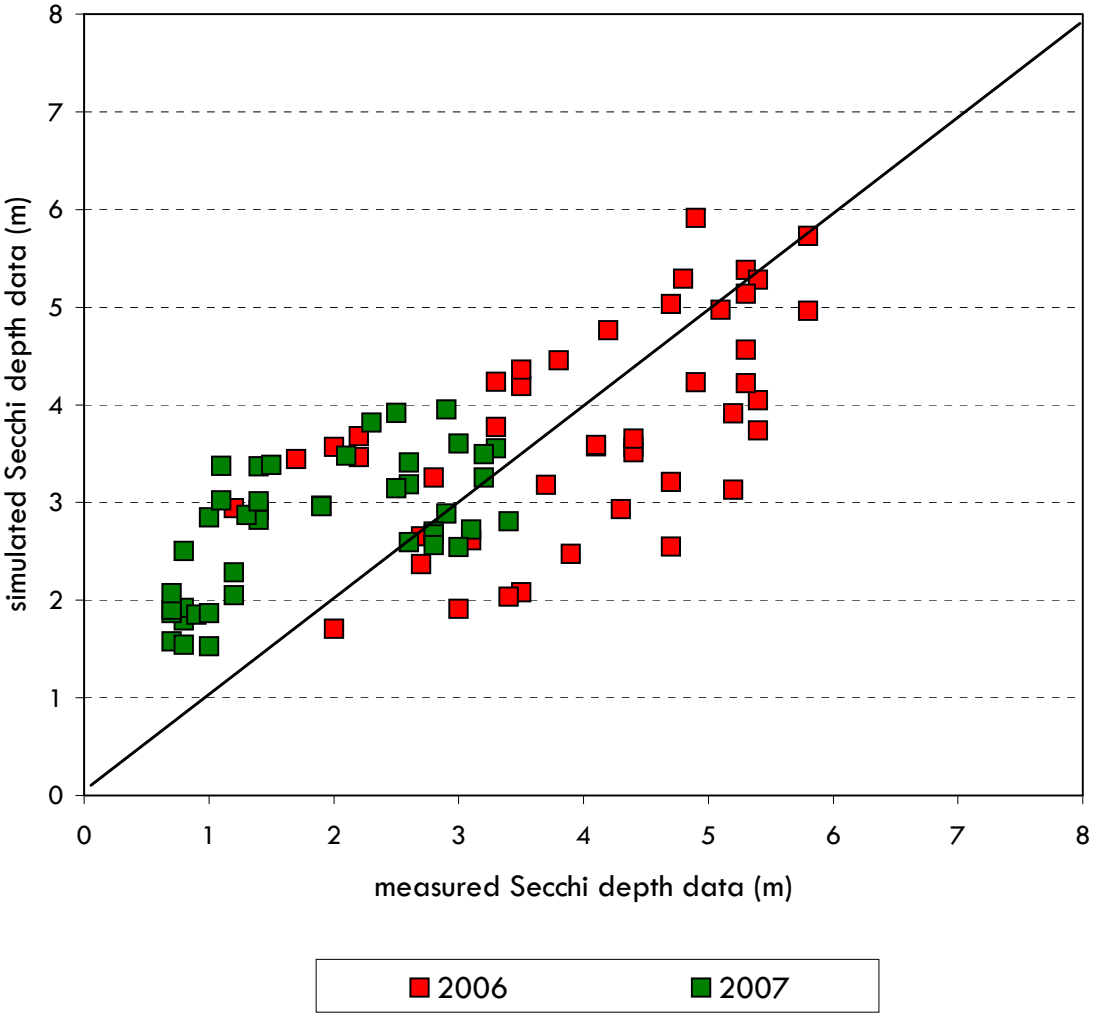

Figure 50

FSI V094005
May 01, 2012

FLOW SCIENCE®

APPENDIX A

DESCRIPTION OF ELCOM/CAEDYM MODELS AND EVIDENCE OF VALIDATION

DESCRIPTION OF ELCOM/CAEDYM MODELS AND EVIDENCE OF VALIDATION

1.0 INTRODUCTION

The coupling of biogeochemical and hydrodynamic processes in numerical simulations is a fundamental tool for research and engineering studies of water quality in coastal oceans, estuaries, lakes, and rivers. A modeling system for aquatic ecosystems has been developed that combines a three-dimensional hydrodynamic simulation method with a suite of water quality modules that compute interactions between biological organisms and the chemistry of their nutrient cycles. This integrated approach allows for the feedback and coupling between biogeochemical and hydrodynamic systems so that a complete representation of all appropriate processes can be included in an analysis. The hydrodynamic simulation code is the Estuary and Lake Computer Model (ELCOM) and the biogeochemical model is the Computational Aquatic Ecosystem Dynamics Model (CAEDYM).

The purpose of this document is to demonstrate that ELCOM and CAEDYM are accepted models that have been systematically tested and debugged, and then successfully validated in numerous applications. A history of the models is provided, followed by an outline of the general model methodology and evolution that emphasizes the basis of the ELCOM/ CAEDYM codes in previously validated models and research. Then the process of code development, testing, and validation of ELCOM/CAEDYM is detailed. Specific model applications are described to illustrate how the ELCOM/CAEDYM models have been applied to coastal oceans, estuaries, lakes, and rivers throughout the world and the results successfully validated against field data. Finally, a general description of the governing equations, numerical models, and processes used in the models is provided along with an extensive bibliography of supporting material.

A comprehensive description of the equations and methods used in the models is provided in the "The CWR Estuary and Lake Computer Model, User Guide" by Hodges (1999), "Estuary and Lake Computer Model, ELCOM Science Manual Code Version 1.5.0" by Hodges and Dallimore (2001), "Computational Aquatic Ecosystem Dynamics Model, CAEDYM: User Manual" (1999), and the "Computational Aquatic Ecosystem Dynamics Model (CAEDYM), An Ecological Water Quality Model Designed for Coupling with Hydrodynamic Drivers, Scientific Manual" by Hamilton and Herzfeld (1999).

2.0 MODEL HISTORY

The ELCOM/CAEDYM models were originally developed at the Centre for Water Research (CWR) at the University of Western Australia, although the hydrodynamics code ELCOM is an outgrowth of a hydrodynamic model developed earlier by Professor Vincenzo Casulli in Italy and now in use at Stanford University under the name TRIM-3D. The CAEDYM model was essentially developed at CWR as an outgrowth of earlier water quality modules used in the one-dimensional model, Dynamic Reservoir Simulation Model - Water Quality (DYRESM-WQ, Hamilton and Schladow, 1997).

The original ELCOM/CAEDYM models, as developed by CWR, were implemented in Fortran 90 (with F95 extensions) on a UNIX computer system platform. In 2001, the codes for both models were ported to a personal computer (PC) platform through an extensive recompiling and debugging effort by Flow Science Incorporated (Flow Science) in Pasadena, California.

3.0 MODEL METHODOLOGY

ELCOM is a three-dimensional numerical simulation code designed for practical numerical simulation of hydrodynamics and thermodynamics for inland and coastal waters. The code links seamlessly with the CAEDYM biogeochemical model undergoing continuous development at CWR, as shown graphically in **Figure 1**. The combination of the two codes provides three-dimensional simulation capability for examination of changes in water quality that arise from anthropogenic changes in either quality of inflows or reservoir operations.

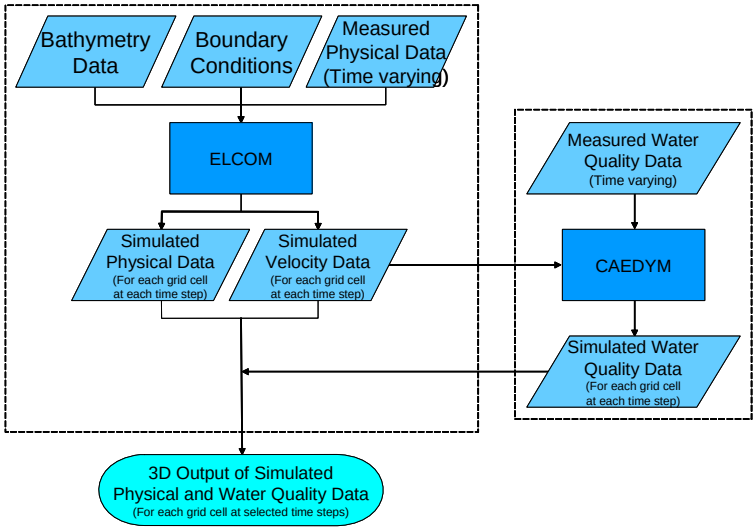

Figure 1 Flow chart showing the integration of the linked ELCOM/CAEDYM models.

The numerical method used in ELCOM is based on the TRIM-3D model scheme of Casulli and Cheng (1992) with adaptations made to improve accuracy, scalar conversion, numerical diffusion, and implementation of a mixed-layer model. The ELCOM model also extends the TRIM-3D scheme by including conservative advection of scalars. The unsteady Reynolds-averaged, Navier-Stokes equations, and the scalar transport equations serve as the basis of ELCOM. The pressure distribution is assumed hydrostatic and density changes do not impact the inertia of the fluid (the Boussinesq approximation), but are considered in the fluid body forces. There is an eddy-viscosity approximation for the horizontal turbulence correlations that represent the turbulent momentum transfer. Vertical momentum transfer is handled by a Richardson number-based diffusion coefficient. Since numerical diffusion generally dominates molecular processes, molecular diffusion in the vertical direction is neglected in ELCOM.

Both ELCOM and TRIM-3D are three-dimensional, computational fluid dynamics (CFD) models. CFD modeling is a validated and well-established approach to solving the equations of fluid motions in a variety of disciplines. Prior to the development of TRIM-3D, there were difficulties in modeling density stratified flows and such flows required special numerical methods. With TRIM-3D, Casulli and Cheng (1992) developed the first such successful method to model density-stratified flows, such as occur in the natural environment. Since then, TRIM-3D has been validated by numerous publications. ELCOM is based on the same proven method, but incorporates additional improvements as described above. Furthermore, the ELCOM model is based on governing equations and numerical algorithms that have been used in the past (e.g., in validated models such as TRIM-3D), and have been validated in refereed publications. For example:

- The hydrodynamic algorithms in ELCOM are based on the Euler-Lagrange method for advection of momentum with a conjugate gradient solution for the free-surface height (Casulli and Cheng, 1992).
- The free-surface evolution is governed by vertical integration of the continuity equation for incompressible flow applied to the kinematic boundary condition *(e.g.*, Kowalik and Murty, 1993).
- The numerical scheme is a semi-implicit solution of the hydrostatic Navier-Stokes equations with a quadratic Euler-Lagrange, or semi-Lagrangian (Staniforth and Côté, 1991).
- Passive and active scalars (*i.e.*, tracers, salinity, and temperature) are advected using a conservative ULTIMATE QUICKEST discretization (Leonard, 1991). The ULTIMATE QUICKEST approach has been implemented in two-dimensional format and demonstration of its effectiveness in estuarine flows has been documented by Lin and Falconer (1997).

- Heat exchange is governed by standard bulk transfer models found in the literature (*e.g.*, Amorocho and DeVries, 1980; Imberger and Patterson, 1981; Jacquet, 1983).
- The vertical mixing model is based on an approach derived from the mixing energy budgets used in one-dimensional lake modeling as presented in Imberger and Patterson (1981), Spigel *et al* (1986), and Imberger and Patterson (1990). Furthermore, Hodges presents a summary of validation using laboratory experiments of Stevens and Imberger (1996). This validation exercise demonstrates the ability of the mixed-layer model to capture the correct momentum input to the mixed-layer and reproduce the correct basin-scale dynamics, even while boundary-induced mixing is not directly modeled.
- The wind momentum model is based on a mixed-layer model combined with a model for the distribution of momentum over depth (Imberger and Patterson, 1990).

The numerical approach and momentum and free surface discretization used in ELCOM are defined in more detail in Hodges, Imberger, Saggio, and Winters (1999). Similarly, the water quality processes and methodology used in CAEDYM are described in more detail in Hamilton and Schladow (1997). Further technical details on ELCOM and CAEDYM are provided in Sections 5.0 and 6.0 below.

4.0 VALIDATION AND APPLICATION OF ELCOM/CAEDYM

Since initial model development, testing and validation of ELCOM and/or CAEDYM have been performed and numerous papers on model applications have been presented, written, and/or published as described in more detail below. In summary:

- ELCOM solves the full three-dimensional flow equations with small approximations.
- ELCOM/CAEDYM was developed, tested, and validated over a variety of test cases and systems by CWR.
- Papers on ELCOM/CAEDYM algorithms, methodology, and applications have been published in peer reviewed journals such as the *Journal of Geophysical Research*, the *Journal of Fluid Mechanics*, the *Journal of Hydraulic Engineering*, the *International Journal for Numerical Methods in Fluids*, and *Limnology and Oceanography*.
- ELCOM/CAEDYM was applied by Flow Science to Lake Mead, Nevada. As part of this application, mass balances were verified and results were presented to a model review panel over a two-year period. The model review panel, the National Park Service, the Bureau of Reclamation, the Southern Nevada Water Authority, and the Clean Water Coalition (a

consortium of water and wastewater operators in the Las Vegas, Nevada, region) all accepted the ELCOM/CAEDYM model use and validity.

- There are numerous applications of ELCOM/CAEDYM in the literature that compare the results to data, as summarized in Section 3.2.

The process of code development, testing, and validation of ELCOM/CAEDYM by CWR, and the ongoing validation and refinement of the codes through further application of the models are detailed in the following subsections. The major components of the development, testing, and validation process are summarized in **Figure 2**.

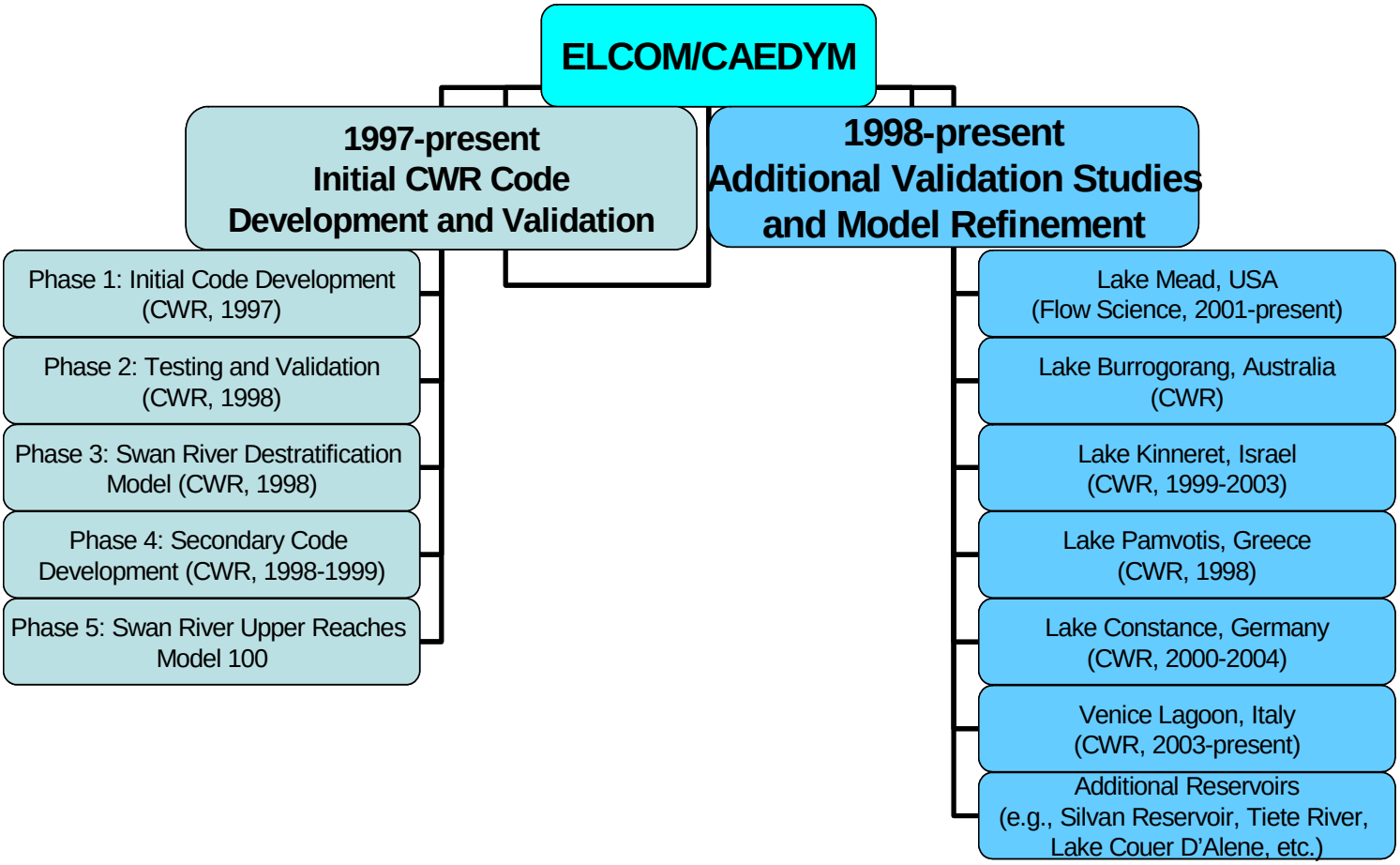

Figure 2 ELCOM/CAEDYM code development, testing, validation, and applications by CWR and Flow Science Incorporated.

4.1 CWR CODE DEVELOPMENT, TESTING, AND VALIDATION

Initial development of the code by CWR occurred from March through December 1997 (Phase 1), followed by a period of testing and validation from January through April 1998 (Phases 2 and 3). Secondary code development by CWR occurred from September 1998 through February 1999 (Phase 4). Testing and validation were performed over a variety of test cases and systems to ensure that all facets of the code were tested. In addition, Phase 5 modeling of the Swan River since 1998 has been used to gain a better understanding of the requirements and limitations of the model (Hodges *et al*, 1999).

4.1.1 Phase 1: Initial Code Development

The ELCOM code was initially conceived by CWR as a Fortran 90/95 adaptation of the TRIM-3D model of Casulli and Cheng (1992) in order to: 1) link directly to the CAEDYM water quality module developed concurrently at CWR and 2) provide a basis for future development in a modern programming language. Although written in Fortran 77, TRIM-3D is considered a state-of-the-art numerical model for estuarine applications using a semi-implicit discretization of the Reynolds-averaged hydrostatic Navier-Stokes equations and an Euler-Lagrange method for momentum and scalar transport.

During development of ELCOM, it became clear that additional improvements to the TRIM-3D algorithm were required for accurate solution of density-stratified flows in estuaries. After the basic numerical algorithms were written in Fortran 90, subroutine-by-subroutine debugging was performed to ensure that each subroutine produced the expected results. Debugging and testing of the entire model used a series of test cases that exercised the individual processes in simplified geometries. This included test cases for the functioning of the open boundary condition (tidal forcing), surface wave propagation, internal wave propagation, scalar transport, surface thermodynamics, density underflows, wind-driven circulations, and flooding/drying of shoreline grid cells. Shortcomings identified in the base numerical algorithms were addressed during secondary code development (Phase 4).

Towards the end of the initial code development, ELCOM/CAEDYM were coupled and test simulations were run to calibrate the ability of the models to work together on some simplified problems. Results showing the density-driven currents induced by phytoplankton shading were presented at the Second International Symposium on Ecology and Engineering (Hodges and Herzfeld, 1997). Further details of modeling of density-driven currents due to combinations of topographic effects and phytoplankton shading were presented at a joint meeting of the American Geophysical Union (AGU) and the American Society of Limnology and Oceanography (ASLO) by Hodges *et al*. (1998), and at a special seminar at Stanford University (Hodges 1998).

Additionally, presentations by Hamilton (1997), Herzfeld *et al*. (1997), and Herzfeld and Hamilton (1998) documented the concurrent development of the CAEDYM ecological model.

4.1.2 Phase 2: Testing and Validation

The simplified geometry tests of Phase I revealed deficiencies in the TRIM-3D algorithm including the inability of the TRIM-3D Euler-Lagrange method (ELM) to provide conservative transport of scalar concentrations (e.g., salinity and temperature). Thus, a variety of alternate scalar transport methods were tested, with the best performance being a flux-conservative implementation of the ULTIMATE filter applied to third-order QUICKEST discretization based on the work of Leonard (1991).

Model testing and validation against simple test cases was again undertaken. In addition, a simulation of a winter underflow event in Lake Burragorang in New South Wales, Australia, was performed to examine the ability of the model to capture a density underflow in complex topography in comparison to field data taken during the inflow event. These tests showed that the ability to model underflows is severely constrained by the cross-channel grid resolution.

4.1.3 Phase 3: Swan River Destratification Model

Phase 3 involved examining a linked ELCOM/CAEDYM destratification model of the Swan River system during a period of destratification in 1997 when intensive field monitoring had been conducted. The preliminary results of this work were presented at the Swan-Canning Estuary Conference (Hertzfeld *et al*, 1998). More comprehensive results were presented at the Western Australian Estuarine Research Foundation (WAERF) Community Forum (Imberger, 1998).

4.1.4 Phase 4: Secondary Code Development

In conducting the Phase 3 Swan River destratification modeling, it became clear to CWR that long-term modeling of the salt-wedge propagation would require a better model for mixing dynamics than presently existed. Thus, the availability of an extensive field data set for Lake Kinneret, Israel, led to its use as a test case for development of an improved mixing algorithm for stratified flows (Hodges *et al*, 1999).

A further problem appeared in the poor resolution of momentum terms using the linear ELM discretization (*i.e.*, as used in the original TRIM-3D method). Since the conservative ULTIMATE QUICKEST method (used for scalar transport, see Phase 1 above) does not lend itself to efficient use for discretization of momentum terms in a semi-implicit method, a quadratic ELM approach was developed for more accurate discretization of the velocities.

4.1.5 Phase 5: Swan River Upper Reaches Model

Phases 1-4 developed and refined the ELCOM code for accurate modeling of three-dimensional hydrodynamics where the physical domain is well resolved. Phase 5 is an ongoing process of model refinement that concentrates on developing a viable approach to modeling longer-term evolution hydrodynamics and water quality in the Swan River where fine-scale resolution of the domain is not practical. The Swan River application is also used for ongoing testing and calibration of the CAEDYM water quality module.

The Swan River estuary is located on the Swan Coastal Plain, Western Australia. It is subject to moderate to high nutrient loads associated with urban and agricultural runoff and suffered from *Microcystis aeruginosa* blooms in January 2000. In an effort to find a viable means of conducting seasonal to annual simulations of the Swan River that retain the fundamental along-river physics and the cross-channel variability in water quality parameters, CWR has developed and tested ELCOM/CAEDYM extensively. A progress report by Hodges *et al* (1999) indicates that ELCOM is capable of accurately reproducing the hydrodynamics of the Swan River over long time scales with a reasonable computational time.

Furthermore, studies conducted by Robson and Hamilton (2002) proved that ELCOM/CAEDYM accurately reproduced the unusual hydrodynamic circumstances that occurred in January 2000 after a record maximum rainfall, and predicted the magnitude and timing of the *Microcystis* bloom. These studies show that better identification and monitoring procedures for potentially harmful phytoplankton species could be established with ELCOM/CAEDYM and will assist in surveillance and warnings for the future.

4.2 MODEL APPLICATIONS

In addition to the initial code development, testing, and validation by CWR, numerous other applications of ELCOM/CAEDYM have been developed by CWR and validated against field data. Additionally, Flow Science has applied ELCOM/CAEDYM extensively at Lake Mead (USA) and validated the results against measured data. The results of numerous ELCOM/CAEDYM model applications are presented below.

4.2.1 Lake Mead (Nevada, USA)

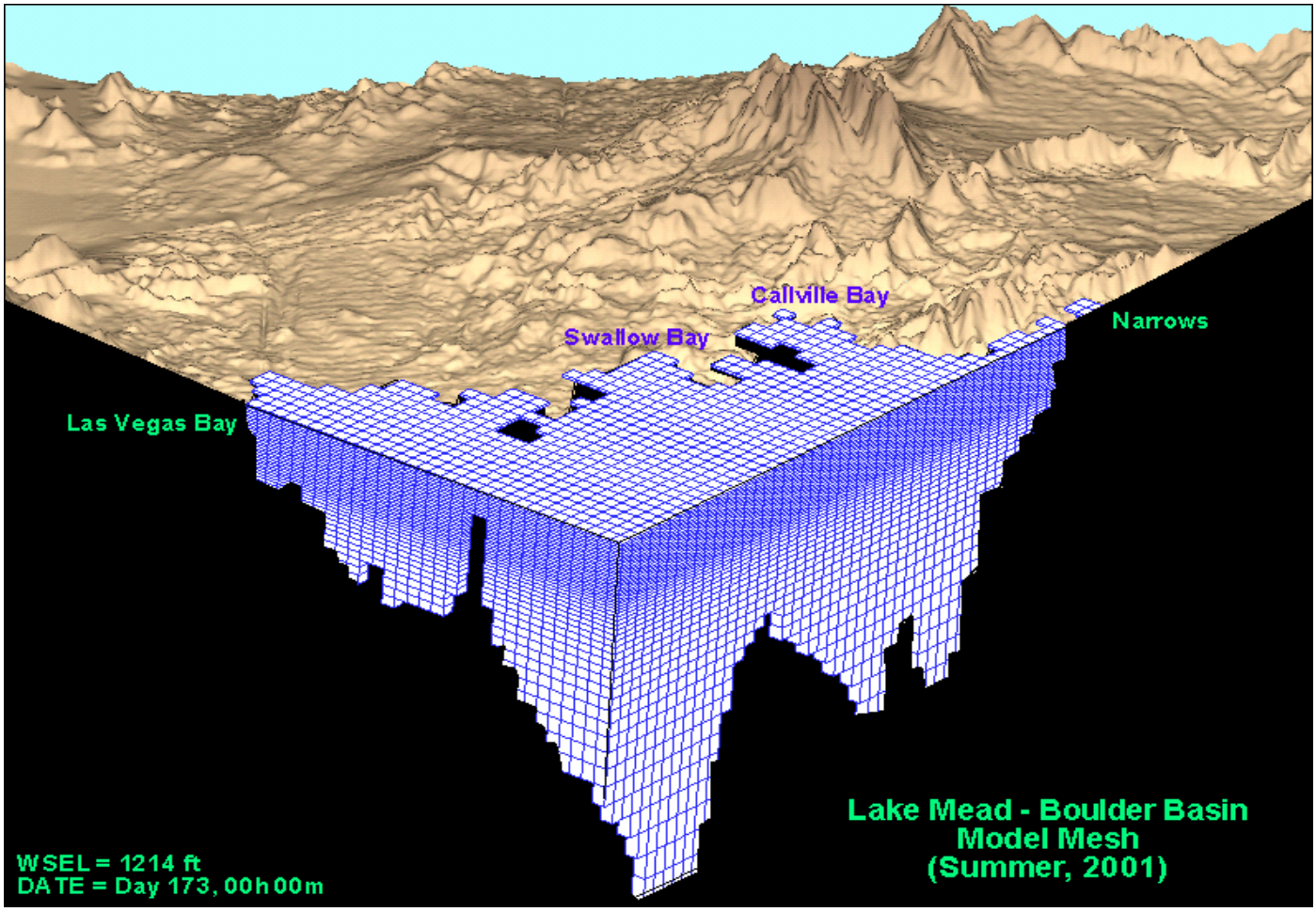

Figure 3 Model Grid for Lake Mead.

An ELCOM/CAEDYM model of Lake Mead near Las Vegas, Nevada, is being used to evaluate alternative discharge scenarios for inclusion in an Environmental Impact Statement (EIS) for the Clean Water Coalition (CWC), a consortium of water and wastewater operators in the Las Vegas region. **Figure 3** is a cut-away of the three-dimensional model grid used for Lake Mead, showing the varying grid spacing in the vertical direction. **Figure 4** is an example of the model output, showing the isopleths of a tracer plume within the reservoir for a sample case.

As part of the EIS process, a model review panel met monthly for two years to review the validation of the ELCOM/CAEDYM model, its calibration against field data, and its application. The modeling committee approved the use of the model.

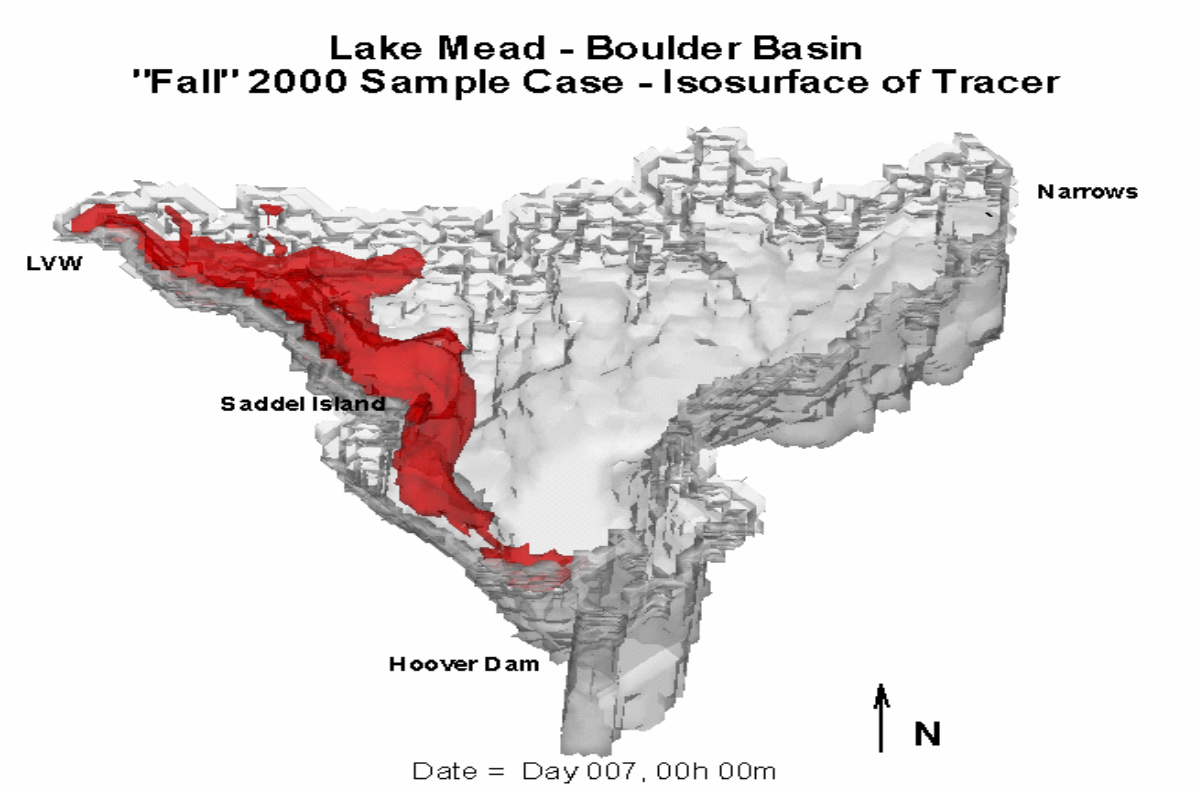

Figure 4 Lake Mead isopleths of tracer for a fall 2000 sample case.

Subsequently, a scientific Water Quality Advisory Panel concluded that the ELCOM/CAEDYM model was applicable and acceptable. The members of the Water Quality Advisory Panel were diverse and included Jean Marie Boyer, Ph.D., P.E. (Water Quality Specialist/Modeler, Hydrosphere), Chris Holdren, Ph.D., CLM (Limnologist, United States Bureau of Reclamation), Alex Horne, Ph.D. (Ecological Engineer, University of California Berkeley), and Dale Robertson, Ph.D. (Research Hydrologist, United States Geological Survey).

More specifically, the Water Quality Advisory Panel agreed on the following findings:

- The ELCOM/CAEDYM model is appropriate for the project.
- There are few three-dimensional models available for reservoirs. ELCOM is one of the best hydrodynamic models and has had good success in Lake Mead and other systems.
- The ELCOM model accurately simulates most physical processes.
- The algorithms used in CAEDYM are widely accepted (a biological consultant, Professor David Hamilton of The University of Waikato, New Zealand, has been retained to review the CAEDYM coefficients and algorithms).

The Lake Mead ELCOM/CAEDYM model was calibrated against four years of measured data for numerous physical and water quality parameters including temperature, salinity, conductivity, dissolved oxygen, pH, nutrients (nitrogen and phosphorus), chlorophyll *a*, perchlorate, chloride, sulfate, bromide, and total organic carbon. Detailed results of this calibration and the subsequent evaluation of alternative discharge scenarios will be made available in late 2005 in the CWC EIS that is currently being prepared for this project. An example of the calibration results for chlorophyll *a* for 2002 is presented in **Figure 5** below. In this figure, simulated concentrations are compared against field data measured in the lake by the United States Bureau of Reclamation (USBR) and the City of Las Vegas (COLV).

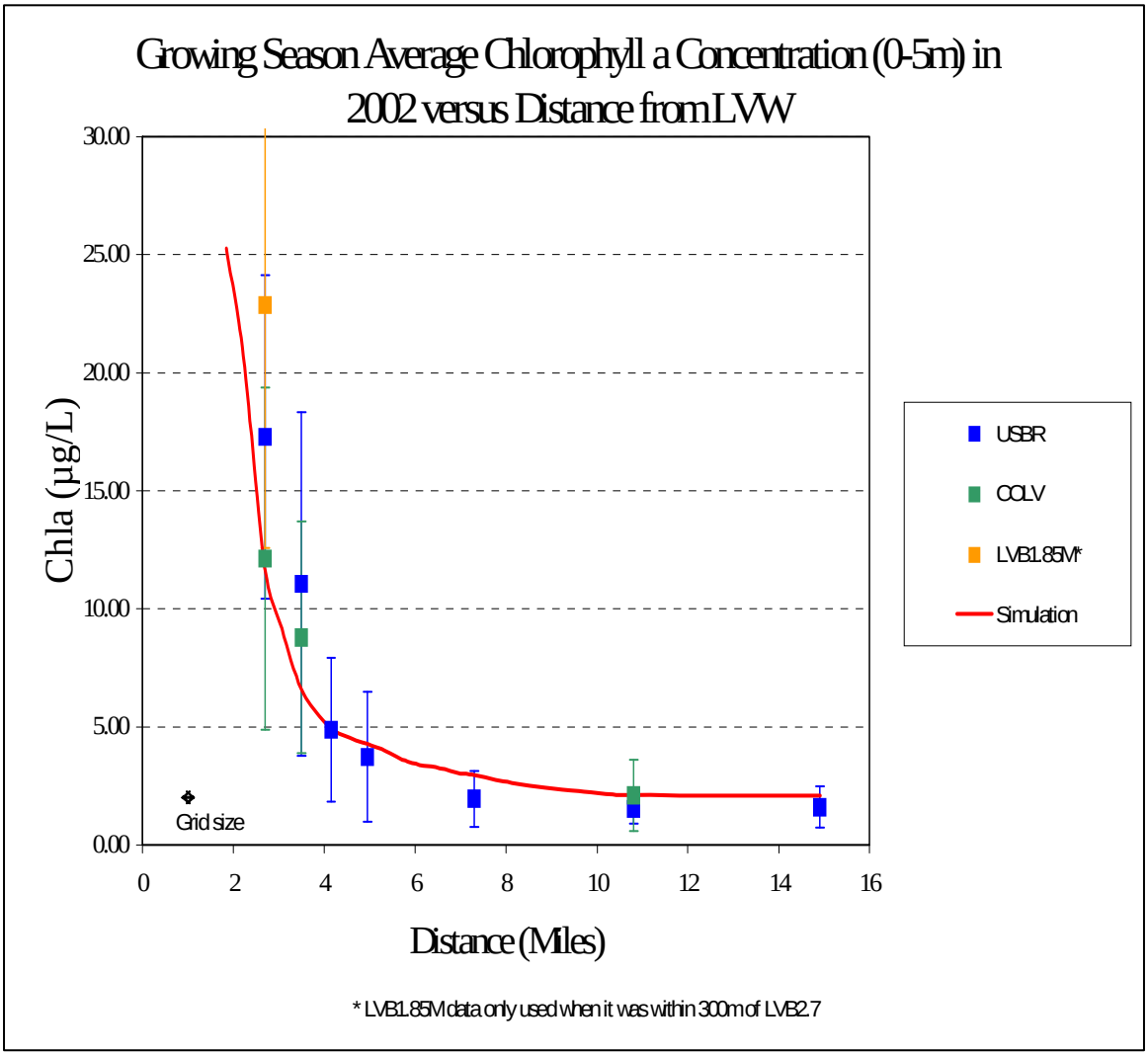

Figure 5 ELCOM/CAEDYM calibration results for chlorophyll a for 2002 as a function of distance from the inflow at Las Vegas Wash.

In addition to the good agreement between the model and field data and the acceptance of the model by the review committees, Flow Science also performed a mass balance on the model to ensure conservation of tracer materials. As a result of such tests and debugging, Flow Science and the CWR have made continuous improvements to the model as necessary including refinements to the ULTIMATE QUICKEST scheme and boundary cell representations.

4.2.2 Lake Burragorang (New South Wales, Australia)

ELCOM was applied and validated for Lake Burragorang in order to rapidly assess the potential impacts on water quality during an underflow event (CWR). Underflows usually occur during the winter when inflow water temperature is low compared to the reservoir. This causes the upheaval of hypolimnetic water at the dam wall, and as a result it transports nutrient rich waters into the euphotic zone.

The thermal dynamics during the underflow event were reproduced accurately by ELCOM for the case with idealized bathymetry data with coarse resolutions (straightened curves and rotating the lake in order to bypass the resolution problem), but not for the simulation with the complex, actual bathymetry. This is because the model tests showed that the ability to model underflows is severely constrained by the cross-channel grid resolution. When the cross-channel direction is poorly resolved at bends and curves, an underflow is unable to propagate downstream without a significant loss of momentum. Nevertheless, the simulations with the coarse idealized domain certainly can be used as aids and tools to visualize the behavior of reservoirs. Particularly, ELCOM was able to capture the traversal of the underflow down the length of Lake Burragorang and then had sufficient momentum to break against the wall causing the injection of underflow waters into the epilimnion near the dam. This simulated dynamic was in agreement with what was measured in the field.

4.2.3 Lake Kinneret (Israel)

ELCOM was applied to model basin-scale internal waves that are seen in Lake Kinneret, Israel, since understanding of basin-scale internal waves behaviors provide valuable information on mixing and transport of nutrients below the wind-mixed layer in stratified lakes. In studies done by Hodges *et al*. (1999) and Laval *et al* (2003), the ELCOM simulation results were compared with field data under summer stratification conditions to identify and illustrate the spatial structure of the lowest-mode basin-scale Kelvin and Poincare waves that provide the largest two peaks in the internal wave energy spectra. The results demonstrated that while ELCOM showed quantitative differences in the amplitude and steepness of the waves as well as in the wave phases, the basin-scale waves were resolved very well by ELCOM. In particular, the model captures the qualitative nature of the peaks and troughs in the thermocline and the depth of the wind-mixed layer at relatively coarse vertical grid resolutions (Hodges *et al*, 1999).

4.2.4 Lake Pamvotis (Greece)

ELCOM/CAEDYM was applied to Lake Pamvotis, a moderately sized (22 km^2), shallow (4 m average depth) lake located in northwest Greece. Since the lake has undergone eutrophication over the past 40 years, many efforts are directed at understanding the characteristics of the lake and developing watershed management and restoration plans.

Romero and Imberger (1999) simulated Lake Pamvotis over a one month period during May to June, 1998, and compared the simulated thermal and advective dynamics of the lake with data obtained from a series of field experiments. The simulation results over-predicted heating; however, diurnal fluctuations in thermal structures were similar to those measured. Since the meteorological site was sheltered from the winds, the wind data used in the simulation was believed to be too low, causing insufficient evaporative heat-loss and subsequent over-heating by ELCOM. An increase in the wind speed by a factor of three gave temperature profiles in agreement with the field data. Moreover, the study demonstrated that the model is capable of predicting the substantial diurnal variations in the intensity and direction of both vertical and horizontal velocities. Romero and Imberger were also able to illustrate the functionality of ELCOM when coupled to the water quality model, CAEDYM, and confirmed that the model could be used to evaluate the effect of various strategies to improve poor water quality in localized areas in the lake.

4.2.5 Lake Constance (Germany, Austria, Switzerland)

Appt (2000) and Appt *et al*. (2004) applied ELCOM to characterize the internal wave structures and motions in Lake Constance since internal waves are a key factor in understanding the transport mechanisms for chemical and biological processes in a stratified lake such as Lake Constance. Lake Constance is an important source of drinking water and a major tourism destination for its three surrounding countries of Germany, Austria, and Switzerland. Due to anthropogenic activities and climatic changes, Lake Constance water quality has deteriorated and its ecosystem has changed.

It was shown that ELCOM was able to reproduce the dominant internal wave and major hydrodynamic processes occurring in Lake Constance. For instance, three types of basin-scale waves were found to dominate the wave motion: the vertical mode-one Kelvin wave, the vertical mode-one Poincare waves, and a vertical mode-two Poincare wave. Moreover, an upwelling event was also reproduced by ELCOM suggesting that the width and length ratio of the basin, spatial variations in the wind, and Coriolis effects play critical roles in the details of the upwelling event. This on-going research has shown that ELCOM can be used as a tool to predict and understand hydrodynamics and water quality in lakes.

4.2.6 Venice Lagoon (Italy)

ELCOM/CAEDYM is being used to develop a hydrodynamic and sediment transport model of Venice Lagoon, Italy, since future gate closures at the mouth of the lagoon are likely to impact flushing patterns. This project is an integral part of the Venice Gate Projects in Italy that was launched in May 2003 to prevent flooding.

ELCOM was validated for the tidal amplitude and phase using the data obtained from 12 tidal stations located throughout the lagoon (Yeates, 2004). Remaining tasks include model validation of temperature, salinity, and velocity against measurements made in the major channels of the lagoon.

4.2.7 Silvan Reservoir (Australia)

ELCOM is currently being applied to reproduce the circulation patterns observed in Silvan Reservoir, Australia, during a field experiment that was conducted in March 2004 to determine the transport pathways in the lake. This experiment confirmed the upwelling behavior of the lake and the strong role of the inflows in creating hydraulic flows in the reservoir (Antenucci, 2004).

4.2.8 Billings and Barra Bonita Reservoirs (Brazil)

ELCOM/CAEDYM is being applied to Billings and Barra Bonita Reservoirs in Brazil. Billings Reservoir is an upstream reservoir that feeds Barra Bonita via the Tiete River. The objective of the project is to develop an integrated management tool for these reservoirs and river reaches for use in the future planning of water resource utilization in Sao Paulo, Brazil (Romero and Antenucci, 2004).

4.2.9 Lake Coeur D'Alene (Idaho, USA)

ELCOM/CAEDYM is being applied to investigate the trade-off between reducing heavy metal concentrations and a potential increase in eutrophication due to remediation procedures in Lake Coeur D'Alene, Idaho. In order to investigate heavy metal fate and transport, CAEDYM is being improved further to include heavy metals and a feedback loop to phytoplankton based on metal toxicity (Antenucci, 2004).

4.2.10 Lake Perris (California, USA)

ELCOM was applied to Lake Perris in order to compare the impacts of several recreational use strategies on measured fecal coliform concentrations at the outlet tower. The physical results of the simulation were validated against measured temperature and salinity data over a one-year period. The comparison of fecal coliform concentrations

against measured data was fair due to a lack of data describing the timing and magnitude of loading and the settling and re-suspension of fecal matter.

4.2.11 Other Applications

Other ELCOM/CAEDYM applications and development in on-going research at CWR include:

- Plume dynamics and horizontal dispersion (Marmion Marine Park, Australia).
- Inflow and pathogen dynamics (Helena, Myponga and Sugarloaf Reservoirs, Australia).
- Mixing and dissipation in stratified environments (Tone River, Japan, and Brownlee Reservoir, USA).
- Tidally forced estuaries and coastal lagoons (Marmion Marine Park and Barbamarco Lagoon, Italy).
- Three-dimensional circulation induced by wind and convective exchange (San Roque Reservoir, Argentina, and Prospect Reservoir, Australia).
- Sea-surface temperature fluctuation and horizontal circulation (Adriatic Sea).
- Response of bivalve mollusks to tidal forcing (Barbamarco Lagoon, Italy).
- Impacts of the additional withdrawals and brine discharge into the ocean from a proposed desalination facility co-located with an existing power plant in the City of Carlsbad (California, USA).

5.0 TECHNICAL DESCRIPTION OF ELCOM

As outlined above, ELCOM solves the unsteady, viscous Navier-Stokes equations for incompressible flow using the hydrostatic assumption for pressure. ELCOM can simulate the hydrodynamics and thermodynamics of a stratified system, including baroclinic effects, tidal forcing, wind stresses, heat budget, inflows, outflows, and transport of salt, heat and passive scalars. Through coupling with the CAEDYM water quality module, ELCOM can be used to simulate three-dimensional transport and interactions of flow physics, biology, and chemistry. The hydrodynamic algorithms in ELCOM are based upon the proven semi-Lagrangian method for advection of momentum with a conjugate-gradient solution for the free-surface height (Casulli and Cheng, 1992) and a conservative ULTIMATE QUICKEST transport of scalars (Leonard, 1991). This approach is advantageous for geophysical-scale simulations since the time step can be allowed to exceed the Courant-Friedrichs-Lewy (CFL) condition for the velocity without producing instability or requiring a fully-implicit discretization of the Navier-Stokes equations.

5.1 GOVERNING EQUATIONS

Significant governing equations and approaches used in ELCOM include:

- Three-dimensional simulation of hydrodynamics (unsteady Reynolds-averaged Navier-Stokes equations).
- Advection and diffusion of momentum, salinity, temperature, tracers, and water quality variables.
- Hydrostatic approximation for pressure.
- Boussinesq approximation for density effects.
- Surface thermodynamics module accounts for heat transfer across free surface.
- Wind stress applied at the free surface.
- Dirichlet boundary conditions on the bottom and sides.

5.2 NUMERICAL METHOD

Significant numerical methods used in ELCOM include:

- Finite-difference solution on staggered-mesh Cartesian grid.
- Implicit volume-conservative solution for free-surface position.
- Semi-Lagrangian advection of momentum allows time steps with CFL > 1.0.
- Conservative ULTIMATE QUICKEST advection of temperature, salinity, and tracers.
- User-selectable advection methods for water quality scalars using upwind, QUICKEST, or semi-Lagrangian to allow trade-offs between accuracy and computational speed.
- Solution mesh is uniform in horizontal directions but allows non-uniformity in vertical direction.

The implementation of the semi-Lagrangian method in Fortran 90 includes sparse-grid mapping of three-dimensional space into a single vector for fast operation using array-processing techniques. Only the computational cells that contain water are represented in the single vector so that memory usage is minimized. This allows Fortran 90 compiler parallelization and vectorization without platform-specific modification of the code. A future extension of ELCOM will include dynamic pressure effects to account for nonlinear dynamics of internal waves that may be lost due to the hydrostatic approximation.

Because the spatial scales in a turbulent geophysical flow may range from the order of millimeters to kilometers, it is presently impossible to conduct a Direct Navier-Stokes (DNS) solution of the equations of motion (*i.e.* an exact solution of the equations).

Application of a numerical grid and a discrete time step to a simulation of a geophysical domain is implicitly a filtering operation that limits the resolution of the equations. Numerical models (or closure schemes) are required to account for effects that cannot be resolved for a particular grid or time step. There are four areas of modeling in the flow physics: (l) turbulence and mixing, (2) heat budgets, (3) hydrodynamic boundary conditions, and (4) sediment transport.

5.3 TURBULENCE MODELING AND MIXING

ELCOM presently uses uniform fixed eddy viscosity as the turbulence closure scheme in the horizontal plane (in future versions a Smagorinsky 1963 closure scheme will be implemented to represent subgrid-scale turbulence effects as a function of the resolves large-scale strain-rates). These methods are the classic "eddy viscosity" turbulence closure. With the implementation of the Smagorinsky closure, future extensions will allow the eddy-viscosity to be computed on a local basis to allow improvements in modeling local turbulent events and flow effects of biological organisms (e.g., drag induced by macroalgae or seagrass).

In the present code, the user has the option to extend the eddy-viscosity approach to the vertical direction by setting different vertical eddy-viscosity coefficients for each grid layer. However, in a stratified system, this does not adequately account for vertical turbulent mixing that may be suppressed or enhanced by the stratification (depending on the stability of the density field and the magnitude of the shear stress). To model the effect of density stratification on turbulent mixing the CWR has developed a closure model based on computation of a local Richardson number to scale. The latter is generally smaller than the time step used in geophysical simulations, so the mixing is computed in a series of partial time steps. When the mixing time-scale is larger than the simulation time step, the mixing ratio is reduced to account for the inability to obtain mixing on very short time scales. This model has the advantage of computing consistent mixing effects without regard to the size of the simulation time-step (*i.e.* the model produces mixing between cells that is purely a function of the physics and not the numerical step size).

5.4 HEAT BUDGET

The heat balance at the surface is divided into short-wave (penetrative) radiation and a heat budget for surface heat transfer effects. The surface heat budget requires user input of the net loss or gain through conduction, convection, and long wave radiation in the first grid layer beneath the free surface. The short wave range is modeled using a user-prescribed input of solar radiation and an exponential decay with depth that is a function of a bulk extinction coefficient (a Beer's law formulation for radiation absorption). This coefficient is the sum of individual coefficients for the dissolved organics ("gilvin"), phytoplankton biomass concentration, suspended solids, and the

water itself. The extinction coefficients can either be computed in the water quality module (CAEDYM) or provided as separate user input.

5.5 HYDRODYNAMIC BOUNDARY CONDITIONS

The hydrodynamic solution requires that boundary conditions on the velocity must be specified at each boundary. There are six types of boundary conditions: (1) free surface, (2) open edge, (3) inflow-outflow, (4) no-slip, (5) free-slip, and (6) a Chezy-Manning boundary stress model (the latter is presently not fully implemented). For the free surface, the stress due to wind and waves is required. The user can either input the wind/wave stress directly, or use a model that relates the surface stress to the local wind speed and direction *via* a bulk aerodynamic drag coefficient. Open boundaries (e.g. tidal inflow boundaries for estuaries) require the user to supply the tidal signature to drive the surface elevation. Transport across open boundaries is modeled by enforcing a Dirichlet condition on the free-surface height and allowing the inflow to be computed from the barotropic gradient at the boundary. Inflow-outflow boundary conditions (e.g. river inflows) are Dirichlet conditions that specify the flow either at a particular boundary location *or inside the domain*. Allowing an inflow-outflow boundary condition to be specified for an interior position (*i.e.* as a source or sink) allows the model to be used for sewage outfalls or water outlets that may not be located on a land boundary. Land boundaries can be considered zero velocity (no-slip), zero-flux (free-slip) or, using a Chezy-Manning model, assigned a computed stress.

5.6 SEDIMENT TRANSPORT

While sediment transport is fundamentally an issue of flow physics, the algorithms for the sediment transport are more conveniently grouped with the water quality algorithms in CAEDYM. Settling of suspended particulate matter is computed using Stokes law to obtain settling velocities for the top and bottom of each affected grid cell. This allows the net settling flux in each cell to be computed. A two-layer sediment model has been developed that computes resuspension, deposition, flocculation, and consolidation of sediment based on (1) the shear stress at the water/sediment interface, (2) the type of sediment (cohesive/non-cohesive), and (3) the thickness of the sediment layer. Determination of the shear stress at the water/sediment interface requires the computation of bottom shear due to current, wind, and waves. A model has been developed to account for the effects of small-scale surface waves that cannot be resolved on a geophysical-scale grid. This model computes the theoretical wave height and period for small-scale surface waves from the wind velocity, water depth, and domain fetch. From these, the wavelength and orbital velocities are calculated. The wave-induced shear stress at the bottom boundary resulting from the wave orbital velocities is combined with a model for the current-induced shear stress to obtain the total bottom shear that effects sediment resuspension. The cohesiveness of the sediment determines the critical shear stresses that are necessary to resuspend or deposit the sediments. A model of

consolidation of the sediments is used to remove lower sediment layers from the maximum mass that may be resuspended.

6.0 TECHNICAL DESCRIPTION OF CAEDYM

CAEDYM is an outgrowth of previous CWR water quality modules in DYRESM-WQ and the Estuary Lake Model - Water Quality (ELMO-WQ) codes. CAEDYM is designed as a set of subroutine modules that can be directly coupled with one, two, or three-dimensional hydrodynamic "drivers", catchment surface hydrological models, or groundwater models. Additionally, it can be used in an uncoupled capacity with specification of velocity, temperature, and salinity distributions provided as input files rather than as part of a coupled computation. The user can specify the level of complexity in biogeochemical process representation so both simple and complex interactions can be studied. Direct coupling to a hydrodynamic driver (*e.g.* ELCOM) allows CAEDYM to operate on the same spatial and temporal scales as the hydrodynamics. This permits feedbacks from CAEDYM into ELCOM for water quality effects such as changes in light attenuation or effects of macroalgae accumulation on bottom currents. **Figure 6** shows an illustration of the interactions of modeled parameters in CAEDYM. Being an “N-P-Z” (nutrient-phytoplankton-zooplankton) model, CAEDYM can be used to assess eutrophication. Unlike the traditional general ecosystem model, CAEDYM serves as a species- or group-specific model (*i.e.* resolves various phytoplankton species). Furthermore, oxygen dynamics and several other state variables are included in CAEDYM.

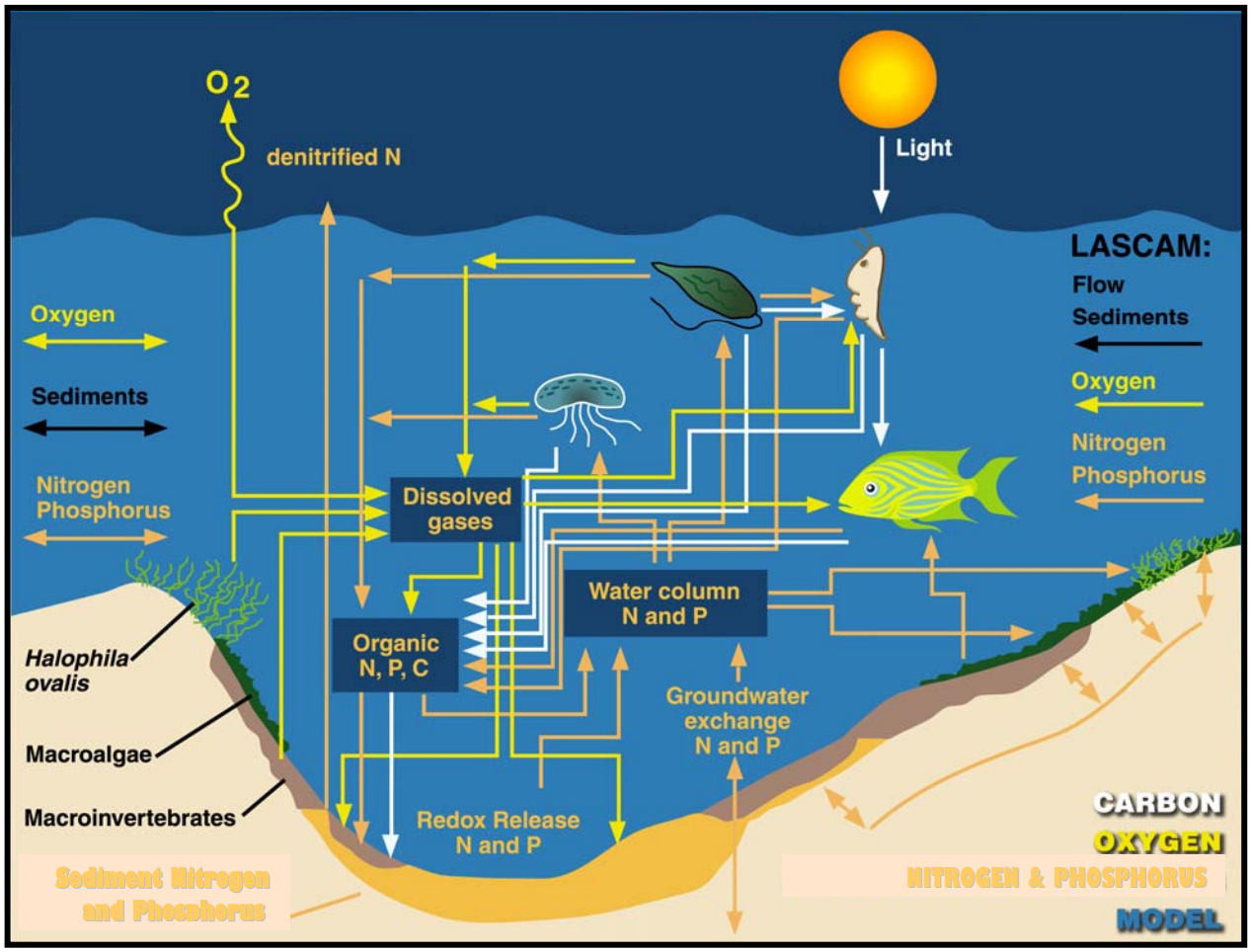

Illustration of interactions of modeled parameters in CAEDYM.

The representation of biogeochemical processes in ecological models has, historically, been treated in a simple manner. In fact, the pioneering work on modeling marine ecosystems (Riley *et al*, 1949; Steel, 1962) is still used as a template for many of the models that are currently used (Hamilton and Schladow, 1997). The level of sophistication and process representation included in CAEDYM is of a level hitherto unseen in any previous aquatic ecosystem model. This enables many different components of the system to be examined, as well as providing a better representation of the dynamic response of the ecology to major perturbations to the system (e.g. the response to various management strategies). **Figure 7** shows the major state variables included in the CAEDYM model. Using CAEDYM to aid in management decisions and

system understanding requires (1) a high level of process representation, (2) process interactions and species differentiation of several state variables, and (3) applicability over a spectrum of spatial and temporal scales. The spectrum of scales relates to the need for managers to assess the effects of temporary events, such as anoxia at specific locations, through to understanding long-term changes that may occur over seasons or years. There is considerable flexibility in the time step used for the ecological component. Long time steps (relative to the hydrodynamic advective scale) may be used to reduce the frequency of links to ELCOM when long-term (*i.e.* seasonal or annual) simulations are run.

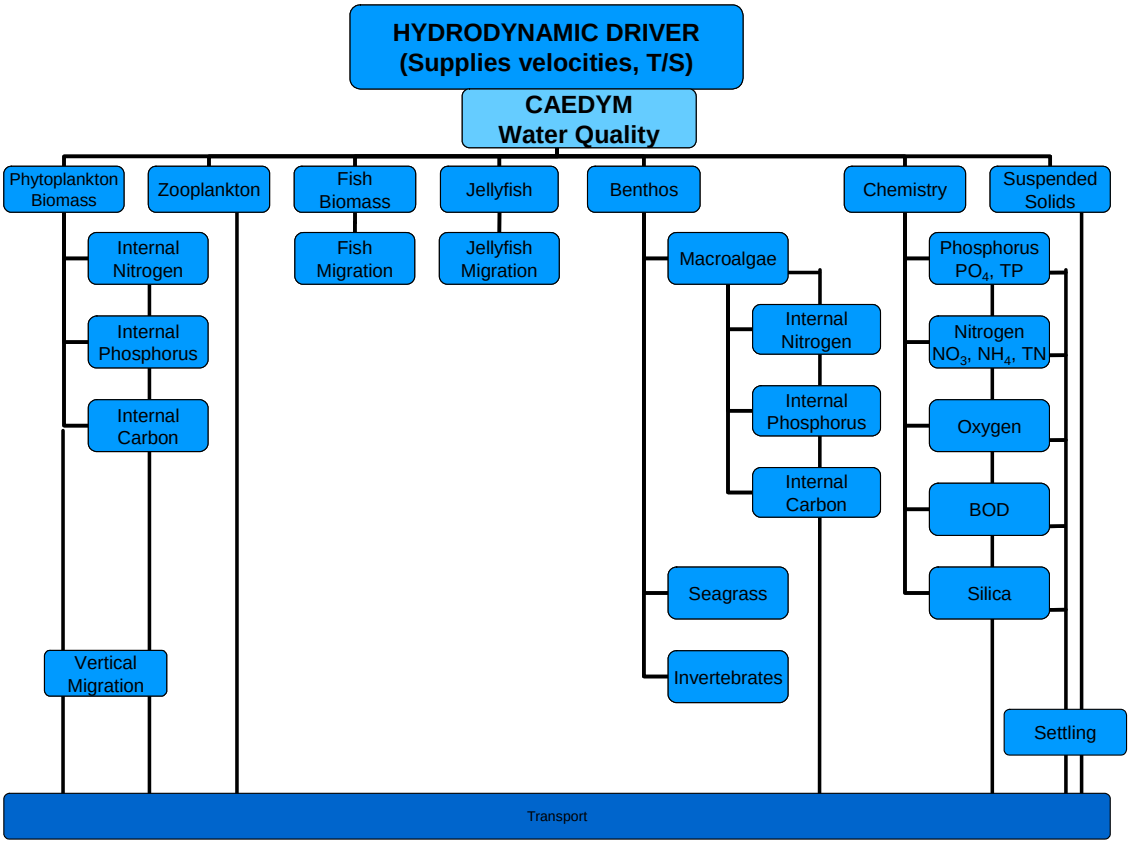

Figure 7 Major state variables included in the CAEDYM model.

6.1 BIOLOGICAL MODEL

The biological model used in CAEDYM consists of seven phytoplankton groups, five zooplankton groups, six fish groups, four macroalgae groups and three invertebrate groups, as well as models of seagrass and jellyfish. This set will be expanded as biological models are developed, tested, and calibrated to field data. There is flexibility for the user in choosing which species to include in a simulation. Vertical migration is simulated for motile and non-motile phytoplankton, and fish are migrated throughout the model domain according to a migration function based on their mortality. A weighted grazing function is included for zooplankton feeding on phytoplankton and fish feeding on zooplankton. The biomass grazed is related to both food availability and preference of the consumer for its food supply. Improved temperature, respiration and light limitation functions have been developed to represent the environmental response of the organisms. The benthic processes included a self-shading component and beach wrack function for macroalgae, sediment bioturbation and nutrient cycling by polychaetes, and effects of seagrass on sediment oxygen status.

In particular, the seven phytoplankton groups modeled are dinoflagellates, freshwater diatoms, marine/estuarine diatoms, freshwater cyanobacteria, marine estuarine cyanobacteria, chlorophytes, and cryptophytes. Phytoplankton biomass is represented in terms of chlorophyll *a*. Phytoplankton concentrations are affected by the following processes:

- Temperature growth function
- Light limitation
- Nutrient limitation by phosphorus and nitrogen (and when diatoms are considered, silica)
- Loss due to respiration, natural mortality, excretion, and grazing
- Salinity response
- Vertical migration and settling

6.2 NUTRIENTS, METALS, AND OXYGEN DYNAMICS

The transport and chemical cycling of nutrients is an important part of simulating the interaction of biological organisms in an ecosystem. CAEDYM includes as state variables the following:

- Nutrients (dissolved inorganic phosphorus, total phosphorus, total nitrogen, ammonium nitrate, and silica).
- Dissolved oxygen and biochemical oxygen demand.
- Metals (dissolved and particulate forms of iron and manganese).

- Suspended sediment (the particulate and colloidal fractions).
- pH

The model incorporates oxygen dynamics and nutrient cycling in both the sediments and water column. A sediment pool of organic detritus and inorganic sediments, both of which may be resuspended into the water column, is included. Redox-mediated release of dissolved nutrients is simulated from the sediments to the water column.

Processes included in the water and sediment oxygen dynamics include:

- Atmospheric exchange (Wanninkhof, 1992).
- Oxygen production and consumption through phytoplankton, macroalgae, and seagrass/macrophyte photosynthesis and respiration, respectively.
- Utilization of dissolved oxygen due to respiration of higher organisms such as zooplankton and fish and due to photosynthesis and respiration in jellyfish
- Water column consumption of oxygen during nitrification.
- Biochemical oxygen demand due to mineralization of organic matter in the water column and in the sediments.
- Oxygen flux from the water column to the sediments, sediment oxygen demand (SOD), as developed from Fick's law of diffusion.

The last two processes are used together with a sediment porosity and diffusion coefficient (Ullman and Aller, 1982) in order to define the depth of the toxic layer in the sediments.

Nutrient processes included in the sediment and water column dynamics include:

- Phytoplankton nutrient uptake, with provision for luxury storage of nutrients.
- Release of dissolved inorganic nutrients from phytoplankton excretion.
- Excretion of nutrients as fecal material by zooplankton.
- Nitrification and denitrification by bacterial mediated action.
- Generation of inorganic nutrients from organic detritus.
- Transfer of nutrients through the food chain (*e.g.* phytoplankton--zooplankton--fish).
- Uptake of nutrients by macroalgae and seagrasses.
- Adsorption/desorption of nutrients from inorganic suspended sediments.
- Sediment/water transfer of nutrients (*via* such processes as sediment resuspension, sedimentation, redox-mediated nutrient release, and bioturbation).

In essence, CAEDYM represents the type of interactive processes that occur amongst the ecological and chemical components in the aquatic ecosystem. As a broad generalization, one component of the system cannot be manipulated or changed within the model without affecting other components of the system. Similarly in nature, changing an integral component in the aquatic system will have wide-ranging and follow-on effects on many of the other system components. CAEDYM is designed to have the complexity and flexibility to be able to handle the continuum of responses that will be elicited as components of a system that are manipulated. Thus, the model represents a valuable tool to examine responses under changed conditions, as for example, when new approaches to managing an ecosystem are adopted.

7.0 BIBLIOGRAPHY

7.1 REFERENCED IN TEXT

(1999), "Computational aquatic ecosystem dynamics model, CAEDYM: User manual," TTF/4/Nov99, Centre for Water Research, University of Western Australia, 51pp.

Amorocho, J. and DeVries, J.J. (1980). "A new evaluation of the wind stress coefficient over water surfaces," Journal of Geophysical Research, 85:433-442.

Antenucci, Jason (2004). "Tracing Short-Circuiting Potential," from CWR Models: Bytes and Nybbles, Autumn 2004, Issue 10, page 2.

Antenucci, Jason (2004). "New Metals Model for CAEDYM," from CWR Services: Bytes and Nybbles, December 2004, Issue 11, page 1.

Appt, Jochen (January 2000), "Review on the modeling of short period internal waves in lakes with focus on Lake Constance," Pfaffenwaldring 61, D-70550 Stuttgart, Universität Stuttgart, Institut für Hydraulik und Grundwasser, Stuttgart.

Appt, J., Imberger, J., Kobus, H. (2004), "Basin-scale motion in stratified Upper Lake Constance," Limnology and Oceanography, 49(4), 919-933

Casulli, Vincenzo and Cheng, Ralph T. (1992), "Semi-implicit finite difference methods for three-dimensional shallow water flow," *International Journal for Numerical Methods in Fluids*, **15**, 629-48.

CWR, "Limnological Study of Lake Burragorang," Centre For Water Research, The University of Western Australia, Chapter 4 excerpt from report, pp. 104-126.

Hamilton, D. (1997). "An integrated ecological model for catchment hydrology and water quality for the Swan and Canning Rivers," presented at the 2nd International

Symposium on Ecology and Engineering, 10-12 November 1997, Freemantle, Australia. IAHR Eco-Hydraulics section.

Hamilton, David and Herzfeld, Michael (November 11, 1999), "Computational aquatic ecosystem dynamics model (CAEDYM), An ecological water quality model designed for coupling with hydrodynamic drivers, Scientific manual," Centre for Water Research, The University of Western Australia, Nedlands, Australia, 101pp.

Hamilton, D.P. and S.G. Schladow (1997), "Prediction of water quality in lakes and reservoirs: Part I: Model description," *Ecological Modelling, 96,* 91-110.

Herzfeld, M. and Hamilton, D. (1998), "A computational aquatic ecosystem dynamics model for the Swan River," *EOS Trans. AGU*, **79**(1), Ocean Sciences Meet. Suppl. OS11P-02.

Herzfeld, M.; Hodges, B.R.; and Hamilton, D. (1998), "Modelling the Swan River on small temporal and spatial scales," The Swan Canning Estuary conference, York, Australia, Apr., 1998.

Herzfeld, M.; Hamilton, D.; and Hodges, B.R. (1997), "Reality vs. management: The role of ecological numerical models," *2nd International Symposium on Ecology and Engineering*, 10-12 November 1997, Fremantle, Australia, IAHR Eco-Hydraulics section.

Hodges, B.R. (1998), "Hydrodynamics of differential heat absorption," *Environmental Mechanics Laboratory Seminar*, Dept. of Civil Eng., Stanford University, Feb. 1998.

Hodges, B.R. and Dallimore C. (2001), "Estuary and lake computer model, ELCOM Science Manual Code Version 1.5.0," Centre for Water Research, The University of Western Australia.

Hodges, B.R. and Herzfeld, M. (1997), "Coupling of hydrodynamics and water quality for numerical simulations of Swan River," *2nd International Symposium on Ecology and Enginnering*, 10-12 November, Fremantle, Australia, IAHR Eco-Hydraulics section.

Hodges, B.R.; Herzfeld, M.; Winters, K.; and Hamilton, D. (1998), "Coupling of hydrodynamics and water quality in numerical simulations," *EOS Trans. AGU*, **79**(1), Ocean Sciences Meet. Suppl. OS11P-01.

Hodges, Ben R. (May 25, 1999), "The CWR estuary and lake computer model, User guide," Centre for Water Research, The University of Western Australia, 47pp.

Hodges, B.R., Imberger, J., Saggio, A., and K. Winters (1999), "Modeling basin-scale internal waves in a stratified lake," *Limnology and Oceanography*), **45**(7), 1603-20.

Hodges, B.R., Yue, N., and Bruce, L. (May 27, 1999), "Swan River hydrodynamic model progress report," Centre For Water Research, The University of Western Australia, 14pp.

Jacquet, J. (1983). "Simulation of the thermal regime of rivers," In Orlob, G.T., editor, Mathematical Modeling of Water Quality: Streams, Lakes and Reservoirs, pages 150-176. Wiley-Interscience.

Kowalik, Z. and Murty, T.S. (1993). "Numerical Modeling of Ocean Dynamics," World Scientific.

Laval, B., Imberger, J., Hodges, B.R., and Stocker, R. (2003), "Modeling circulation in lakes: spatial and temporal variations," Limnology and Oceanography 48(3), 983-994.

Leonard, B.P. (1991), "The ULTIMATE conservative difference scheme applied to unsteady one-dimensional advection," *Computational Methods in Applied Mechanics and Engineering*, **88**, 17-74.

Lin, B. and Falconer, R.A. (1997). "Tidal flow and transport modeling using ULTIMATE QUICKEST," Journal of Hydraulic Engineering, 123:303-314.

Robson, B.J. and Hamilton, D. P. (2002). "Three-Dimensional Modeling of a Microcystis bloom event in a Western Australian Estuary." Centre For Water Research, The University of Western Australia, 491- 496 pp.

Romero, J.R. and Antenucci, J. (2004). "The Tiete River: Supply for Sao Paolo, Brazil," from CWR Models: Bytes and Nybbles, Autumn 2004, Issue 10, page 4.

Romero, J.R. and Imberger, J. (1999). "Lake Pamvotis Project-Final report", ED report WP 1364 JR, Centre for Water Research, Crawley, Western Australia, Australia.

Spigel, R.H.; Imberger, J.; and Rayner, K.N. (1986), "Modeling the diurnal mixed layer," *Limnology and Oceanography,* **31**, 533-56.

Staniforth, A. and Côté, J. (1991). "Semi-Lagrangian integration schemes for atmospheric models – a review," Monthly Weather Review, 119:2206-2223.

Stevens, C. and Imberger, J. (1996). "The initial response of a stratified lake to a surface shear stress," Journal of Fluid Mechanics, 312:39-66.

Ullman, W.J. and R.C. Aller (1982), "Diffusion coefficients in nearshore marine sediments," *Limnol. Oceanogr., 27,* 552-556.

Wanninkhof, R. (1992), "Relationship between wind speed and gas exchange over the ocean," *J. Geophys. Res., 97(C5)*, 7373-7382.

Yeates, Peter (2004). "ELCOM in the Venice Lagoon," from CWR Models: Bytes and Nybbles, Autumn 2004, Issue 10, page 2.

7.2 SUPPLEMENTAL REFERENCES

(November 1999), "Course notes, Computational aquatic ecosystem dynamics model, CAEDYM, Special introduction work session," TTF/3/Nov99, Centre for Water Research, University of Western Australia, 51pp.

(January 2000), "Course notes, Estuary & lake computer model, ELCOM, Special introduction training session," TTF/3/JAN2000, Centre for Water Research, University of Western Australia, 21pp+app.

(January 21, 2000) "Instructions for the use of the graphical user interface *modeler* in the configuration & visualization of DYRESM-CAEDYM," Draft version 2, 42pp.

Antenucci, J. and Imberger, J. (1999), "Seasonal development of long internal waves in a strongly stratified lake: Lake Kinneret," *Journal of Geophysical Research* (in preparation).

Antenucci, J. and Imberger, J. (2000), "Observation of high frequency internal waves in a large stratified lake," *5th International Symposium on Stratified Flows, (ISSF5)*, Vancouver, July 2000, **1**, 271-6.

Bailey, M.B. and Hamilton, D.H. (1997), "Wind induced sediment re-suspension: a lake wide model," *Ecological Modeling*, **99**, 217-28.

Burling, M.; Pattiaratchi, C.; and Ivey, G. (1996), "Seasonal dynamics of Shark Bay, Western Australia," *3rd National AMOS Conference*, 5-7 February 1996, University of Tasmania, Hobart, 128.

Chan, C.U.; Hamilton, D.P.; and Robson, B.J. (2001), "Modeling phytoplankton succession and biomass in a seasonal West Australian estuary," *Proceedings, SIL Congress XXVIII* (in press).

Chan, T. and Hamilton, D.P. (2001), "The effect of freshwater flow on the succession and biomass of phytoplankton in a seasonal estuary," *Marine and Freshwater Research* (in press).

De Silva, I.P.D.; Imberger, J.; and Ivey, G.N. (1997), "Localized mixing due to a breaking internal wave ray at a sloping bed," *Journal of Fluid Mechanics*, **350**, 1-27.

Eckert, W.; Imberger, J.; and Saggio, A. (1999), "Biogeochemical evolution in response to physical forcing in the water column of a warm monomictic lake," *Limnology and Oceanography* (submitted).

Gersbach, G.; Pattiaratchi, C.; Pearce, A.; and Ivey, G. (1996), "The summer dynamics of the oceanography of the south-west coast of Australia – The Capes current" *3rd National AMOS Conference*, 5-7 February 1996, University of Tasmania, Hobart, 132.

Hamilton, D.P. (1996), "An ecological model of the Swan River estuary: An integrating tool for diverse ecological and physico-chemical studies," *INTECOL's V International Wetlands Conference 1996 "Wetlands for the Future,"* September 1996, Perth, Australia.

Hamilton, D.P.; Chan, T.; Hodges, B.R.; Robson, B.J.; Bath, A.J.; and Imberger, J. (1999), "Animating the interactions of physical, chemical and biological processes to understand the dynamics of the Swan River Estuary," Combined Australian-New Zealand Limnology Conference, Lake Taupo.

Hamilton, D.P. (2000), "Record summer rainfall induces first recorded major cyanobacterial bloom in the Swan River," *The Environmental Engineer*, **1**(1), 25.

Hamilton, D.; Hodges, B.; Robson, B.; and Kelsey, P. (2000), "Why a freshwater blue-green algal bloom occurred in an estuary: the Microcystis bloom in the Swan River Estuary in 2000," Western Australian Marine Science Conference 2000, Path, Western Australia.

Hamilton, D.P.; Chan, T.; Robb, M.S.; Pattiaratchi, C.B.; Herzfeld, M.; and Hodges, B. (2001), "Physical effects of artificial destratification in the upper Swan River Estuary," *Hydrological Processes*.

Heinz, G.; Imberger, J.; and Schimmele, M. (1990), "Vertical mixing in Überlinger See, western part of Lake Constance," *Aquat. Sci.*, **52**, 256-68.

Herzfeld, M. (1996), "Sea surface temperature and circulation in the Great Australian bight," Ph.D. Thesis, School of Earth Science, Flinders University, South Australia.

Herzfeld, M. and Hamilton, D. (1997), "A computational aquatic ecosystem dynamics model for the Swan River, Western Australia," *MODSIM '97, International Congress on Modeling and Simulation Proceedings*, 8-11 December, 1997, University of Tasmania, Hobart, **2**, 663-8.

Herzfeld, Michael (May 28, 1999), "Computational aquatic ecosystem dynamics model (CAEDYM), An ecological water quality model designed for coupling with

hydrodynamic drivers, Programmer's guide," Centre for Water Research, The University of Western Australia, Nedlands, Australia, 133pp.

Hodges, Ben R. (July 1991), "Pressure-driven flow through an orifice for two stratified, immiscible liquids," M.S. thesis, The George Washington University, School of Engineering and Applied Science.

Hodges, Ben R. (March 1997), "Numerical simulation of nonlinear free-surface waves on a turbulent open-channel flow," Ph.D. dissertation, Stanford University, Dept. of Civil Engineering.

Hodges, Ben R. (June 9, 1998), "Heat budget and thermodynamics at a free surface: Some theory and numerical implementation (revision 1.0c)," Working manuscript, Centre for Water Research, The University of Western Australia, 14pp.

Hodges, Ben R. (1999), "Numerical techniques in CWR-ELCOM," Technical report, Centre for Water Research, The University of Western Australia. (in preparation)

Hodges, Ben R. (2000), "Recirculation and equilibrium displacement of the thermocline in a wind-driven stratified lake," *5th International Symposium on Stratified Flows, (ISSF5)*, Vancouver, July 2000, **1**, 327-30.

Hodges, B.R., Herzfeld, M., and Hamilton, D. (1998), "A computational aquatic ecosystem dynamics model for the Swan River," *EOS Trans. AGU*, **79**(1), Ocean Sciences Meet. Suppl. OS11P-02.

Hodges, B.; Herzfeld, M.; Winters, K.; and Hamilton, D. (1998), "Interactions of a surface gravity waves and a sheared turbulent current," *EOS Trans. AGU*, **79**(1), Ocean Sciences Meet. Suppl. OS53.

Hodges, B.R. and Street, R.L. (1999), "On simulation of turbulent nonlinear free-surface flow," *Journal of Computational Physics*, **151**, 425-57.

Hodges, B.R.; Imberger, J.; Laval, B.; and Appt, J. (2000), "Modeling the hydrodynamics of stratified lakes," *Fourth International conference on HydroInformatics*, Iowa Institute of Hydraulic Research, Iowa City, 23-27 July 2000.

Hodges, B.R. and Imberger, J. (2001), "Simple curvilinear method for numerical methods of open channels," *Journal of Hydraulic Engineering*, **127**(11), 949-58.

Hodges, Ben R. and Street, Robert L. (1996), "Three-dimensional, nonlinear, viscous wave interactions in a sloshing tank," *Proceedings of the Fluid Engineering Summer Meeting 1996*, Vol. **3**, FED-Vol. **238**, ASME, 361-7.

Hodges, Ben R. and Street, Robert L. (1998), "Wave-induced enstrophy and dissipation in a sheared turbulent current," *Proceedings of the Thirteenth Australian fluid Mechanics Conference*, M.C. Thompson and K. Hourigan (eds.), Monash University, Melbourne, Australia, 13-18 December 1998, Vol. **2**, 717-20.

Hodges, B.R., Street, R.L., and Zang, Y. (1996), "A method for simulation of viscous, non-linear, free-surface flows," *Twentieth Symposium on Naval Hydrodynamics*, National Academy Press, 791-809.

Hollan, E. (1998), "Large inflow-driven vortices in Lake Constance," in J. Imberger (ed.), *Physical Processes in Lakes and Oceans. Coastal and Estuarine Studies*, **54,** American Geophysical Union, 123-36.

Hollan, E.; Hamblin, P.F.; and Lehn, H. (1990), "Long-term modeling of stratification in Large Lakes: Application to Lake Constance," in: Tilzer, M.M. and C. Serruya (eds.). *Large Lakes, Ecological Structure and Function***,** Berlin: Springer Verlag, 107-24.

Horn, D.A.; Imberger, J.; and Ivey, G.N. (1999), "Internal solitary waves in lakes – a closure problem for hydrostatic models," *Proceedings of 'Aha Halikoa Hawaiian Winter Workshop*, January 19-22, 1999, University of Hawaii, Manoa.

Horn, D.A.; Imberger, J.; and Ivey, G.N. (1999), "The degeneration of large-scale interfacial gravity waves in lakes," under consideration for publication in *Journal of Fluid Mechanics*.

Horn, D.A.; Imberger, J.; Ivey, G.N.; and Redekopp, L.G. (2000), "A weakly nonlinear model of long internal waves in lakes," *5th International Symposium on Stratified Flows, (ISSF5)*, Vancouver, July 2000, **1**, 331-6.

Imberger, J. (1985), "The diurnal mixed layer," *Limnology and Oceanography*, **30**(4), 737-70.

Imberger, J. (1985), "Thermal characteristics of standing waters: an illustration of dynamic processes," *Hydrobiologia*, **125,** 7-29.

Imberger, J. (1994), "Mixing and transport in a stratified lake," Preprints of *Fourth International Stratified on Flows Symposium*, Grenoble, France, June-July 1994, **3** 1-29.

Imberger, J. (1994), "Transport processes in lakes: a review," in R. Margalef (ed.), *Limnology Now: A Paradigm of Planetary Problems*, Elsevier Science, 99-193.

Imberger, J. (1998), "Flux paths in a stratified lake: A review," in J. Imberger (ed.), *Physical Processes in Lakes and Oceans. Coastal and Estuarine Studies,* **54,** American Geophysical Union, 1-18.

Imberger, J. (1998), "How does the estuary work?" WAERF Community Forum, 25 July 1998, The University of Western Australia.

Imberger, J.; Berman, T; Christian, R.R.; Sherr, E.B.; Whitney, D.E.; Pomeroy, L.R.; Wiegert, R.G.; and Wiebe, W.J. (1983), "The influence of water motion on the distribution and transport of materials in a salt marsh estuary," *Limnology and Oceanography,* **28**, 201-14.

Imberger, J. and Hamblin, P.F. (1982), "Dynamics of lakes, reservoirs, and cooling ponds," *Journal of Fluid Mechanics,* **14**, 153-87.

Imberger, J. and Head, R. (1994), "Measurement of turbulent properties in a natural system," reprinted from *Fundamentals and Advancements in Hydraulic Measurements and Experimentation*.

Imberger, J. and Ivey, G.N. (1991), "On the nature of turbulence in a stratified fluid. Part II: Application to lakes," *Journal of Physical Oceanography,* **21**(5), 659-80.

Imberger, J. and Ivey, G.N. (1993), "Boundary mixing in stratified reservoirs," *Journal of Fluid Mechanics,* **248**, 477-91.

Imberger, J. and Patterson, J.C. (1981), "A dynamic reservoir simulation model – DYRESM: 5," In H.B. Fischer (ed.) *Transport Models for Inland and Coastal Waters,* Academic Press, 310-61.

Imberger, J. and Patterson, J.C. (1990), "Physical limnology," In: *Advances in Applied Mechanics,* **27**, 303-475.

Ivey, G.N. and Corcos, G.M. (1982), "Boundary mixing in a stratified fluid," *Journal of Fluid Mechanics,* **121**, 1-26.

Ivey, G.N. and Imberger, J. (1991), "On the nature of turbulence in a stratified fluid. Part I: The energetics of mixing," *Journal of Physical Oceanography,* **21**(5), 650-8.

Ivey, G.N.; Imberger, J.; and Koseff, J.R. (1998), "Buoyancy fluxes in a stratified fluid," in J. Imberger (ed.), *Physical Processes in Lakes and Oceans. Coastal and Estuarine Studies,* **54,** American Geophysical Union, 377-88.

Ivey, G.N.; Taylor, J.R.; and Coates, M.J. (1995), "Convectively driven mixed layer growth in a rotating, stratified fluid," *Deep-Sea Research I.,* **42**(3), 331-49.

Ivey, G.N.; Winters, K.B; and De Silva; I.P.D. (1998), "Turbulent mixing in an internal wave energized benthic boundary layer on a slope," submitted to *Journal of Fluid Mechanics*.

Jandaghi Alaee, M.; Pattiaratchi, C.; and Ivey, G. (1996), "The three-dimensional structure of an island wake," *8th International Biennial Conference. Physics of Estuaries and coastal Seas (PECS)* 9-11 September 1996, the Netherlands, 177-9.

Javam, A; Teoh, S.G.; Imberger, J.; and Ivey, G.N. (1998), "Two intersecting internal wave rays: a comparison between numerical and laboratory results," in J. Imberger (ed.), *Physical Processes in Lakes and Oceans. Coastal and Estuarine Studies*, **54,** American Geophysical Union, 241-50.

Kurup, R.; Hamilton, D.P.; and Patterson, J.C. (1998), "Modeling the effects of seasonal flow variations on the position of a salt wedge in a microtidal estuary," Estuarine Coastal *and Shelf Science*, **47**(2), 191-208.

Kurup, R.G.; Hamilton, D.P.; and Phillips, R.L. (2000), "Comparison of two 2-dimensional, laterally averaged hydrodynamic model applications to the Swan River Estuary," *Mathematics and Computers in Simulation*, **51**(6), 627-39.

Laval, B.; Hodges, B.R.; and Imberger, J. (2000), "Numerical diffusion in stratified lake," *5th International Symposium on Stratified Flows, (ISSF5)*, Vancouver, July 2000, **1**, 343-8.

Lemckert, C. and Imberger, J. (1995), "Turbulent benthic boundary layers in fresh water lakes," Iutam Symposium on Physical Limnology, Broome, Australia, 409-22.

Maiss, M.; Imberger, J.; and Münnich, K.O. (1994), "Vertical mixing in Überlingersee (Lake Constance) traced by SF6 and heat," *Aquat. Sci.*, **56**(4), 329-47.

Michallet, H. and Ivey, G.N. (1999), "Experiments on mixing due to internal solitary waves breaking on uniform slopes," *Journal of Geophysical Research*, **104**, 13467-78.

Nishri, A; Eckert, W.; Ostrovosky, I.; Geifman, J.; Hadas, O.; Malinsky-Rushansky, N.; Erez, J.; and Imberger, J. (1999), "The physical regime and the respective biogeochemical processes in Lake Kinneret lower water mass," *Limnology and Oceanography*, (in press).

Ogihara, Y.; Zic, K.; Imberger, J.; and Armfield, S. (1996), "A parametric numerical model for lake hydrodynamics," *Ecological Modeling*, **86**, 271-6.

Patterson, J.C; Hamblin, P.F.; and Imberger, J. (1984), "Classification and dynamic simulation of the vertical density structure of lakes," *Limnology and Oceanography*, **29**(4), 845-61.

Pattiaratchi, C.; Backhaus, J.; Abu Shamleh, B.; Jandaghi Alaee, M.; Burling, M.; Gersbach, G.; Pang, D.; and Ranasinghe, R. (1996), "Application of a three-dimensional numerical model for the study of coastal phenomena in south-western Australia," *Proceedings of the Ocean & Atmosphere Pacific International Conference*, Adelaide, October 1995, 282-7.

Riley, G.A., H. Stommel and D.F. Bumpus, "Quantitative ecology of the plankton of the Western North Atlantic," *Bull. Bingham Oceanogr. Coll., 12(3)*, 1-69, 1949.

Robson, B.J.; Hamilton, D.P.; Hodges, B.R.; and Kelsey, P. (2000), "Record summer rainfall induces a freshwater cyanobacterial bloom in the Swan River Estuary," *Australian Limnology Society Annual Congress*, Darwin, 2000.

Saggio, A. and Imberger, J. (1998), "Internal wave weather in a stratified lake," *Limnology and Oceanography*, **43**, 1780-95.

Schladow, S.G. (1993), "Lake destratification by bubble-plume systems: Design methodology," *Journal of Hydraulic Engineering*, **119**(3), 350-69.

Smagorinsky, J. (1963) "General circulation experiments with the primitive equations, ´*Monthly Weather Review, 91*, 99-152.

Spigel, R.H. and Imberger, J. (1980), "The classification of mixed-layer dynamics in lakes of small to medium size," *Journal of Physical Oceanography*, **10**, 1104-21.

Steele, J.H. (1962), "Environmental control of phytosynthesis in the sea," *Limnol. Oceanogr., 7*, 137-150.

Taylor, J.R. (1993), "Turbulence and mixing in the boundary layer generated by shoaling internal waves," *Dynamics of Atmospheres and Oceans*, **19**, 233-58.

Thorpe, S.A. (1995), "Some dynamical effects of the sloping sides of lakes," *IUTAM Symposium on Physical Limnology*, Broome, Australia, 215-30.

Thorpe, S.A. (1998), "Some dynamical effects of internal waves and the sloping sides of lakes," in J. Imberger (ed.), *Physical Processes in Lakes and Oceans. Coastal and Estuarine Studies*, **54,** American Geophysical Union, 441-60.

Thorpe, S.A. and Lemmin, U. (1999), "Internal waves and temperature fronts on slops," *Annales Geophysicae*, **17**(9), 1227-34.

Unlauf, L; Wang, Y.; and Hutter, K. (1999), "Comparing two topography-Following primitive equation models for lake circulation," *Journal of Computational Physics*, **153**, 638-59.

Winter, K.B. and Seim, H.E. (1998), "The role of dissipation and mixing in exchange flow through a contracting channel," submitted to *Journal of Fluid Mechanics*.

Winter, K.B.; Seim, H.E.; and Finnigan, T.D. (1998), "Simulation of non-hydrostatic, density-stratified flow in irregular domains," submitted to *International Journal of Numerical Methods in Fluids*.

Zhu, S. and Imberger, J. (1994) "A three-dimensional numerical model of the response of the Australian North West Shelf to tropical cyclones," in: *J. Austral. Math. Soc. Ser.***, B 36,** 64-100.

APPENDIX B

HISTORICAL RESERVOIR DATA

San Vicente Reservoir

Measured Water Surface Elevations

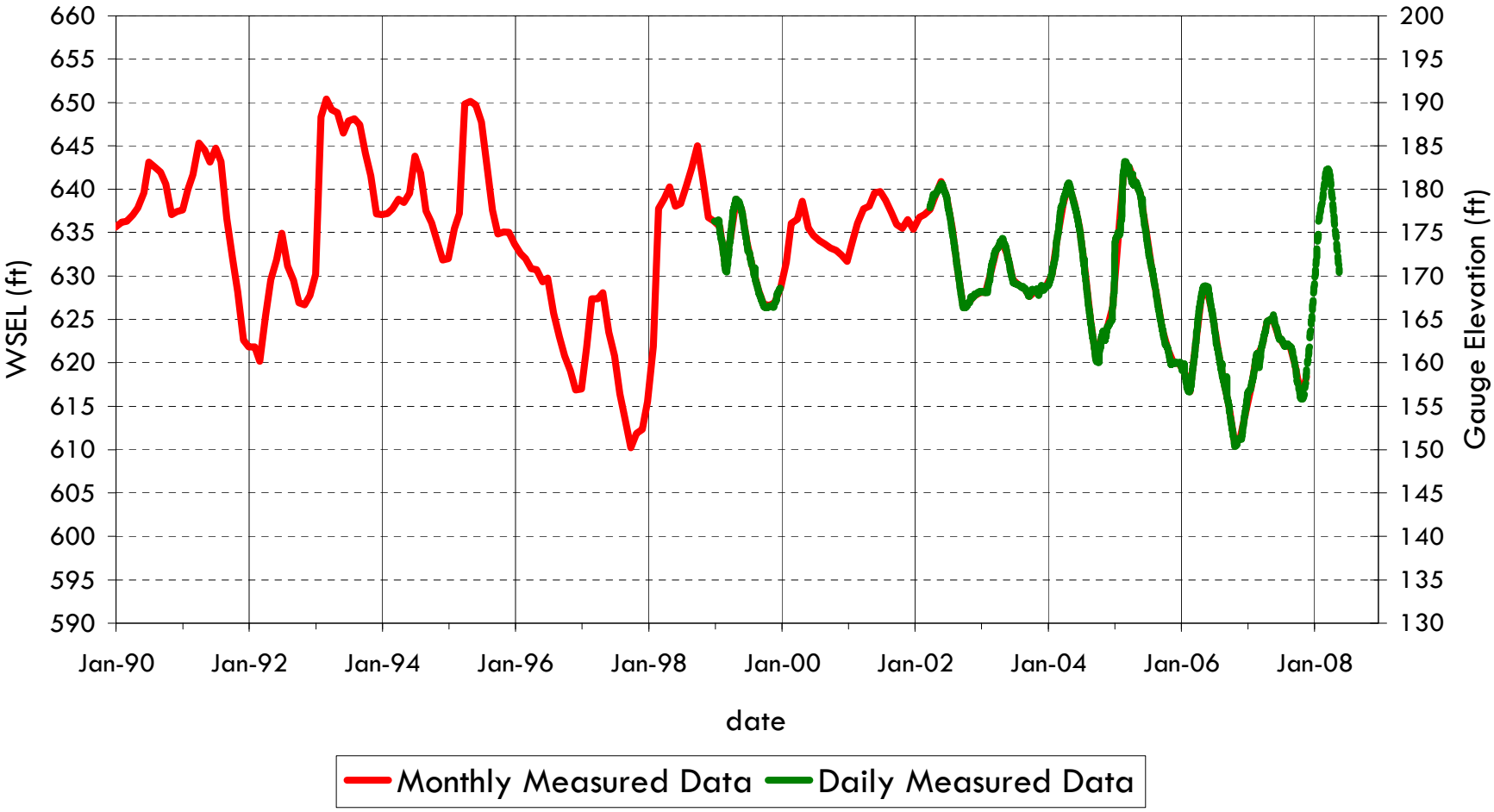

FSI V094005
May 01, 2012

Figure B-1

FLOW SCIENCE®

San Vicente Reservoir (1992)

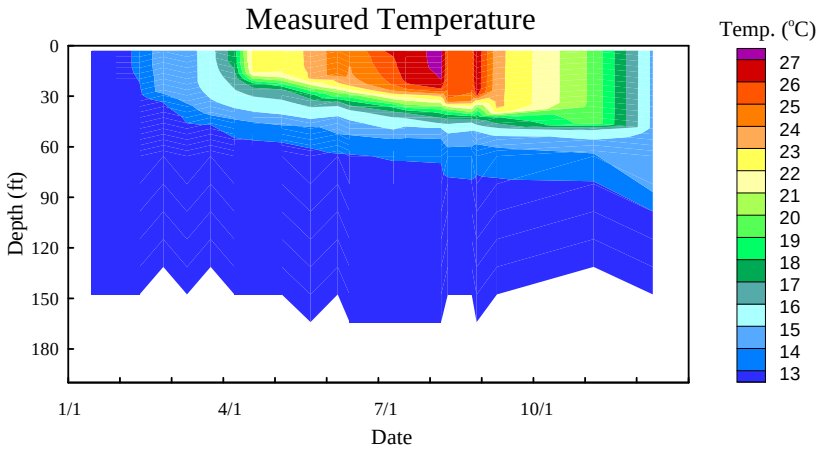

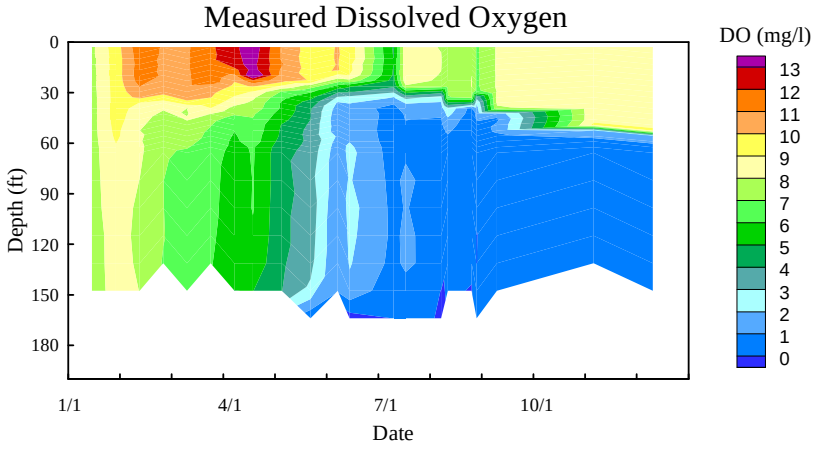

San Vicente Reservoir (1993)

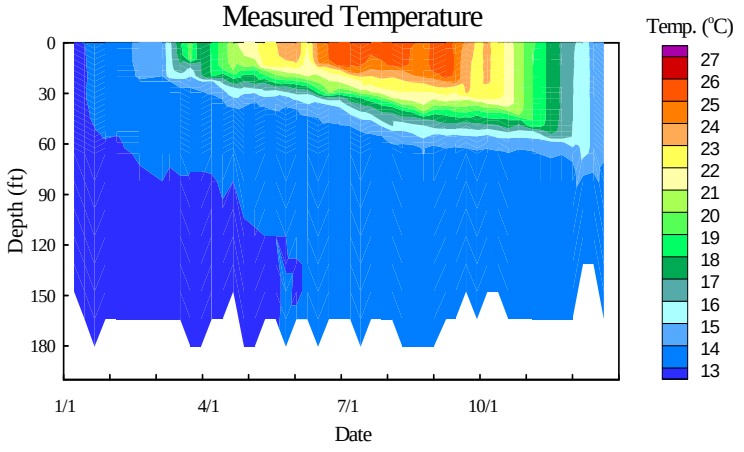

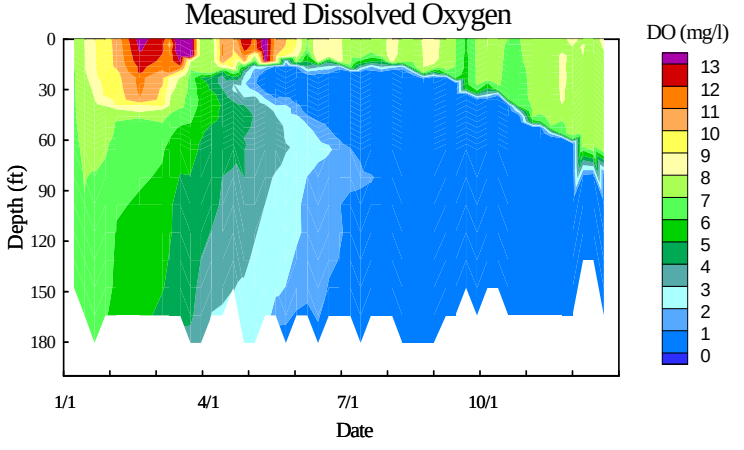

FSI V094005
May 01, 2012

Figure B-2

FLOW SCIENCE®

San Vicente Reservoir (1994)

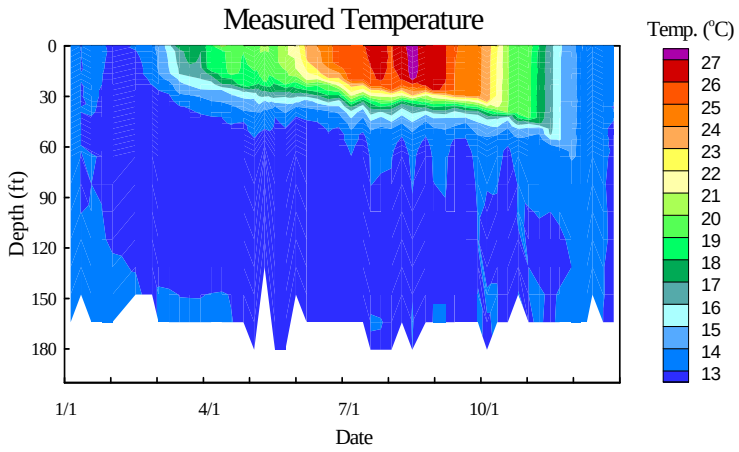

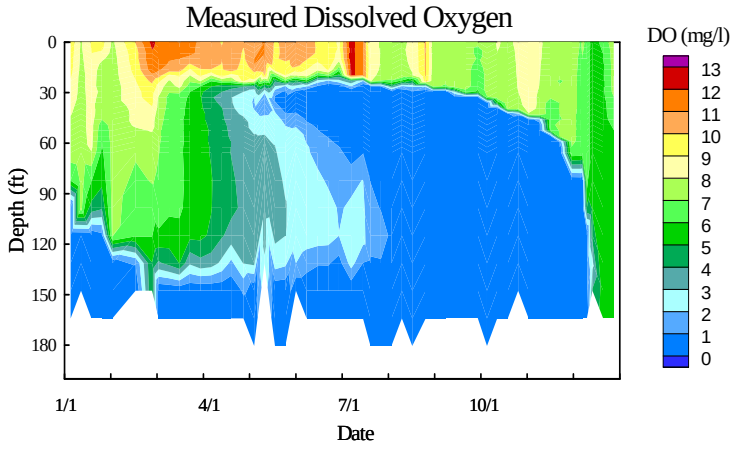

San Vicente Reservoir (1995)

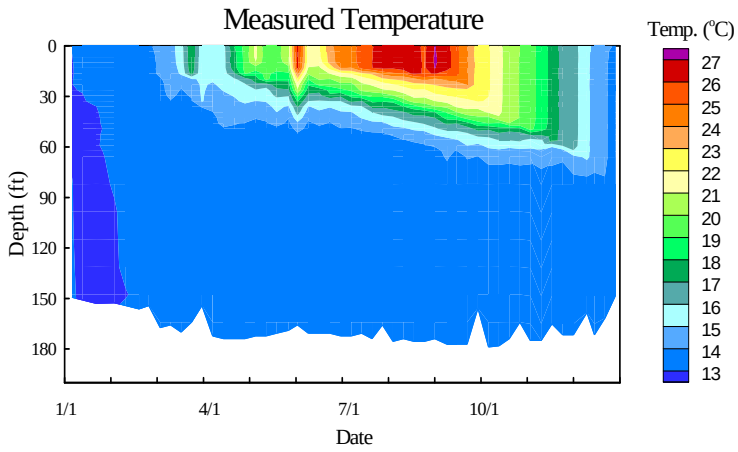

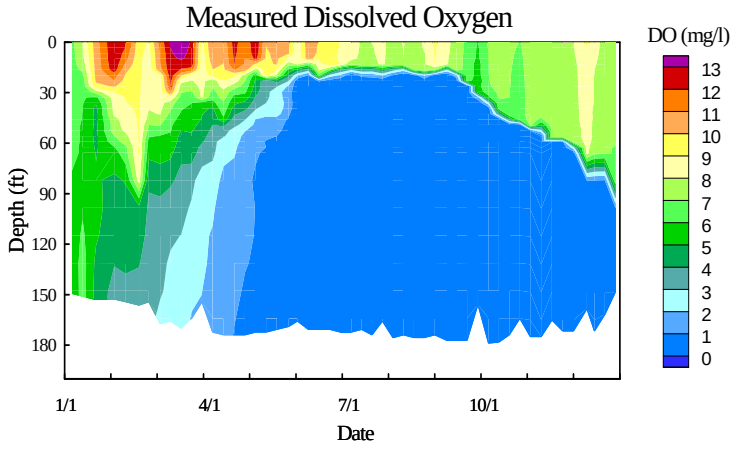

FSI V094005
May 01, 2012

Figure B-3

FLOW SCIENCE®

San Vicente Reservoir (1996)

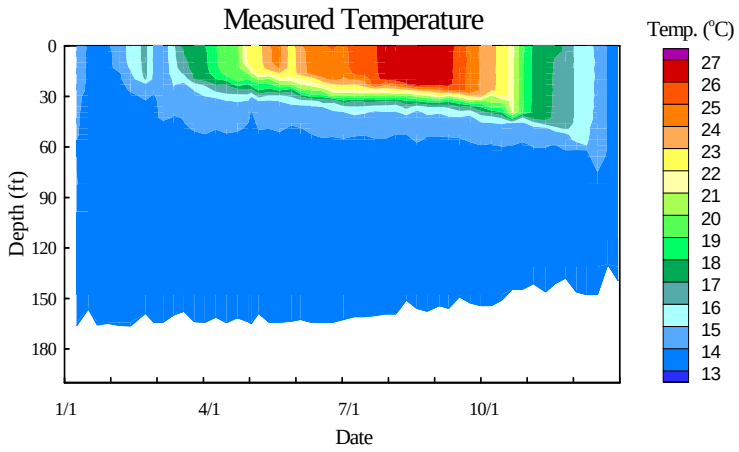

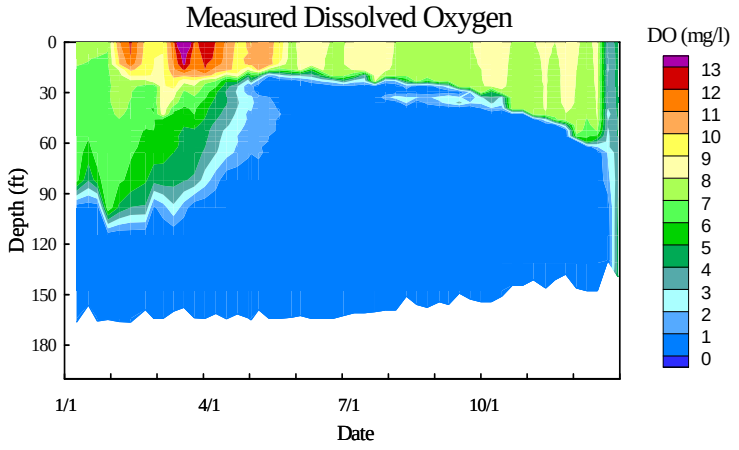

San Vicente Reservoir (1997)

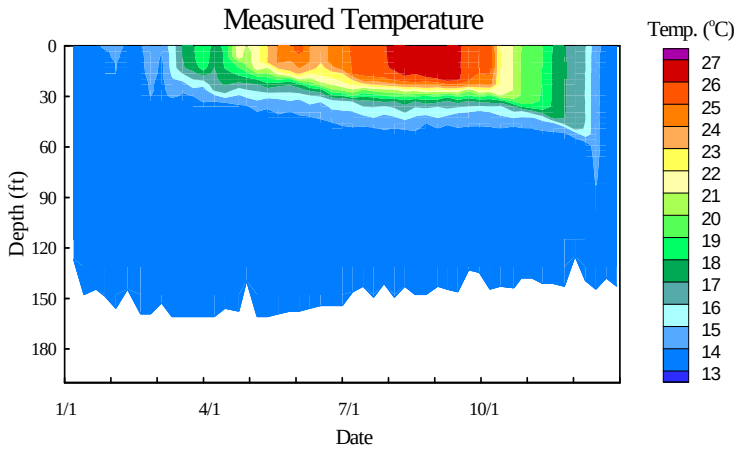

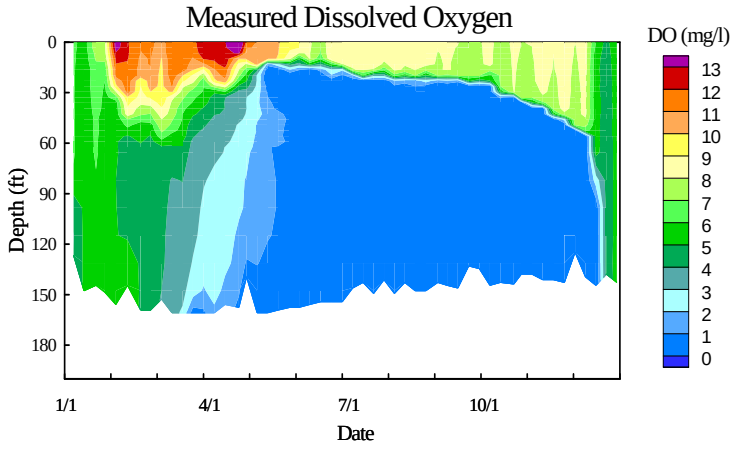

FSI V094005
May 01, 2012

Figure B-4

FLOW SCIENCE®

San Vicente Reservoir (1998)

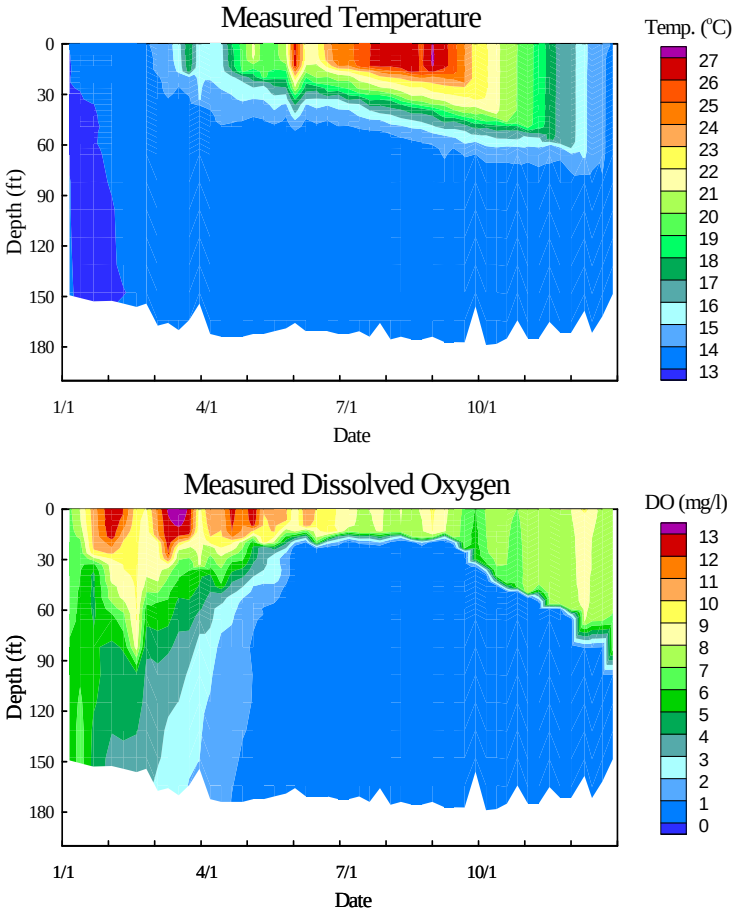

FSI V094005
May 01, 2012

Figure B-5

FLOW SCIENCE®

San Vicente Reservoir (1999)

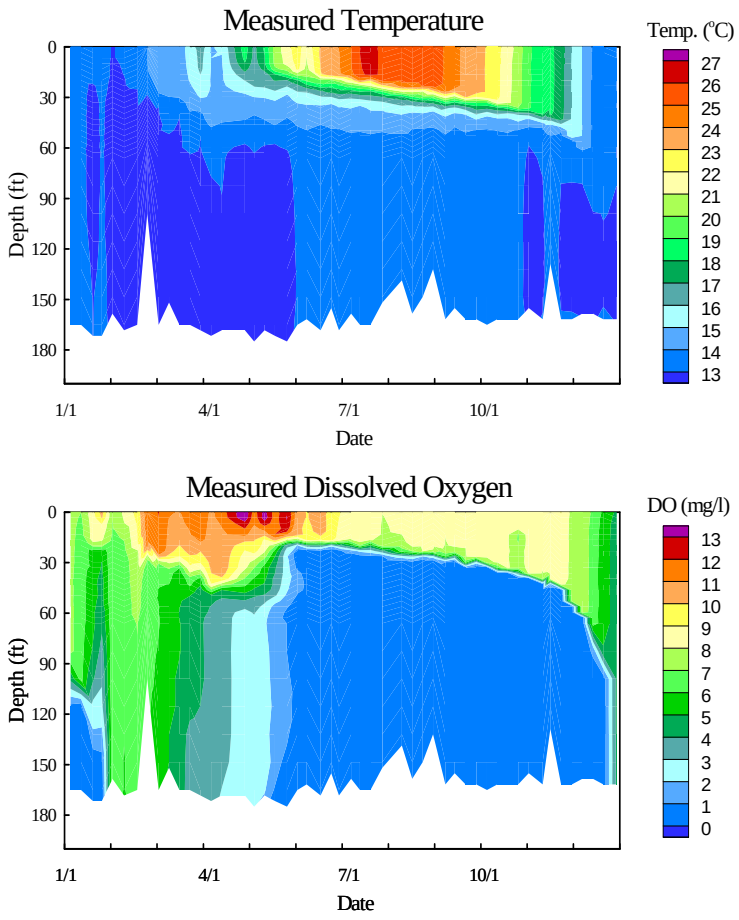

San Vicente Reservoir (1999)

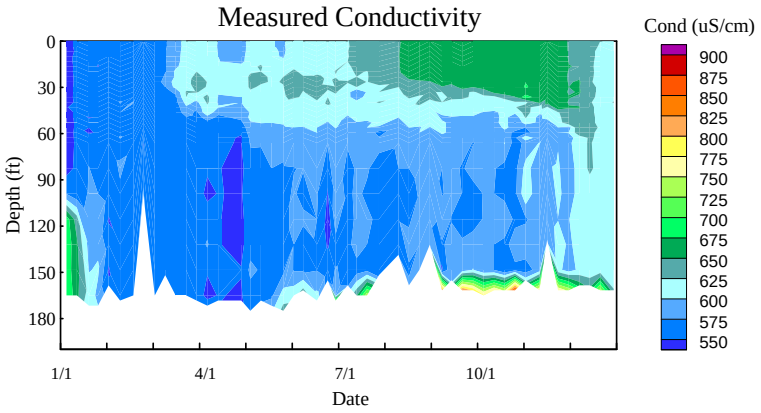

FSI V094005
May 01, 2012

Figure B-6

FLOW SCIENCE®

San Vicente Reservoir (2000)

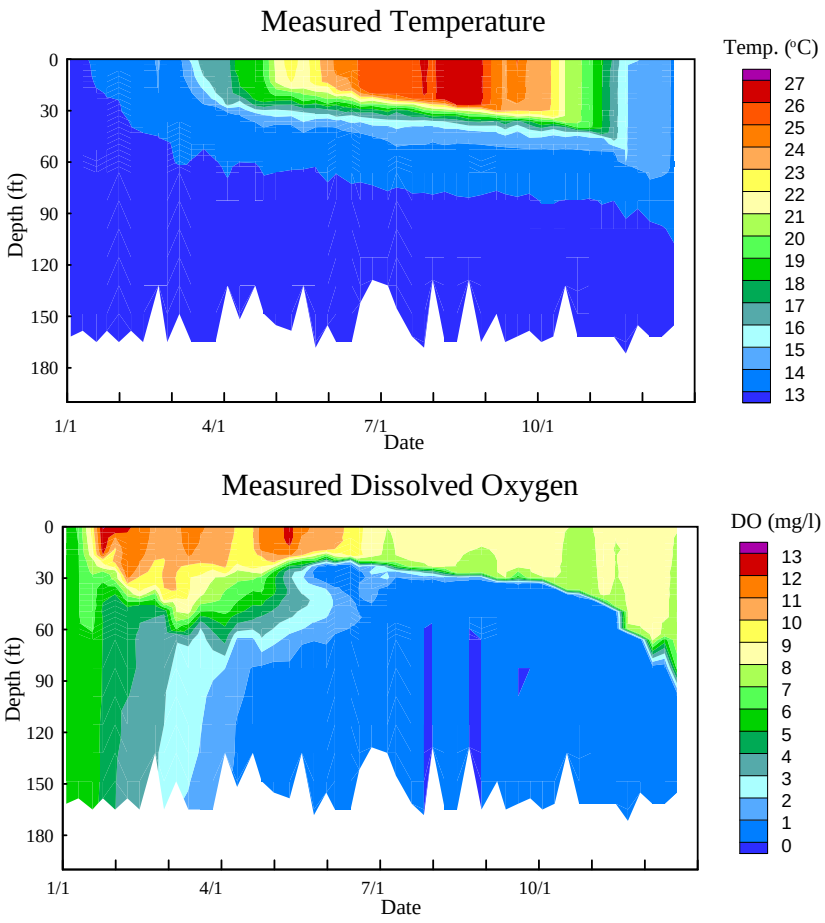

San Vicente Reservoir (2000)

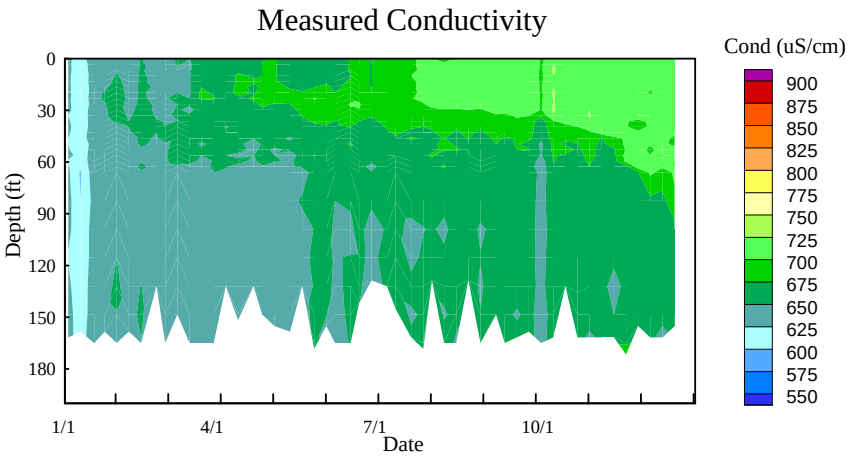

FSI V094005
May 01, 2012

Figure B-7

FLOW SCIENCE®

San Vicente Reservoir (2001)

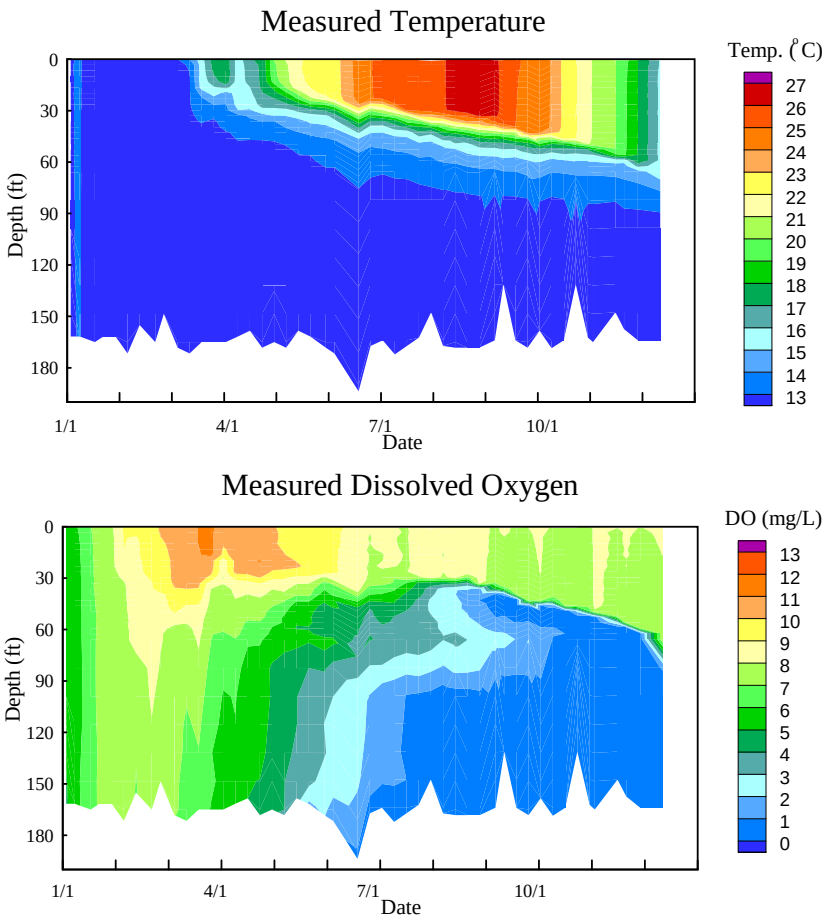

San Vicente Reservoir (2001)

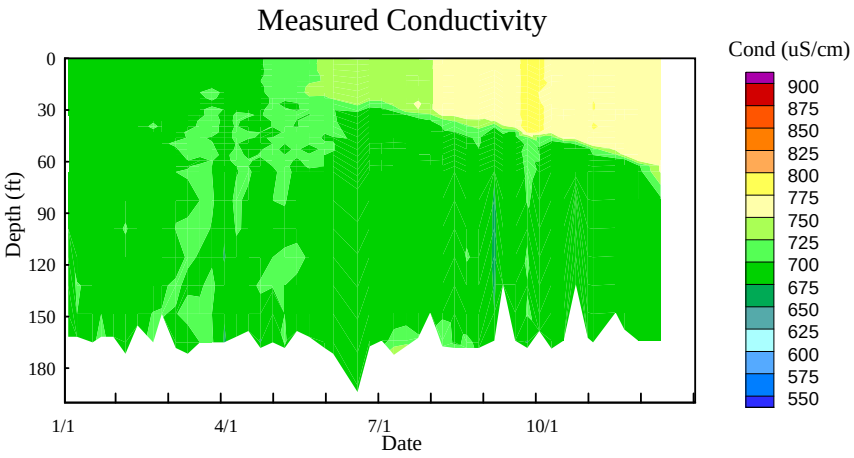

FSI V094005
May 01, 2012

Figure B-8

FLOW SCIENCE®

San Vicente Reservoir (2002)

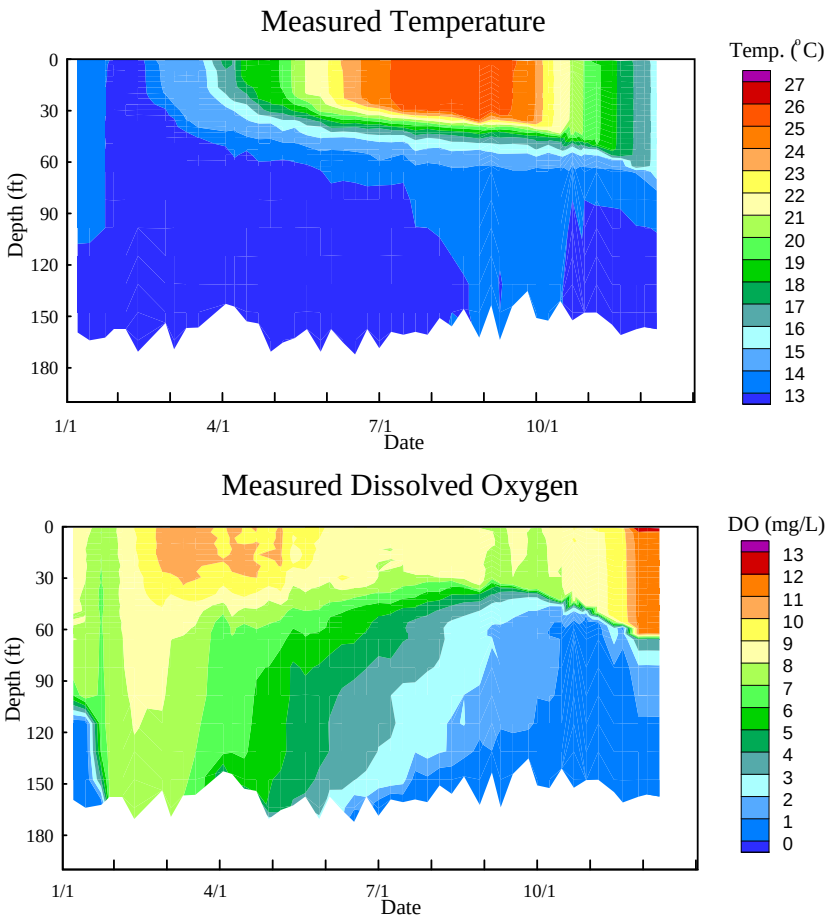

San Vicente Reservoir (2002)

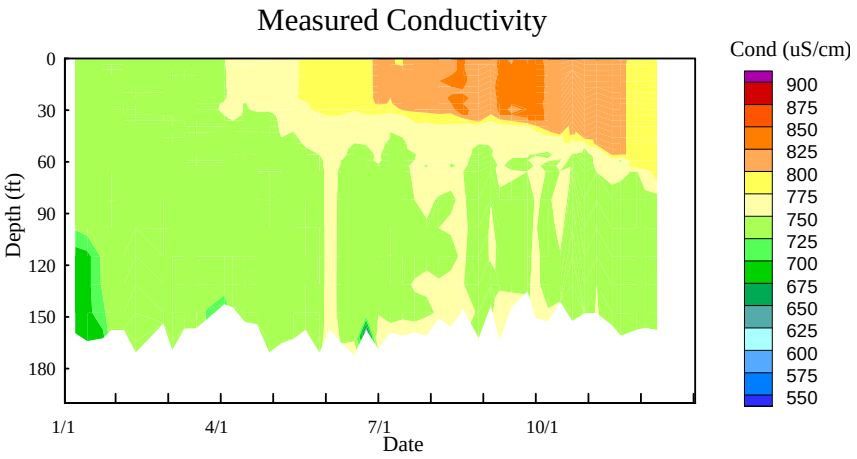

FSI V094005
May 01, 2012

Figure B-9

FLOW SCIENCE®

San Vicente Reservoir (2003)

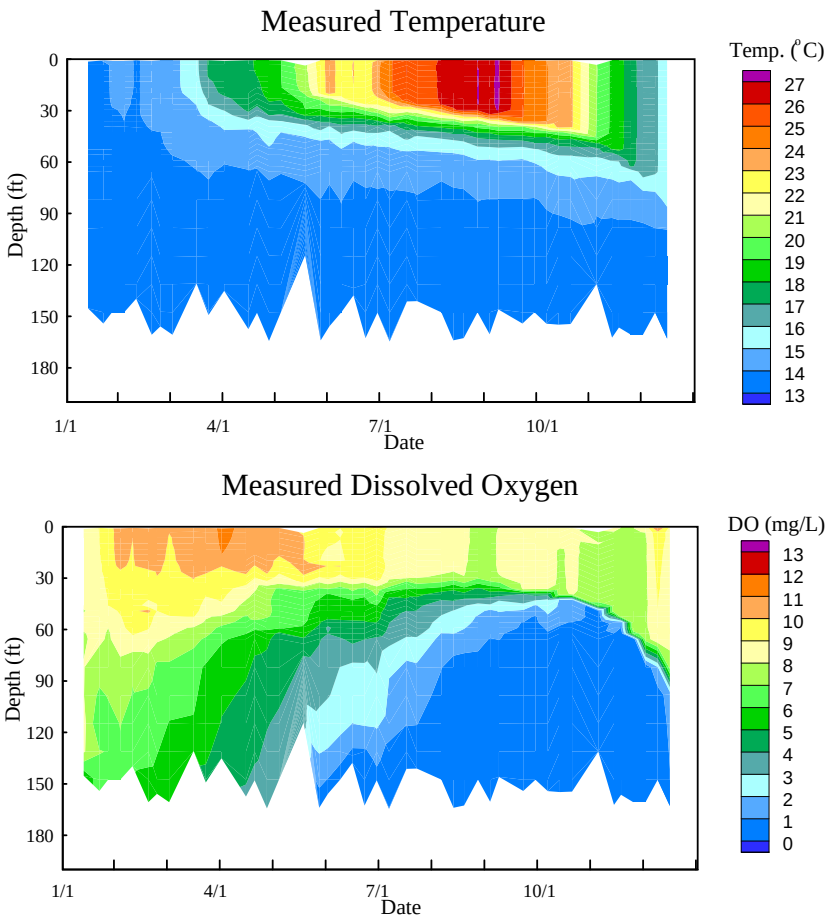

San Vicente Reservoir (2003)

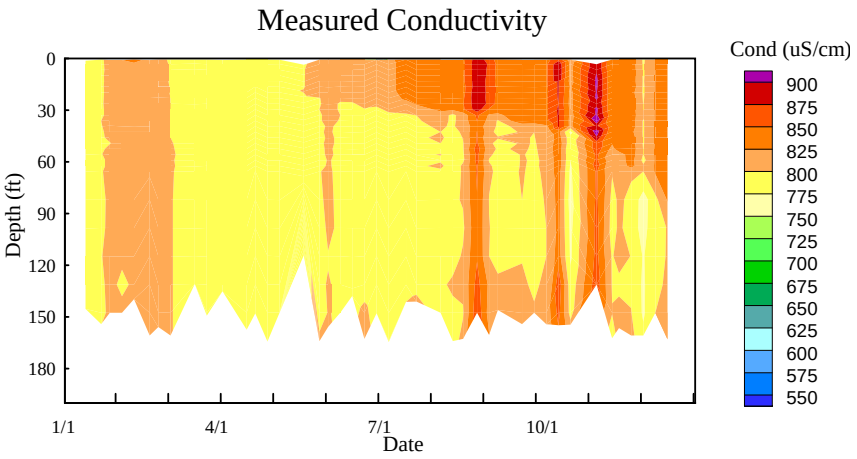

FSI V094005
May 01, 2012

Figure B-10

FLOW SCIENCE®

San Vicente Reservoir (2004)

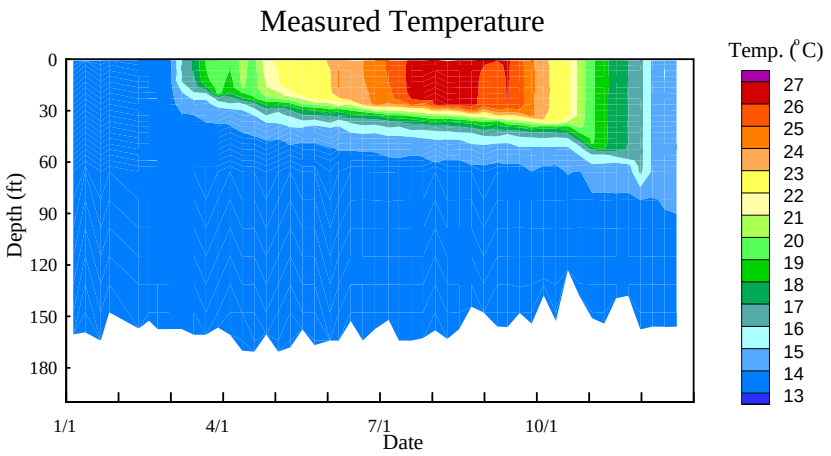

San Vicente Reservoir (2004)

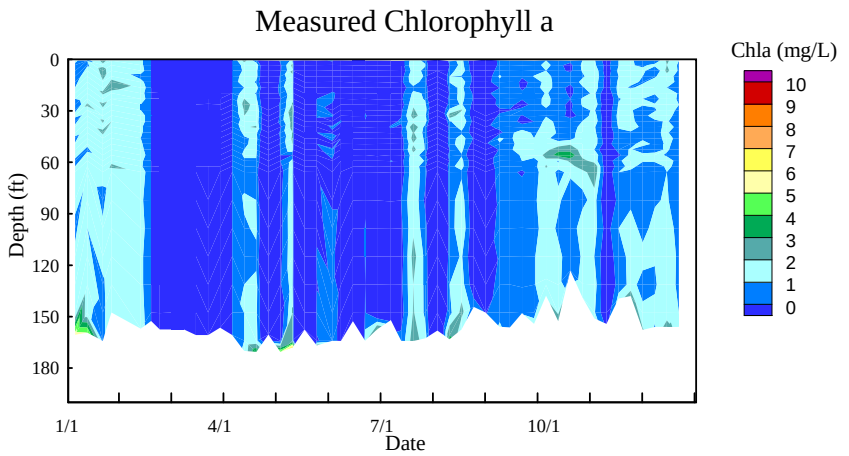

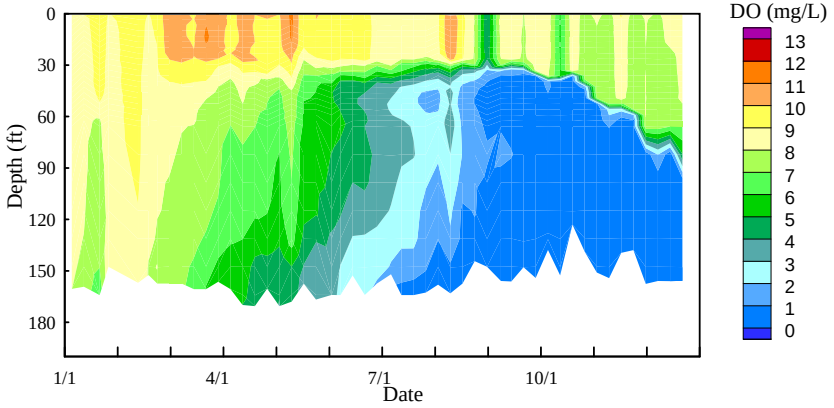

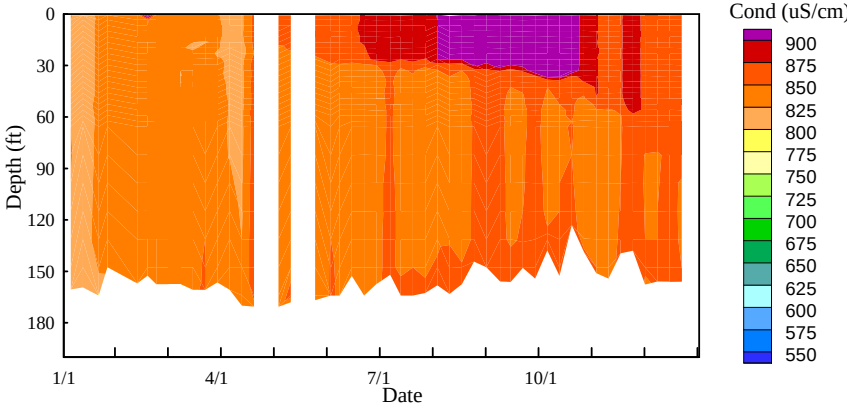

FSI V094005
May 01, 2012

Figure B-11

FLOW SCIENCE®

San Vicente Reservoir (2005)

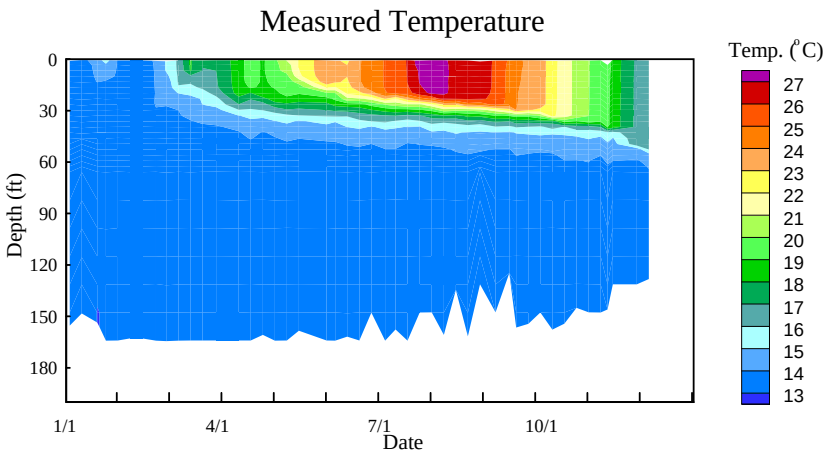

San Vicente Reservoir (2005)

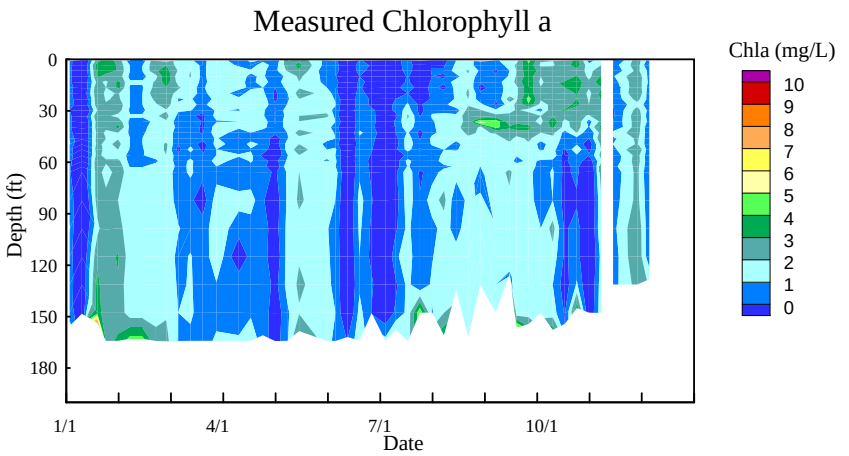

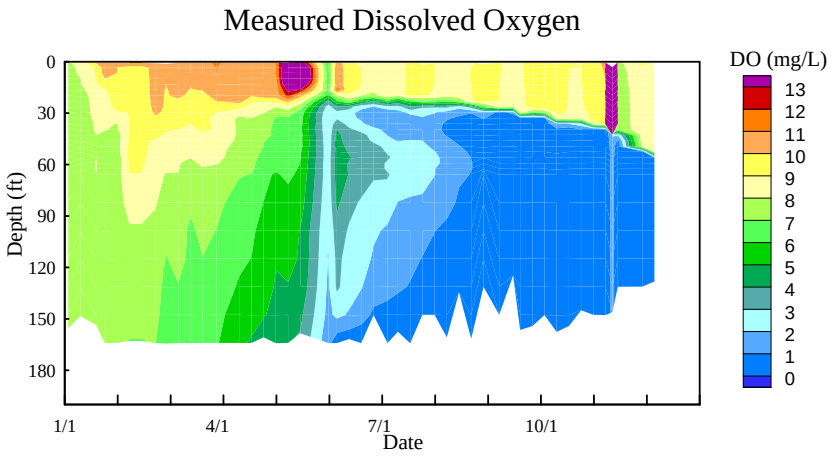

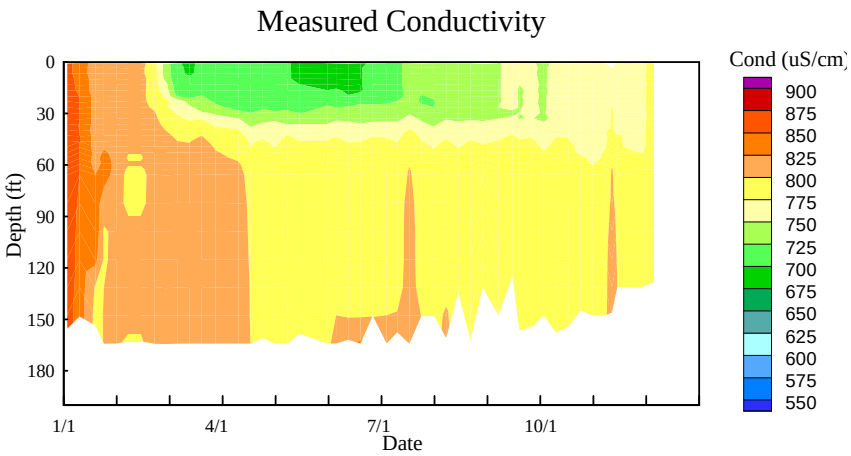

FSI V094005
May 01, 2012

Figure B-12

FLOW SCIENCE®

San Vicente Reservoir (2006)

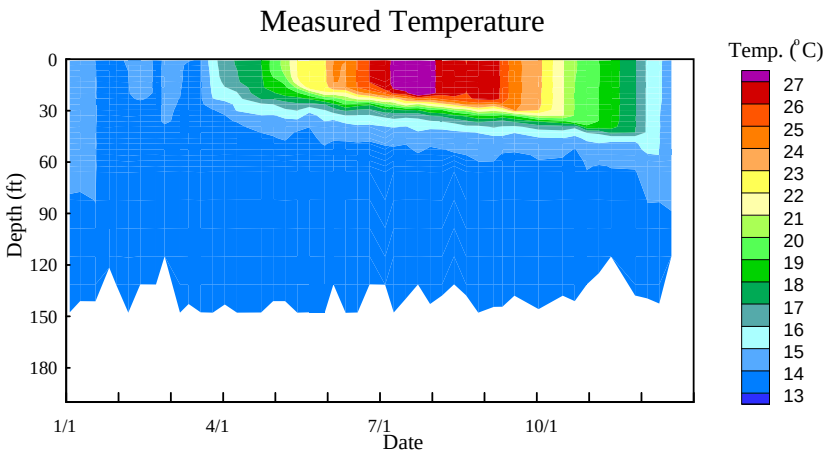

San Vicente Reservoir (2006)

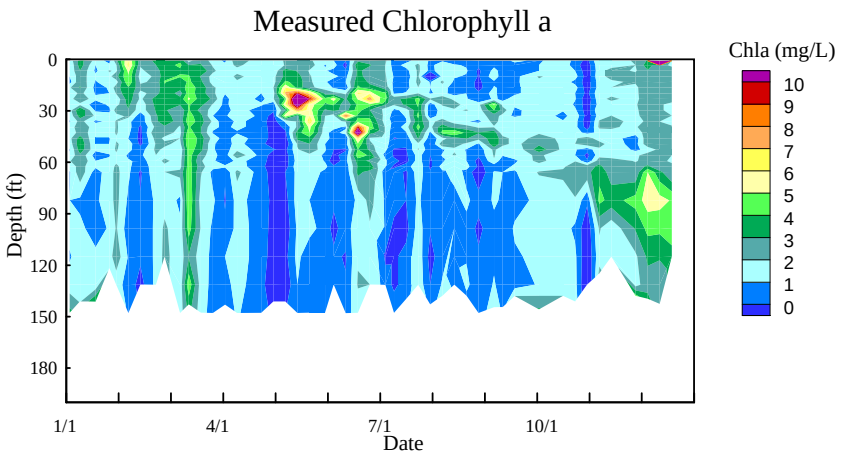

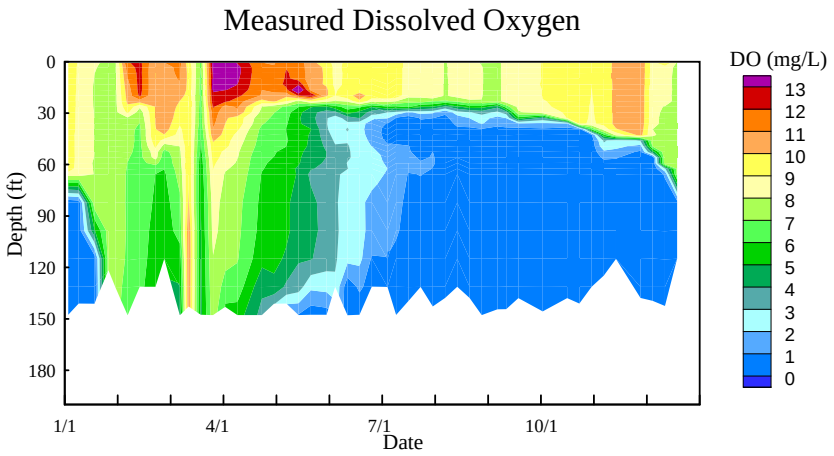

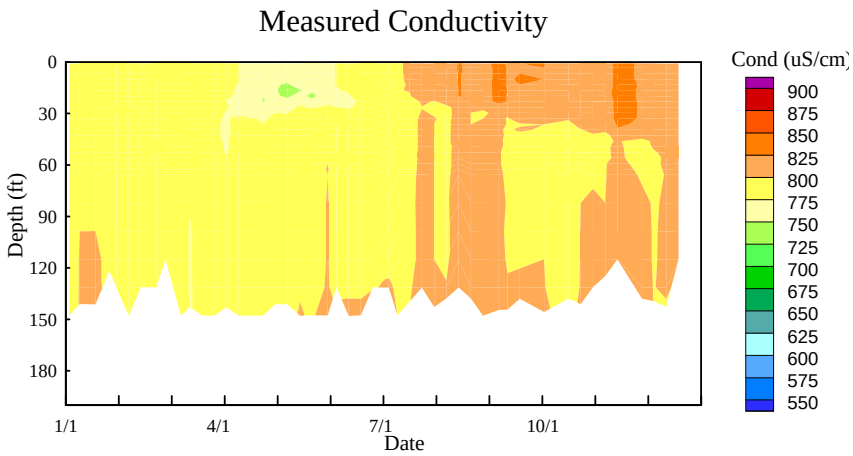

FSI V094005
May 01, 2012

Figure B-13

FLOW SCIENCE®

San Vicente Reservoir (2007)

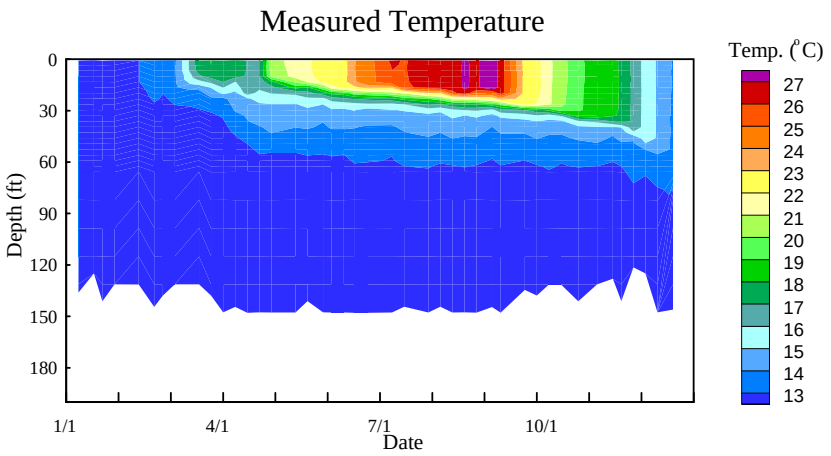

San Vicente Reservoir (2007)

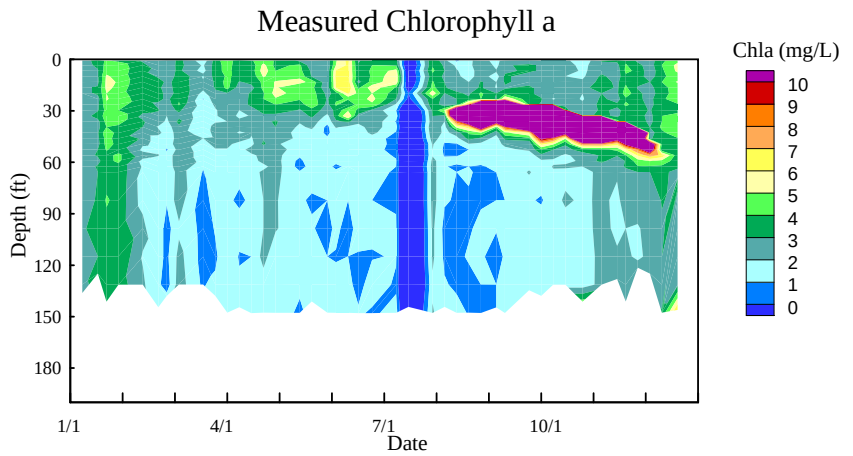

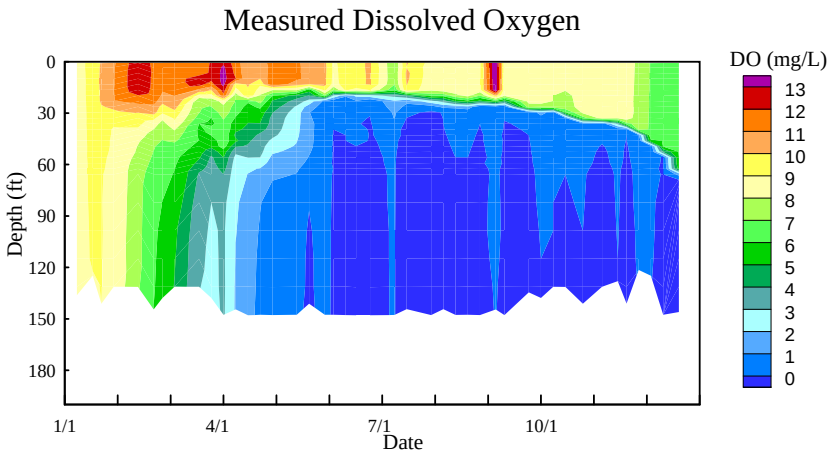

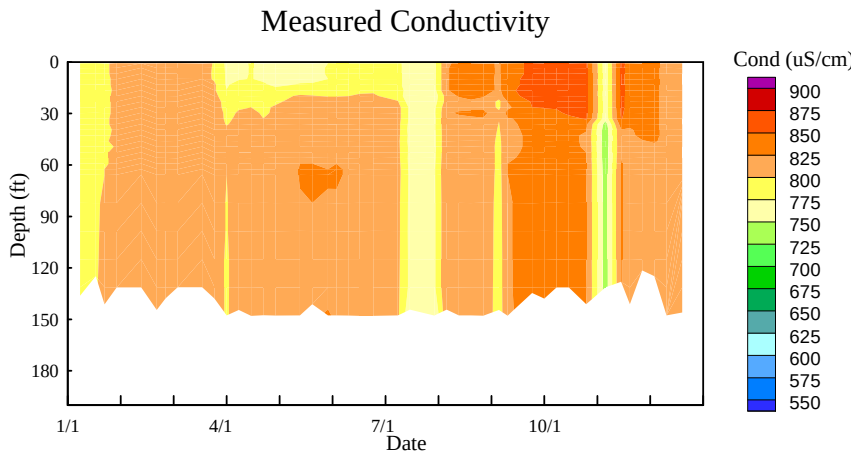

FSI V094005
May 01, 2012

Figure B-14

FLOW SCIENCE®

San Vicente Reservoir (2008)

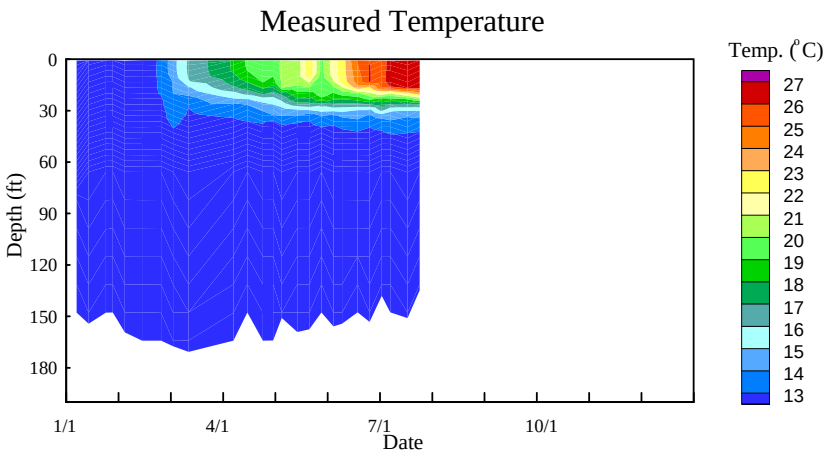

San Vicente Reservoir (2008)

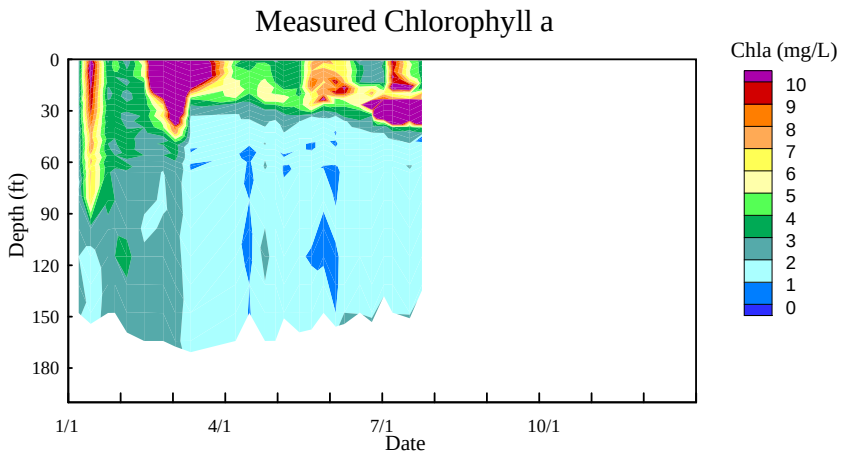

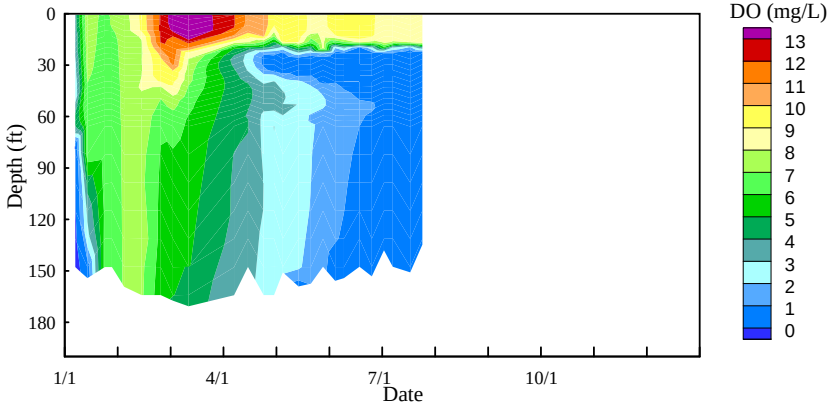

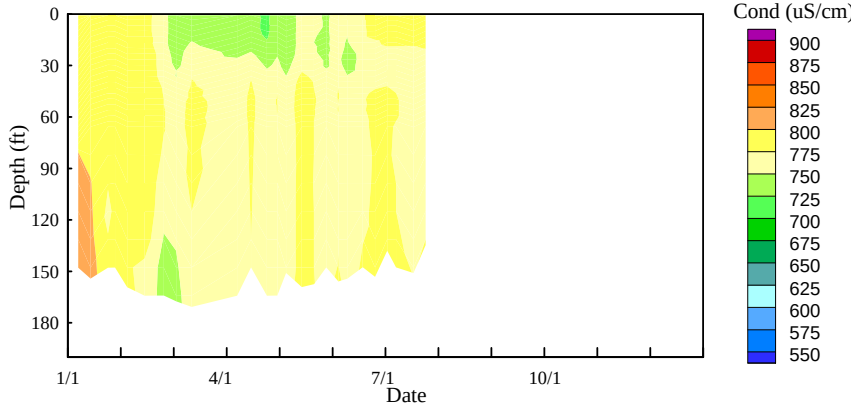

FSI V094005
May 01, 2012

Figure B-15

FLOW SCIENCE®

San Vicente Reservoir

In Reservoir Total Phosphorus Data

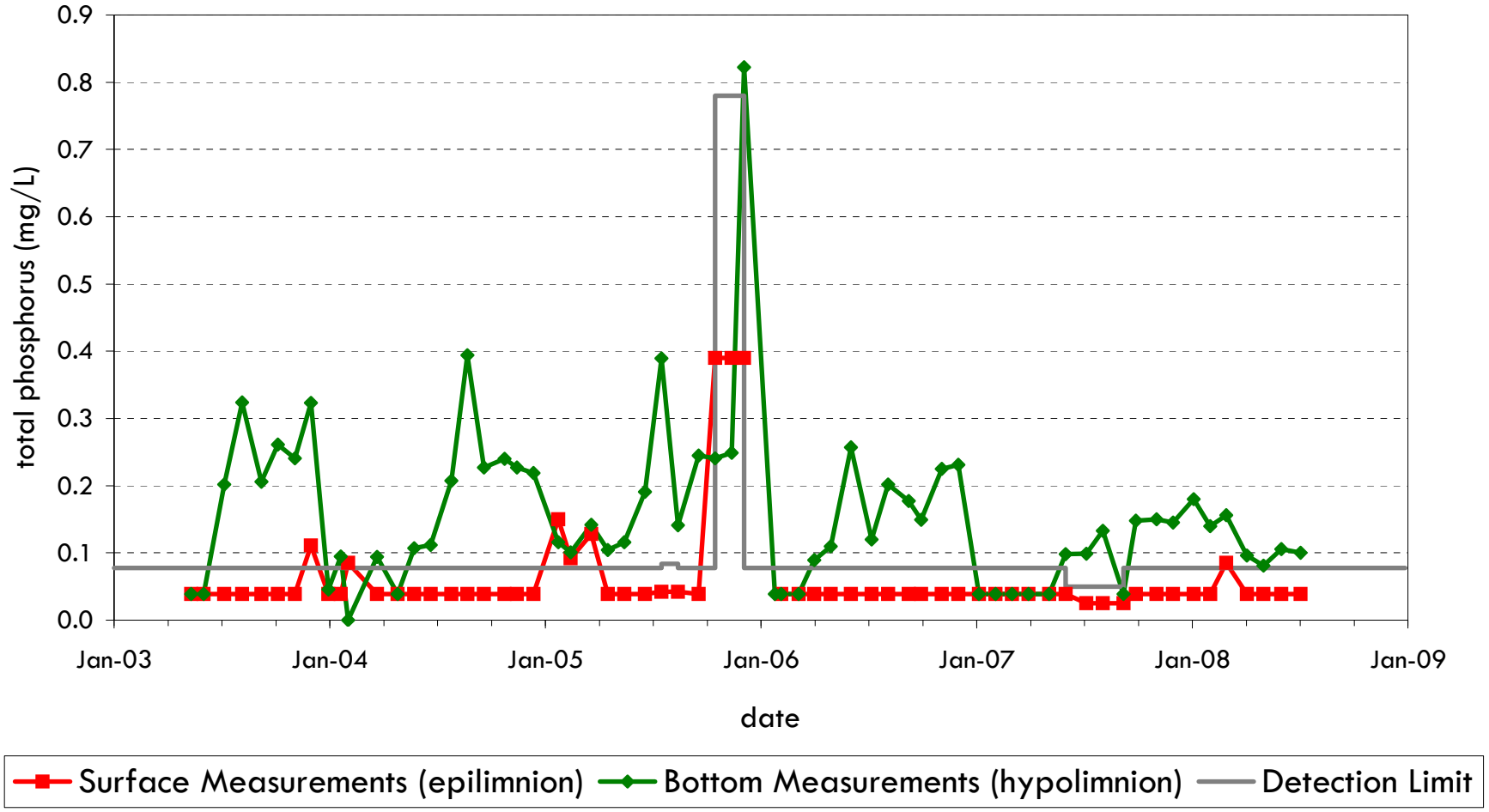

FSI V094005
May 01, 2012

Figure B-16

FLOW SCIENCE®

San Vicente Reservoir

In Reservoir Soluble Reactive Phosphorus Data

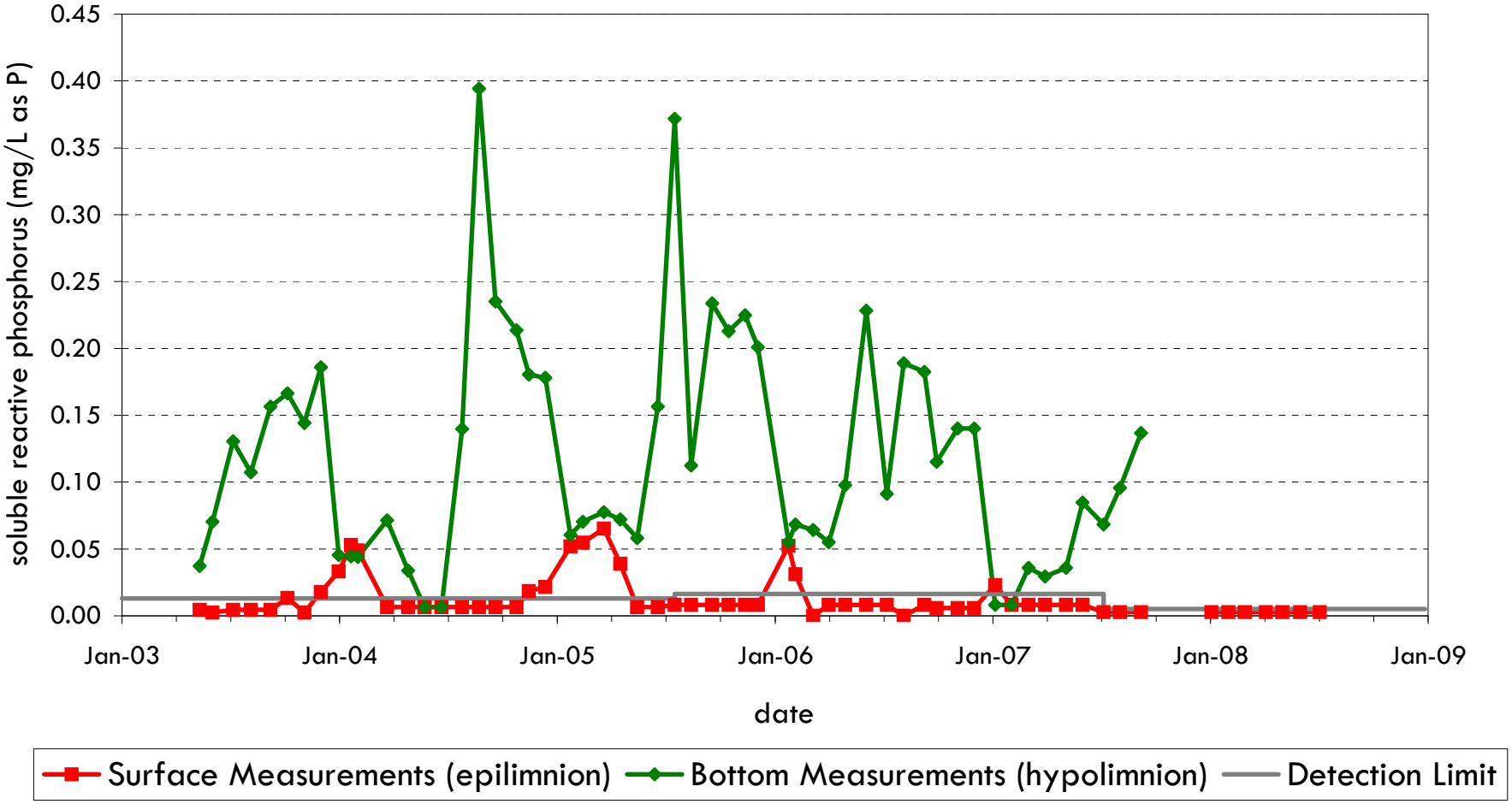

FSI V094005
May 01, 2012

Figure B-17

FLOW SCIENCE®

San Vicente Reservoir

In Reservoir Total Nitrogen Data

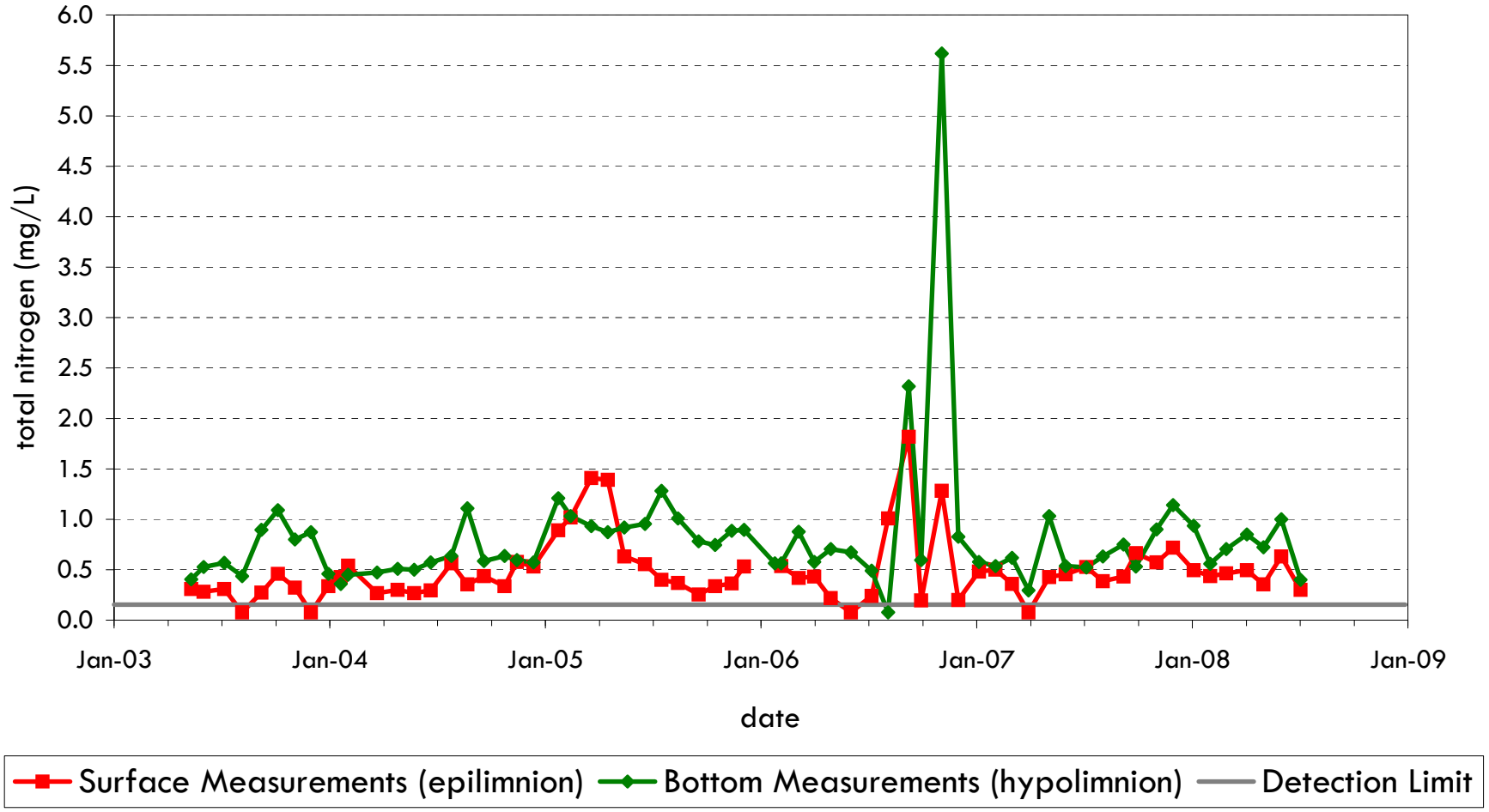

FSI V094005
May 01, 2012

Figure B-18

FLOW SCIENCE®

San Vicente Reservoir

In Reservoir Nitrate Data

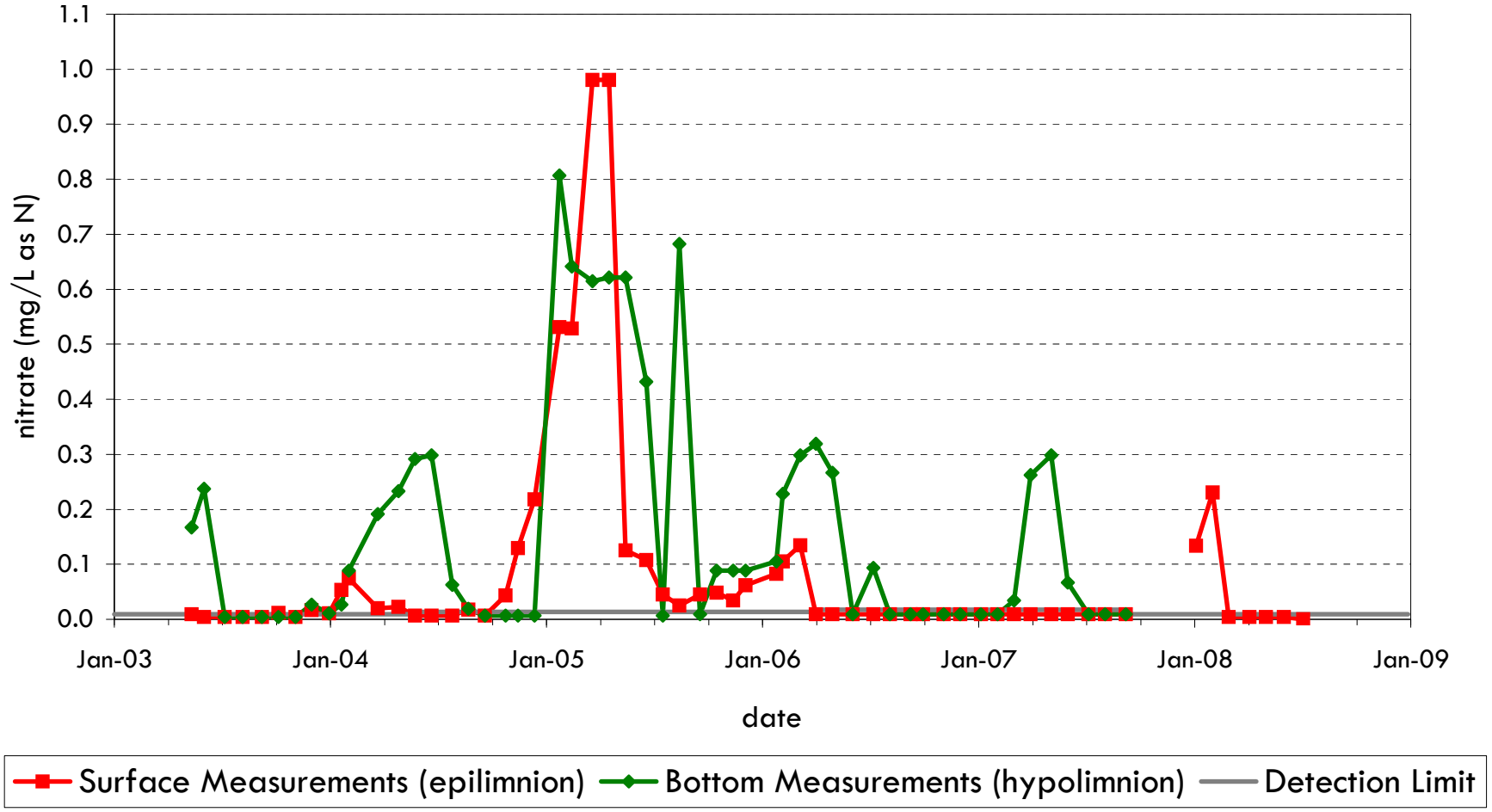

FSI V094005
May 01, 2012

Figure B-19

FLOW SCIENCE®

San Vicente Reservoir

In Reservoir Ammonia Data

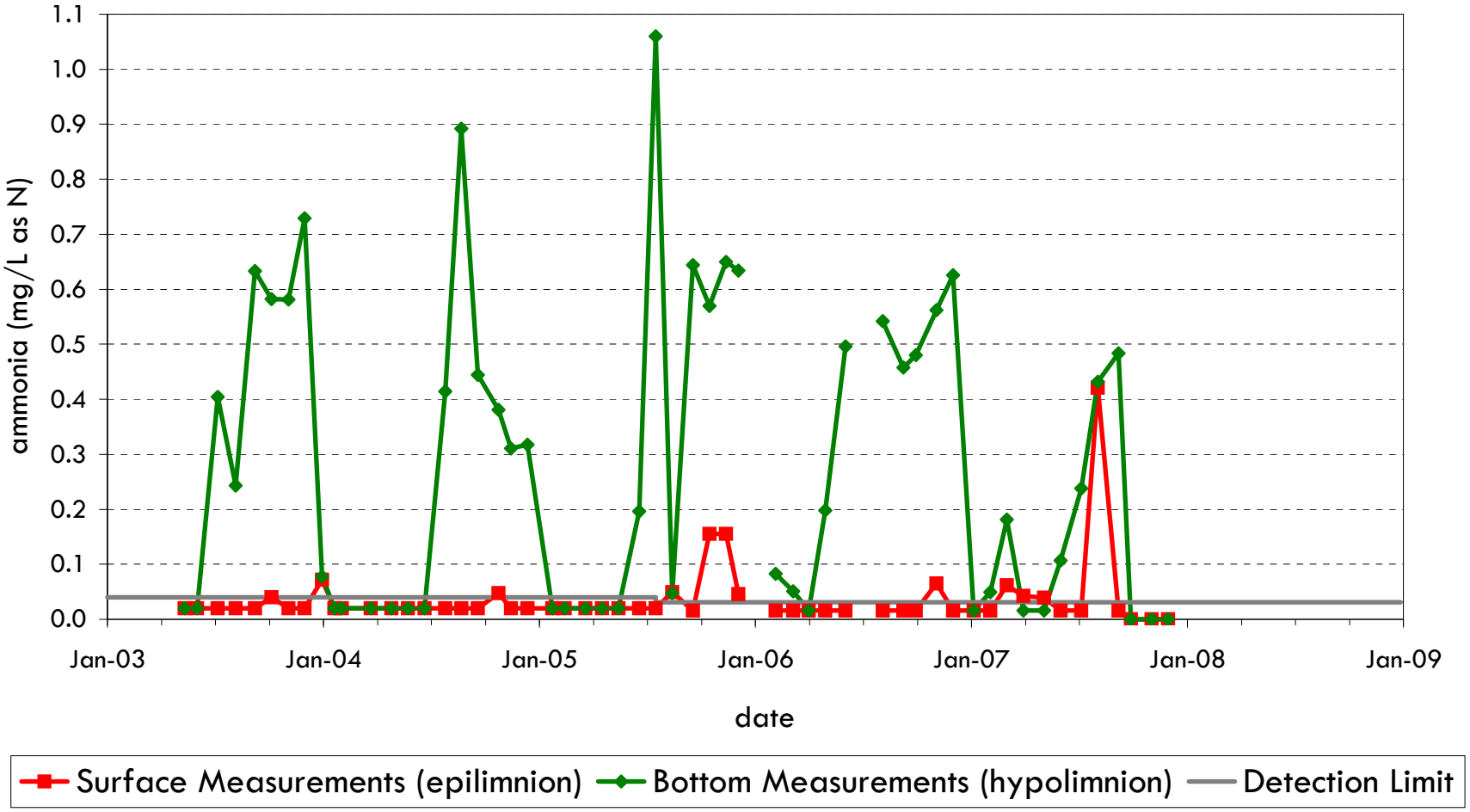

FSI V094005
May 01, 2012

Figure B-20

FLOW SCIENCE®

San Vicente Reservoir

In Reservoir Chlorophyll a Data

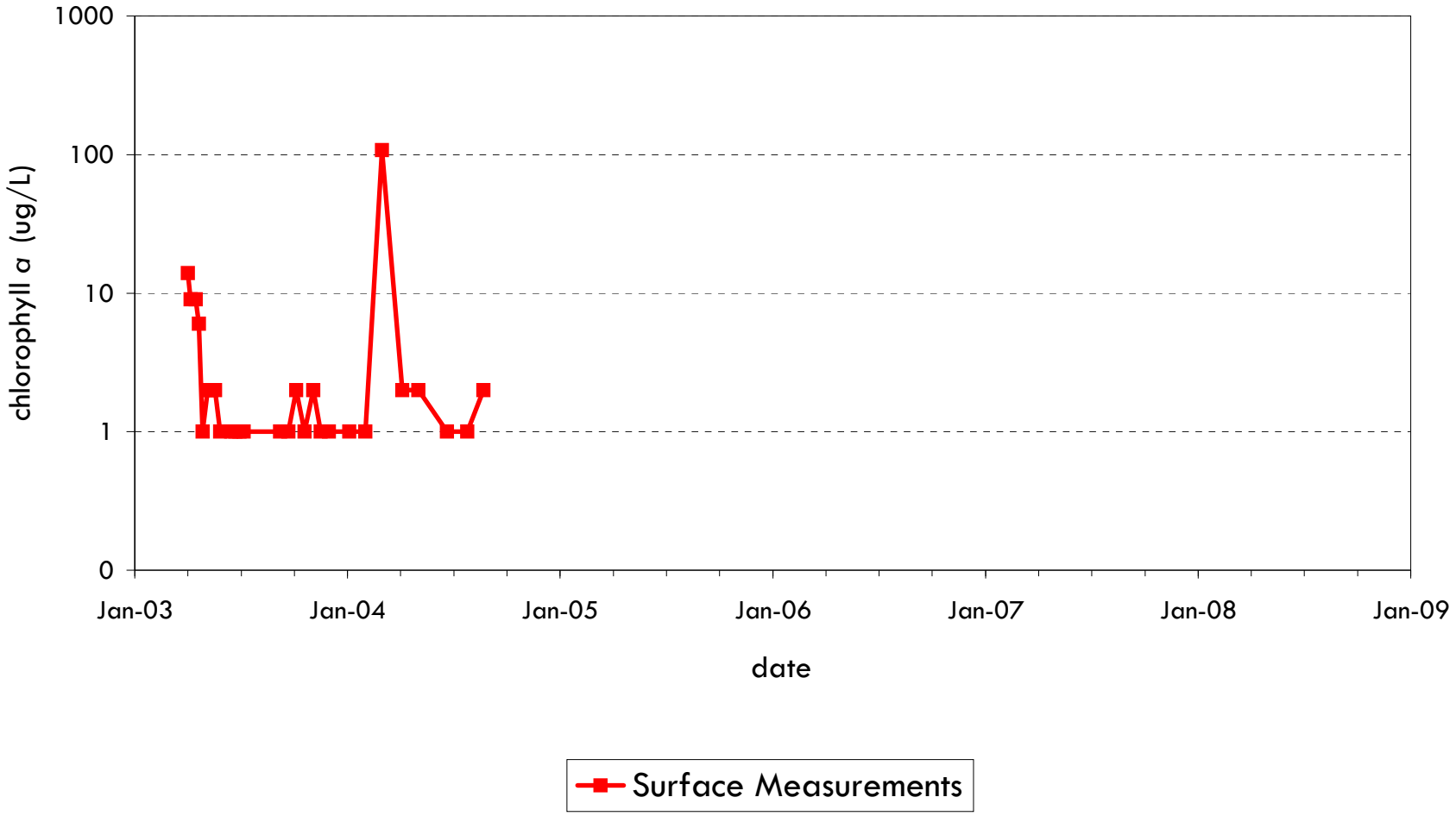

FSI V094005
May 01, 2012

Figure B-21

FLOW SCIENCE®

San Vicente Reservoir

In Reservoir Transparency Data

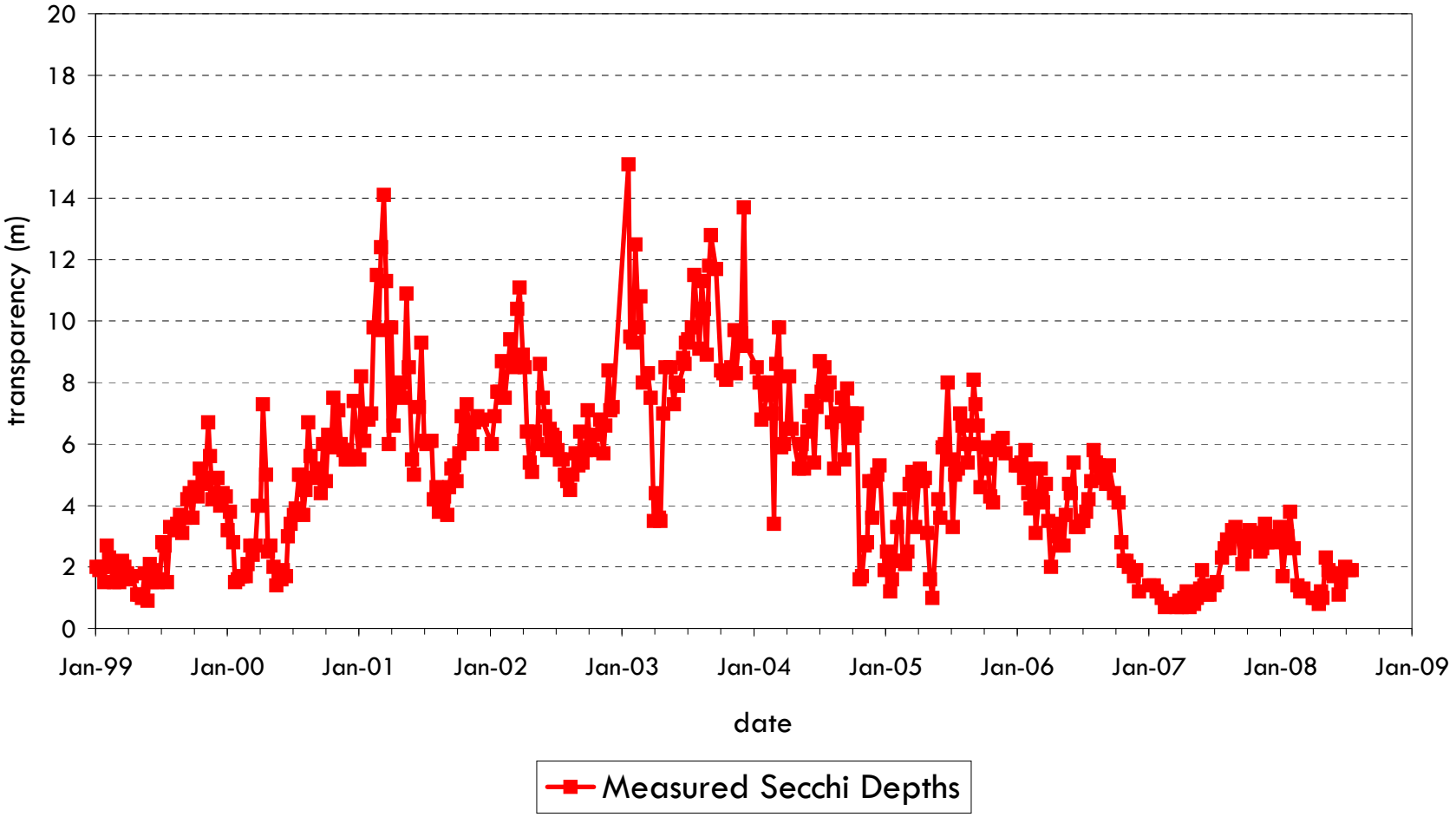

FSI V094005
May 01, 2012

Figure B-22

FLOW SCIENCE®

APPENDIX C

INPUTS FOR CALIBRATION
CALIBRATION/VALIDATION RESULTS

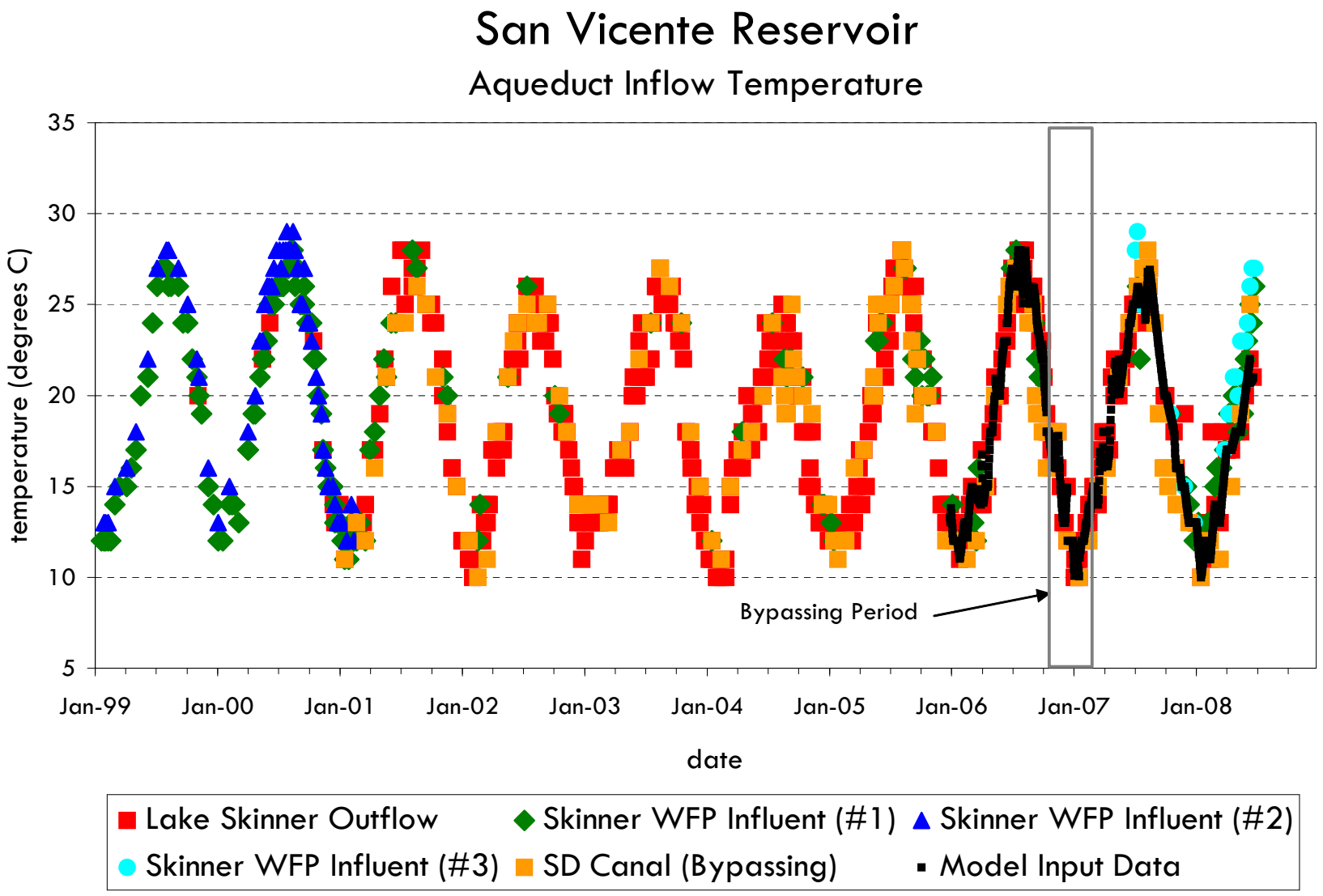

FSI V094005
May 01, 2012

Figure C-1

FLOW SCIENCE®

San Vicente Reservoir

Aqueduct Inflow Salinity/TDS

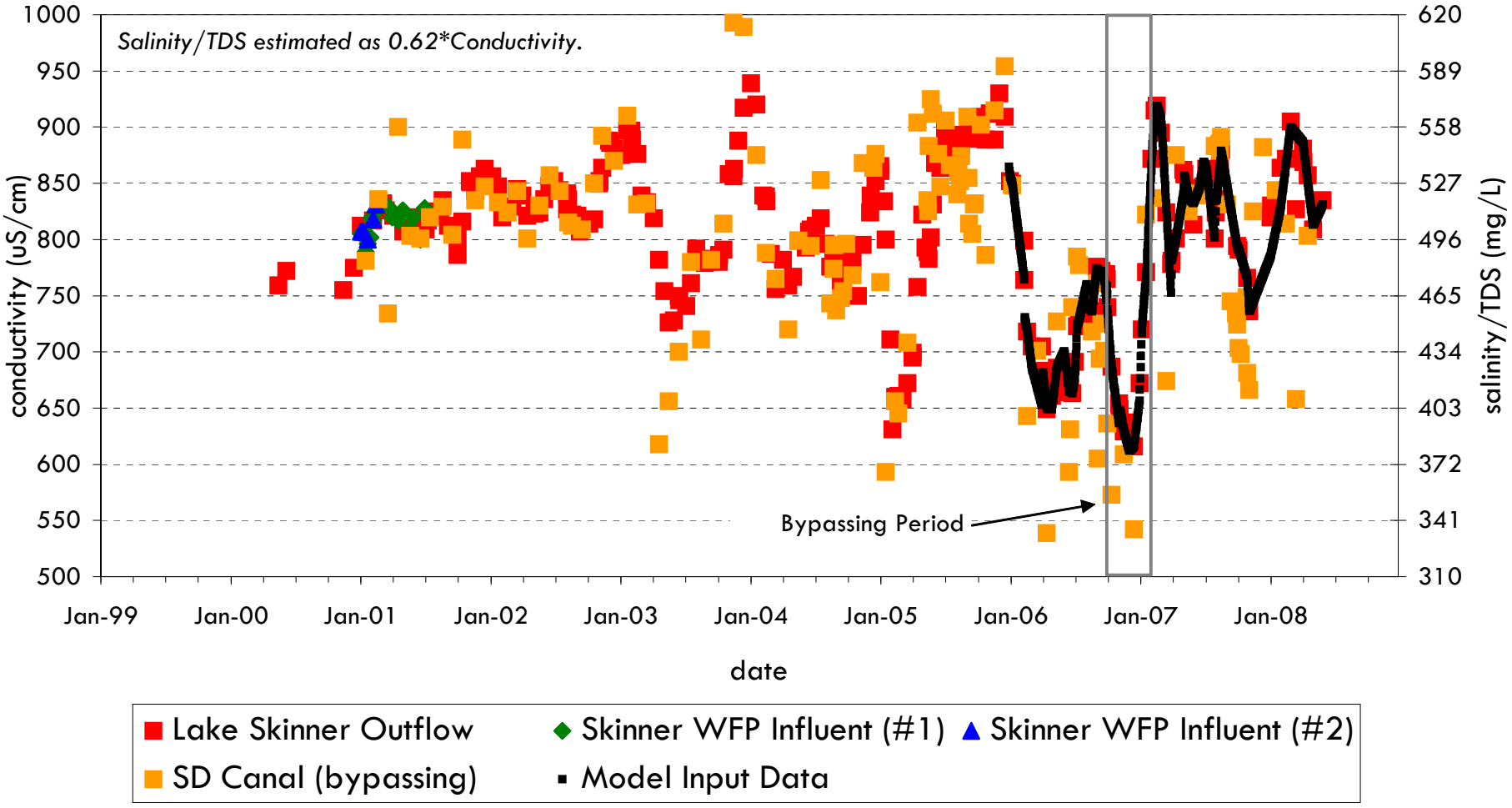

FSI V094005
May 01, 2012

Figure C-2

FLOW SCIENCE®

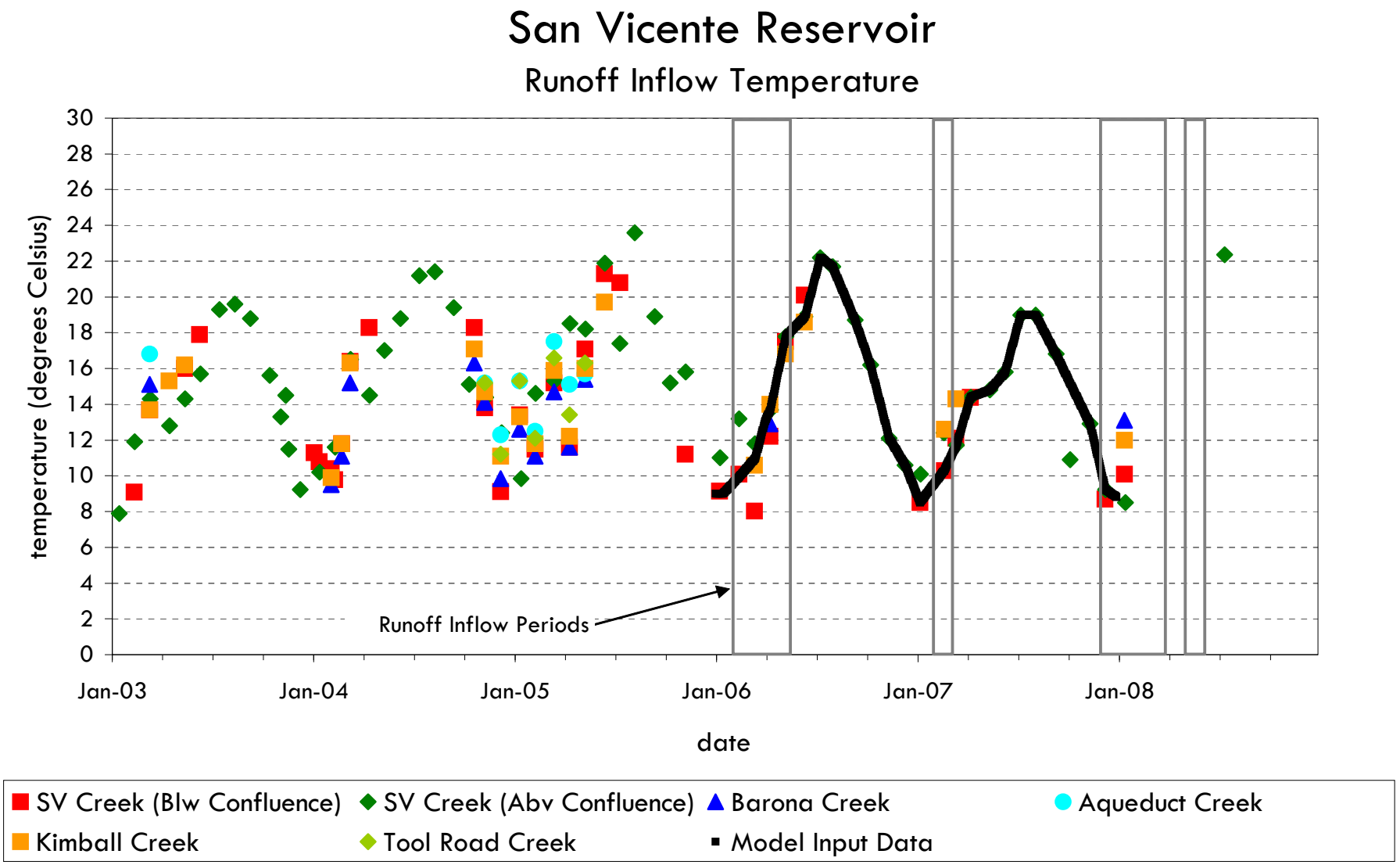

FSI V094005
May 01, 2012

Figure C-3

FLOW SCIENCE®

San Vicente Reservoir

Runoff Inflow Salinity/TDS

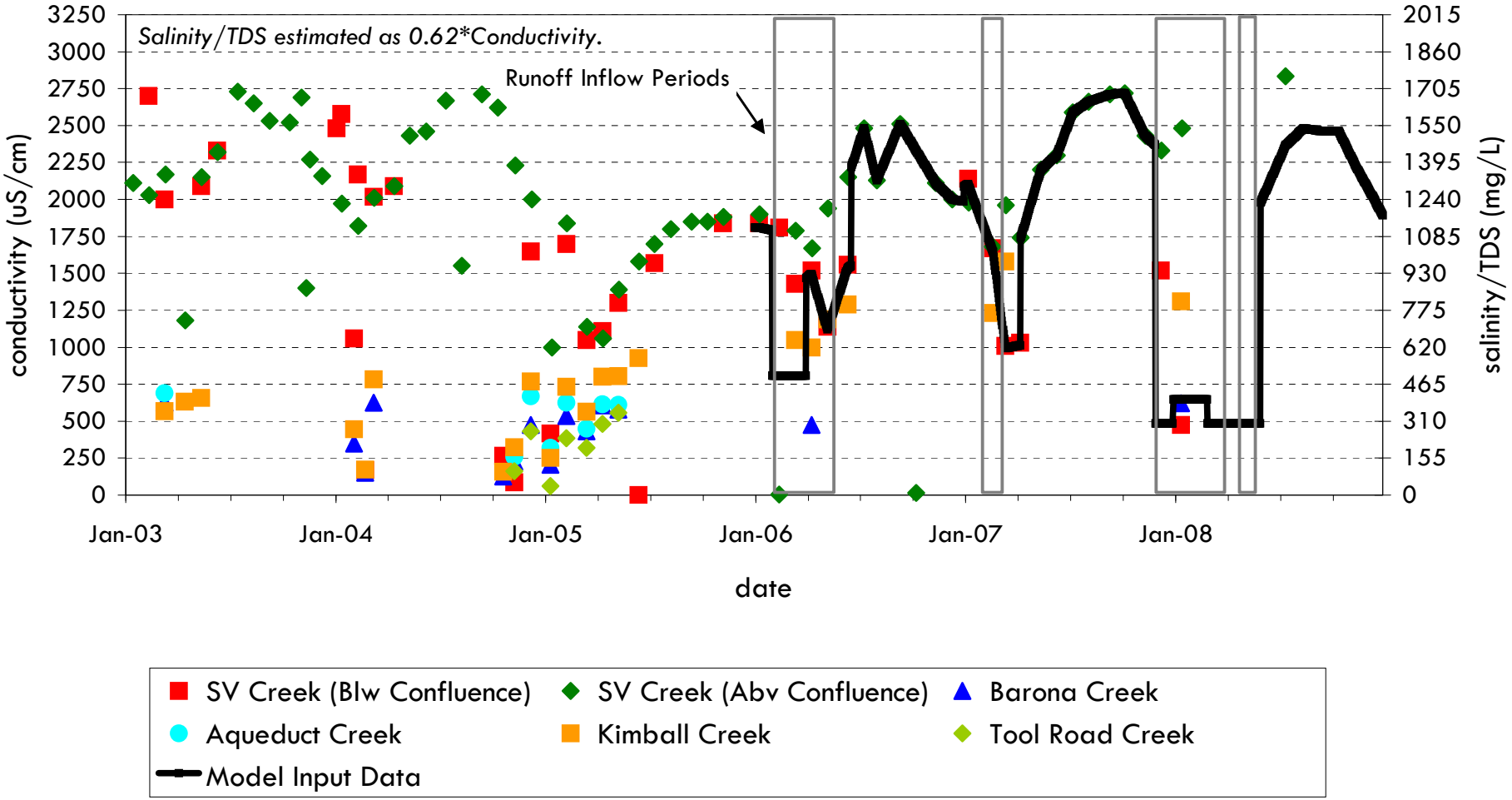

FSI V094005
May 01, 2012

Figure C-4

FLOW SCIENCE®

San Vicente Reservoir

Sutherland Reservoir Temperatures Near Outlet (El 1940 ft)

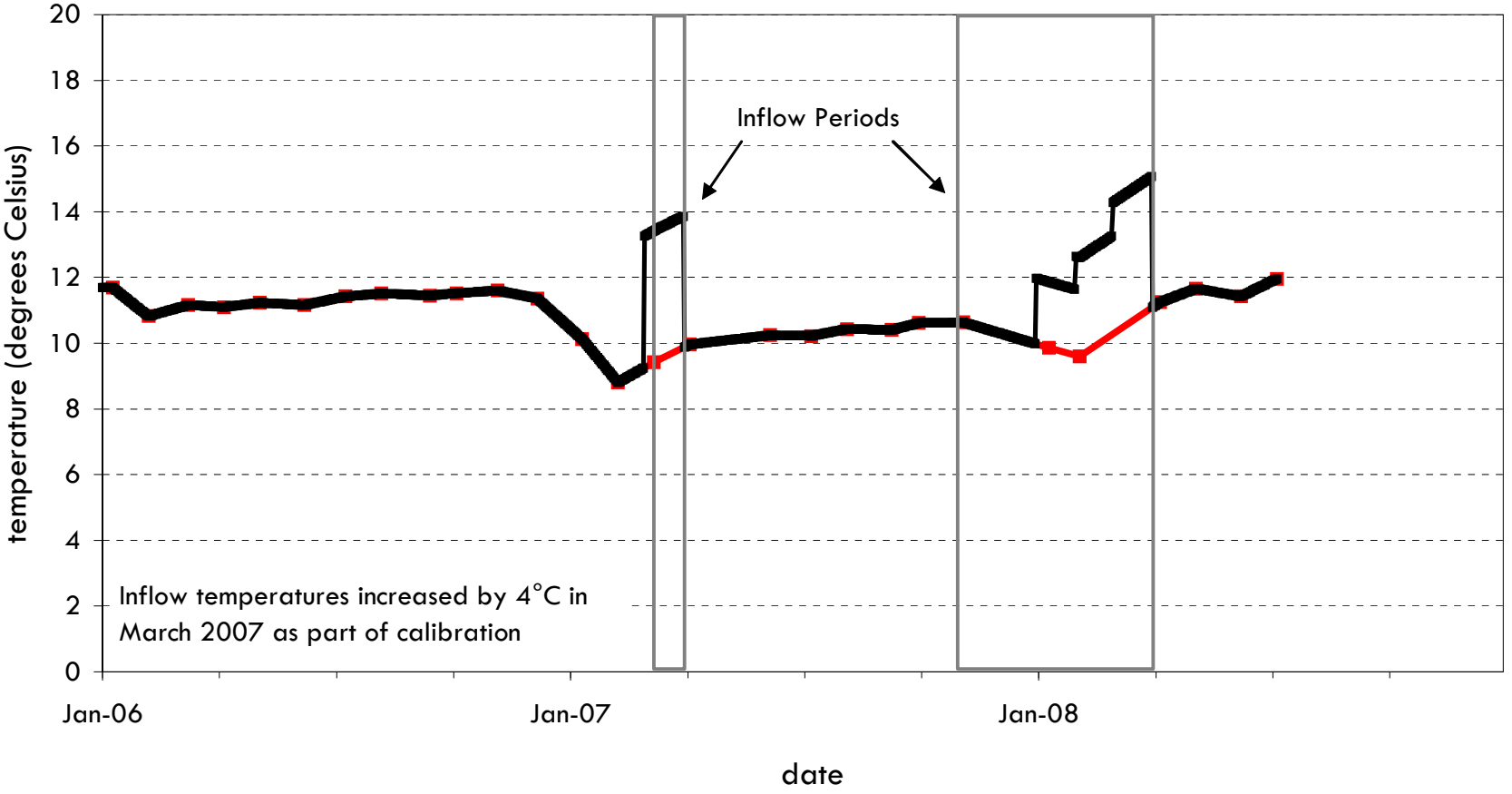

FSI V094005
May 01, 2012

Figure C-5

FLOW SCIENCE®

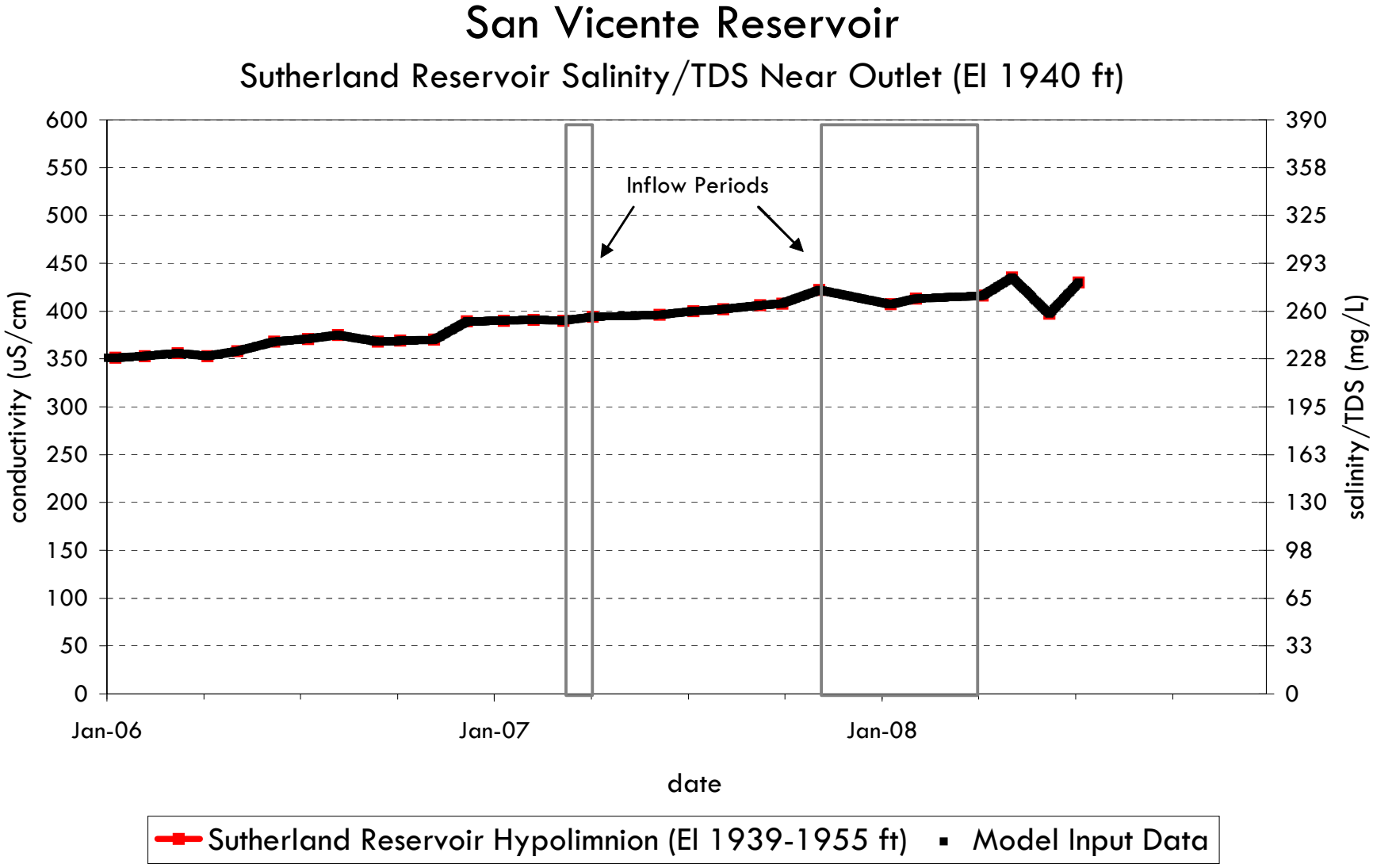

FSI V094005
May 01, 2012

Figure C-6

FLOW SCIENCE®

San Vicente Reservoir

Input Meteorological Data - Solar Radiation

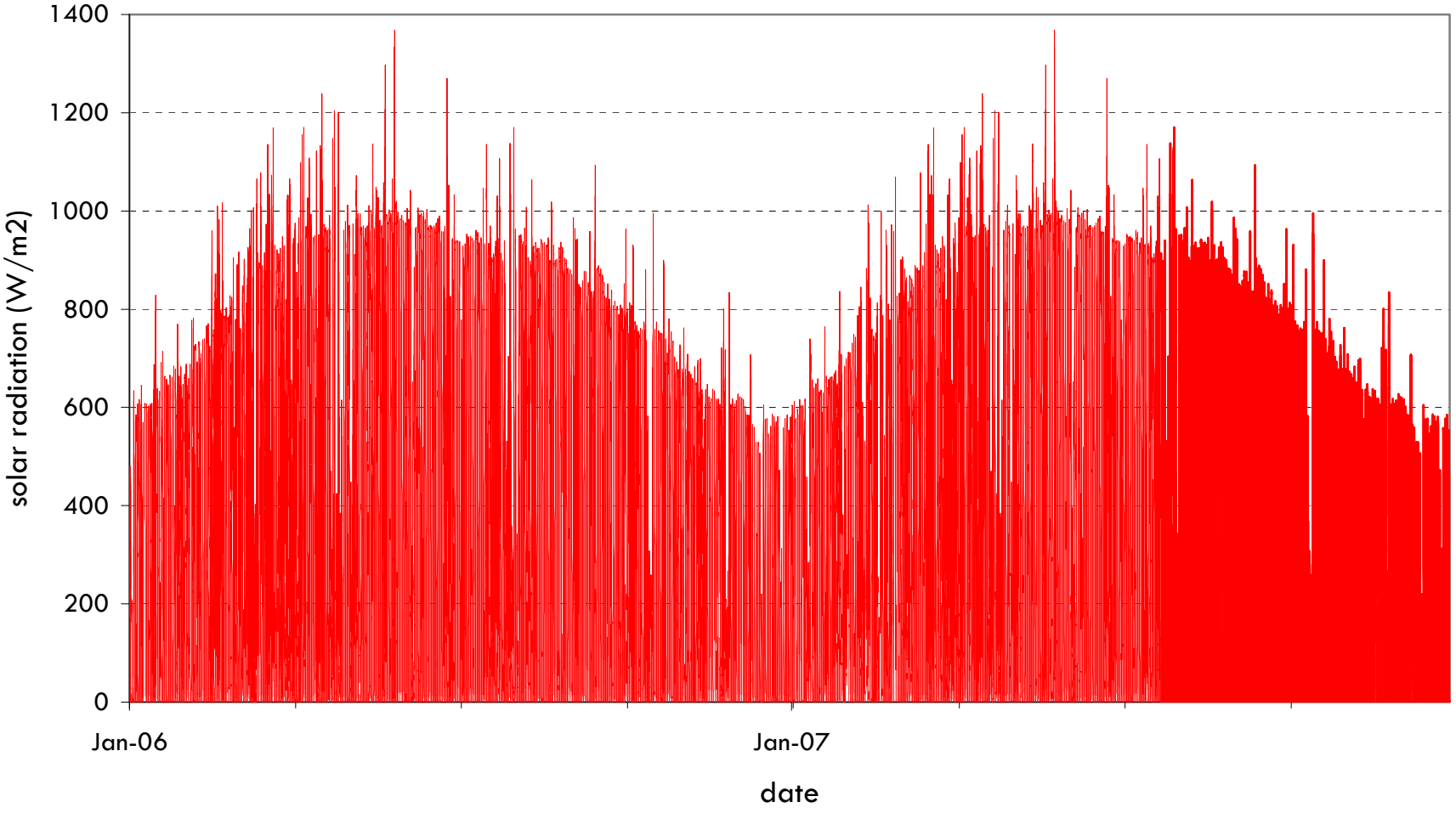

Figure C-7

FSI V094005
May 01, 2012

FLOW SCIENCE®

San Vicente Reservoir

Input Meteorological Data - Air Temperature

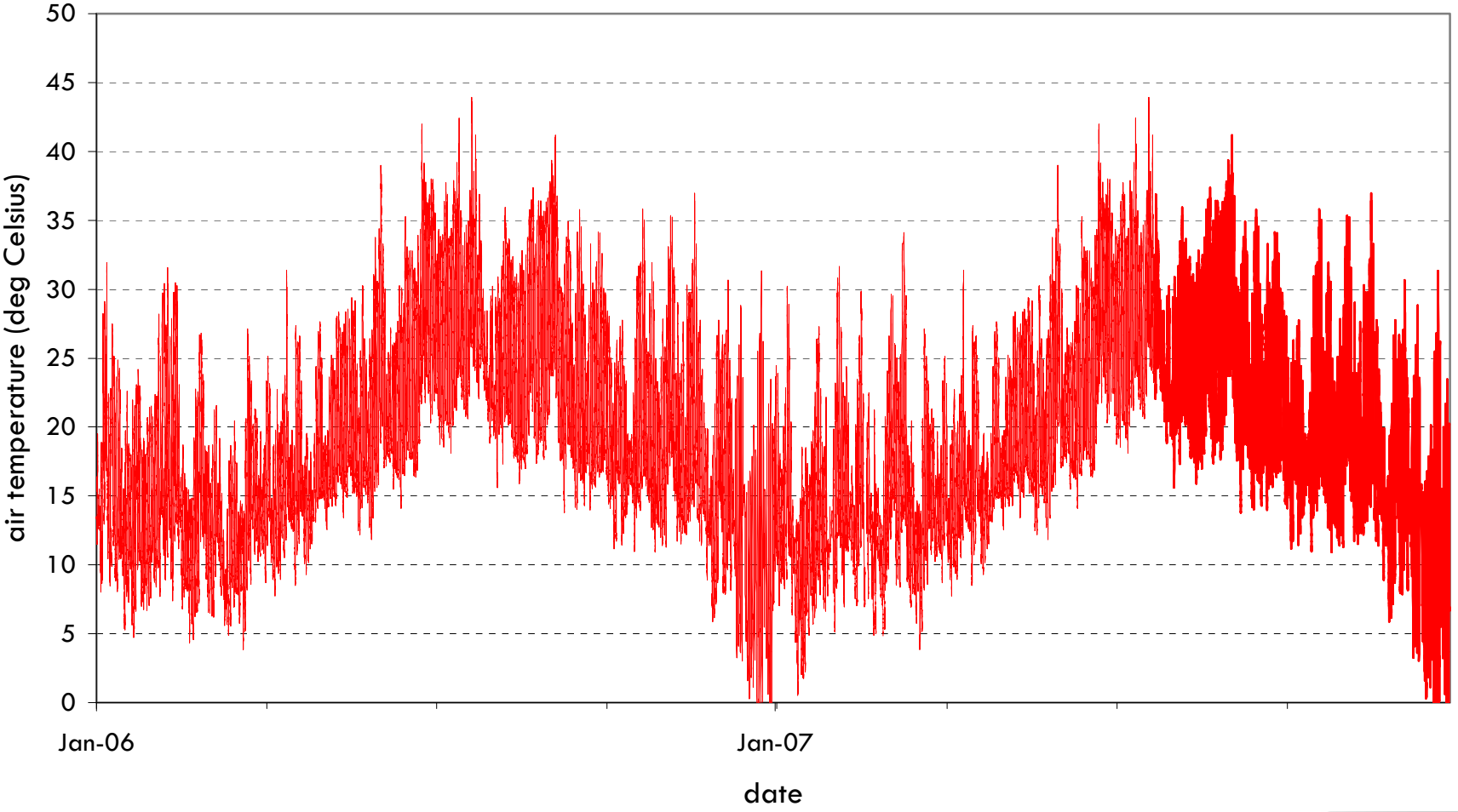

Figure C-8

FSI V094005
May 01, 2012

FLOW SCIENCE®

San Vicente Reservoir

Input Meteorological Data - Wind Speed

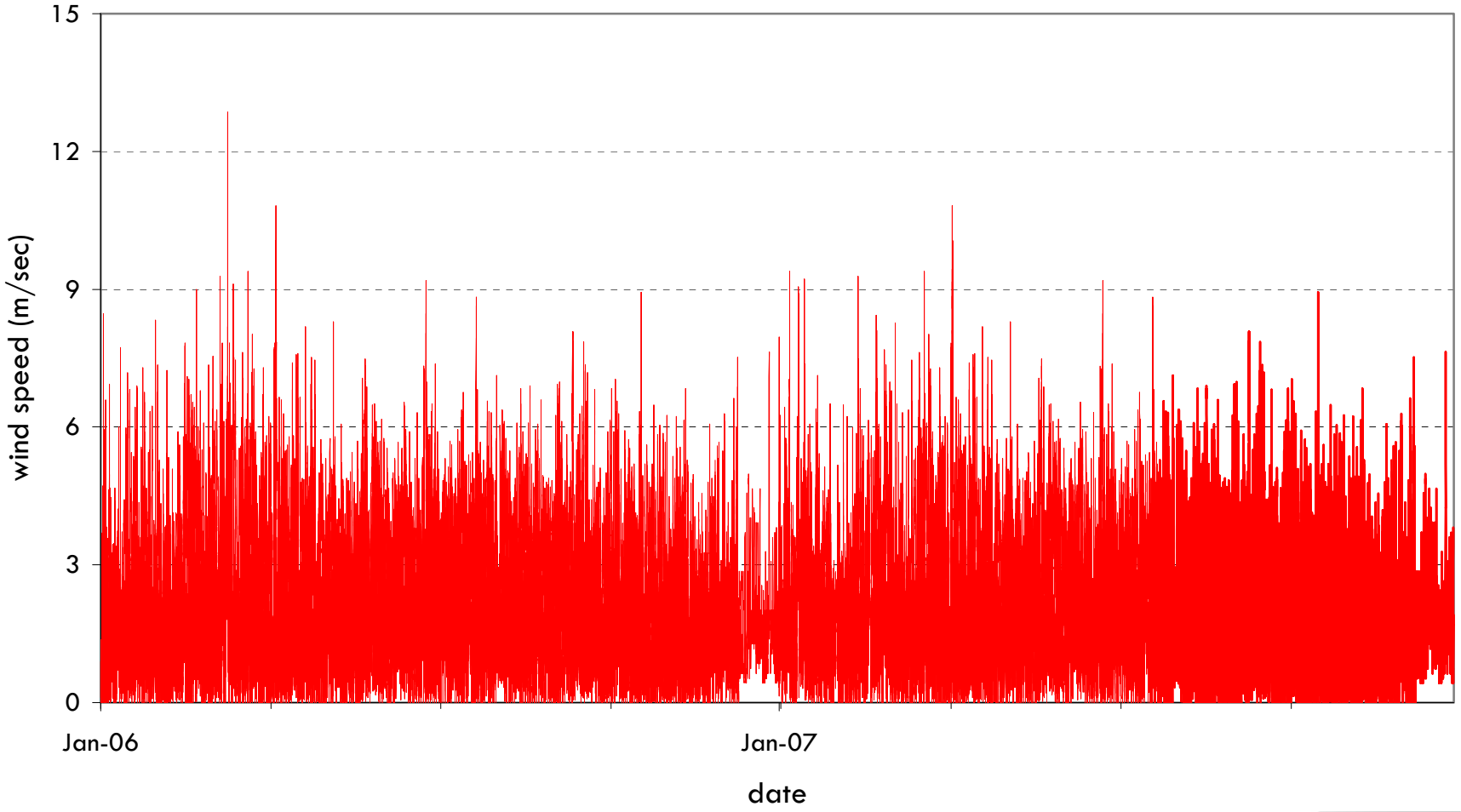

Figure C-9

FSI V094005
May 01, 2012

FLOW SCIENCE®

San Vicente Reservoir

Input Meteorological Data - Wind Direction

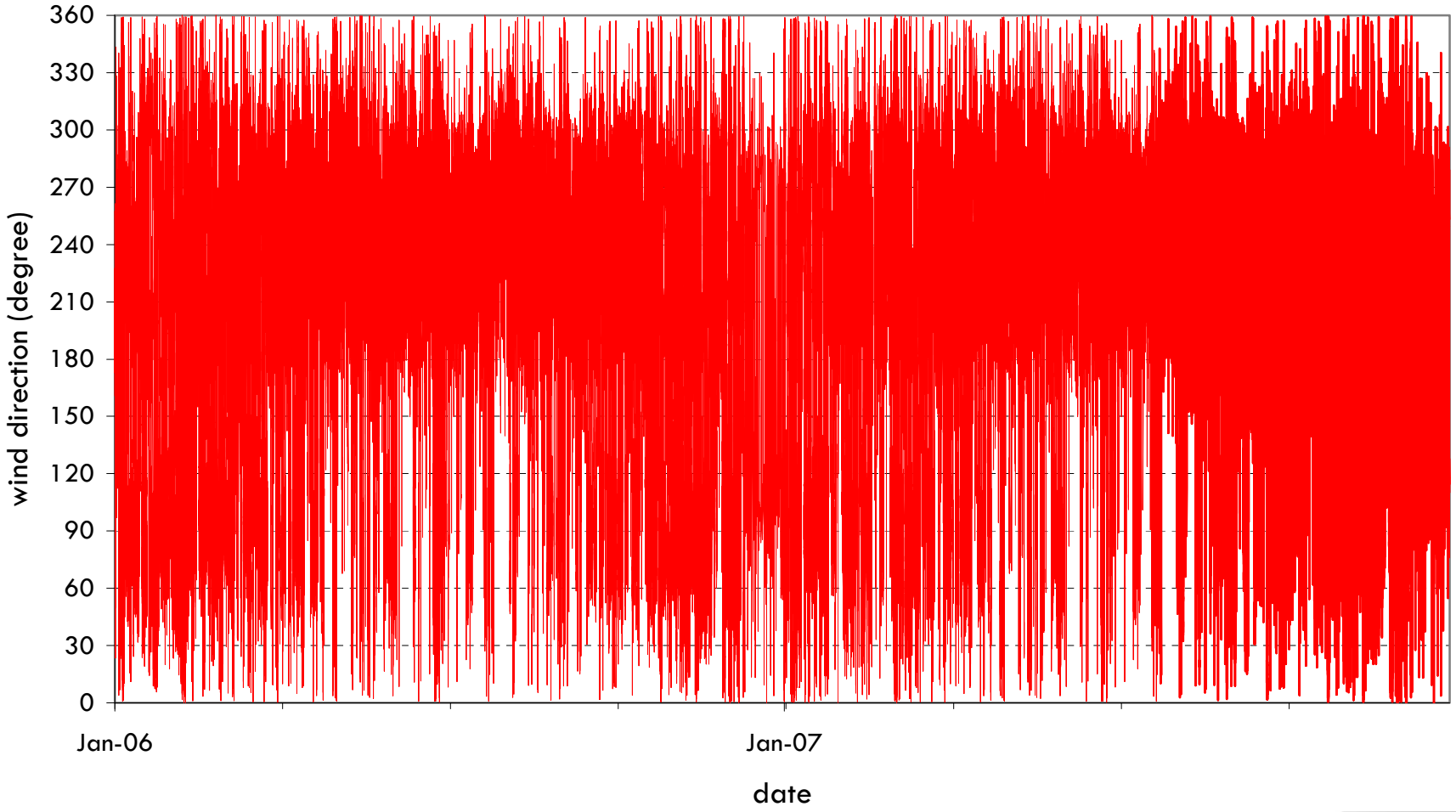

Figure C-10

FSI V094005
May 01, 2012

FLOW SCIENCE®

San Vicente Reservoir

Input Meteorological Data - Relative Humidity

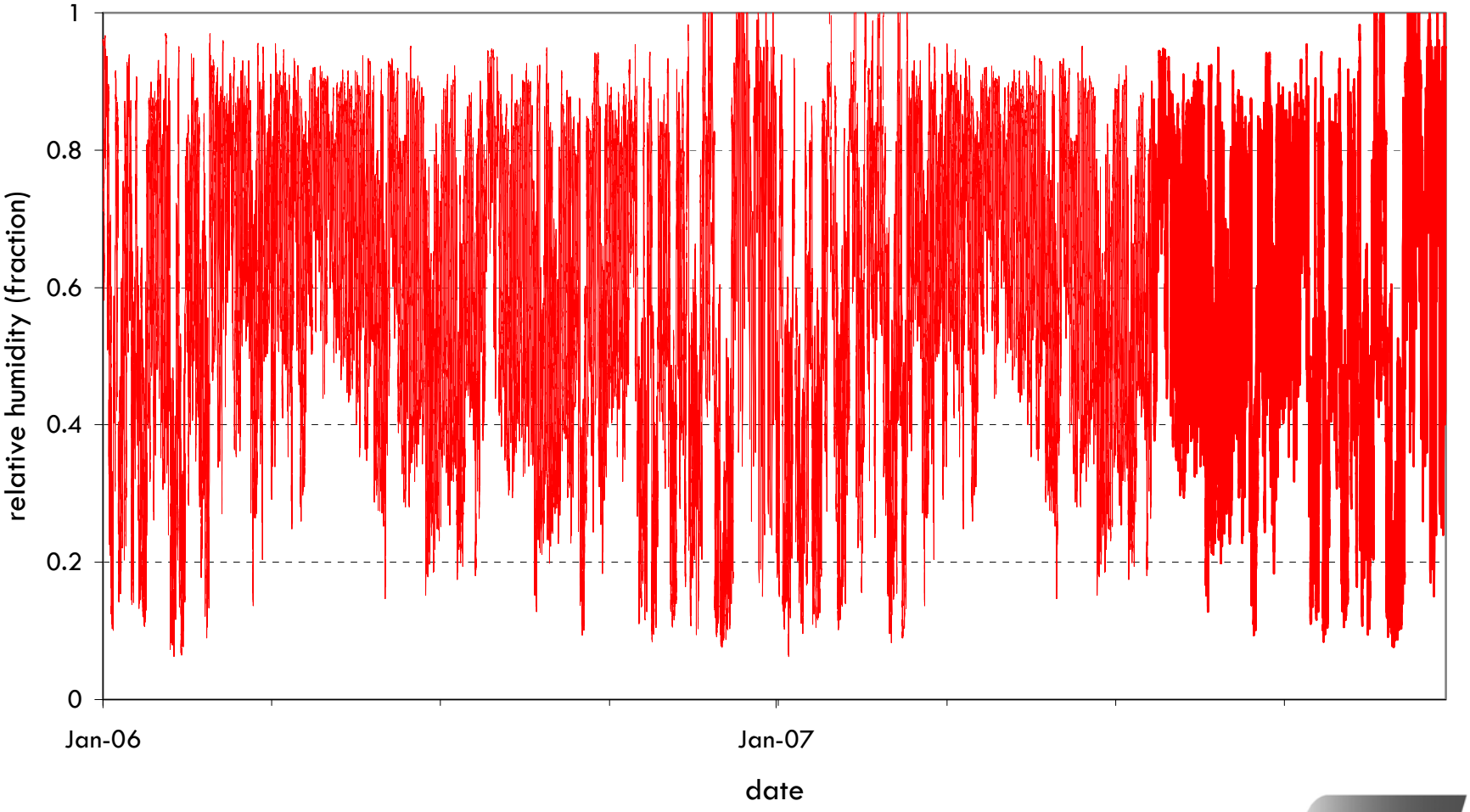

Figure C-11

FSI V094005
May 01, 2012

FLOW SCIENCE®

San Vicente Reservoir

Input Meteorological Data - Precipitation Rate

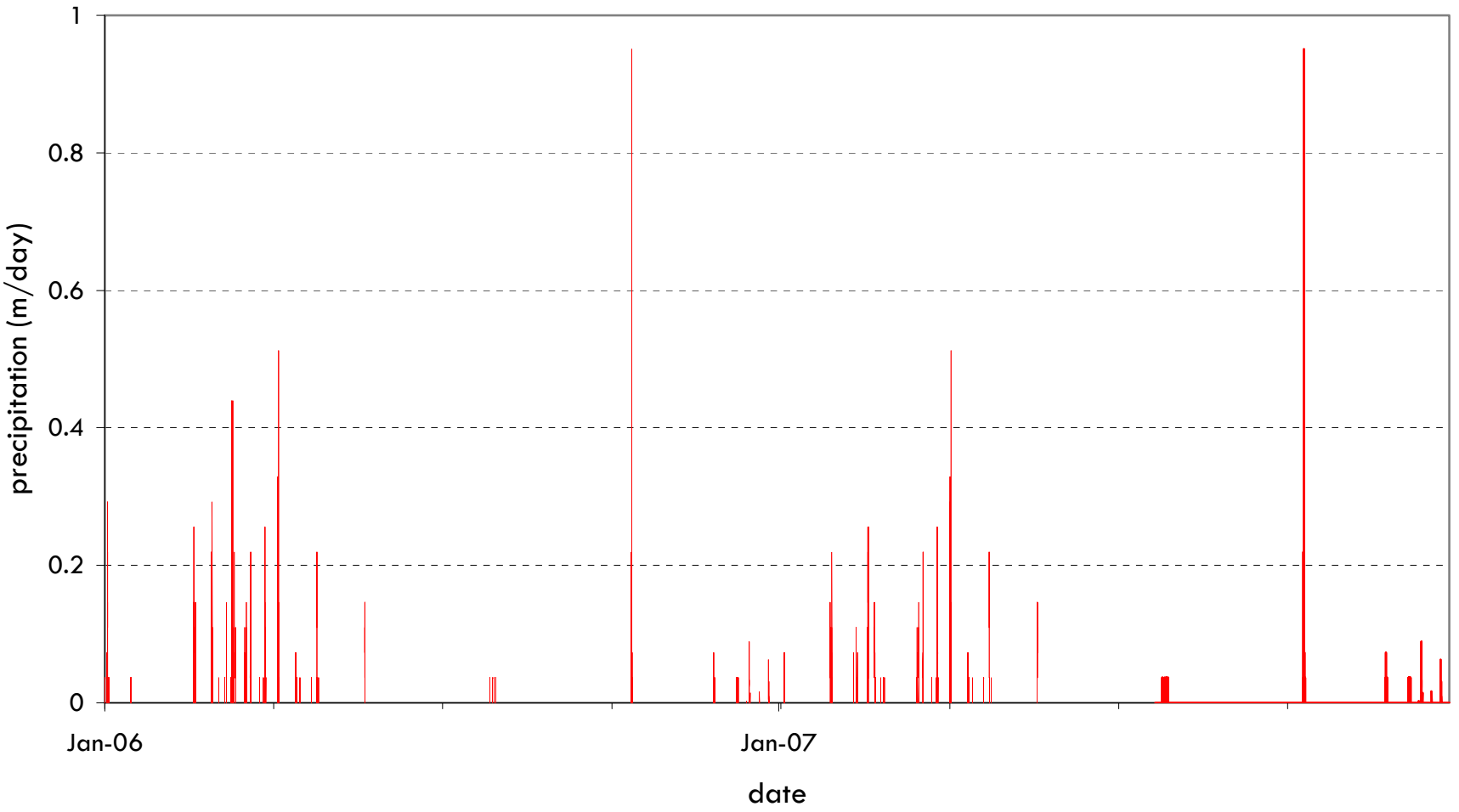

Figure C-12

FSI V094005
May 01, 2012

FLOW SCIENCE®

San Vicente Reservoir Station A - Water Temperature Calibration

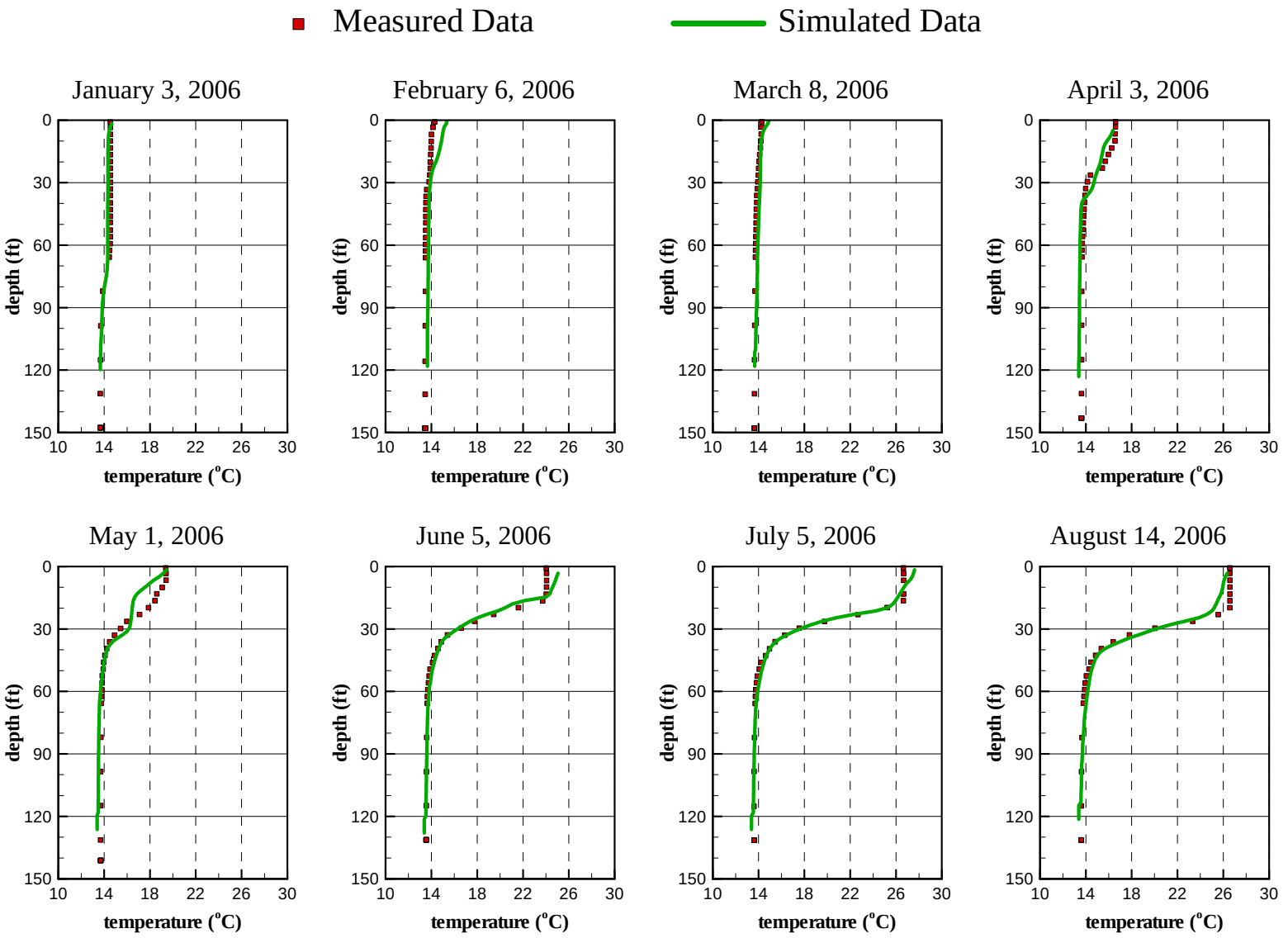

FSI V094005
May 01, 2012

Figure C-13

FLOW SCIENCE®

San Vicente Reservoir Station A - Water Temperature Calibration

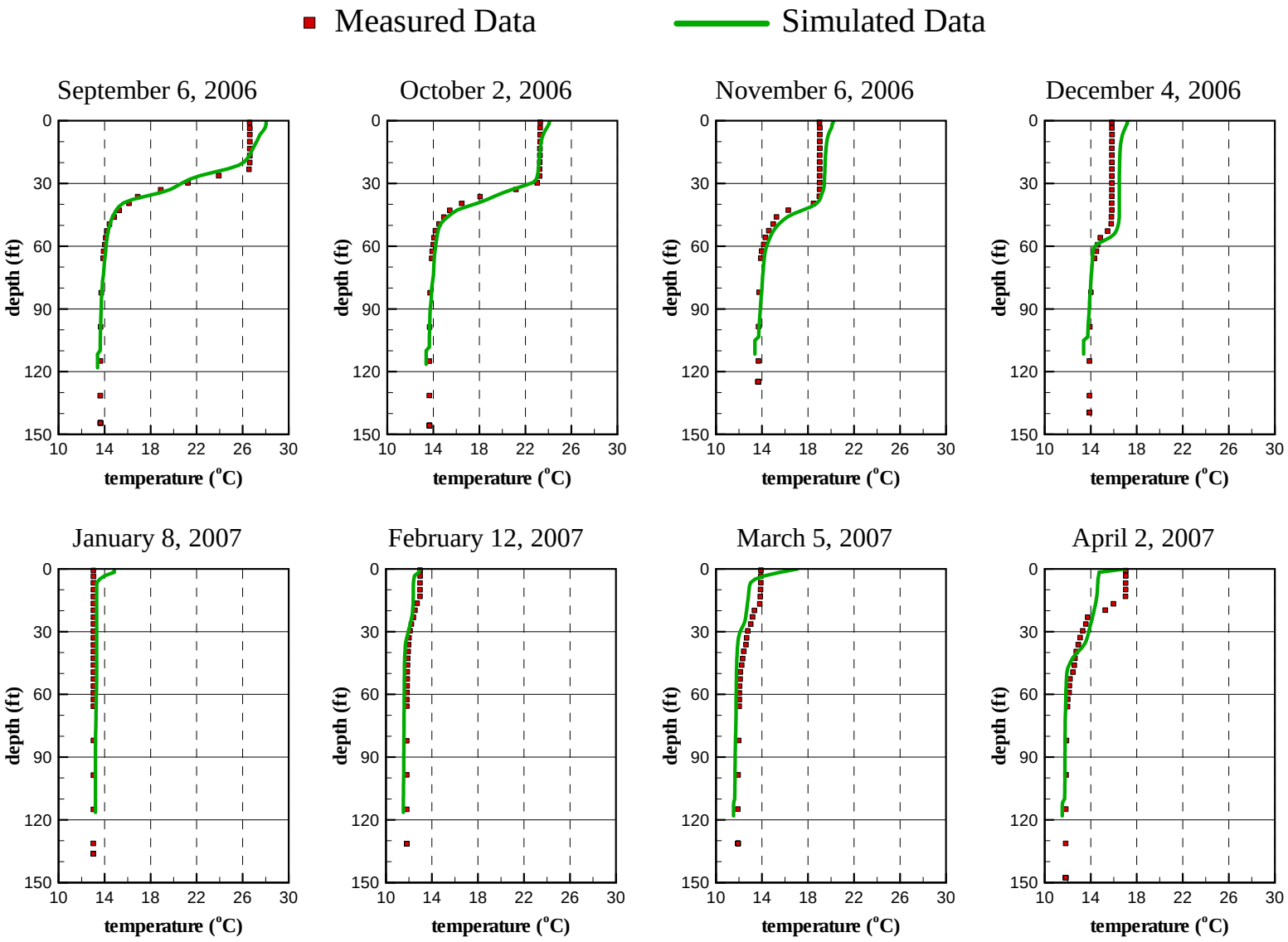

Figure C-14

FSI V094005
May 01, 2012

FLOW SCIENCE®

San Vicente Reservoir Station A - Water Temperature Calibration

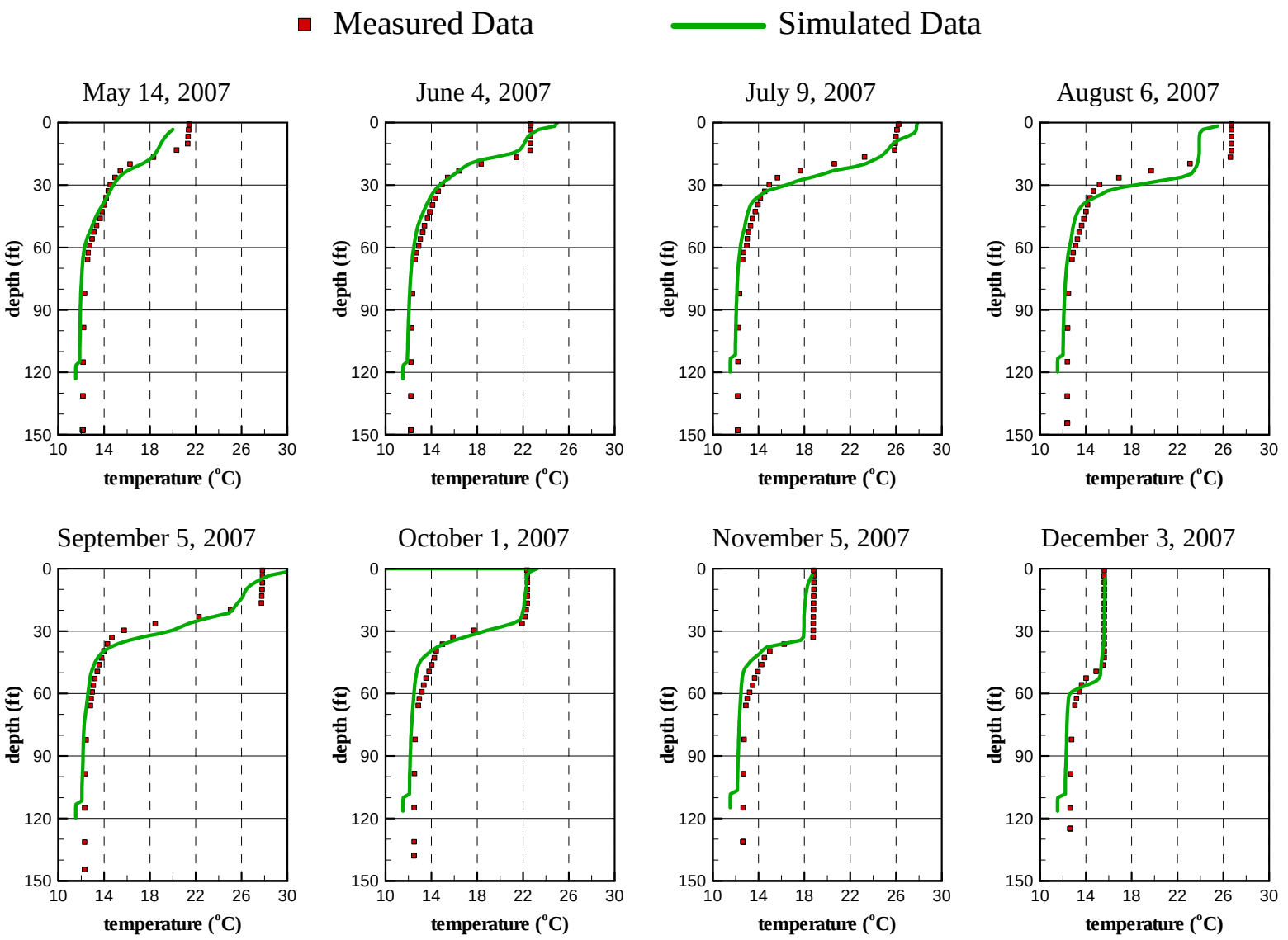

FSI V094005
May 01, 2012

Figure C-15

FLOW SCIENCE®

San Vicente Reservoir

1995 Tracer Winter Study – Measured Tracer versus Simulated Conservative Tracer

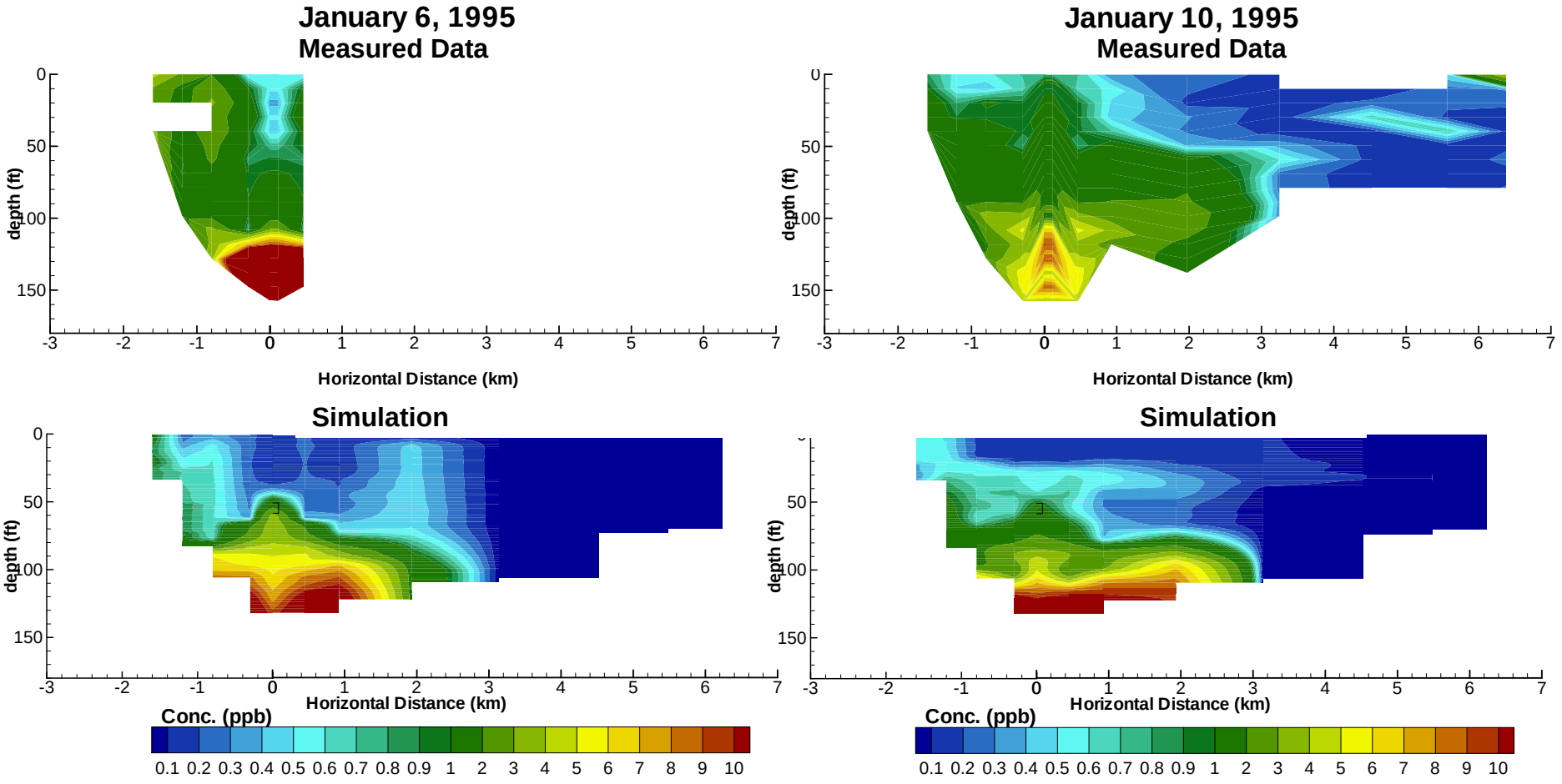

FSI V094005
May 01, 2012

Figure C-16

FLOW SCIENCE®

San Vicente Reservoir

1995 Tracer Winter Study – Measured Tracer versus Simulated Conservative Tracer

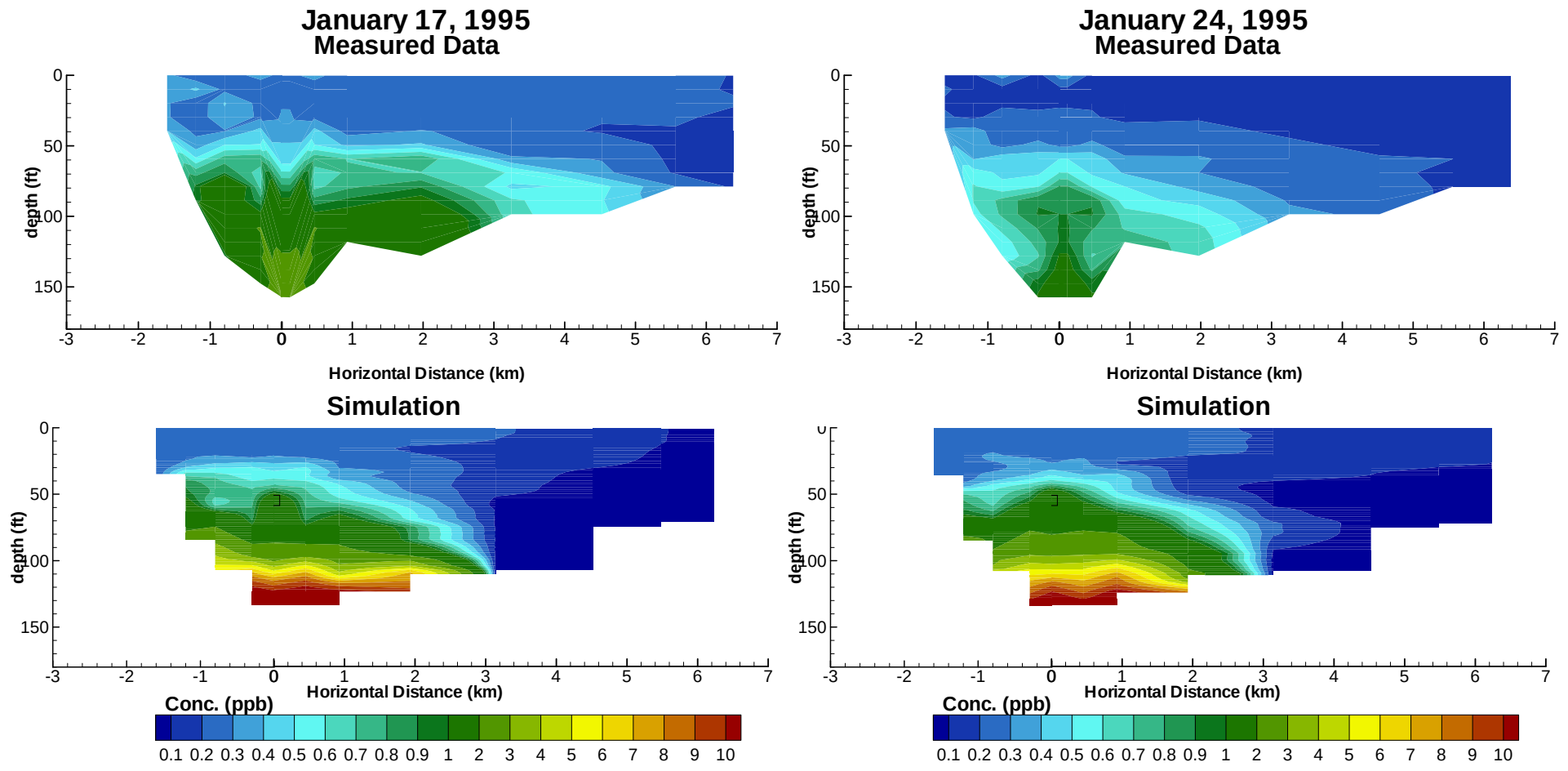

FSI V094005
May 01, 2012

Figure C-17

FLOW SCIENCE®

San Vicente Reservoir

1995 Tracer Winter Study – Measured Tracer versus Simulated Conservative Tracer

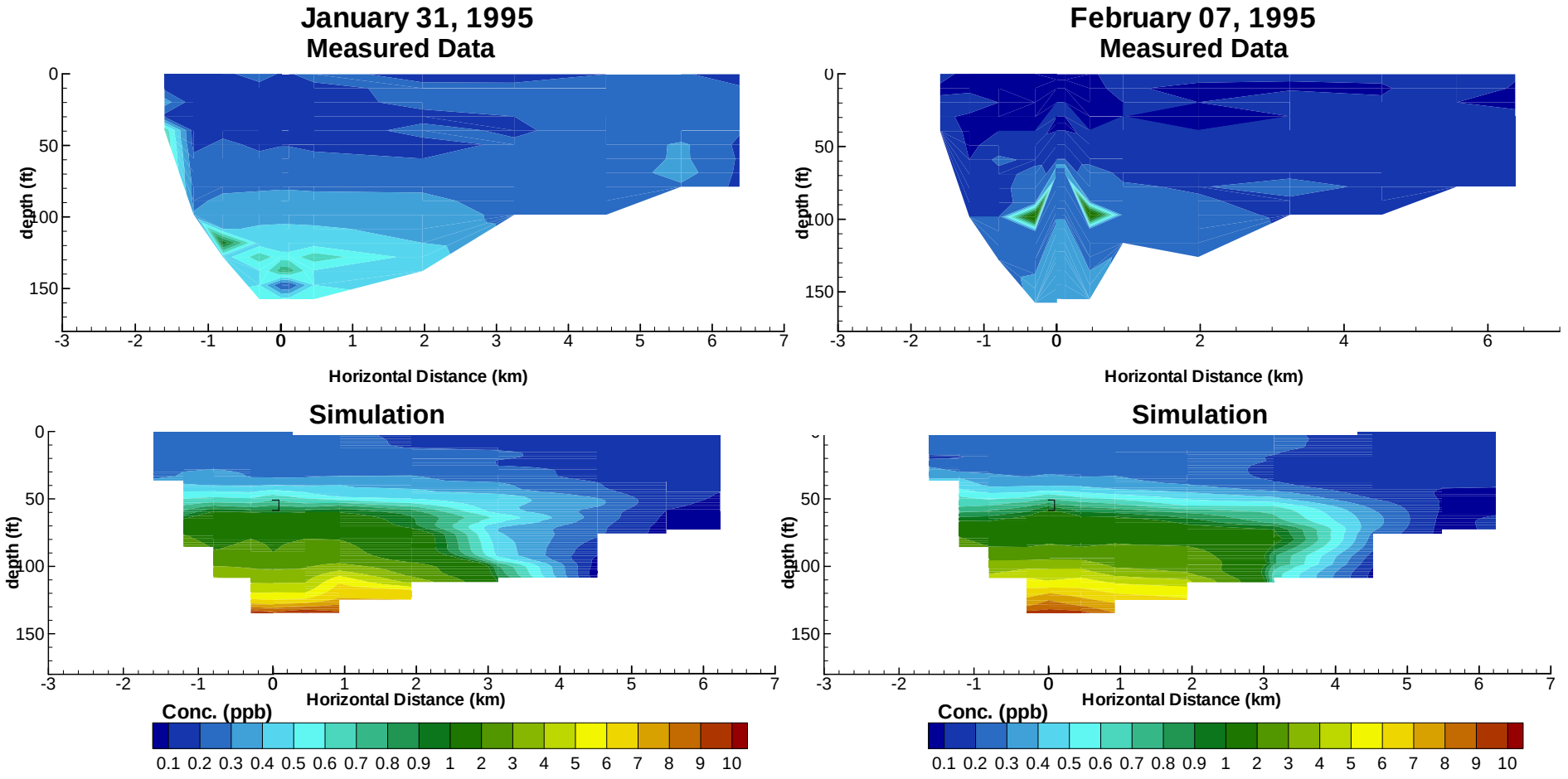

FSI V094005
May 01, 2012

Figure C-18

FLOW SCIENCE®

San Vicente Reservoir

1995 Tracer Summer Study – Measured Tracer versus Simulated Conservative Tracer

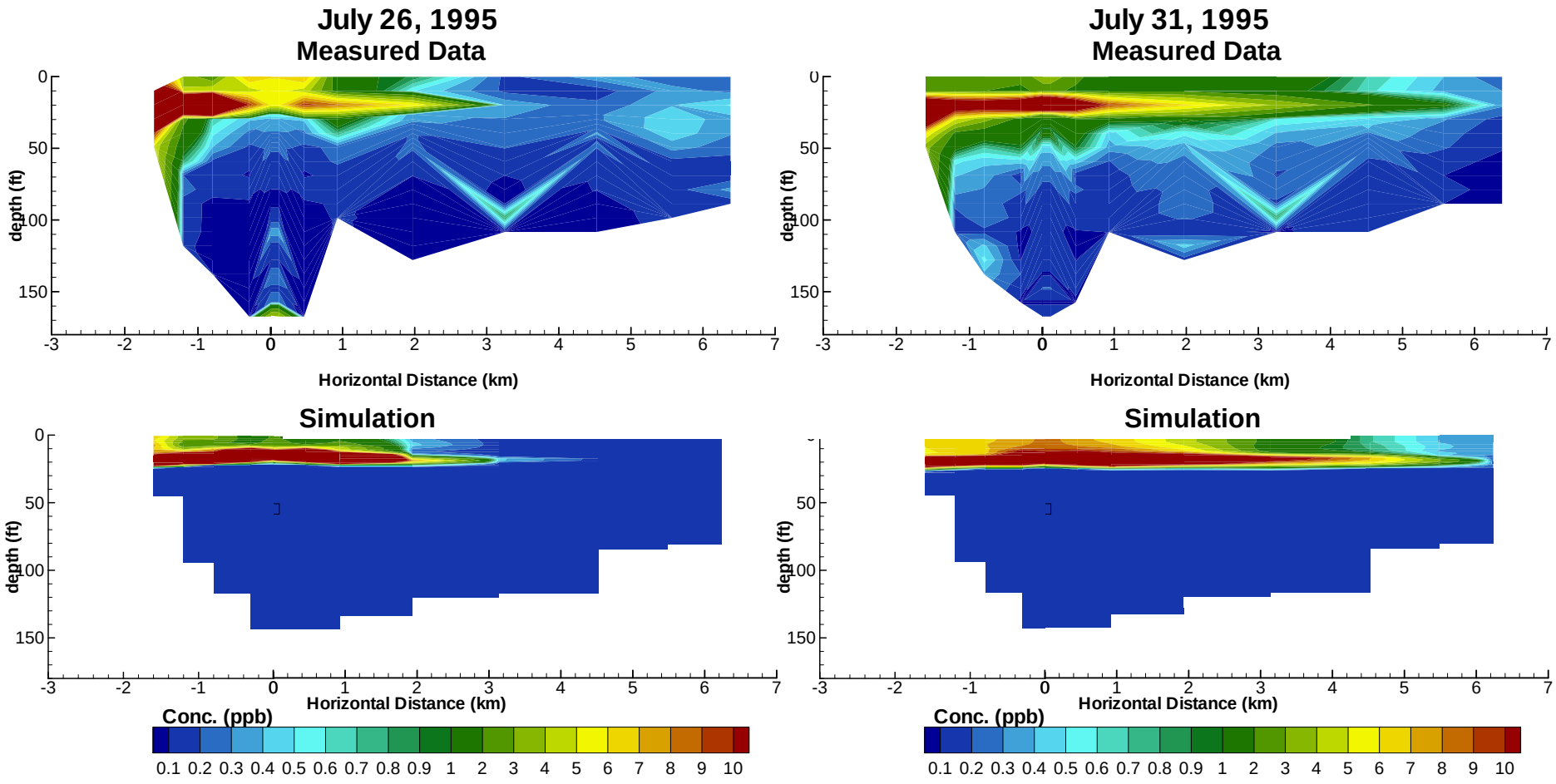

FSI V094005
May 01, 2012

Figure C-19

FLOW SCIENCE®

San Vicente Reservoir

1995 Tracer Summer Study – Measured Tracer versus Simulated Conservative Tracer

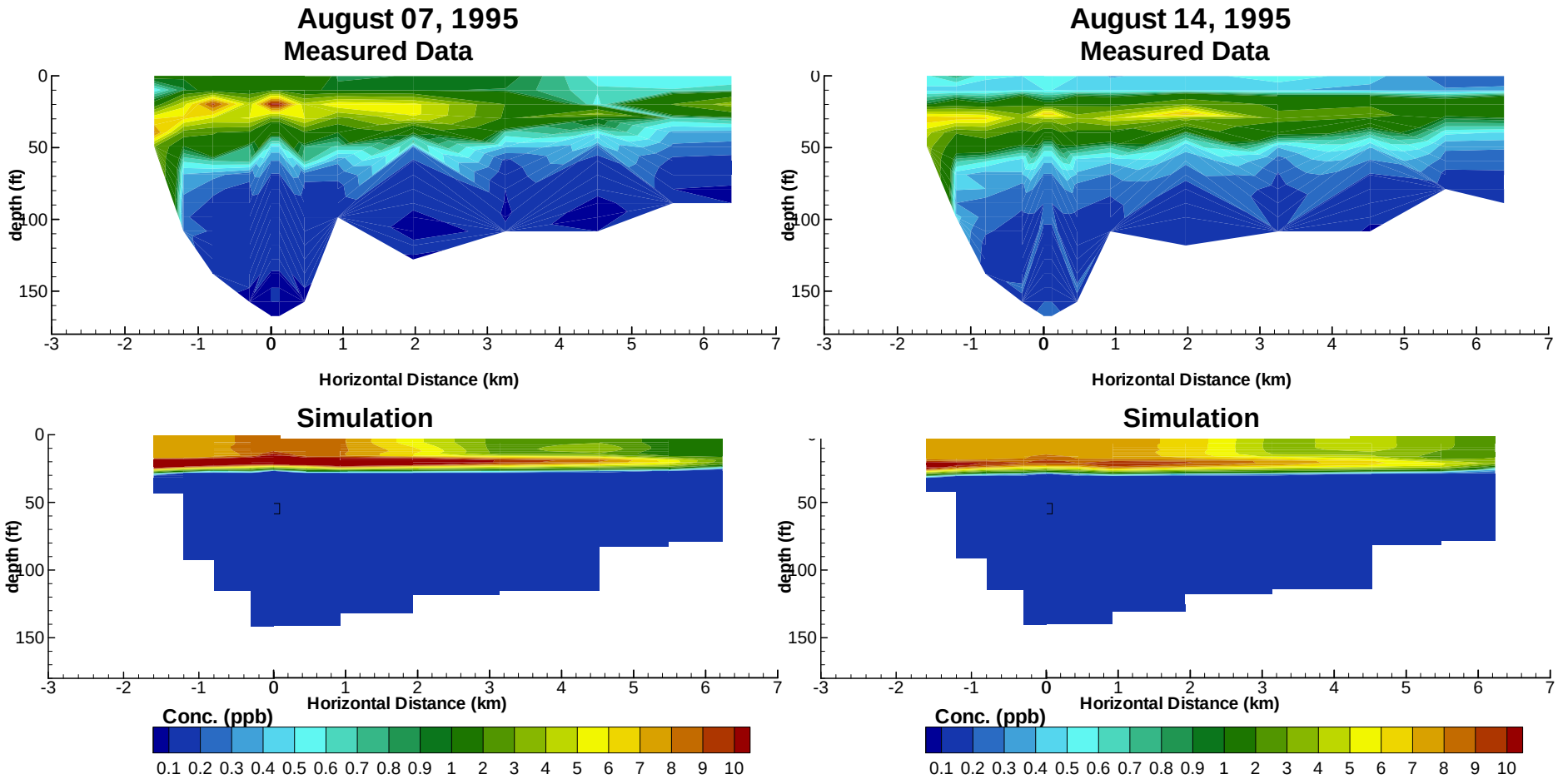

FSI V094005
May 01, 2012

Figure C-20

FLOW SCIENCE®

San Vicente Reservoir

1995 Tracer Summer Study – Measured Tracer versus Simulated Conservative Tracer

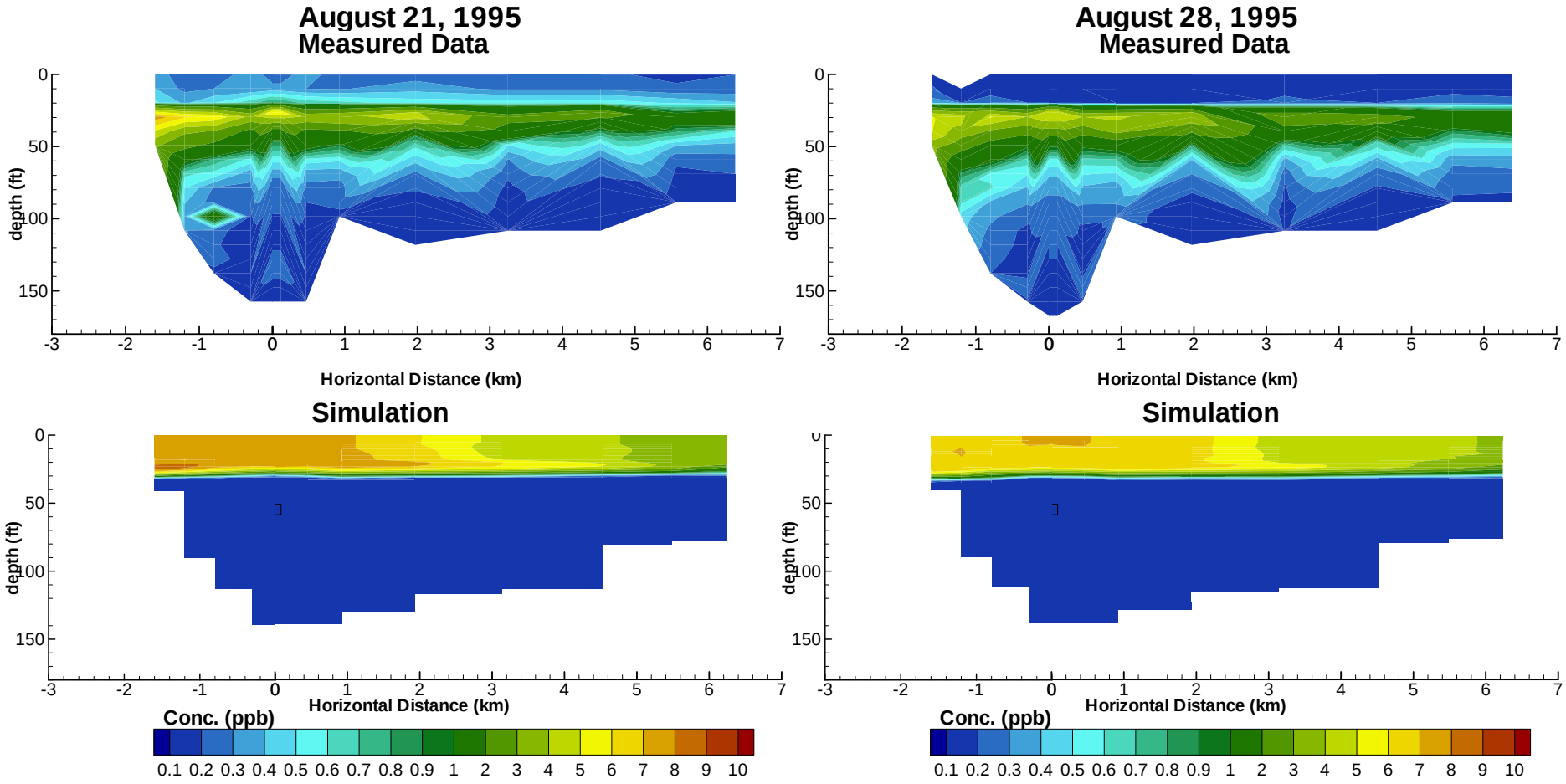

FSI V094005
May 01, 2012

Figure C-21

FLOW SCIENCE®

San Vicente Reservoir

1995 Tracer Summer Study – Measured Tracer versus Simulated Conservative Tracer

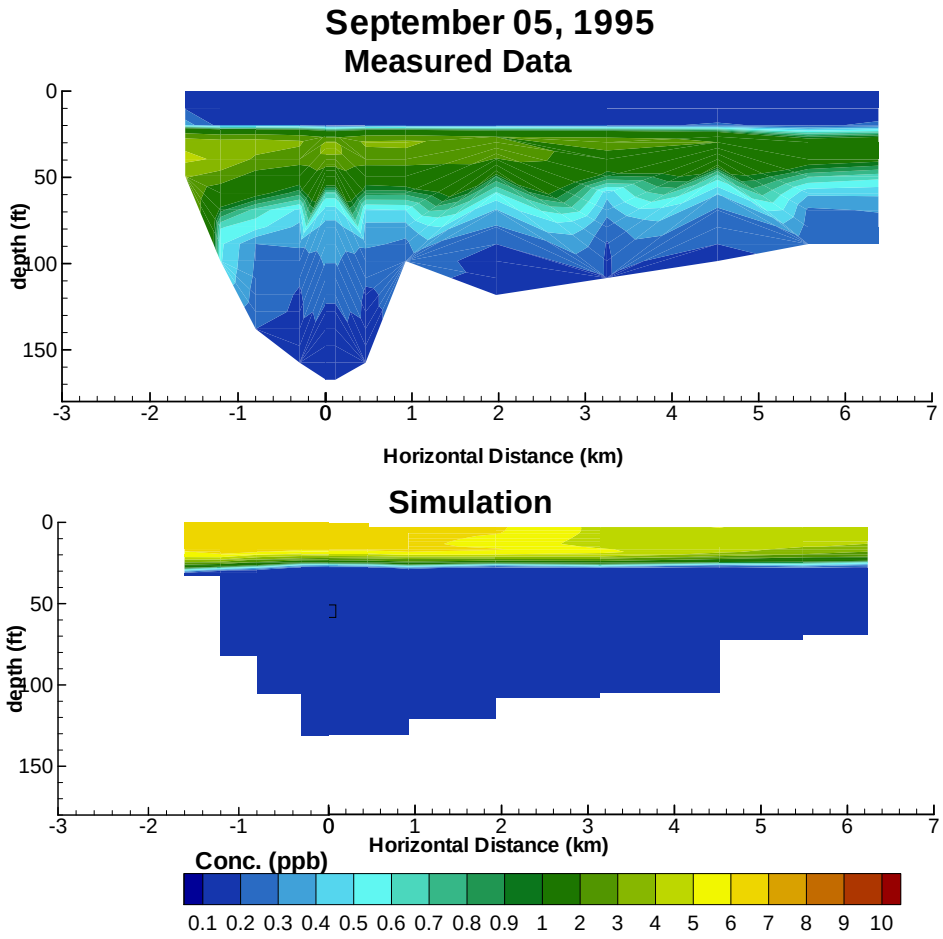

FSI V094005
May 01, 2012

Figure C-22

FLOW SCIENCE®

San Vicente Reservoir

Aqueduct Inflow Ammonia Data

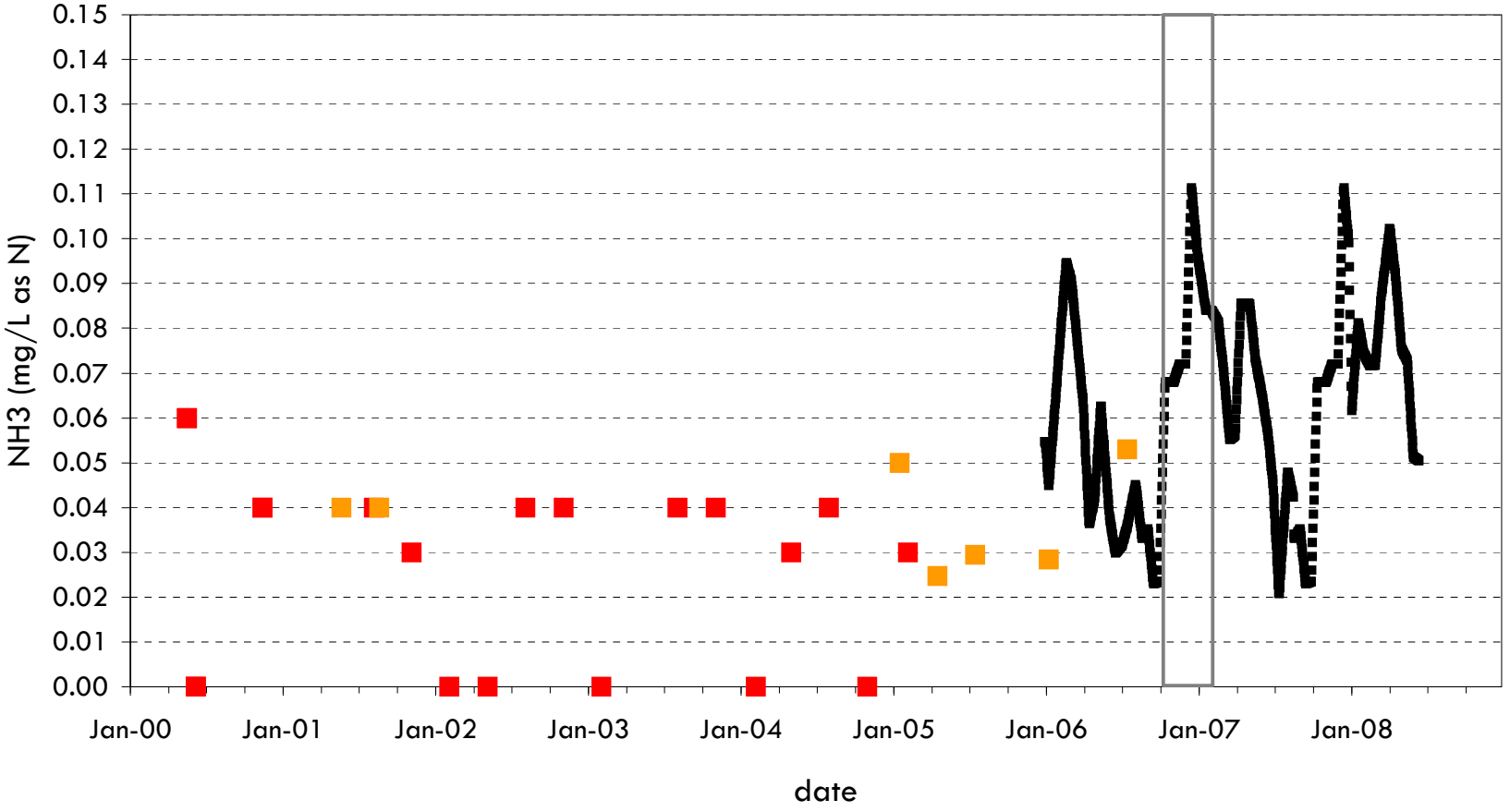

FSI V094005
May 01, 2012

Figure C-23

FLOW SCIENCE®

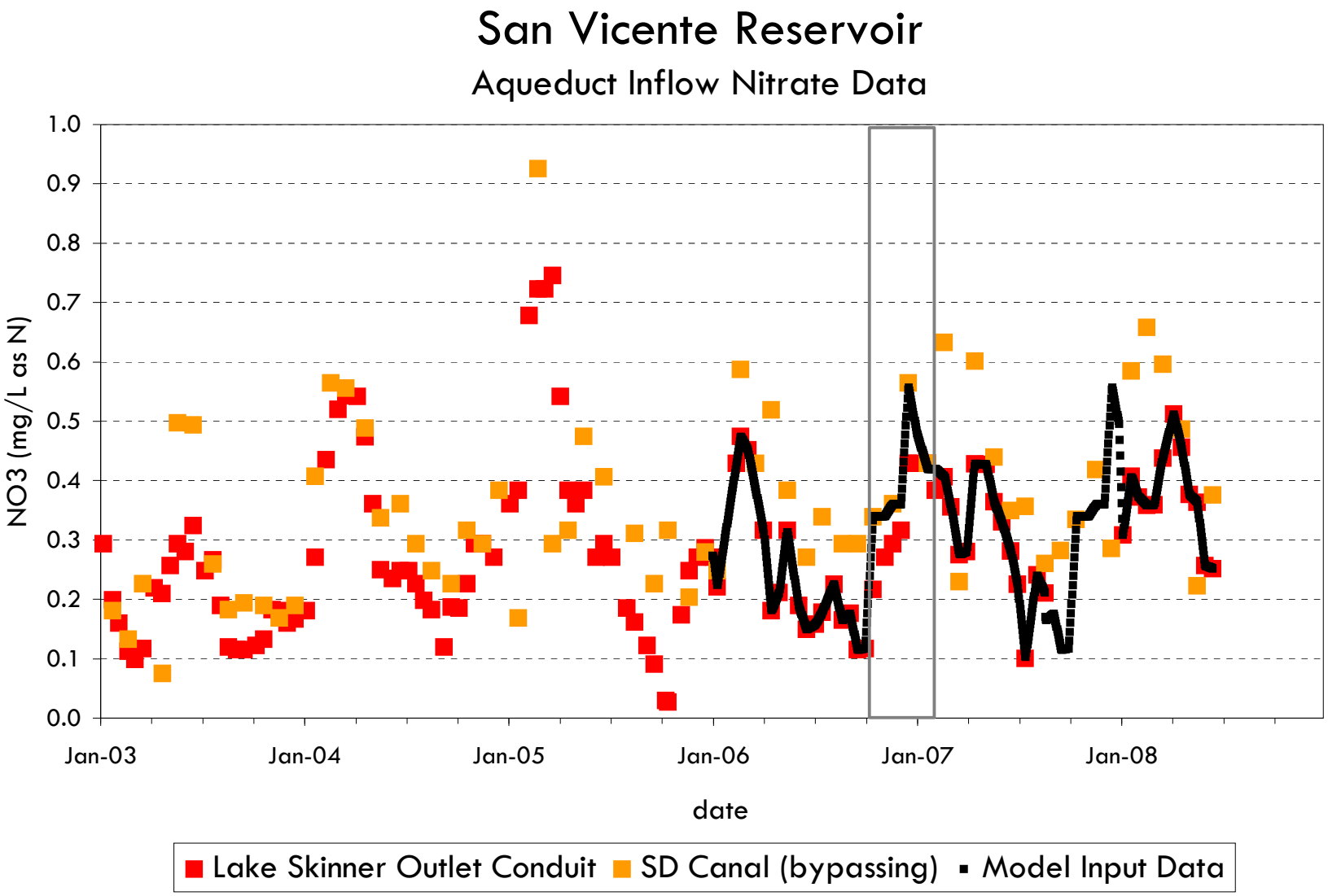

FSI V094005
May 01, 2012

Figure C-24

FLOW SCIENCE®

San Vicente Reservoir

Aqueduct Inflow Total Nitrogen Estimate

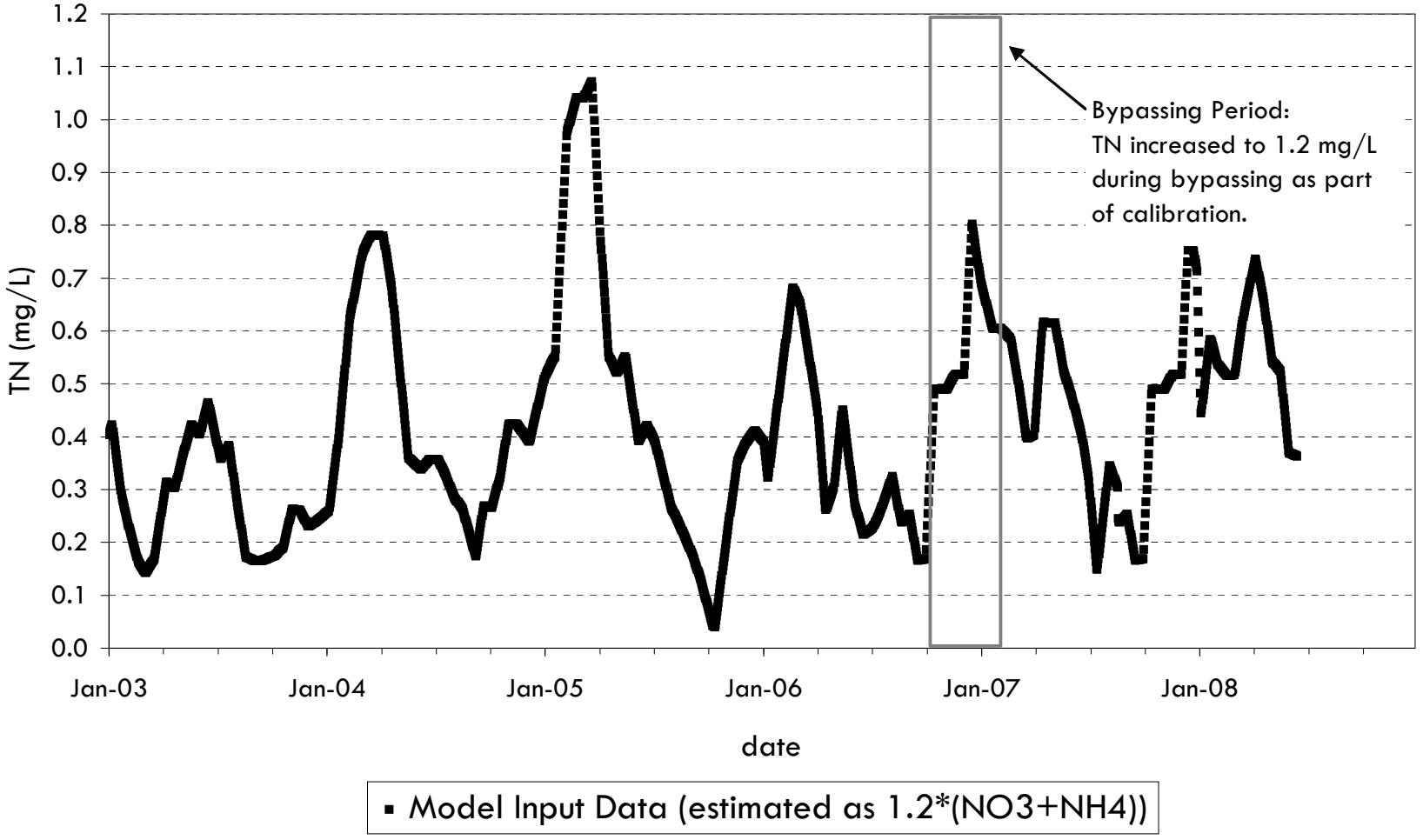

FSI V094005
May 01, 2012

Figure C-25

FLOW SCIENCE®

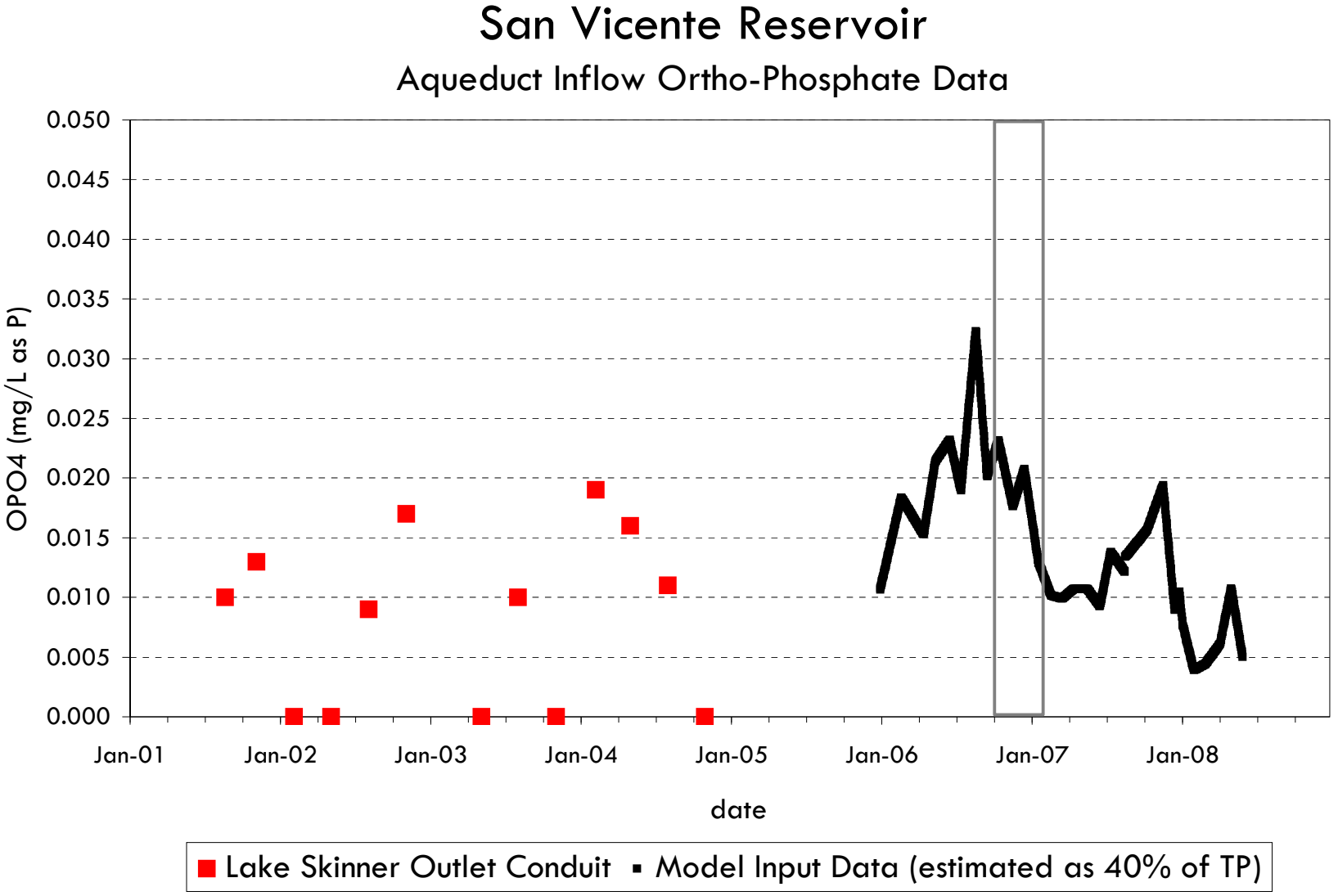

FSI V094005
May 01, 2012

Figure C-26

FLOW SCIENCE®

San Vicente Reservoir

Aqueduct Inflow Total Phosphorus Data

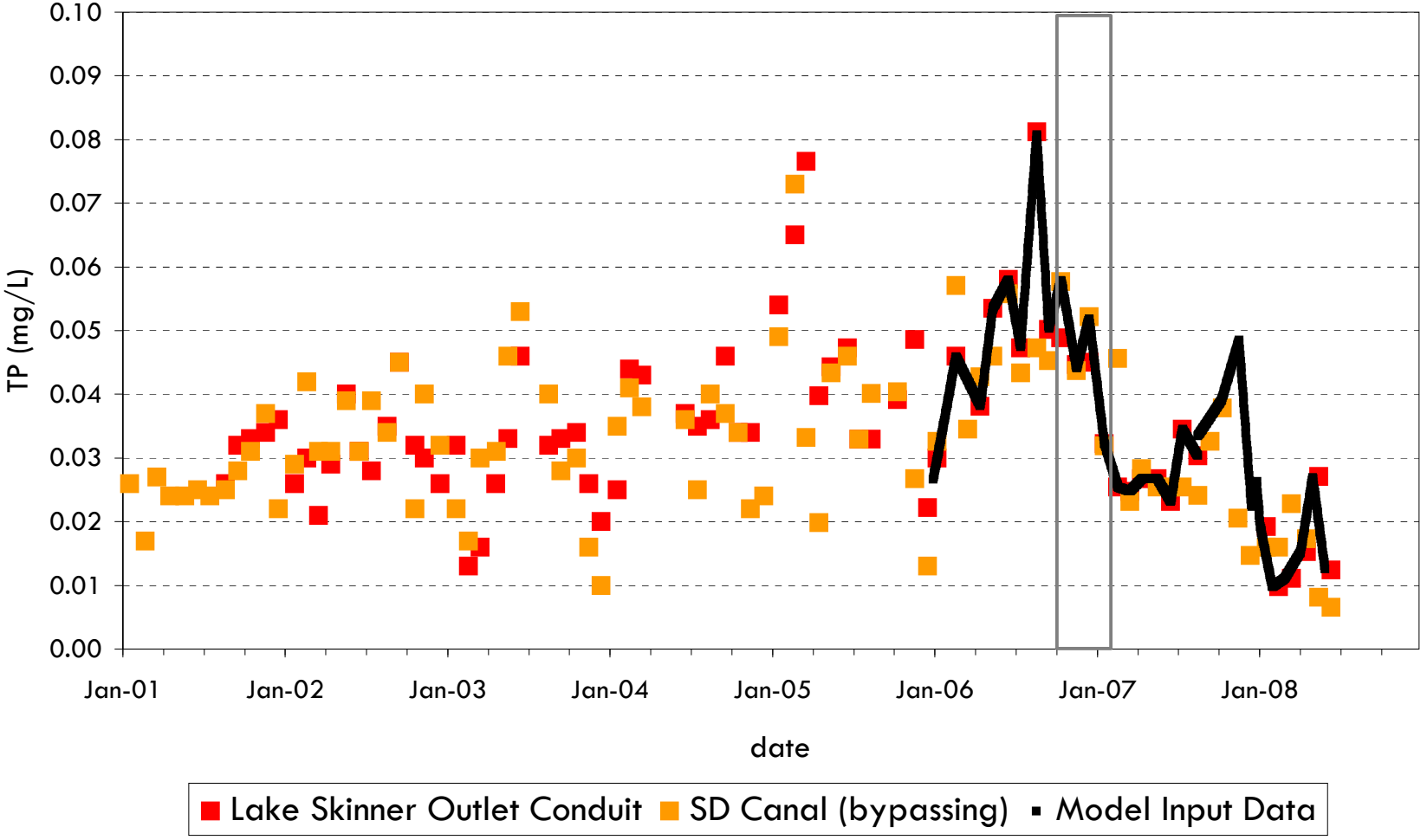

FSI V094005
May 01, 2012

Figure C-27

FLOW SCIENCE®

San Vicente Reservoir

Aqueduct Inflow Dissolved Oxygen

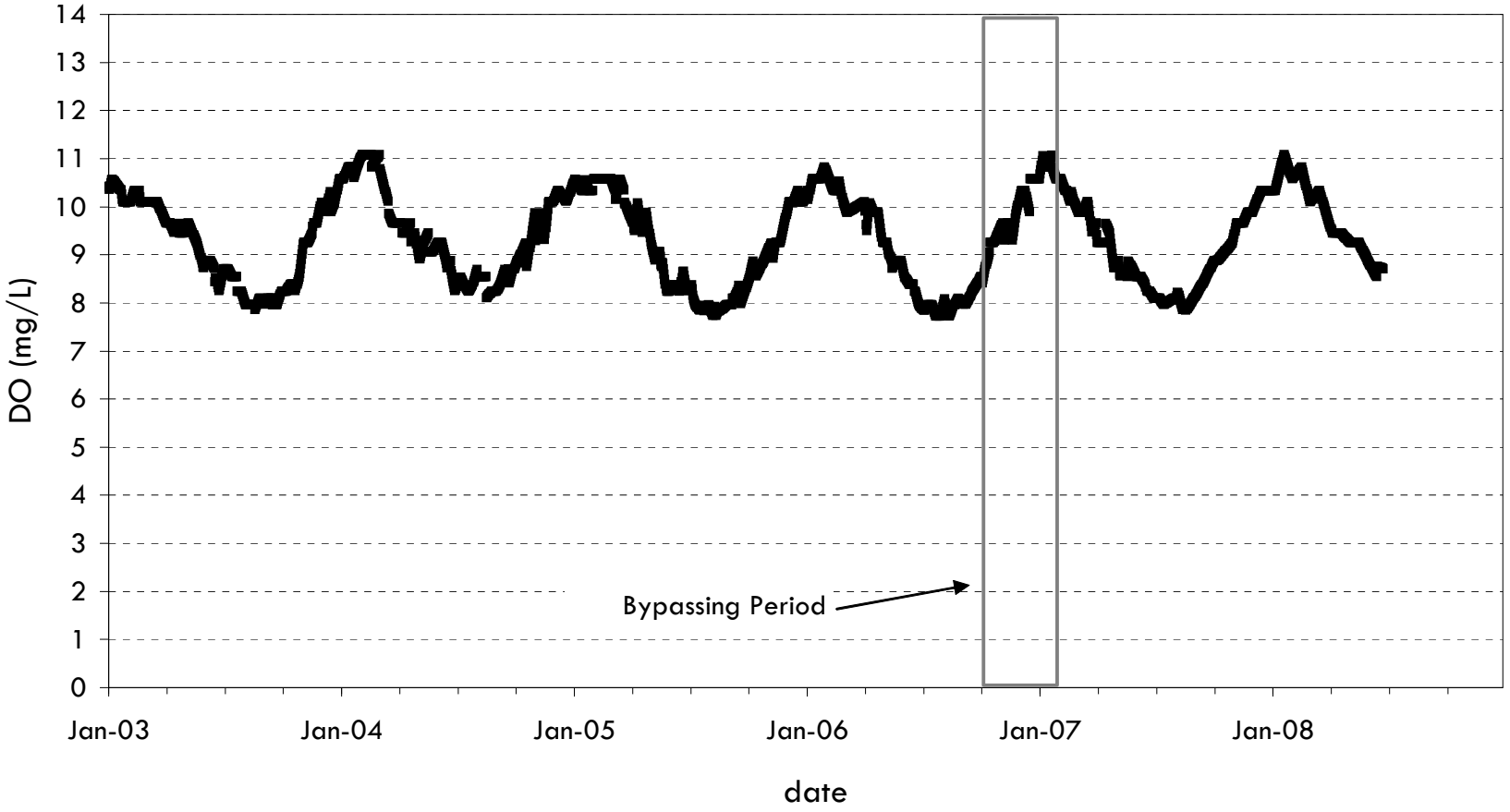

FSI V094005
May 01, 2012

Figure C-28

FLOW SCIENCE®

San Vicente Reservoir

Aqueduct Inflow pH Data

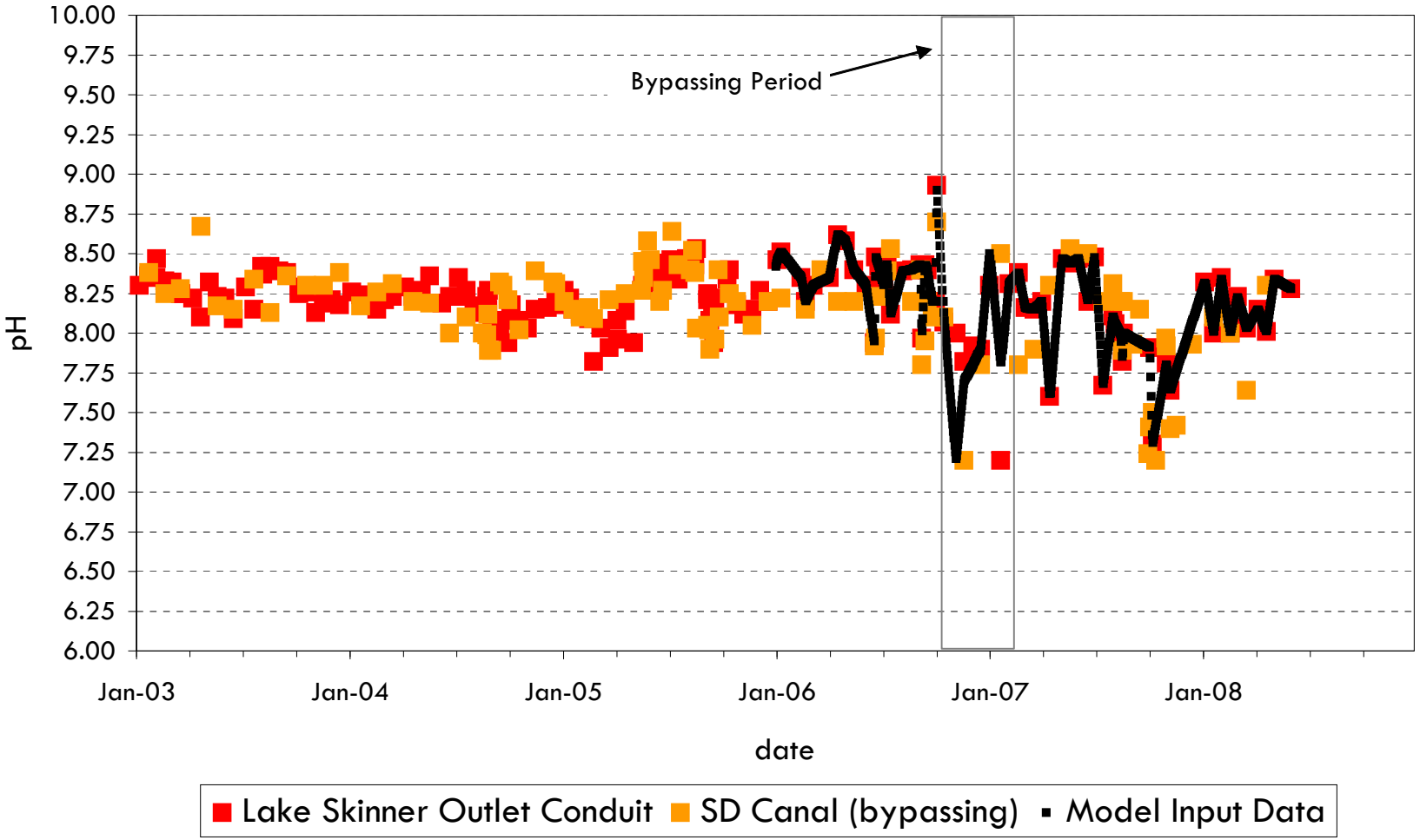

FSI V094005
May 01, 2012

Figure C-29

FLOW SCIENCE®

San Vicente Reservoir

Runoff Inflow Ammonia

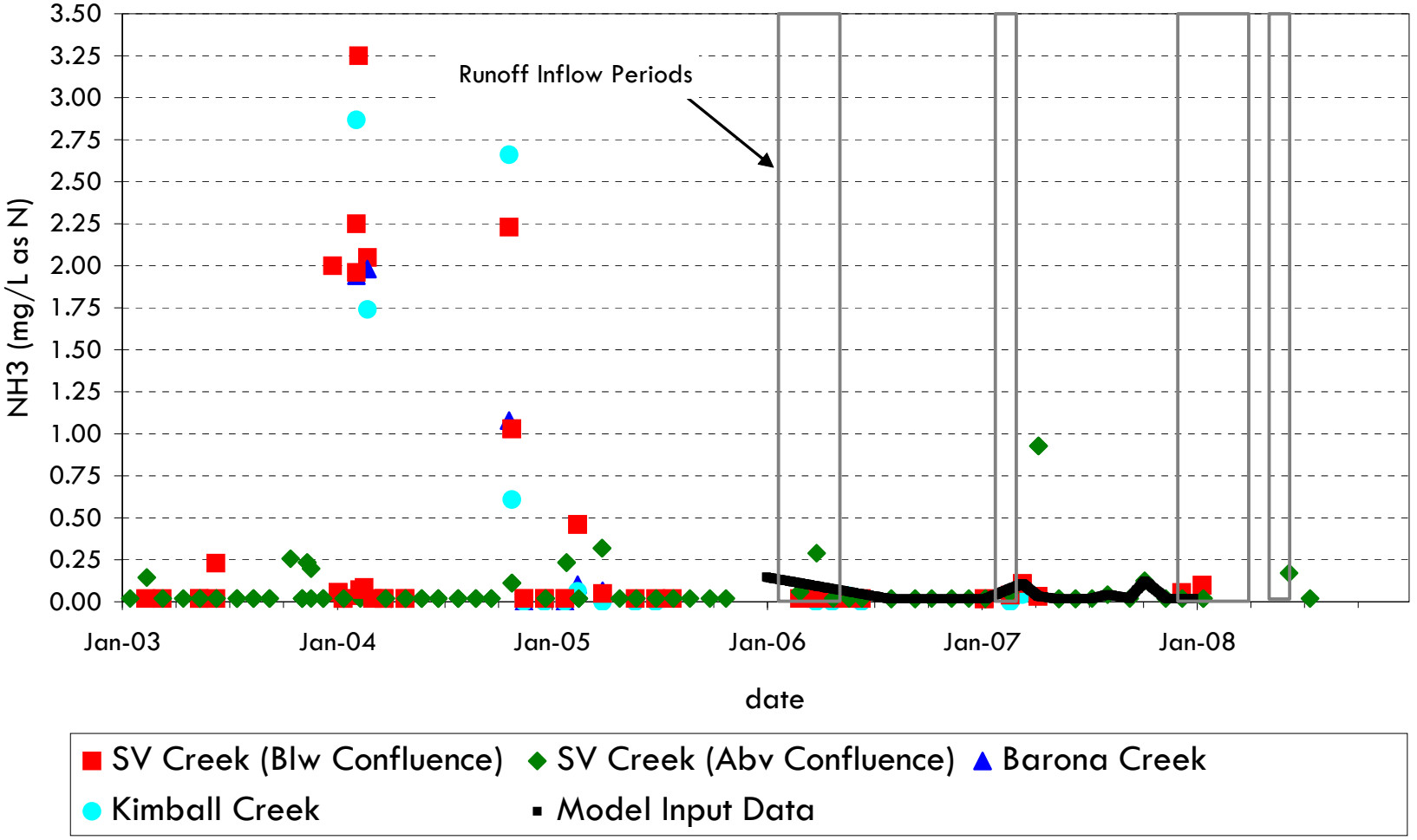

FSI V094005
May 01, 2012

Figure C-30

FLOW SCIENCE®

San Vicente Reservoir

Runoff Inflow Nitrate

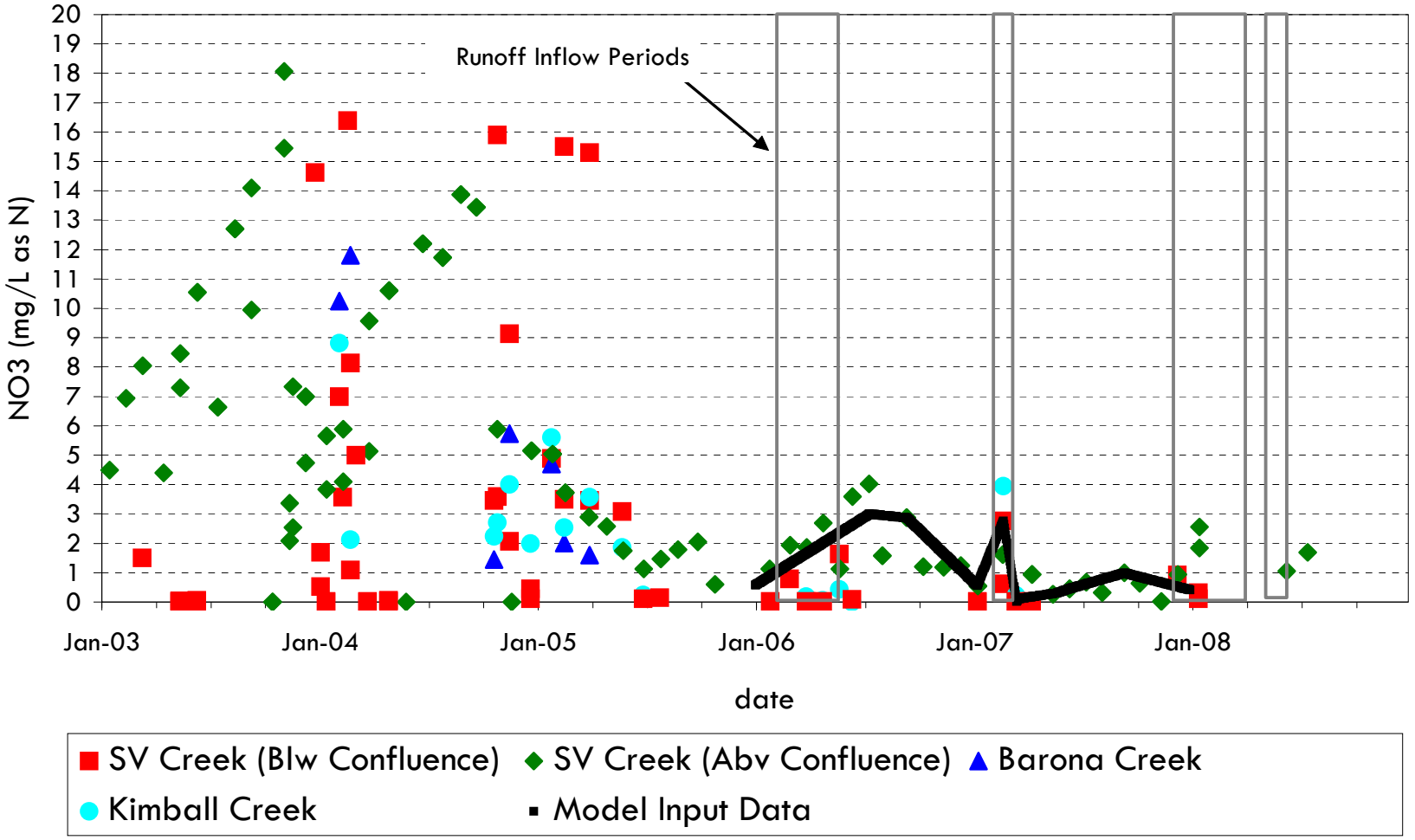

FSI V094005
May 01, 2012

Figure C-31

FLOW SCIENCE®

San Vicente Reservoir

Runoff Inflow Total Nitrogen

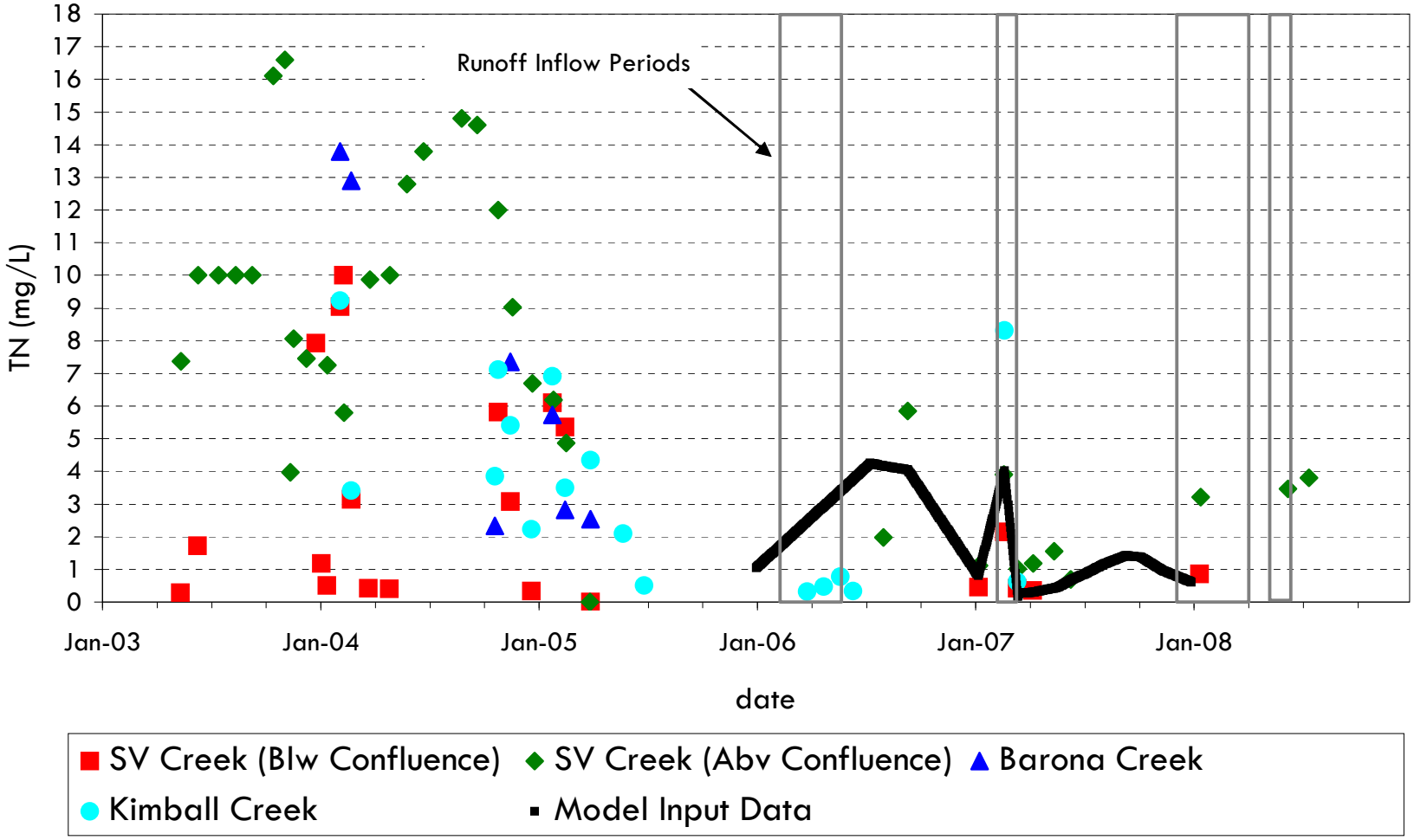

FSI V094005
May 01, 2012

Figure C-32

FLOW SCIENCE®

San Vicente Reservoir

Runoff Inflow Ortho-Phosphate

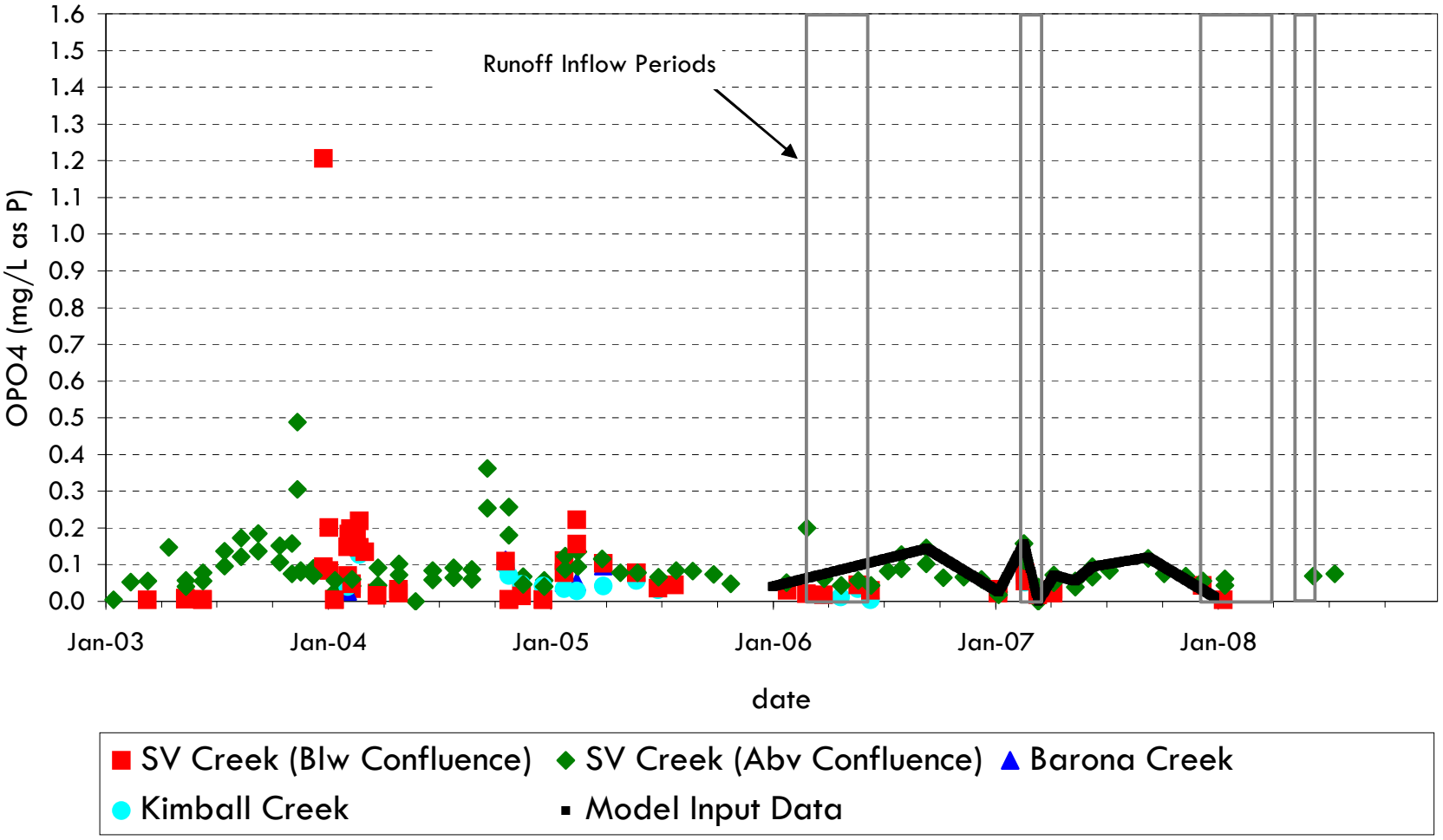

FSI V094005
May 01, 2012

Figure C-33

FLOW SCIENCE®

San Vicente Reservoir

Runoff Inflow Total Phosphorus

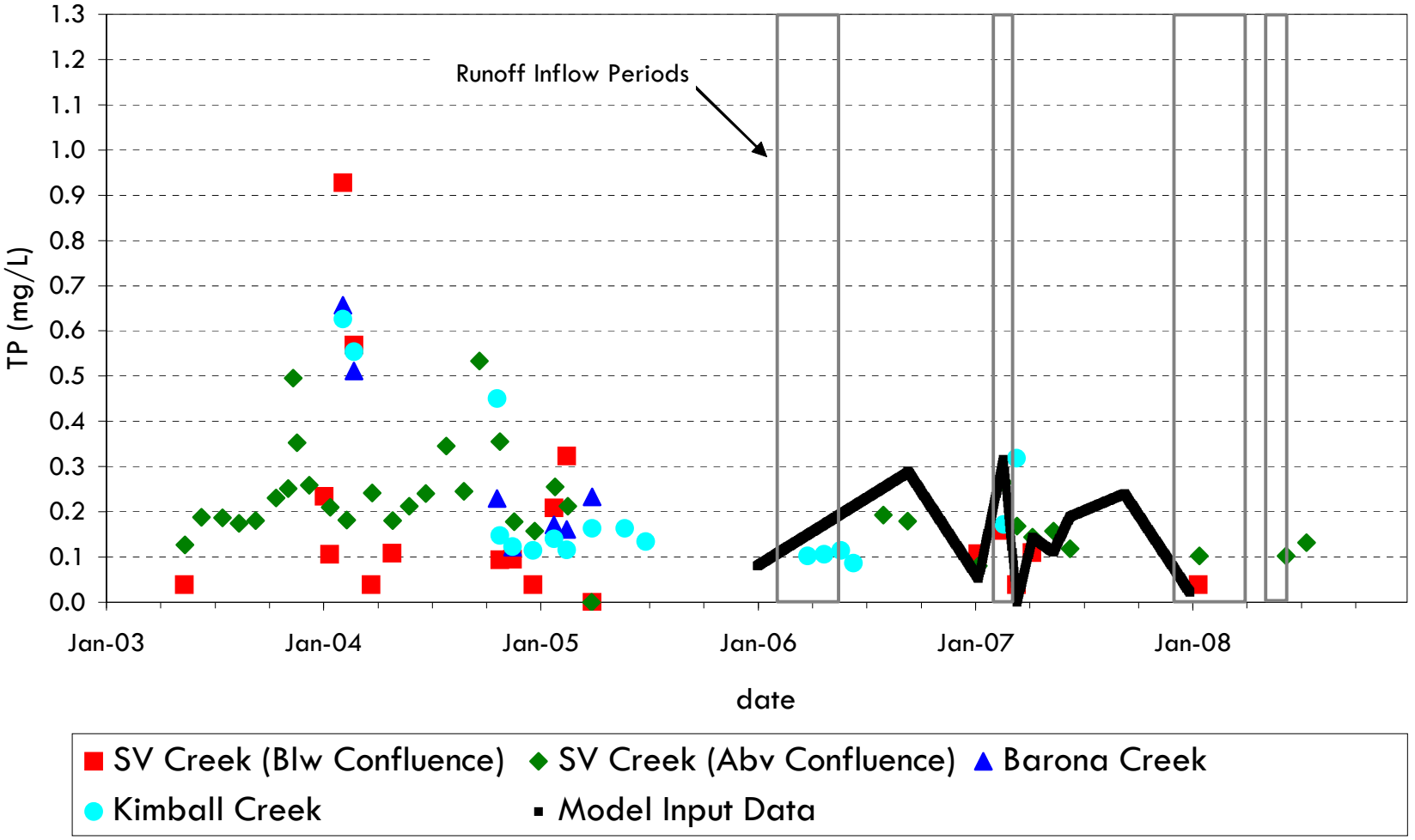

FSI V094005
May 01, 2012

Figure C-34

FLOW SCIENCE®

San Vicente Reservoir

Runoff Inflow Dissolved Oxygen

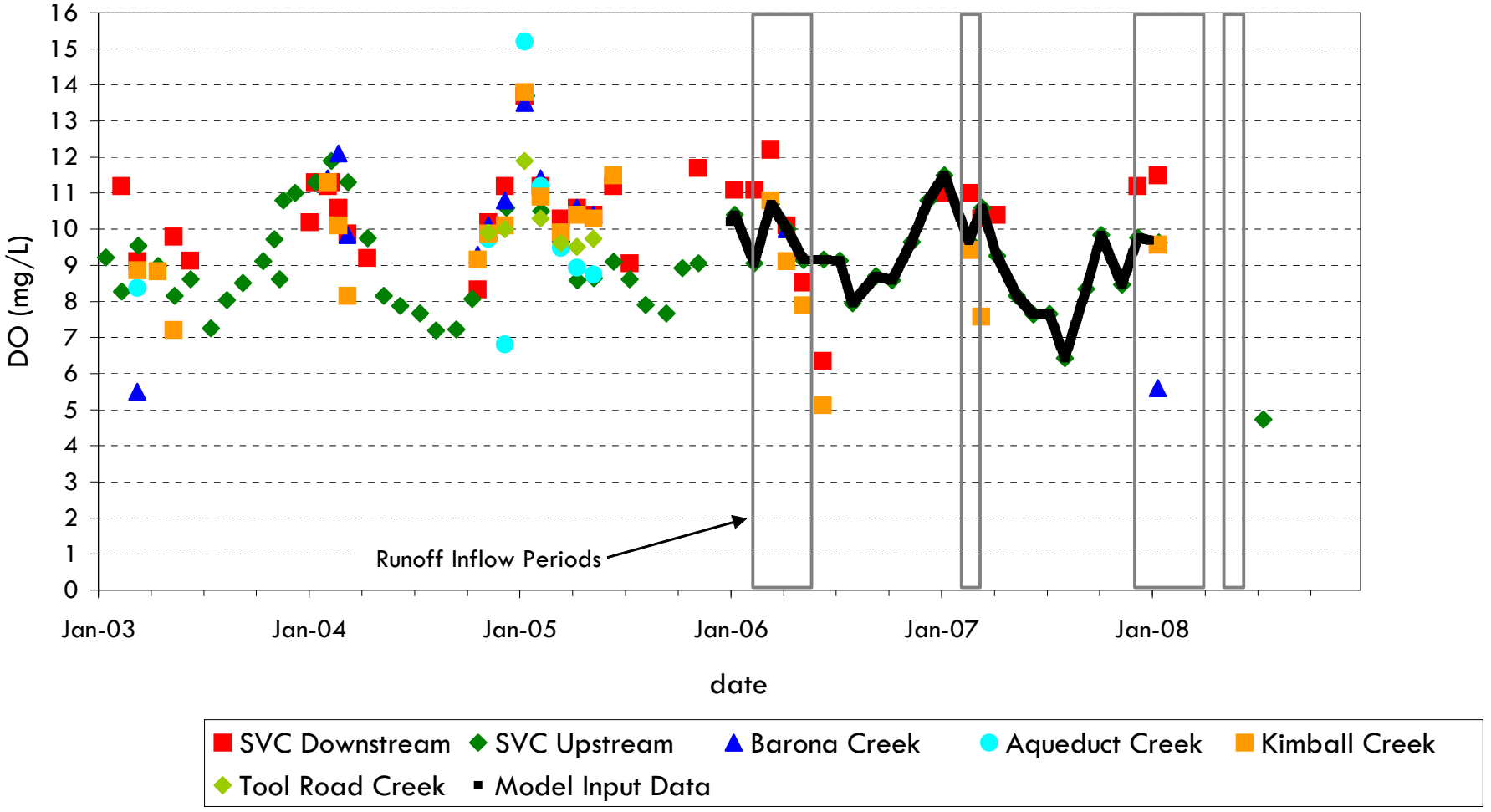

FSI V094005
May 01, 2012

Figure C-35

FLOW SCIENCE®

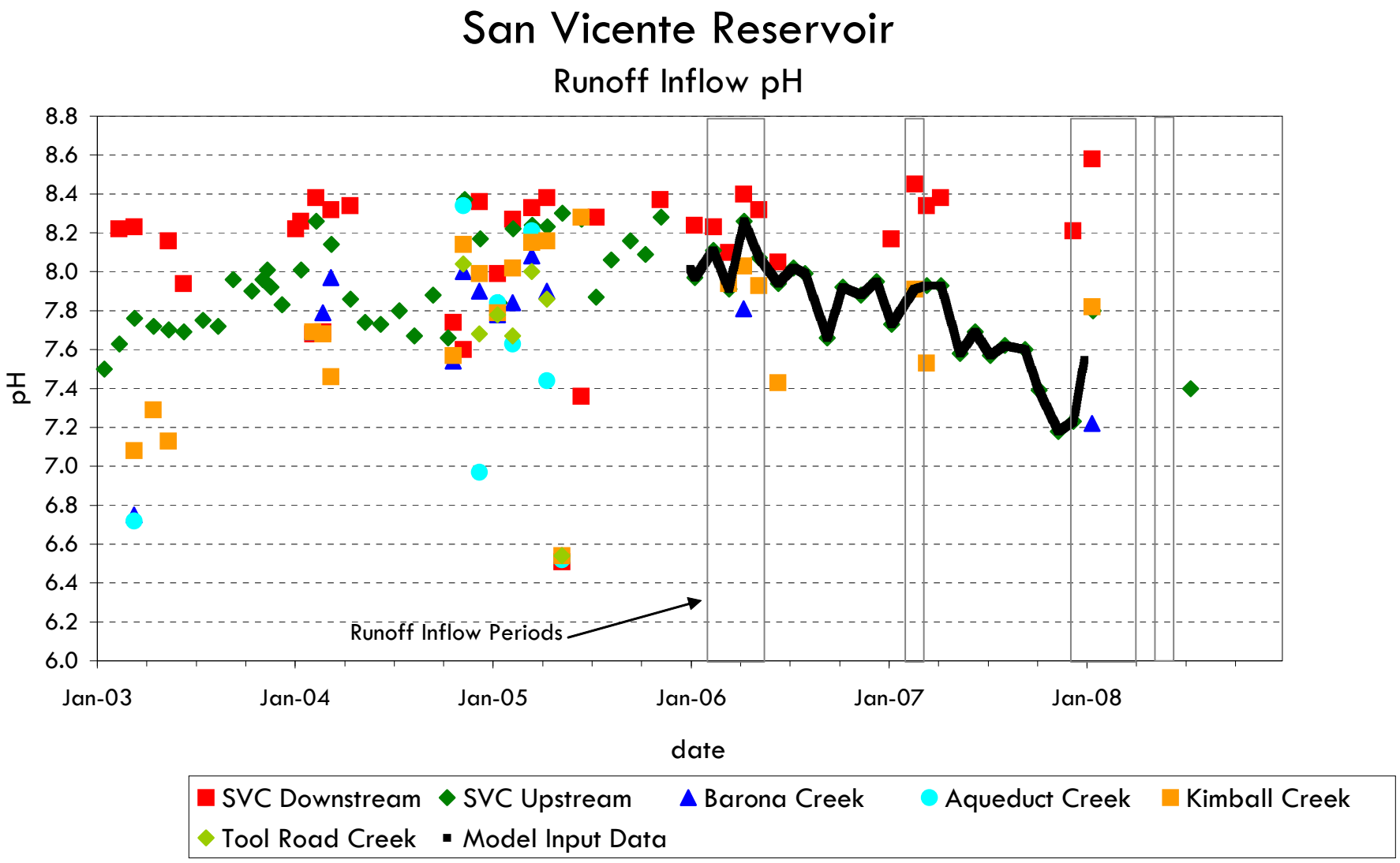

FSI V094005
May 01, 2012

Figure C-36

FLOW SCIENCE®

City of San Diego
Water Quality Laboratory
Sutherland Reservoir Station A Data
January 01, 2006 thru December 31, 2007

Sample Date	Nitrate (mg/L)	Total Nitrogen (mg/L)	Ortho-phosphate (mg/L)	Total Phosphorus (mg/L)
9-Jan-06	< 0.4	0.869	0.253	0.103
6-Apr-06	**< 0.4**	**0.578**	**< 0.2**	**0.109**
10-Jul-06	N/A	0.522	N/A	< 0.078
5-Oct-06	N/A	0.3	N/A	< 0.078
11-Jan-07	< 0.4	0.823	< 0.2	0.264
5-Apr-07	**N/A**	**0.62**	**N/A**	**< 0.078**
9-Jul-07	N/A	0.639	N/A	< 0.078
1-Oct-07	**< 0.4**	**0.493**	**< 0.2**	**< 0.078**
11-Jan-08	< 0.4	0.946	N/A	< 0.078
7-Apr-08	< 0.4	0.779	< 0.2	< 0.078
7-Jul-08	< 0.4	0.363	< 0.2	< 0.078

San Vicente Reservoir

Sutherland Reservoir Dissolved Oxygen Near Outlet (El 1940 ft)

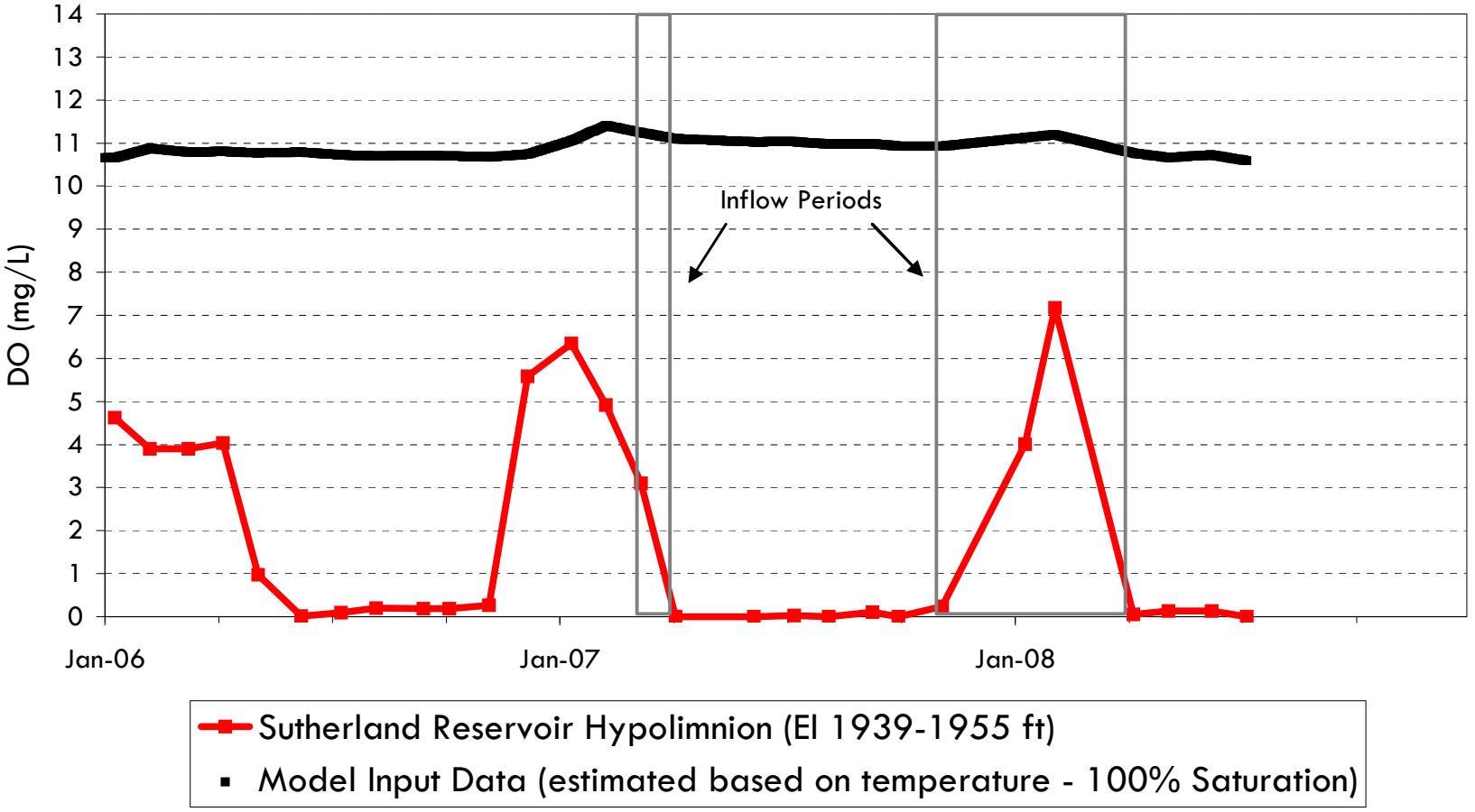

FSI V094005
May 01, 2012

Figure C-38

FLOW SCIENCE®

San Vicente Reservoir

Sutherland Reservoir pH Near Outlet (El 1940 ft)

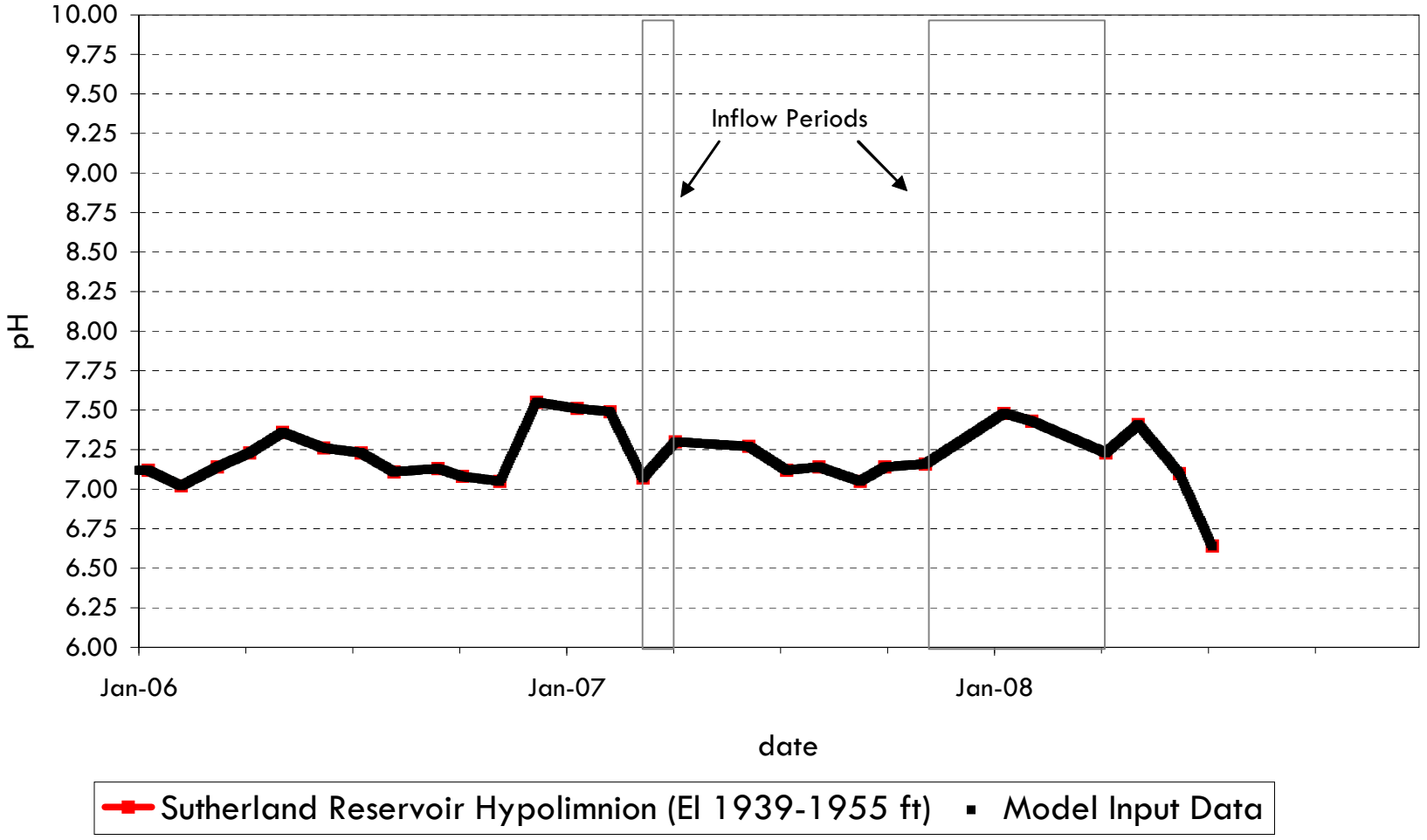

FSI V094005
May 01, 2012

Figure C-39

FLOW SCIENCE®

San Vicente Reservoir

Sutherland Reservoir Chlorophyll a Near Outlet (El 1940 ft)

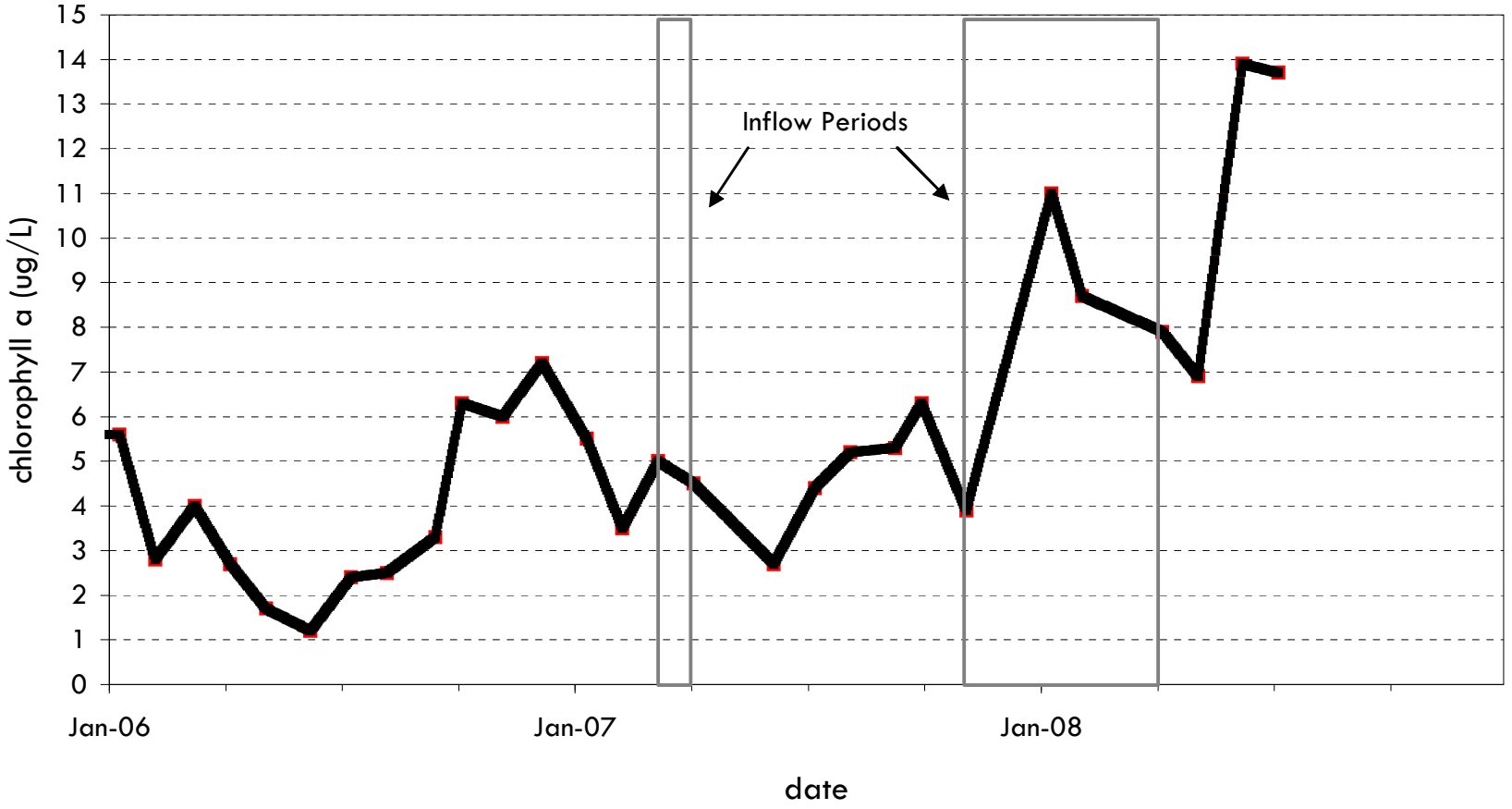

FSI V094005
May 01, 2012

Figure C-40

FLOW SCIENCE®

APPENDIX D

LIST OF ANIMATIONS

INSTRUCTIONS FOR INSTALLING AND USING FRAMER TO VIEW ANIMATION FILES

Installation of Framer

Copy the files from the CD(s) to a directory on your computer.

Running Framer

1) In the Start Menu, choose "run." In this window, type "framer.exe." This should open a "Framer Open File" window, in which you find the proper directory and choose the file that you wish to view.

2) Commands for running the animation files are in the toolbar in the upper left corner of the framer window.

LIST OF ANIMATIONS

1) Appendix D_SVR_Aqueduct_Tracer.rm